GEOCHEMISTRY AND BASIN MODELING OF DEVONIAN-MISSISSIPPIAN

PETROLEUM SYSTEMS IN THE ANADARKO BASIN

A Dissertation

by

IBRAHIM AL ATWAH

Submitted to the Office of Graduate and Professional Studies of
Texas A&M University
in partial fulfillment of the requirements for the degree of

DOCTOR OF PHILOSOPHY

Chair of Committee,	Franco Marcantonio
Committee Members,	Mauro Becker
	Andrea Miceli Romero
	Anthony Knap
Head of Department,	Michael Pope

August 2019

Major Subject: Geology

ABSTRACT

The Woodford Shale and the overlying Mississippian Limestone constitute one of the prolific unconventional and conventional hydrocarbon targets in Northern Oklahoma. Technological advancement in drilling and production has allowed for the economic recovery of hydrocarbon from tight source-rock reservoirs. However, many challenges remain unexplained related to the variation in well performance and hydrocarbon composition. Many factors control hydrocarbon producibility from Devonian-Mississippian reservoirs, including rock mineralogy, thermal maturity and organic-richness. A collection of rock, crude-oil and fluid-inclusion samples were geochemically investigated to gain insight into their origin and thermal maturity. This study introduces an entirely new geochemical approach for the correlation of high-temperature fluid inclusions with their source rocks, using quantitative extended diamondoid analysis (QEDA).

Mississippian mudrocks exhibit organic-rich units capable of generating hydrocarbon. Petroleum from Mississippian rocks is proven through source-rock and crude-oil correlation, sharing similar biomarker fingerprints. A collection of Mississippian biomarkers has been identified, including diterpenoids and extended tricyclic terpenes, reflecting the organic-matter source and depositional environment. Macerals of Mississippian rocks are characterized by the amorphous morphologies, whereas Woodford Shale macerals exhibit intact structures. According to mineralogy and sedimentology, six main facies were identified within the Mississippian mudrocks. Furthermore, Organic and sedimentological characteristics suggest shoaling-upward sequences in the Mississippian formation. Examined crude oil was grouped into three major families, each of which exhibits a unique geochemical signature. The first crude-oil family is derived from Mississippian end-member source rocks, while the third family is closely related to Woodford Shale source rock, and the second oil family represents a mixture of the two end-

members. Diamondoids shed light into on mixed hydrocarbons at various levels of maturity, in which oils within the Anadarko Shelf and Sooner Trend Anadarko Basin Canadian and Kingfisher Counties (STACK) plays are mixed oils of uncracked and cracked hydrocarbons, whereas oils within central Oklahoma are unmixed and uncracked hydrocarbons. Based on geochemical evidence derived from fluid inclusions and crude oil, petroleum-migration timing is defined over four major episodes, with long-distance petroleum migration west of the Nemaha Uplift, and short-distance petroleum migration at the east of the Nemaha Uplift. All generated geochemical data were integrated into a basin and petroleum systems approach with the aim of understanding major factors controlling the distribution and quality of hydrocarbons across the Devonian-Mississippian petroleum systems.

DEDICATION

Dedicated to the strongest lymphoma fighter.

ACKNOWLEDGMENTS

CONTRIBUTORS AND FUNDING SOURCES

TABLE OF CONTENTS

LIST OF FIGURES

LIST OF TABLES

CHAPTER I

INTRODUCTION

Unconventional Petroleum Systems

A pioneering petroleum geologist who helped prove the value of geology to the petroleum industry, Wallace Pratt once stated, "Where oil is first found is, in the final analysis, in the minds of men" (AAPG Foundation, 1958). The task of a petroleum geologist to visualize and interpret ancient natural phenomenon embedded in observable and measurable data sets is challenging and complex. Similarly, the generation of petroleum in the geological strata is complicated, requiring certain elements of organic material, as well as specific regimes of temperature and pressure. In the quest to understand the principles of petroleum generation, migration and accumulation, scientists have proposed many theoretical models, such as models centered on oil habitat, oil system, generative basin and petroleum system (Demaison, 1984; Dow, 1974; Knebel and Rodriguez-Eraso, 1956; Meissner et al., 1984; Perrodon, 1992). These concepts were further refined by Magoon and Dow (1994), who defined the petroleum system as the presence of an active source rock and a genetically related hydrocarbon accumulation resulting from the petroleum system elements and processes. The elements of a conventional petroleum system consist of the source rock, reservoir rock, seal rock and overburden rock, whereas petroleum system processes encompass trap formation and the generation-migration-accumulation of petroleum (Magoon and Dow, 1994). Ultimately, the petroleum system concept is a petroleum investigation tool usually used at a regional scale as opposed to petroleum prospect, which is an investigation of a single trapped hydrocarbon accumulation. The most critical element of the petroleum system is the source rock, and it is what defines the petroleum system. Without a source

rock, there is no petroleum system. The presence or the lack of other elements and processes of the petroleum system dictates whether the petroleum system is conventional or unconventional.

Unlike conventional petroleum systems, unconventional petroleum systems do not necessitate the presence of all the petroleum system elements and processes; however, they require the source rock's presence. Figure 1 summarizes the different types of unconventional petroleum systems. Examples of these unconventional hydrocarbon systems include shale gas, shale oil, coalbed methane, bituminous sands, and so on (Sonnenberg and Meckel, 2016; Zou, 2017). In general, the unconventional petroleum systems discussed in this dissertation (i.e., shale gas and shale oil) exhibit unique characteristics such as tight reservoir properties (i.e., ultra-low porosity and permeability), extensive continuous distribution, and low or high oil viscosity; these unconventional systems thus require advanced technology (e.g., horizontal drilling and fracking) to economically produce the associated hydrocarbon resources.

Figure 1: Schematic diagram showing different types of unconventional petroleum systems together with conventional oil and gas accumulations, modified from (Sonnenberg and Meckel, 2016).

Global Outlook

Historically, oil and gas exploration and production have been primarily focused on conventional oil and gas fields. However, over the last two decades, the importance of unconventional shale oil and shale gas has dramatically increased. In considering estimations of unconventional oil and gas resource and reserves, either globally or locally, one must note discrepancies in numbers between varying sources, and sometimes such differences are found even within the same source. As methodologies for estimation of unconventional resources and recovery technology improve, better and more accurate volumetric calculations can be made. Crucially, however, such a resource assessment often lacks certainty. Hence, estimates of unconventional resources continue to improve with further time, expertise and technological progress. Today, the largest unconventional shale oil and shale gas resources are located in the United States, Russia, Eastern Asia and South America (Figure 2).

Several other large reserves exist in the Middle East, Africa and Europe; however, the resources for those basins are currently not estimated (Kuuskraa et al., 2013). With respect to shale gas basins globally, China, Argentina, Algeria, and the United States are among the countries with the largest technically recoverable shale gas resources (Kuuskraa et al., 2013). As of 2013, China was assessed to have 1115 trillion cubic feet of gas resources, while the United States was estimated to have 665 trillion cubic feet of shale gas resources. It is important to note that "technically recoverable" does entail "economically recoverable"; a massive amount of oil or gas may exist in the subsurface, but the cost of extracting it would be far more than a company could ever make off of the product. Concerning global shale oil, the highest amounts of *in-situ* shale oil resources, by nation, reside in Russia, the United States, Argentina and Libya (Dyni, 2006). Russia

is assessed to have roughly 75 billion barrels of oil in technically recoverable oil resources, while

the United States is estimated to have 58 billion (Kuuskraa et al., 2013).
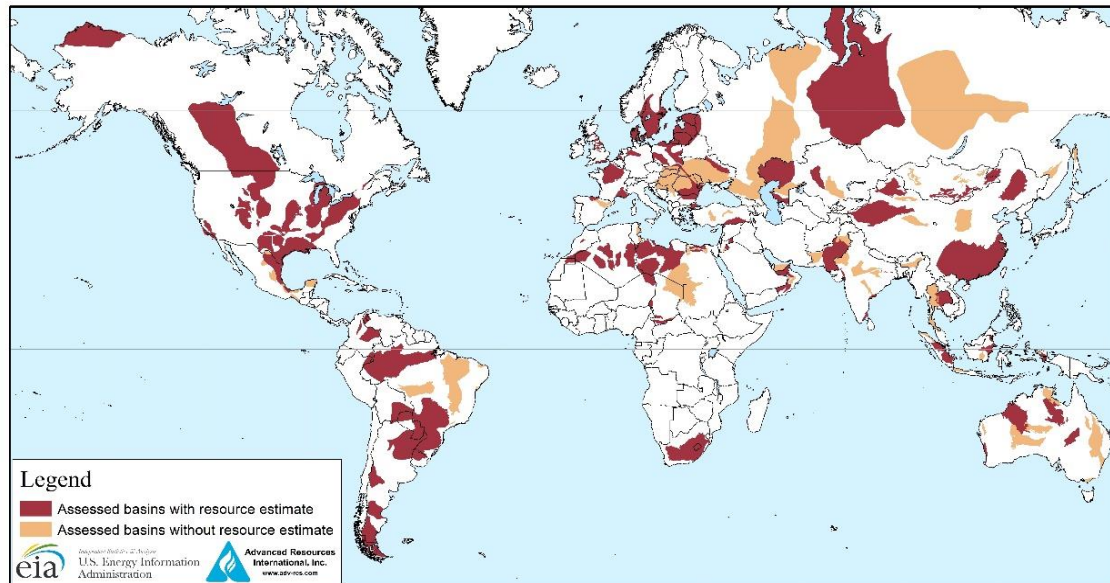
Figure 2: Global distribution of sedimentary basins with significant shale oil and shale gas resources (Kuuskraa et al., 2013).

U.S. Unconventional Shale Plays

Unconventional shale plays in the United States contribute significantly to hydrocarbon

production, with estimates of 2014 reaching at a total of 3.6 million barrels of oil per day and

around 35 billion cubic feet of gas per day (Sieminski, 2014b). Some of the major oil- and gas-

producing shale formations are Eagle Ford and Spraberry in Texas, Bakken in North Dakota, and

Woodford in Oklahoma (Figure 3) (EIA, 2015). As of 2013, the United States required 18.4 million

barrels of oil per day to meet energy requirements. Of those 18.4 million, 7.4 million were

produced from U.S. plays, while the other 11 million were imported from various countries

(Sieminski, 2014a). Although the amount imported appears high, it is the lowest per-day amount

of oil that the United States has ever had to import. This reduction in imports can be attributed to

4
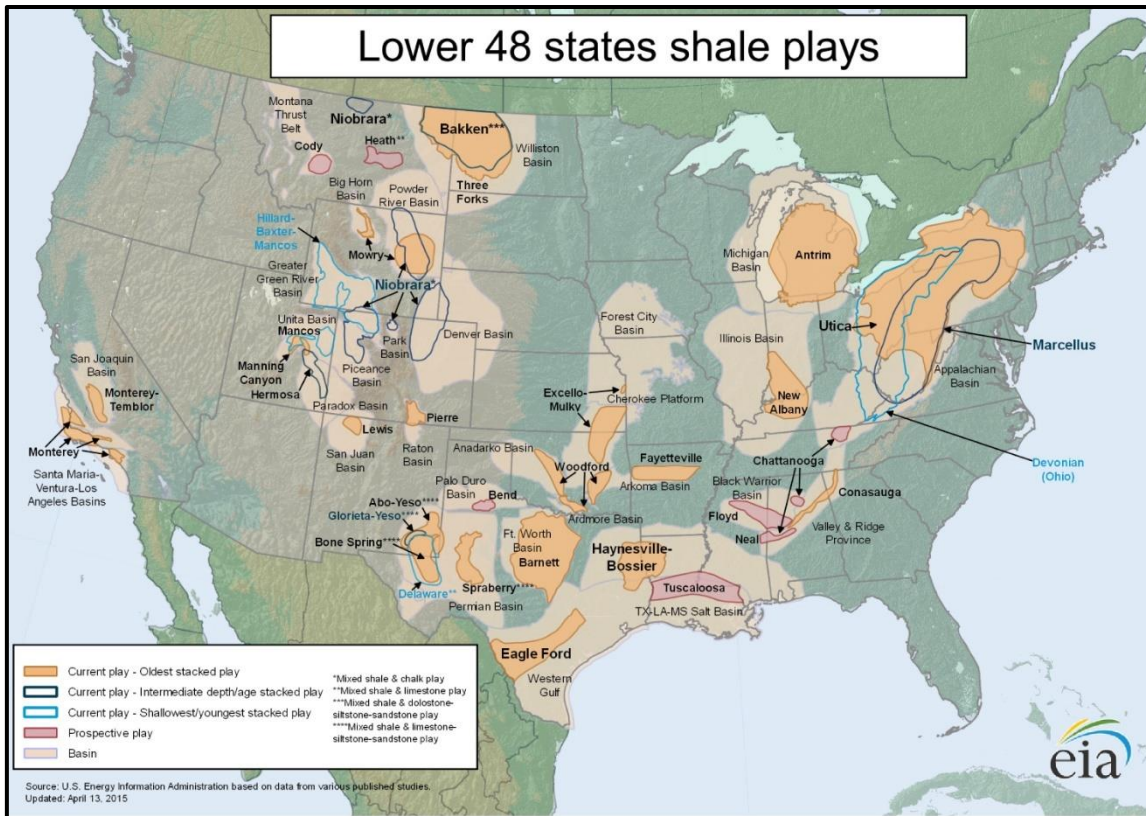
Figure 3: Geographic distribution of major unconventional shale plays showing both oil- and gas- producing plays, and outlining sedimentary basins (EIA, 2015).

the contribution of unconventional shale resources. As of 2016, the United States' proven oil resources were reported to be 35.2 billion, with a total increase of 3% in the lower 48 states. Meanwhile, proven gas resources are estimated at 341.1 trillion cubic feet, which exhibits a total 5% increase of reserves compared to previous assessments (EIA, 2018). Of these states with oil- and gas-proven resources, seven contain the majority: Texas, North Dakota, the Gulf of Mexico, Oklahoma, California, New Mexico, and Alaska. Of these states, most showed a total decrease in oil reserves assessments from 2012 to 2016, with exception of Texas and Oklahoma, for which proven oil reserves have grown over time (EIA, 2018). This increase of reserves is clear evidence of the great potential of tight oil resources, which, with time and technology advancement, yield more hydrocarbons. Texas exhibited the largest increase in oil discoveries, with proven crude oil

and condensate reserves at 941 million barrels, a 7% increase in oil reserves over the figures for 2017. Such a gain is primarily due to drilling activities in the Permian Basin of West Texas, in particular oil plays such as the Wolfcamp and Spraberry shale plays. Moreover, Oklahoma had the second largest proven crude-oil and condensate reserves after Texas, with a total of 386 million barrels in 2016 a total increase of 23% compared with proven oil reserves in 2015 (EIA, 2018). Oklahoma's oil-reserves gain is attributed to successful discoveries in the stacked zones of a number of tight-shale plays encompassing the Woodford, Caney and Meramec succession of tight shales and carbonate rocks (EIA, 2018).

Hydrocarbon Plays in Oklahoma

The Anadarko Basin and adjacent shelves are major hydrocarbon-producing areas in Oklahoma. The first commercial crude-oil-producing well (Nellie Johnstone No. 1, Fig.4) was drilled in 1897 near oil seeps at Bartlesville, Oklahoma (Franks, 1980). Since then, the Anadarko Province has been known for its prolific crude-oil and gas production. Hydrocarbon richness in the Anadarko Basin results from the presence of multiple petroleum systems, spanning in age from Ordovician to Pennsylvanian (Burruss and Hatch, 1989a; Da Wang and Philp, 1997).
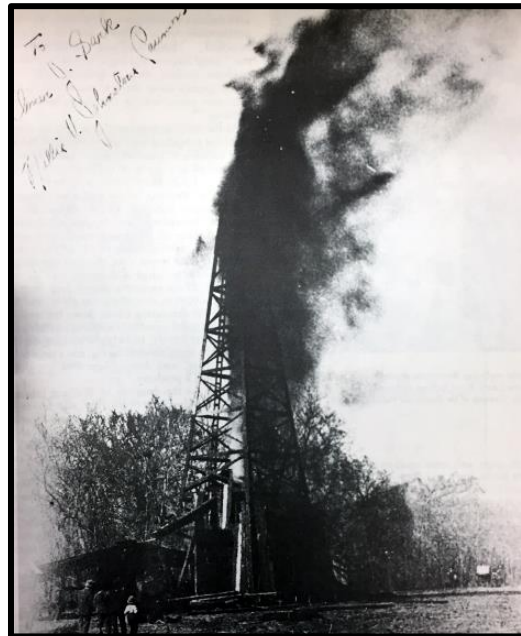
Figure 4: Nellie Johnstone No. 1 first commercial oil well in Oklahoma, drilled in 1897 (Franks, 1980).

.

In recent years, the advantage of horizontal drilling and hydraulic fracturing technologies have made unconventional tight reservoirs attractive targets. More specifically, they are unconventional targets within the Devonian-Mississippian stratigraphic interval located in central Oklahoma and extending across the eastern side of the Anadarko Basin and Shelf, known as the STACK/SCOOP plays (Figure 5). The unconventional "STACK" play corresponds to "Sooner Trend Anadarko Basin Canadian and Kingfisher Counties," while "SCOOP" stands for "South Central Oklahoma Oil Province." Oil production from the STACK play is primarily from Mississippian Meramec tight and naturally fractured carbonates, whereas the SCOOP play's main production is from the Woodford Shale (Milam, 2013; Molinares-Blanco and Slatt, 2014).
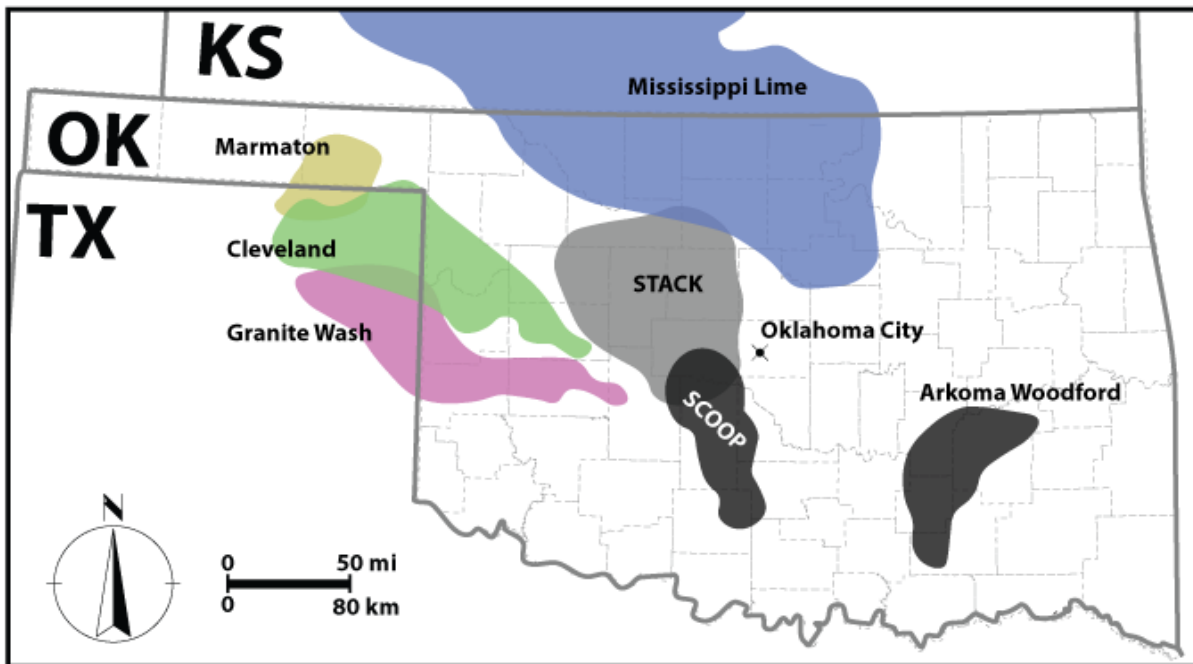
Figure 5: Generalized boundaries of major conventional and unconventional hydrocarbon plays in the Anadarko Basin, Oklahoma. The graph is adapted from WoodMackenzie.
.

Devonian-Mississippian Petroleum Systems in Oklahoma

Oklahoma's Devonian-Mississippian interval constitutes the richest productive zones, due to the presence of several unconventional and conventional reservoir beds. Organic-rich source rocks include the well-known Devonian Woodford Shale, and the Mississippian Meramec, Caney and Springer Shales. These source rocks have been correlated with genetically related crude oils, suggesting at least two geochemically distinct petroleum systems operating with a variable degree of mixing. For instance, the presence of extended tricyclic terpene biomarkers in Mississippian crude oils is attributed to petroleum charge from Mississippian age source rocks .

The Devonian-Mississippian petroleum systems exhibit a number of conventional and unconventional reservoirs. As an example of a conventional petroleum play, the Mississippi Lime
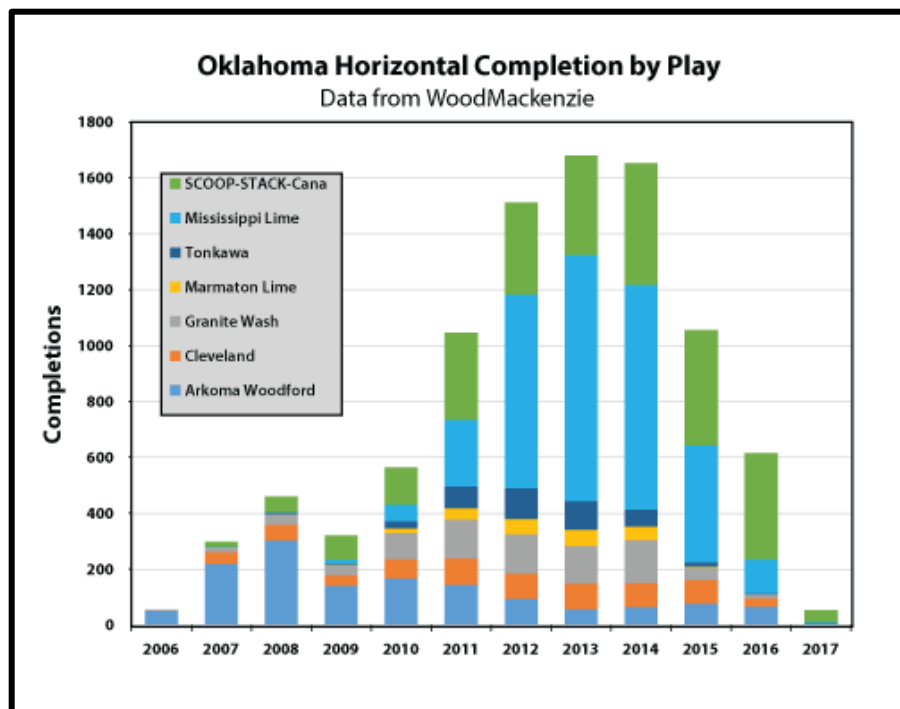
Figure 6: Number of horizontal well completions by petroleum play type (including conventional and unconventional reservoirs) registered from 2006 to 2017. Data from WoodMackenzie (2017).

was discovered in the 1900s, whereas emerging STACK/SCOOP plays are considered unconventional targets that account for the majority of the current drilling activities in the Anadarko Basin.

In recent years, the Devonian-Mississippian petroleum systems account for more than 50% of wells completed, which reflects the economic success of producing large volumes of hydrocarbons contained in these reservoirs, which sustained profitability even during the 2014 downturn in oil markets (Figure 6). The STACK/SCOOP plays together with the Mississippi Lime play account for the majority of the completed wells in Oklahoma after the year of 2011, with completion activity maximizing at a total of 880 wells targeting the Mississippi Lime play during 2013, representing 52% of Oklahoma's completed wells in 2013. The STACK/SCOOP play reached the maximum of 436 completions, accounting for 26% of the total completions in 2014. Moreover, in recent years, including in 2016 and 2017, the STACK/SCOOP plays and Mississippi Lime play represent 81% and 90%, respectively, of total completed wells in Oklahoma.

Oil and gas production records attest to the significant contribution of hydrocarbon resources trapped in Devonian-Mississippian rock formations. Figure 7 compares Oklahoma's annual oil and gas production by barrels of oil equivalent, subdivided by play type. Since 2012, production from both, the Mississippi Lime and STACK/SCOOP plays represent more than 54% of the produced crude oil and 90% of the produced gas. Moreover, since 2014 the Mississippi Lime play was the top oil-producing interval, averaging 33.1 million barrels of oil equivalent (Figure 7). However, in subsequent years, the unconventional reservoirs surged in the production of oil and gas. The STACK/SCOOP play reached maximum production in 2016, with a total of 46.7 million barrels of crude oil and 137.5 million barrels of gas equivalent, which equates to 107 trillion cubic feet of natural gas. In 2017, the magnitude of production for oil and gas dropped by

almost half. This drop was largely driven by the market for the oil industry and was definitely not due to resource depletion. In addition, even with the downturn in the oil market, the Devonian-Mississippian plays remain the top-producing hydrocarbon intervals. Therefore, the aforementioned drilling activity and production performance reflect the significant economic value of those rock formations and hence the importance of understanding the geological evolution and the petroleum systems in this basin. Particularly, in delineating "sweet spots" resulting in the increased recovery of good hydrocarbon quality while minimizing the geological risk associated with fluids migration and accumulation.
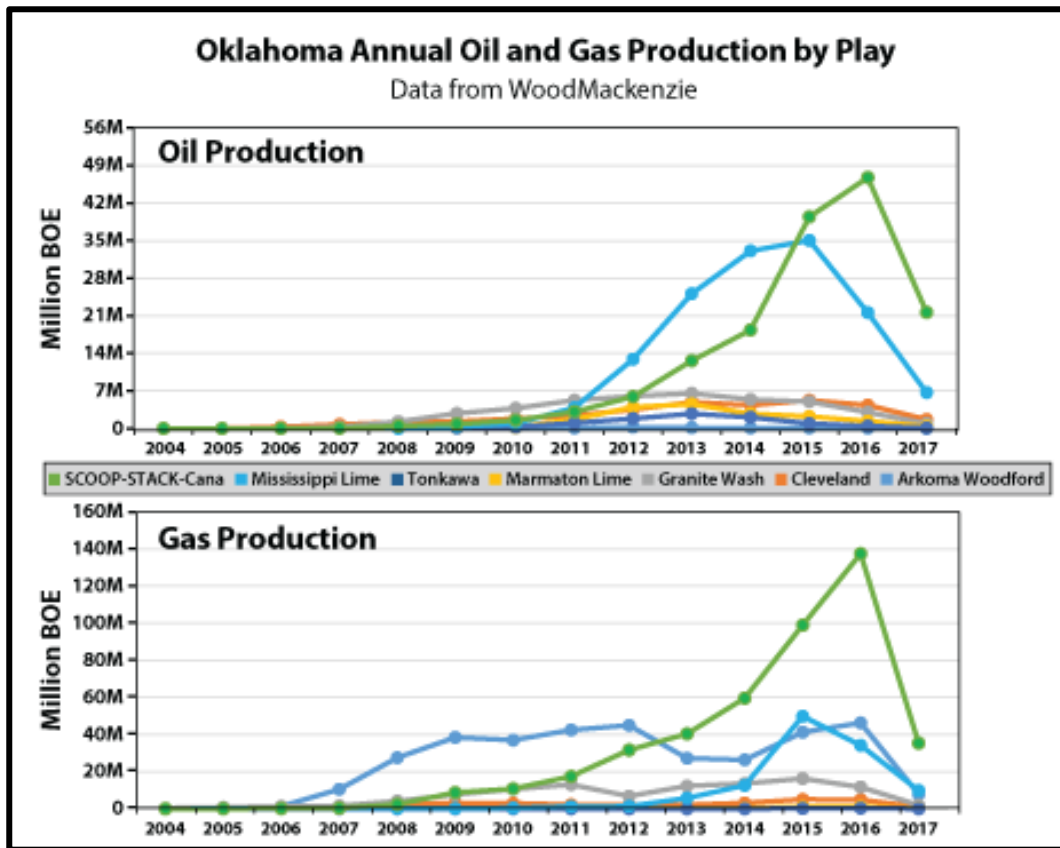
Figure 7: Oklahoma's annual production of oil and gas in barrel of oil equivalent (boe) from year 2004 through 2017. The data curves are colored by play name. Data from WoodMackenzie (2017).

Study Objective and Scope

The objective of this study is to understand the origin and migration history of petroleum reservoired in conventional and unconventional reservoirs of Devonian-Mississippian petroleum systems, in the Anadarko Basin. An important step in this research is to geochemically characterize the produced petroleum and correlate these fluid samples with source rocks from Devonian-Mississippian ages. Molecular geochemistry provides a tool to understand fluids sources, organic-matter maturity, depositional environment, and migration history. The characterization of Devonian-Mississippian mudrocks' kerogen is achieved by the identification of the organic-matter type that contributes to petroleum generation. Moreover, petroleum generation kinetics from organic-rich Mississippian carbonates is further investigated by means of hydrous pyrolysis techniques to simulate natural petroleum generation. Insight into petroleum migration is examined through microthermometry and organic geochemistry of oil-bearing fluid inclusions within Mississippian rocks. Additionally, the geochemical data of rock and fluids, together with measurements of petroleum generation kinetics, are integrated into basin and petroleum-systems modeling to shed light on major geological factors controlling petroleum migration, timing, and the types of hydrocarbons generated within the Devonian-Mississippian petroleum systems of the Anadarko Basin.

Study Motivation

Despite the great potential of reserves contained within Devonian-Mississippian reservoirs, the industry faces many unanswered questions whose answers could help improve the exploration and development of these reservoirs. Much of the research on Devonian-Mississippian petroleum

systems up to now has been essentially descriptive in nature, and lacking an integrated petroleum systems analysis approach.

Devonian-Mississippian unconventional targets remain attractive, even in light of the 2015 oil industry downturn. However, they can be unpredictable due to the unknown controls of the basin evolution on hydrocarbon composition and maturity, together with the variable distribution and thickness of source rock and reservoir depth throughout the Anadarko Basin. These regional variations make finding sweet-spot production areas very challenging although economically rewarding.

One of the challenges for this research is the unexplained variability in Anadarko Basin-produced fluids phase and composition from a single reservoir, the Mississippian Meramec (Figure.8). Gas-to-oil ratio (GOR) maps show regions with a predominance of condensate and dry
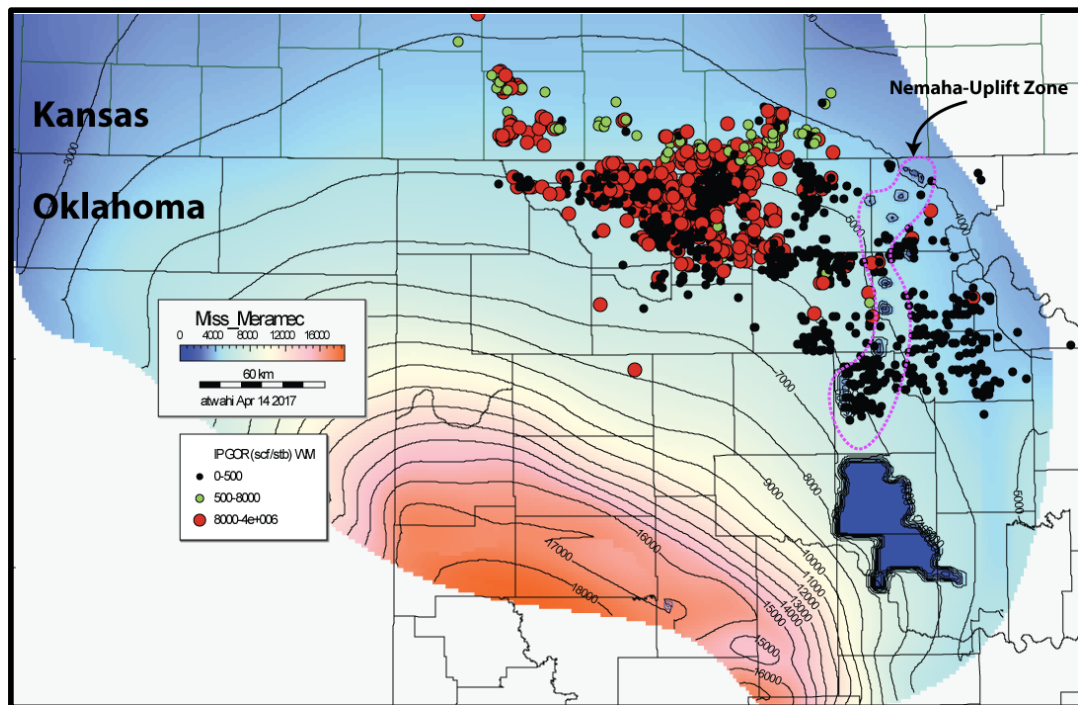
Figure 8: Structural top of the Mississippian Formation and colored circles represent gas-to-oil ratio (GOR) of hydrocarbons produced from all Mississippian reservoirs across northern Oklahoma. Note the variation in gas–oil ratios west of the Nemaha Uplift

12

gas, while in other areas fluid-type black oil dominates (e.g. east of the Nemaha Uplift). By the same token, the variability of fluids composition is widely observed in the STACK/SCOOP plays, for example, with crude oil showing a predominance of diamondoids (highly mature petroleum) over biomarkers in one region and the reverse concentration in another. All geochemical evidence reinforces the complexity of the Devonian-Mississippian petroleum systems and presents an opportunity to develop in-depth modeling and simulation analysis aiming to produce geologically reasonable scenarios compatible with the observed fluids' heterogeneity.

Significance

The significance of this research resides in providing a geologically thorough understanding of factors causing variability in produced hydrocarbon from Devonian-Mississippian targets, based on geochemical approaches combined with comprehensive literature review and petroleum-systems modeling. Geochemical data and analysis, when integrated with other geological and geophysical data, can significantly improve the forecasting efficiency of prospects prior to drilling, hence reducing exploratory geological risks (Murris., 1984; Peters and Fowler, 2002).

The basin modeling workflow adds value to the data generated in this study and to the data published in the literature by integrating them into a dynamic model through geological time, rather than being isolated datasets. The calibrated basin models can be used as an assessment tool for different estimated fluid and rock properties at a very low cost, prior to drilling a prospect or appraising reservoir continuity (Baur et al., 2018). Moreover, in unconventional source-rock reservoirs, petroleum geochemistry principles and applications can contribute significantly to thermal maturity assessment, together with organic-richness evaluation (Curiale and Curtis, 2016).

Geological Settings

Overview

Oklahoma state is situated in the southern part of the U.S. Midcontinent Region, featuring a number of complex geological structures including basins (i.e., Anadarko, Arkoma and Ardmore Basins) bounded by shallow broad shelf (i.e., Anadarko Shelf and Cherokee Platform) and uplifts (e.g., Nemaha, Wichita, Arbuckle Uplifts) (Figure 9). In this study, the emphasis is laid on the Anadarko Basin and Shelf, the Nemaha Uplift, and the Cherokee Platform areas. The Anadarko Basin is the deepest basin located within the cratonic interior of North America, bounded to the north by the Anadarko Shelf and Hugoton Embayment, to the east by the Nemaha Uplift and
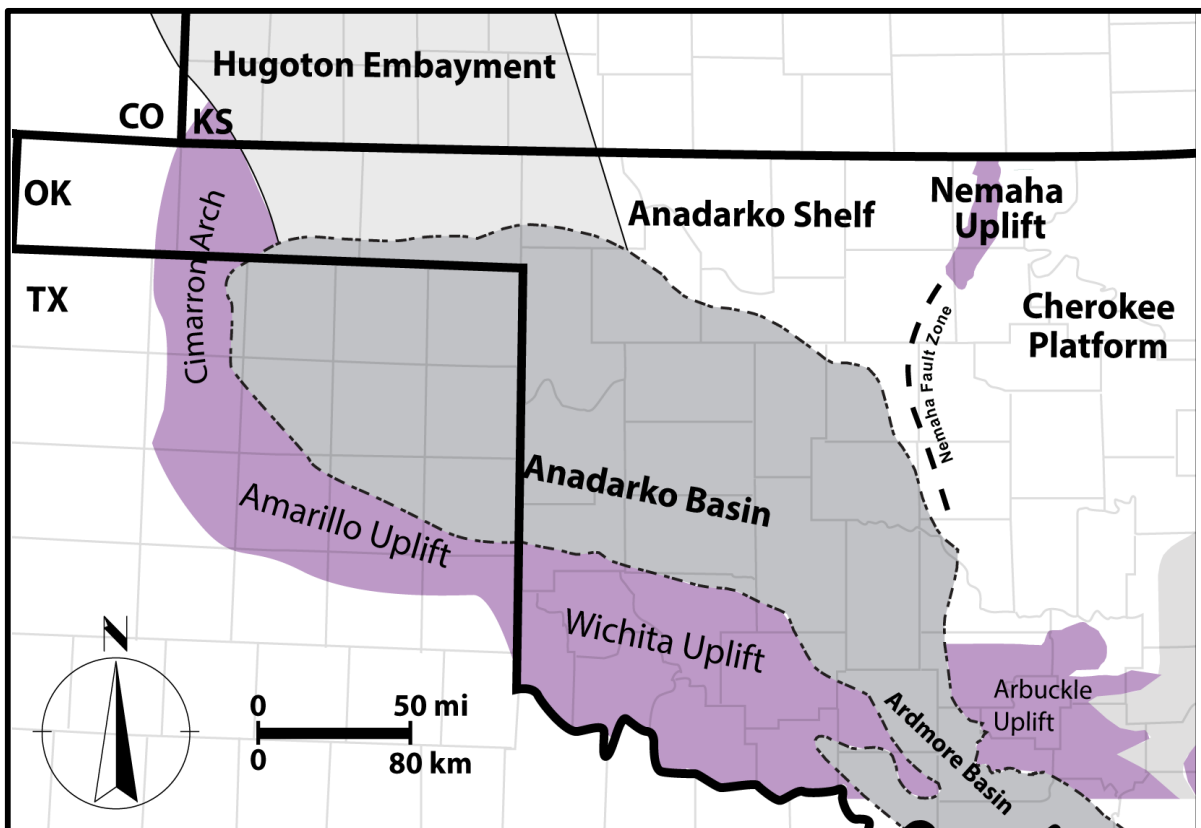
Figure 9: Map showing major geological provinces in close proximity to the Anadarko Basin. Modified from Johnson (1989b).

Cherokee Platform, to the south by the Wichita and Amarillo Uplifts, and to the west by Cimarron arch (Brewer et al., 1983; Ham et al., 1964; Johnson, 1989a). The Anadarko Basin and its broad shallow shelf are separated from the Cherokee Platform in the east of Oklahoma by the Nemaha Uplift (Figure 9).

Anadarko Basin Evolution

The Anadarko Basin in the present-day structural settings can be classified as foreland basin. However, over geological time, the Anadarko Basin is considered to be a polyhistory basin that initially started as aulacogen rifting (known as the Southern Oklahoma Aulacogen [SOA]), which developed into a cratonic basin and later into foreland basin (Gilbert, 1992). According to Johnson et al. (1989), the Anadarko Basin's evolution can be divided into four major episodes: a first-phase igneous episode during Precambrian to Middle Cambrian time; a second-phase epeirogenic episode during Cambrian through Mississippian time; a third-phase orogenic episode during Pennsylvanian time; and a final-phase epeirogenic episode from the Permian to the present day.

The failed arm of the triple junction known as the SOA marks the first episode in the Anadarko Basin's evolution, which took place during Precambrian to Middle Cambrian times (Gilbert, 1992). The SOA is believed to extend around 700 km northwest from the Ouachita fold-thrust belt of the Paleozoic continental margin into southwestern Oklahoma and northern Texas (Figure 10) (Ham et al., 1964). Moreover, it has been estimated that the SOA was situated in present-day northern portion of the Amarillo/Wichita Uplifts and the southern portion of the present-day Anadarko Basin. This estimation is evidenced from a Cambrian through Lower Ordovician isopach map indicating the depocenter of the southern Oklahoma trough, with a

thickness reaching 8000 ft in the depocenter (Figure 10) (Gatewood, 1979). The SOA is thought to have initially developed as a graben-like structure, with the rise of basaltic liquid forming layered complexes associated with the rift magmatism (Gilbert, 1983). The beginning of this rifting stage also caused the intrusive Glen Mountains Layered Complex, which is presently exposed about 3 miles southeast of Roosevelt town in Kiowa County, Oklahoma (Ham et al., 1964). Based on subsidence curves and thermal history evidence of the SOA, Feinstin (1981) postulates that continuing subsidence of the aulacogen trough by the means of initial elastic flexure was followed by detachment and differential subsidence due to thermally controlled isostatic subsidence
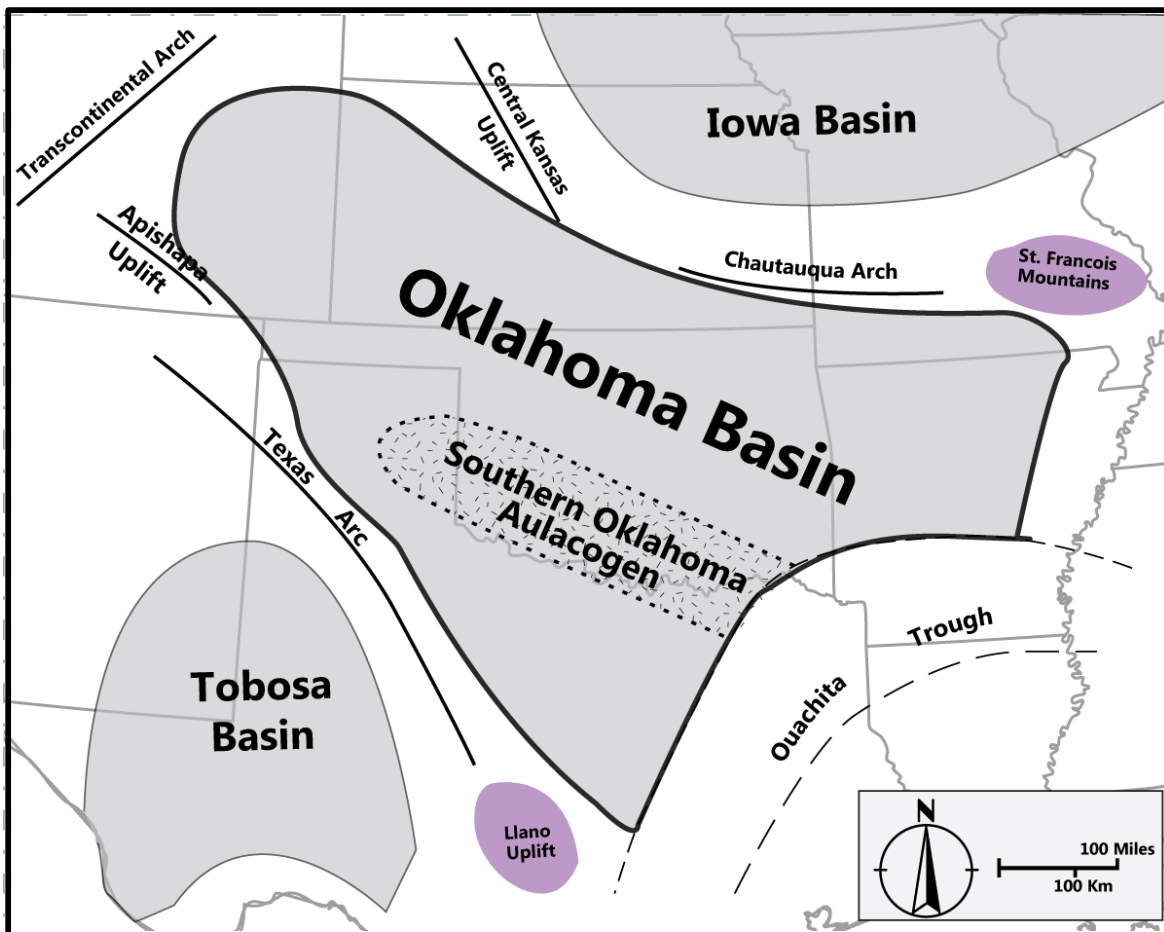
Figure 10: Map showing approximate boundaries of the Oklahoma Basin and the Southern Oklahoma Aulacogen (SOA) during early to middle Paleozoic time and prior to the development of the present-day Anadarko Basin. Modified from Johnson (1989b).

16

(Feinstein, 1981). These extrusive and intrusive igneous mafic rocks subsequently resulted in cooling and sinking of the continual crust, forming the proto-basin also known in the literature as the Oklahoma Basin and the Southern Oklahoma geosyncline (Ham et al., 1964; Ham and Wilson, 1967; Johnson, 1989a).

The development of the Oklahoma Basin across the epicontinental sea marks the second episode of the Anadarko Basin's evolution during the period from the Late Cambrian to Late Mississippian time (Johnson et al., 1988b). During this episode, a major shift in tectonic and depositional settings from an aulacogen and magmatic activity into passive-margin settings with marine sediments, ultimately resulting in cratonic basin settings. Moreover, the early phase of this episode is influenced by the slow subsidence rates of the Oklahoma Basin due to both passive margin settings, suggesting decreased tectonic activity and cooling associated with Cambrian crustal thinning and magmatic actives (Donovan, 1986; Feinstein, 1981; Garner and Turcotte, 1984). Particularly during the Silurian and Devonian period, subsidence rate was the slowest, with estimated total deposited sediment of one-half kilometer in thickness at the deepest part of the basin (Gilbert, 1992; McConnell, 1987). Notably, the subsidence rate of the basin rapidly increased significantly during Late Mississippian time. This phenomenon has been attributed tectonically to the onset of a subduction activity along the southern continental margin of the Ouachita plate (Donovan, 1986; Garner and Turcotte, 1984). More specifically, Garner and Turcotte (1984) proposed a thermomechanical model to explain accelerated isostatic subsidence during Late Mississippian time (Springer) by crustal and lithospheric thinning, which was accompanied by an increase in heat-flow. Ultimately, this subsidence resulted in the deposition of a thick marine carbonate formation interbedded with shales and sandstone with limited occurrence (Johnson et al., 1988b).

17

The third period of the Anadarko Basin's development is characterized by an orogenic episode during Late Mississippian to Pennsylvanian time (Johnson, 1989b; Perry, 1989). This phase marks the shift of a passive margin and cratonic basin to foreland basin settings This period of foreland deformation was additionally accompanied by intense crustal shortening, folding, uplifts and downwarping, ultimately disjointing the Oklahoma Basin into tectonic provinces comparable to present-day structural features (Ham et al., 1964; Johnson, 1989b). More specifically, during this period the Anadarko Basin started to develop into an asymmetric foreland basin. Structural events during the Late Carboniferous remain a topic of debate, with mainly two tectonic interpretations; one interpretation suggests the control of wrench-fault tectonics (Carter, 1982; Tanner, 1967), while the other interpretation emphasizes the role of compressional tectonics (Brewer et al., 1983; Brown, 1984; Dott, 1934; Peterson, 1983). Kluth (1986) further argues that both tectonic mechanisms took place; that is to say, both wrenching and compression stresses resulted in the formation of the Ouachita-Marathon orogeny, subsequently forming the Anadarko Basin and adjacent uplifts, such as the Arbuckle and Wichita Uplifts. From a plate-tectonic perspective, the mentioned orogenic deformation is believed to result from the collision of the
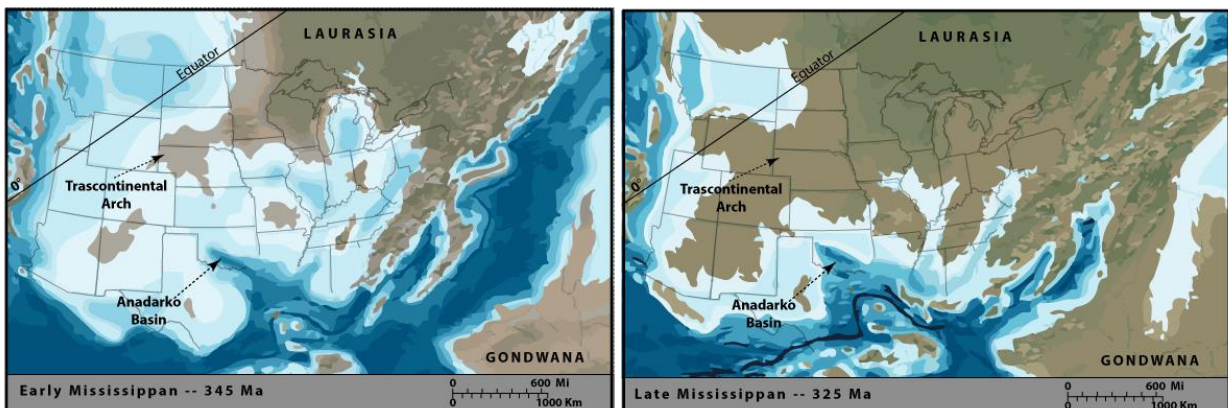
Figure 11: Paleogeography maps showing the transition from the second to the third phase of the Anadarko Basin evolution from epicontinental sea during early the Mississippian (left) to the orogenic events during the Late Mississippian to the Early Pennsylvanian (right), modified from (Blakey, 2011)

North American plate with South American plate, as well as the African plate to the east (Gondwana) (Figure 11) (Keller et al., 1983; Kluth, 1986; Ross, 1979). Moreover, this episode of the Anadarko Basin is crucial, as it marks the onset of petroleum generation and migration in Devonian-Mississippian petroleum systems (Al Atwah et al., 2018b; Higley, 2013). Further evidence from oil-bearing fluid inclusions and basin modeling are presented in Chapters VI and VII.

Lastly, the fourth episode of the Anadarko Basin evolution is an epeirogenic movement that started in the Permian time and has persisted to the present day (Johnson, 1989b). During this period, most of the dramatic tectonic activates have ceased, and hence slow subsidence rates are observed due to thermal subsidence, as the lithosphere reached thermal equilibrium (Garner and Turcotte, 1984). However, some aspects of the Permian subsidence remain enigmatic, as Gilbert (1992) noted: the Permian strata's thickest centerline does not coincide with the deepest part of the basin, which he speculated could be controlled by a crustal sinking in the northern part of the basin (Gilbert, 1992). Nevertheless, the Anadarko Basin during this phase reached its maximum burial depth around Middle to Late Cretaceous time (Carter et al., 1998; Gilbert, 1992; Higley, 2013). It is important to note the influence of the Western Interior Seaway and the associated Laramide orogeny on the Anadarko Basin. The scarcity of Cretaceous rocks is observed in the Anadarko Province, so exhumation and erosion of Cretaceous rocks are inferred, also resulting in a subtle eastward tilt in the basin caused by the Laramide orogeny (Adler, 1971; Johnson et al., 1988b). Additionally, localized and mild tectonic activity has also been observed during the Quaternary period within the southern part of the Anadarko Basin (Crone and Luza, 1990; Donovan et al., 1983).

The Anadarko Basin contains thick Paleozoic sedimentary rocks, reaching up to 40,000ft in thickness at the deepest portion (Adler, 1971; Ham et al., 1964; Johnson, 1989b). Figure 12 shows a cross-section of the Anadarko Basin depicting the asymmetrical shape of the basin with its depocenter situated in the south. The thickness of deposited sedimentary sequences is thought to be primarily controlled by an underlain basement rock type (Ham et al., 1964). In general, sediments tend to be thicker in areas where the overlay Middle Cambrian basement rocks are associated with the aulacogen (Ham et al., 1964; Ham and Wilson, 1967). Figure 13 shows a generalized stratigraphic column of the Anadarko Basin, its petroleum systems and major source rocks. In the following paragraphs, each major stratigraphic subdivision will be discussed, emphasizing Devonian-Mississippian formations

Anadarko Province's Basement rocks can be categorized into two rock types, according to their ages. The first type is a Precambrian basement rock composed of massive granites and believed to be part of the North American craton. The second type is the Early-to-Middle Cambrian basement rock composed of a mixture of sediments (i.e., greywacke, chert) and intrusive igneous rocks (i.e., spilite, gabbro, anorthosite, and rhyolite) (Ham et al., 1964). The latter corresponds to a thick sedimentary cover, which marks the first stages of the SOA that ultimately evolved into the Anadarko Basin depocenter (Feinstein, 1981; Gilbert, 1992). The thickness of these later basement rocks as observed within the Wichita Uplift is around 20,000ft, however, under the Anadarko Basin, it remains unknown, with an estimated thickness range from 5,000 to 20,000ft (Ham et al., 1964; Johnson, 1989b).

Cambrian through Mississippian sedimentary rocks are primarily shallow-water carbonates interbedded with shale and clastic sediments. Overlaying basement is a transgressive sand facies of the Regan Sandstone Formation, which grades into the Cambrian Arbuckle Formation. The Arbuckle Formation marks the shift in depositional from the SOA to passive margin with epeirogenic setting of the Oklahoma Basin (Ham et al., 1964; Johnson, 1989b). In terms of lithology, the Arbuckle is primarily limestone with secondary dolomite, and the formation is dated as Late Cambrian to Early Ordovician (Figure 13) (Donovan, 1986). The Arbuckle Group features
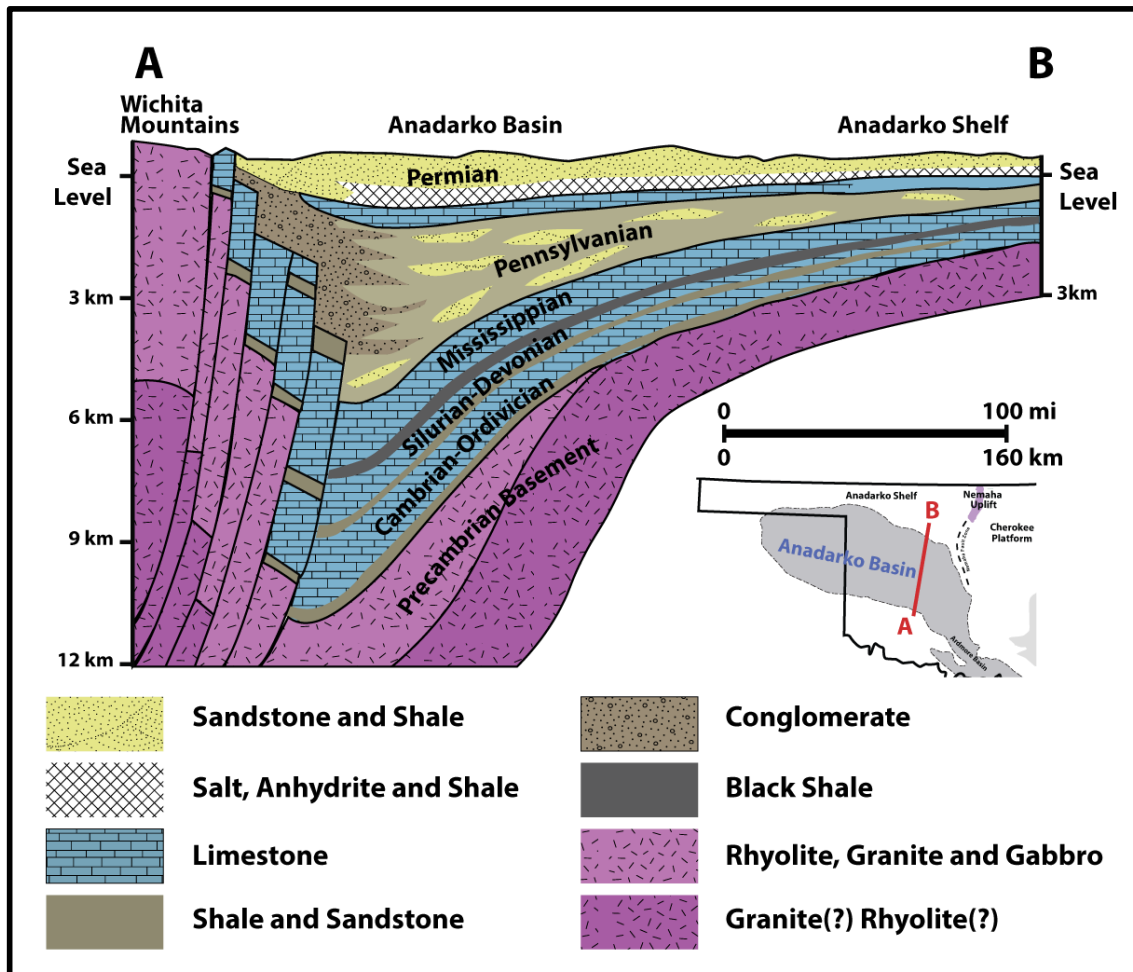
Figure 12: Schematic South–North cross-section of the Anadarko Basin and Anadarko Shelf. Note the asymmetrical architecture of the basin with the depocenter towards the southern portion of the basin, modified from (Johnson, 1989a).

System	Lithostratigraphic Unit		Source Rock Potential	Petroleum Systems
	Sandstone (legend)			
	Limestone			
	Organic-rich Shale			
	Shale			
	Glauconitic Sandstone			
Permian	**Summer Gp.; Enid Gp.; Hennessy Gp.**			
	Chase Group / Council Grove Group / Admire Group	**Pontotoc Group**		
Pennsylvanian	Wabaunsee Group / Shawnee Group	**Ada Group**		
	Douglas Group			
	Lasing Group	**Hoxbar Group**		Penn. Petroleum System
	Cherokee Group	**Deese Group**	Fair	
	Atoka Gp.; Thirteen Finger limestone		Fair-Good	
	Morrow Formation		Fair-Good	
Mississippian	**Springer Formation** Chester Group	(Miss Chat)		
	Meramec lime	**Mayes Group**	Good	Miss-Devonian Petroleum Systems
	Osage lime	**Caney Shale**		
	Kinderhook Shale		Very Good	
Devonian	**Woodford Shale**		Excellent	
	Misener Sand			
Silurian	**Hunton Group**			
Ordovician	**Sylvan Shale**			
	Viola Group/Formation		Fair-Good	Ordovician Petroleum System
	Simpson Group			
Cambrian	**Arbuckle Group**		Possible?	Cambrian Petroleum System

Figure 13: Generalized stratigraphic column of the Anadarko Basin showing the major formations' lithology, source rock potential and major petroleum systems by age.

enhanced porosity of different types, making it a primary target for reinjection of disposable water produced during hydraulic fracturing as part of unconventional source rock stimulation (Keranen et al., 2014). Arbuckle Group thickness can reach more than 6,000ft in the depocenter and thins gradually towards the northern shelf, and the Hugoton Embayment (Johnson et al., 1988b). Source rock potential within the Arbuckle Group has been suggested in the literature; more specifically, the lower shale member of the Oil Creek Formation has shown fair petroleum-generation potential, evaluated using Rock-Eval pyrolysis data (Curtiss and Wavrek, 1997). The Ordovician Simpson Group overlays the Arbuckle Group (Figure 13). In general, the Simpson Group is composed of a combination of approximately equal thicknesses of sandstone, shale and carbonates (Statler, 1965). The sandstone is indicative of high-energy environments with subangular to well-rounded grains, with well-sorted and clean quartzose, while the Simpsons Group carbonates range from fine-grained dense limestone to oolitic and fragmental limestones. Simpson's shales are clay-rich mostly in illite, with their color ranging from green to gray (Statler, 1965). Late Ordovician strata include Viola carbonate and Sylvian Shale, both of which overlay the Simpson Group (Figure 13). The Viola Formation is composed of different carbonate facies encompassing wackestone and packstone deposited within the deeper section of the SOA, which transition into high-energy facies moving upward north to the craton, which includes well-washed, cross-bedded crinoidal and grainstone (Amati and Westrop, 2006). Interestingly, fauna diversity during the deposition of the Viola Formation was high in the shallow platform and low within the depocenter of the aulacogen (Amati and Westrop, 2006). The Late Ordovician (Ashgillian age) Sylvian Shale is a distinctive lithological marker because it is situated between two carbonate formations: the Viola Formation on the bottom and the Hunton Formation on the top. The Sylvian Shale is fissile graptolitic brown to green shale transitioning upward into clay-enriched facies (Jenkins, 1970). Sylvian Shale

thickness is nonuniformly distributed, with a thickness of approximately 100 ft and thickening towards the depocenter reaching 400 ft, but anomalies of 700 ft thickness have also been reported (Amsden, 1975). Like the Sylvian Shale, the Hunton Group has an easily distinguishable marker in the subsurface, with a distinctive well-log response, being a carbonate rock underlain by Sylvian Shale and overlain by the Woodford Shale (Figure 13). The Hunton Group extends in age from Late Ordovician to Early Devonian, as evidenced from brachiopod assemblage zones (Shannon Jr, 1962). The Hunton Group consists of a number of formations, including ones at the base of the skeletal limestones and dolomite of the Chimney-hill Formation, overlain by dolomite and argillaceous and silty limestones of the Henryhouse and Bois d'Arc Limestone Formations. At the top of the Hunton is the skeletal packstone and grainstone of the Frisco Limestone (Al Shaieb and Puckette, 2002; Gaswirth and Higley, 2013). Hunton Group thickness ranges between approximately 1600 ft, in the deeper part of the Anadarko Basin, to 100 ft, as observed from the fault blocks bordering the Wichita Uplift (Amsden, 1975). The deposition of the Hunton Group was interrupted by epeirogenic uplifts, which resulted in localized unconformities during the Early Devonian (pre-Frisco) and Late Devonian (pre-Woodford) (Amsden, 1975). The latter is accompanied by the deposition of the Misener Sandstone Formation, which deposited over channelized surface in north-central Oklahoma, composed of sandy dolomite and dolomitic sandstones with a thickness not exceeding 20 ft (Figure 13) (Amsden and Klapper, 1972).

The Misener Sandstone grades into the Late Devonian organic-rich Woodford Shale. Deposition of the Misener and Woodford Shale mark a shift to the first episode of clastic deposition, compared to Early Paleozoic carbonate depositional systems (Ham and Wilson, 1967). The Woodford Shale is characterized by highly radioactive, low-density, high resistivity well-log response (Kirkland et al., 1992). The thickness of the Late Devonian Woodford Shale reaches a

maximum thickness (600 ft) aligning with the depocenter, which is located in the southern part of the Anadarko Basin (Comer, 1992). The thickness gradually thins towards the Anadarko Shelf in the north and northwest, reaching a thickness of 50 ft; similarly, within the Nemaha Uplift area the Woodford thickness is around 50 ft or is completely eroded (Comer, 1992). The Woodford Shale is an extensively studied formation due to its economic significance as a prolific source rock and unconventional target (Cardott, 1989; Cardott et al., 2015; Jacobi et al., 2009; Miceli Romero and Philp, 2012; Quan et al., 2013). Moreover, the exposure of the Woodford Shale at McAlester Cemetery Quarry provides a unique opportunity to study and characterize the Woodford Shale. Stratigraphically, the Woodford Shale is informally subdivided into three members: upper, middle and lower, each exhibiting a distinctive well-log response, palynomorphs, geochemistry, kerogen content and sequence stratigraphy interpretation (Figure 14) (Hester et al., 1990; Kirkland et al., 1992; Romero and Philp, 2012; Sullivan, 1985; Turner et al., 2015). Upper Woodford member is dominantly black to dark-gray laminated siliceous mudrock with some localized occurrence of phosphate nodules (Turner et al., 2015), composed of carbonate apatite, primarily calcium phosphate ($Ca_5(PO_4, CO_3)_3$) (Kirkland et al., 1992). Moreover, the nodules range in size from 1.2 cm to 7.6 cm occurring parallel to bedding with spherical to slightly flattened structures (Kirkland et al., 1992). As an unconventional reservoir, the presence of phosphate nodules within the Upper Woodford interval is postulated to enhance storage capacity and brittleness, providing a sweet-spot zone within the Woodford Shale (Puckette et al., 2013).

Black to gray siliceous laminated mudrock comprises the dominant lithofacies of the Woodford's Middle member, with limited occurrence of mixed siliceous-argillaceous mudrock together with massive siliceous mudrock, with highest clay minerals (as observed from enrichment

in clay proxies including potassium and aluminum) and organic-richness deposited during anoxic conditions (Figure 14) (Romero and Philp, 2012; Turner et al., 2015).

Lithofacies of the Lower Woodford member is primarily siliceous laminated and mixed siliceous and argillaceous mudrock (Figure 14) (Turner et al., 2015). The presence of the Lower member is not as uniformly preserved, due to deposition interruption during pre-Late Devonian (pre-Woodford) resulting from epeirogenic uplifts, especially in north-center Oklahoma along the Nemaha Uplift region (Amsden, 1975; Johnson, 1989a). The Lower Woodford member deposition is recorded in close proximity to the paleoshoreline, as evidenced from a number of microfossil
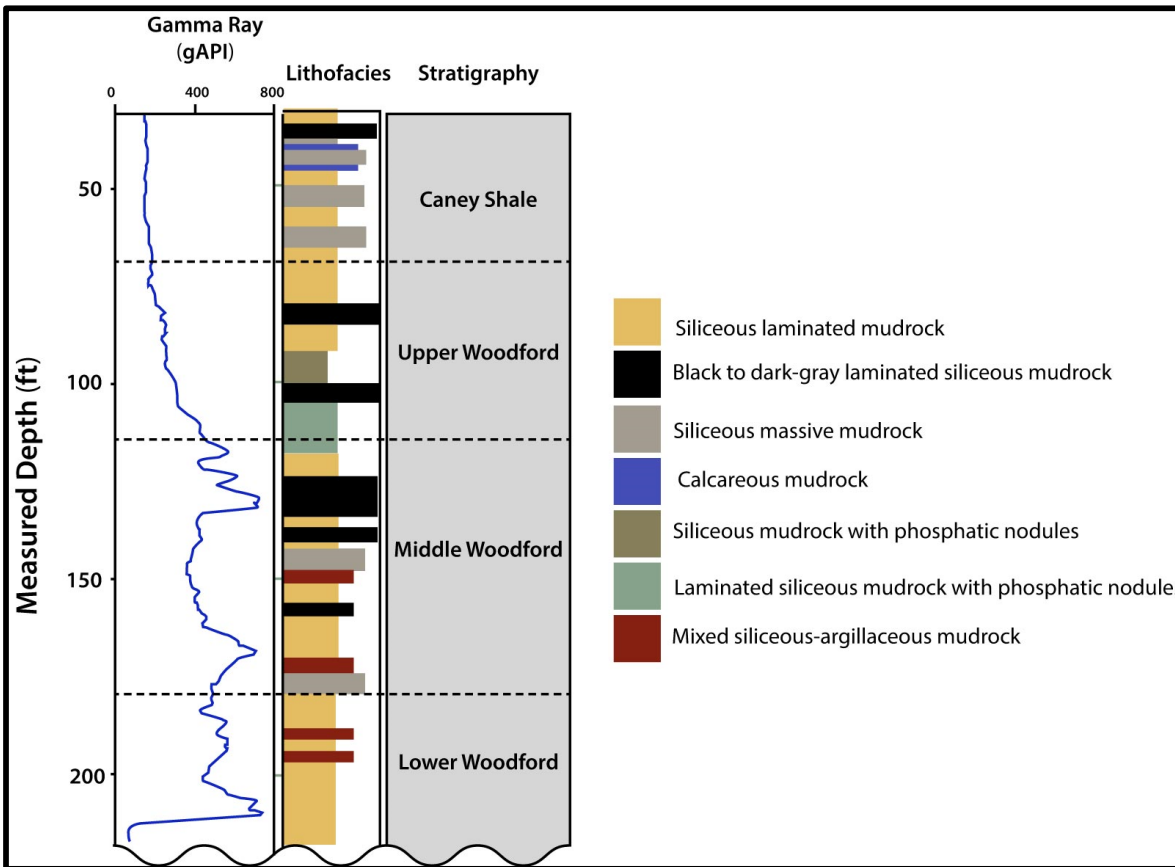
Figure 14: Generalized stratigraphic column and core lithofacies of the Woodford Shale from the Wyche-Farm-1 core located at Wyche shale pit, Pontotoc County, Oklahoma. Diagram is modified from (Buckner et al., 2009; Turner et al., 2015).

assemblages, together with the presence vitrinite macerals suggesting terrigenous organic-matter input (Cardott, 2012; Turner et al., 2015). Overall, the mineralogy of the Woodford Shale is rich in quartz (30–40% by weight) and illite-smectite (30–50% by weight), and to a lesser extent of orthoclase (7–16% by weight), kaolinite (1–7% by weight) and pyrite (3–12% by weight).

Thick and regionally widespread Mississippian carbonates strata overlaying the Woodford Shale extend over the Anadarko Basin and Shelf, Cherokee Platform, Arkoma Basin and the southern portion of Kansas. As with the Woodford, the thickest zone of the Mississippian carbonate is present along the Anadarko depocenter, with a thickness reaching 14,000ft (Johnson et al., 1988b). In general, the Mississippian strata is subdivided into four main geological-time stages ranging from base to top: the Kinderhookian, Osagean, Meramecian and Chesterian Series

	Series	Anadarko Basin	Hugoton Embayment	Cherokee Platform
Mississippian		Springer Fm		
	Chesterian	Chester Group	Chester Group	Mayes Group
	Meramecian	"Meramec Lime"		
	Osagean		"Mississippian Lime"	Boone Group
		"Osage Lime"		St. Joe Group
	Kinderhookian	Kinderhookian Shale		

Figure 15: Generalized stratigraphic column and associated Formation and Group nomenclature of Mississippian age in Anadarko Basin, Hugton Embayment (Anadarko Shelf) and Cherokee Platform, modified from (Johnson et al., 1988b).

(Figure 15) (Huffman, 1955). The Kinderhookian Series is primarily composed of thin silt to sand grains with glauconitic sandstone, dark-gray limestone and gritty shale (Braun, 1961a). Informally, that formation sometimes is referred to as Kinderhookian shale, pre-Sycamore shale or the Welden Formation (Figure 13) (Braun, 1961a). Osagean through Meramecian Series consist of heterogeneous carbonate facies that can have dramatic lateral change in lithofacies within a single formation, creating a series of clinoforms with deep-water muddier facies towards the depocenter and shallower-weathered carbonates at the shallower shelf, typifying a gently sloped carbonate-ramp depositional environment (Grammer, 2017; Johnson et al., 1988b; Rogers, 2001; S. J. Mazzullo, 2017). Lithologically, they can range from medium gray wackestone to packstone, sometimes with fractured intervals with healed or open fractures. Additionally, there is burrowed wackestone associated with thin organic-rich micritic black shale, potentially representing a flooding event. Overall, those limestone sections usually alternate between laminated, cross-bedded and burrowed sections, with the latter being more prevalent. Osagean and Meramecian rocks are usually referred to by operators as "Osage Limestone," Meramec Limestone," "Sycamore Limestone" and "Mays Group" formations. Moreover, the weathered facies of the top Osagean, informally known as "Miss Chat," is composed of cherty limestones with the initial rock fabric being skeletal grainstone that has been replaced by silica-forming chert clasts occurring as angular discolored typifying small-scale debris flow texture (Rogers, 2001). Moreover, Caney Shale is a key formation of Upper Meramecian, characterized by black, bituminous fissile shale with spherical calcareous bedrock with intervals with rich-clay content, occurring within the Arkoma Basin Province known for its shale-gas production (Elias and Branson, 1959; Maughan and Deming, 2006).

The top of the Mississippian strata is the Chesterian Series which in general encompasses the Chester Group and the Springer Formation. The Chester Group consists of limestone rocks, while the Springer Formation consists of tight shales over the deepest areas in the Anadarko Basin, grading into sandstone over the Anadarko Shelf (Adler, 1971). The Springer sandstone and shale record the transition of between Late Mississippian into the Early Pennsylvanian age strata.

For the purposes of this research, the overburden units include Pennsylvanian to Permian formations of primarily marine clastic depositional systems. The Anadarko Basin has received as much as 18,000 ft. of Pennsylvanian sediments, with dominantly sandstones and some carbonates, shale, conglomerates, and coal beds (McKee et al., 1975). The Morrow Formation, which includes sandstone, shales, and limestones, overlays the Springer Formation and marks the contact between Mississippian and Pennsylvanian sediments (Johnson, 1989b). Remarkably, the upper part of Morrow Formation switches into a deltaic sedimentary sequence with sandstones, conglomerates, coals and dark-limestones (Puckette et al., 1996; Swanson, 1979). Overlying the Morrow is the Atoka Group of marine shales, sandstones, and limestones, known as the "thirteen finger limestone." Towards the western edge of the Anadarko Basin and Texas Panhandle, the Atokan lithology abruptly changes to a massive granite wash mixed with clastic deposits with carbonate-rock fragments. This granite wash unit is one of the productive hydrocarbon plays in Oklahoma and Texas (Cunningham, 1961a; Mitchell, 2011).

Desmoinesian Series strata overlay the Atokan Group and include marine carbonates and shales of the Cherokee and Marmaton Groups. Late Pennsylvanian rocks consist of Missourian and Virgilian Series, composed by marine-carbonate interbred with shales with a lateral southeast facies shift into sandstone-shale sequences, while the granite wash persisted through those strata (Figure 12) (Johnson, 1989a).

Permian rock overlays the Virgilian Series, including the Wolfcampian and Leonardian Series, with dominant lithology of carbonates, red beds and evaporites (Johnson, 1989a). Post-Permian strata are encountered in very localized occurrences, mainly on the western region of the Anadarko Basin and Texas Panhandle. Those include the remnants of Triassic, Jurassic, Cretaceous, Tertiary and Quaternary rocks; a mix of fluvial, deltaic and lacustrine depositional systems results in a dominant lithology of red-bed sandstones and shales (Cunningham, 1961a). Post-Permian strata are believed to have extended regionally over the Anadarko Basin, but were subsequently eroded (Johnson, 1989a).

The eroded strata of the Post-Permian has been estimated by a number of studies investigating the Anadarko Basin burial history. The erosion of Post-Permian formations is inferred from the presence of those rocks on the western edge of the Anadarko Basin (Cunningham, 1961a). Additionally, paleo-thermal gradients estimated from the reflectance of vitrinite maceral suggest that the Anadarko Basin strata were buried deeper than the present-day depths, as the current geothermal gradient is inconsistent with measured reflectance values (Cardott and Lambert, 1985). However, varying estimates of eroded thickness are reported in the literature and, hence, varying periods when the Anadarko Basin reached maximum burial (Cardott and Lambert, 1985; Harrison et al., 1987; Pawlewicz, 1866; Schmoker, 1986; Waples, 1980). The estimated exhumed section ranges from 2,600ft to 6,550ft of Post-Permian deposits (Harrison et al., 1987; Schmoker, 1986). This aspect of the Anadarko Basin uplift and erosions is further discussed in Chapter VII.

The Anadarko Basin features a number of mature source rock deposits spanning in age from Cambrian to Pennsylvanian, each of which bears a unique geochemical fingerprint. Molecular, isotopic and bulk geochemical signatures provide a tool to determine the contribution of these source rocks. A summary is presented in Table 1 of the major petroleum systems in Oklahoma.

Oil production from the oldest source rock observed in the basin, the Cambrian Arbuckle Group within Oklahoma and Kansas, dates back to 1912; the production output was light crudes 38° API, as well as black oils enriched in hydrogen-sulfides (Brown and Swetland, 1992; Gatewood, 1992; Webb, 1976). Organic-richness within the Arbuckle carbonate is also observed, indicating fair generation potential with total organic carbon (TOC weight percentage) ranging from 0.8–1.1% (Gatewood, 1992; Webb, 1976). While those studies showed the generation potential of the Arbuckle Group, oil to source-rock correlation evidence is needed to confirm that the Arbuckle rocks are an active petroleum system.

Ordovician source rocks of the Simpson Group has been postulated in the Anadarko Basin, and similarly in the West Texas Permian Basin (Burruss and Hatch, 1989a; Hatch, 1986; Katz et al., 1994). Moreover, Ordovician source rock is present at the Oil- Creek Formation, of lower Ordovician age, at Major County, Oklahoma. The Rock-Eval parameter indicates the presence of fair source-rock potential within the Oil Creek Formation, with TOC ranging from 0.47–2.42%, and averaging at 1.2 wt% in the northern part of the Ames structure, Oklahoma (Curtiss and Wavrek, 1997). Additionally, Ordovician oil geochemistry exhibits odd over even predominance of n-alkane hydrocarbons, with trace amounts of acyclic isoprenoids, together with enrichment in diasteranes relative to regular-sterane biomarkers, and most notably positive excursion stable

carbon isotopes of both the saturate (δ13C = −24.9‰ to −33.9‰) and aromatic (δ13C= −24.3‰ to −33.7‰) hydrocarbons (Burruss and Hatch, 1989a; Hatch et al., 1987; Hatch, 1986; Longman and Palmer, 1987) (Table 1). Furthermore, Ordovician kerogen is known to be rich in *Gloeocapsamorpha prisca (G.prisca)*, so generated oils of Ordovician kerogen bear a similar signature to that of *G.prisca* enrichment (Foster, 1989, 1990; Reed et al., 1986). However, the presence of the G.prisca biomarker has not been observed from oils produced from Oklahoma, which could imply a different type of kerogen of Ordovician age, with possibly marine prokaryotic organisms (Curiale, 1992; Longman and Palmer, 1987).

Late Ordovician source rocks within the Anadarko include both Viola carbonate and Sylvan Shale. Viola carbonate source rock has been reported to have as high as 7.0% TOC and 720 (mgHC/g TOC) on the hydrogen index (HI) from samples collected from the Arbuckle Mountains, Oklahoma (Brown and Sentfle, 1997). Examination of extracted bitumen and crude oils from the Viola Formation exhibit the presence of microbial biomarkers such as drimanes, hopanes, and methylhopanes (Wang and Philp, 1997b). On the other hand, the petroleum generation potential of the Sylvan Shale is low due to lack of organic matter and due to the low thickness of those shales (Wang and Philp, 1997a). Late Ordovician source rocks have only been reported in the southeastern part of the Anadarko Basin and within the Ardmore Basin (Wang and Philp, 1997a; Wavrek et al., 1997) (Table 1).

Devonian-Mississippian source rocks are the most organically rich and, volumetrically, have accounted for the majority of the produced hydrocarbon within the Anadarko Basin (Figure 7). The Woodford Shale is a world-class source rock with an exceptional regional and stratigraphic presence and economic significance. The organic richness of Woodford Shale ranges from 6–17% TOC, with an HI reaching 797 mgHC/g TOC in thermally immature samples (Figure 16) (Kirkland

32

et al., 1992; Romero and Philp, 2012). The TOC distribution of the Woodford Shale as derived from 123 wells suggests an overall trend of increasing TOC towards the east, particularly east of the Nemaha Uplift. However, kerogen conversion due to maturation and retained hydrocarbons can affect TOC distribution, so this map should be used in conjunction with maturity maps (Hester et al., 1990). Petrographic examination of the Woodford kerogen suggests that its dominanted by Type-II marine organic matter, which in some instances will plot within Type I using the pseudo-Van Krevelen diagram due to *Tasmanites* enrichment (Al Atwah et al., 2019). Moreover, examination of the Woodford palynomorphs encountered different species of acritarchs, pollen, spores, and *Tasmanites* (Turner et al., 2015). The geochemistry of Woodford Shale oils and rock extracts share unique signatures, most notably is the predominance of C_{29} regular sterane over its C_{28} and C_{27} counterparts (Jones and Philp, 1990; Romero and Philp, 2012). Moreover, the Woodford Shale exhibits the presence of C_{40} aromatic carotenoids, including paleorenieratane,
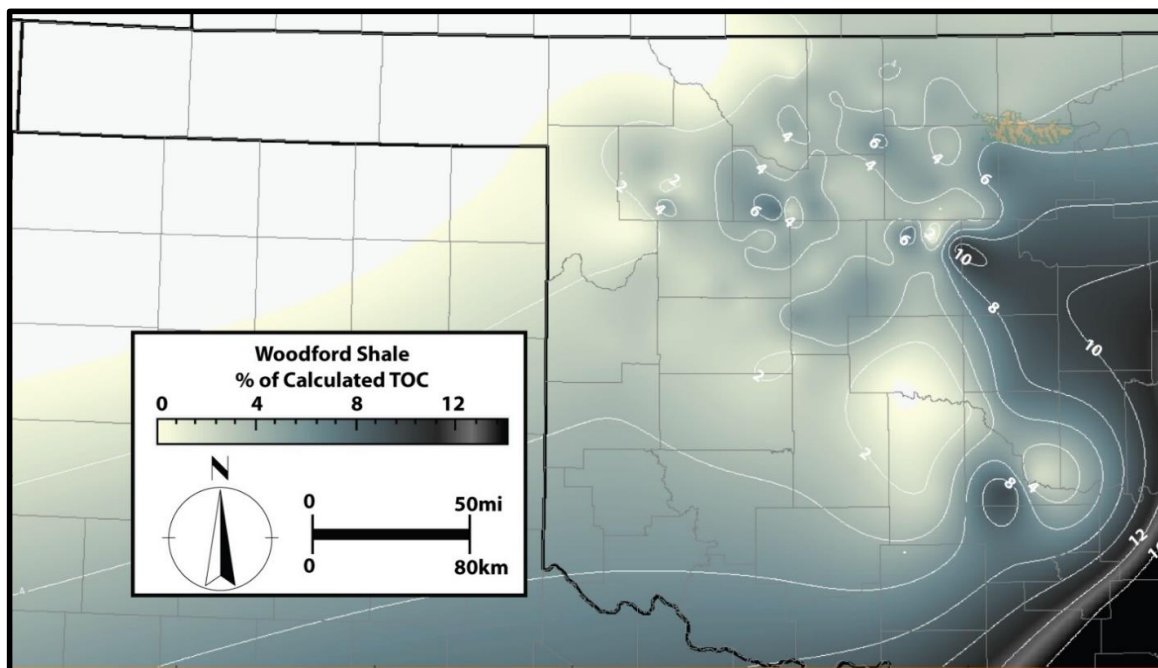
Figure 16: Total organic carbon (TOC) of the Woodford Shale derived from well-log and calibrated to measured TOC values. Map recreated using data sets from (Higley, 2014b).

isorenieratane, renieratane, and renierapurpurane which is believed to be indicative of photic-zone

euxinia (PZE) (Connock et al., 2018). Isotopically, the Woodford oil exhibits a $\delta^{13}C$ value of -

30.0‰ for both, saturate and aromatic hydrocarbon fractions (Wang and Philp, 1997a)(Table 1).

Table 1 Oklahoma's major petroleum systems and associated geochemical fingerprint. Data summarized from (Al Atwah et al., 2017b; Burruss and Hatch, 1989a; Hatch, 1986; Wang and Philp, 1997a; Wavrek, 1992; Wavrek et al., 1997).

Petroleum System age	Extent	Biomarker Character	Isotopic Signature
Cambrian (Arbuckle?)	Southeastern Anadarko, Major County, and Ardmore Basin	Odd over even predominance of n-alkane, enrichment in diasteranes relative to regular-sterane	saturate ($\delta 13C$ = - 24.9 ‰ to- 33.9 ‰) and aromatic($\delta 13C$= - 24.3 ‰ to - 33.7 ‰)
Ordovician (Viola)	Southeastern Anadarko, Ardmore and Marietta Basins	Moderate odd carbon preference in the range of nC_{11}-nC_{20} Drimanes, hopanes, and methylhopanes	saturate ($\delta 13C$ = - 31.3 ‰) and aromatic($\delta 13C$= - 30.9 ‰)
Devonian (Woodford)	Anadarko, Arkoma and Ardmore Basins	Predominance of C29 regular sterane over C28 and C27	saturate ($\delta 13C$ = - 30.0 ‰) and aromatic($\delta 13C$= - 30.0 ‰)
Mississippian	Eastern Anadarko Basin, and Cherokee Platform, Arkoma Basin	Predominance of C27 regular sterane over C29 and C28 Extended tricyclic terpanes reaching up to C_{45}	saturate ($\delta 13C$ = - 31.0 ‰) and aromatic($\delta 13C$= - 30.5.0 ‰)
Pennsylvanian	Anadarko Basin	Moderate abundance of isoprenoids, relative abundance of diahopanes and neohopanes	Saturate ($\delta 13C$ = - 30.8 ‰) and aromatic ($\delta 13C$= - 30.3. ‰)

In addition to the Woodford Shale, Mississippian mudrocks are source rocks, such as Osage

and Meramec carbonates together with Caney Shale formations. Mississippian petroleum source

rocks have been investigated and showed potential for hydrocarbon generation, containing kerogen

of Type II and 6% average TOC (Wang and Philp, 1997a). However, the source-rock geochemistry and macerals of Mississippian source rocks remain poorly understood, partly because Mississippian rocks are usually thought of as a reservoir rock rather than as a source for hydrocarbon (Harris, 1975b). Further details about biomarkers and macerals within Mississippian source rocks and produced hydrocarbons are discussed in Chapters IV and V, with a close comparison to Woodford Shale and associated oils (Table 1).

The youngest petroleum source rocks within the Anadarko Basin are Late Mississippian Early Pennsylvanian in age, including black shales of Springer Formation and Morrow Group. Since a clear shift to the siliciclastic depositional system during Pennsylvanian, it has been suggested that kerogen of Springer Formation and Morrow Group contains primarily Type III with significant oil and gas generation potential Organic richness is fair in the Pennsylvanian source rocks, reaching up to 5% TOC, with an HI averaging at around 100 mg HC/g TOC (Wang and Philp, 1997a). Produced crude oil from Pennsylvanian reservoirs tends to show a mixture signature of Woodford contribution; however, some Pennsylvanian oil exhibits a unique signature indigenous to Pennsylvanian source rocks. These signatures include a moderate abundance of isoprenoids, and the dominance of diasteranes relative to regular steranes, along with a relative abundance of diahopane and neohopane biomarkers, whereas isotopically, the $\delta13C$ value for saturated hydrocarbons is −30.8‰, with −30.3‰ for the aromatic hydrocarbons (Wang and Philp, 1997a; Wavrek, 1992). (Burruss and Hatch, 1989a; Hatch, 1986; Wang and Philp, 1997a; Wavrek, 1992; Wavrek et al., 1997)

The Nemaha Uplift (also known as Nemaha Ridge) is a prominent structural feature that extends from the southeastern part of Nebraska through Kansas, with its southern edge ending in central Oklahoma, adjacent to Oklahoma City (Figure 9). In dimensions, the uplift is a little over 80 miles wide and 500 miles in length, with a total of the area of approximately 17 000 square miles (Dolton and Finn, 1989). In Oklahoma, the Nemaha Uplift isolates the Anadarko Basin and Shelf from the Cherokee Platform and the Arkoma Basin. The Nemaha Province is a productive region of oil with minor production of gas.

The Nemaha Uplift is considered a complex structural system associated with a number of different fault types, including normal, reverse and strike-slip faults (Berendsen and Blair, 1995; Dolton and Finn, 1989; Gay Jr, 1999b, 2003a). Figure 17 shows the detailed pattern of the Nemaha Uplift faults system, after Gay (2003).

Due to its complexity, the mechanism and origin controlling the Nemaha fault system have been debated, and different interpretations have been offered. The discussion over the Nemaha fault system regards whether it originates from compressional, extensional or strike-slip stresses. According to Luza and Lawson (1983), Nemaha Ridge consists of a series of crustal blocks of 3 to 5 miles (5 to 8 km) wide and 5 to 20 miles (8 to 32 km) long, associated with near-vertical normal faults (Luza and Lawson Jr, 1983). Likewise, Sepra et al. (1989) observed east-dipping near-vertical faults bounding the eastern boundary of the Humboldt fault zone a portion of the

36

Nemaha Uplift in Kansas. They interpreted the Humboldt fault zone as originated from extensional stress regime (Serpa et al., 1989). To the contrary, Berendsen and Blair (1995) proposed a wrench faulting with a left-lateral strike-slip motion during the Pennsylvanian time as the main mechanism forming the Nemaha Uplift. Moreover, Gay (2003) provides a comprehensive investigation, he arguing that the Nemaha fault system is a result of primarily compressional and thrust faulting forming a series of reverse faults. Moreover, he suggests that most of Nemaha thrust and reverse faults are listric in nature, and he argues that strike-slip movement within the Nemaha Uplift occurred at a later stage, after most of the thrusting had occurred (Gay Jr, 2003a). Additionally, Gary (2003) attributes observed normal faults within the Nemaha Uplift to post-compressional relaxation via isostatic adjustments. All in all, it seems a reasonable argument for the origin of the Nemaha Uplift being due to compressional and
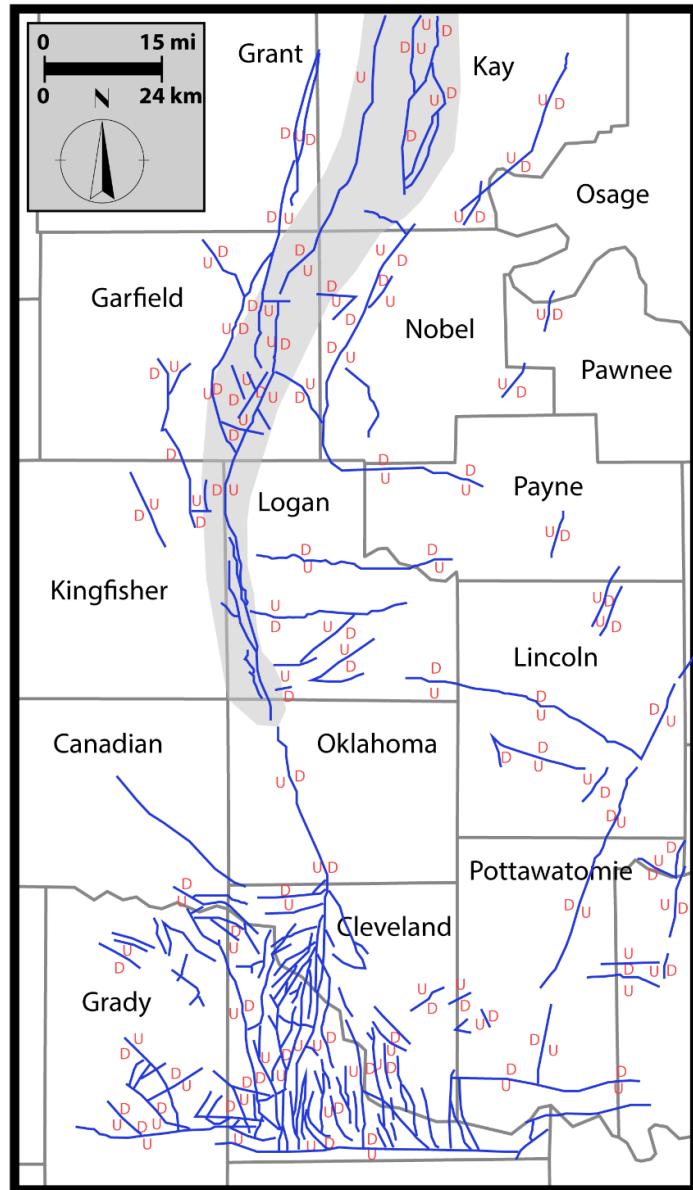
Figure 17: Nemaha-Uplift province showing faults patterns with location of reverse faulting. Map modified from (Gay Jr, 2003b).

thrusting forces associated with a foreland basin setting such as the Anadarko Basin. In addition, from the discussed structural features of the Anadarko Basin above, the compressional thrust-fold, the strike-slip model is geologically consistent with the Anadarko Basin structural evolution (Gay Jr, 1999b, 2003a; Gilbert, 1992; Johnson, 1989b; Perry, 1989).

The timing of the Nemaha Uplift development is believed to have persisted as a positive (paleo-high) feature from the Proterozoic through Paleozoic (Berendsen and Blair, 1995). Moreover, minor uplift movements are proposed during the Ordovician and Devonian, resulting from the Taconic and Acadian orogenies, respectively (Gay Jr, 2003a). The most prominent period in the development of the Nemaha Uplift is interpreted as the Early Pennsylvanian, due to the Ouachita orogeny (Berendsen and Blair, 1995; Gay Jr, 2003a; Luza and Lawson Jr, 1983).

Petroleum production from the Nemaha Uplift Province started in the early 1900s. The first discovery in the Nemaha Uplift took place in 1903 at Cowley County in Kansas, which produced gas from Permian sandstones (Dolton and Finn, 1989). El Dorado is one of the largest oil fields in Kansas, typifying the petroleum prospectivity within the Nemaha Uplift Province. El Dorado was discovered in 1915 by Cities Service Oil Co., and since its discovery, it has produced approximately 300 million barrels of oil from stacked reservoirs ranging from Cambrian to Pennsylvanian in age (Ramondetta, 1990). In Oklahoma, the Oklahoma City oil field is one largest oil-fields within the Nemaha Uplift, and since its discovery in 1928, it has produced nearly 600 million barrels of oil from the Ordovician Simpson Formation alone (Gatewood, 1970). Today, the Nemaha Uplift Province is considered mature in terms of petroleum development, with the last large oil field discovery in 1969, from the S. Peckham field (Dolton and Finn, 1989).

Petroleum occurrence within the Nemaha Uplift area can be divided into three major hydrocarbon plays, each of which exhibits a unique trap style. The first target is Paleozoic

structural and truncation traps, with reservoirs ranging in age from Ordovician through Mississippian featuring anticlines or truncation traps sealed by the overlying shales of Early Pennsylvanian unconformity. El Dorado and the Oklahoma City fields are a typical example of these Paleozoic plays (Dolton and Finn, 1989). The second play comprises shallow structural traps, with reservoirs ranging in age from Pennsylvanian to Permian, predominantly with sandstones and minor limestone reservoirs. This play is characterized by shallow average reservoir depths at 500 ft (152.4 m), with reservoirs being charges by vertical petroleum migration from underlying source rocks (Dolton and Finn, 1989). The third play type comprises the Middle Pennsylvanian stratigraphic traps, primarily with sandstones of the Cherokee Formation and sealed by overlying Missourian shales. These type of traps are associated with relatively small oil accumulations, averaging at about 1 million barrels of oil and 6 billion cubic feet of gas (Dolton and Finn, 1989)

With the emerging unconventional production, the Nemaha Uplift region remains attractive to test production from tight organic-rich intervals. Notably, thermal maturity is a key aspect for the success in hydrocarbon production from unconventional reservoirs. The formations in the Nemaha Uplift region are marginally mature, with values ranging from 0.4 to 0.7%Ro, the range of the early-oil generation window (Al Atwah et al., 2019; Cardott, 2012). However, the Nemaha Uplift region has been known to be associated with geothermal anomalies associated with hot hydrothermal fluids, as well as anomalies associated with basement rock type, as depicted from magnetic and gravity maps. For example, a magnetic and gravity outlier is observed within Osage County, Oklahoma, located at the eastern flank of the Nemaha Uplift (Elebiju et al., 2011; Mohammadi et al., 2017). Such anomalies could influence kerogen maturation and associated organic porosity, and hence oil and gas potential from unconventional targets at the Nemaha Uplift Province remain to be investigated.

CHAPTER II

MOLECULAR GEOCHEMISTRY AS A TOOL IN PETROLEUM SYSTEMS ANALYSIS

Introduction

Petroleum geochemistry as a field of study has matured over the past 30 years, making significant contributions to oil and gas exploration and development. More recently, the application of organic geochemistry principles to unconventional source-rock reservoirs has proven a critical and renewed challenge. Moreover, since unconventional source-rock reservoirs are principally controlled by organic-matter quality, quantity and thermal maturity, organic geochemistry concepts and applications provide the best assessment tools (Curiale and Curtis, 2016). Furthermore, the development of the petroleum geochemistry field is closely related to the technological developments in analytical chemistry instruments. For example, the recent development in gas chromatography and mass spectrometry with the exceptional triple quadrupole mass spectrometer has allowed the analysis of whole crude oil, without the need to fractionate and to prepare samples. This new tool has minimized sample loss due to evaporation and has reduced analysis time (Adhikari et al., 2017; Mei et al., 2018). Similar improvements have been achieved with compound-specific isotope analysis (CSIA) using direct injection of neat oil samples (Barrie et al., 2016). Parallel improvements in pyrolysis techniques have allowed for better understanding and assessment of hydrocarbon saturation and production capability in the unconventional source-rock reservoirs (Abrams et al., 2017; Jarvie, 2012; Romero-Sarmiento et al., 2016).

In this chapter, the key organic compounds used in this study are discussed in detail, aiming to elucidate their chemical structure, nomenclature, origin and application as a tool in petroleum

systems analysis. Those include normal alkanes, acyclic isoprenoids, terpanes, steranes, diterpenes, diamondoids, aromatic hydrocarbons, carbazoles and phenol.

Biomarkers

Known as molecular fossils, biomarkers are organic compounds found in sedimentary organic matter and in crude oil that can be linked to lipid membranes of a biological precursor. Lipid membranes, found in all living organisms, define the boundary between life and non-life. In sedimentary organic matter and petroleum, lipids are the main source of biomarkers. For example, sterane biomarkers found in sedimentary organic matter and petroleum are biosynthesized by
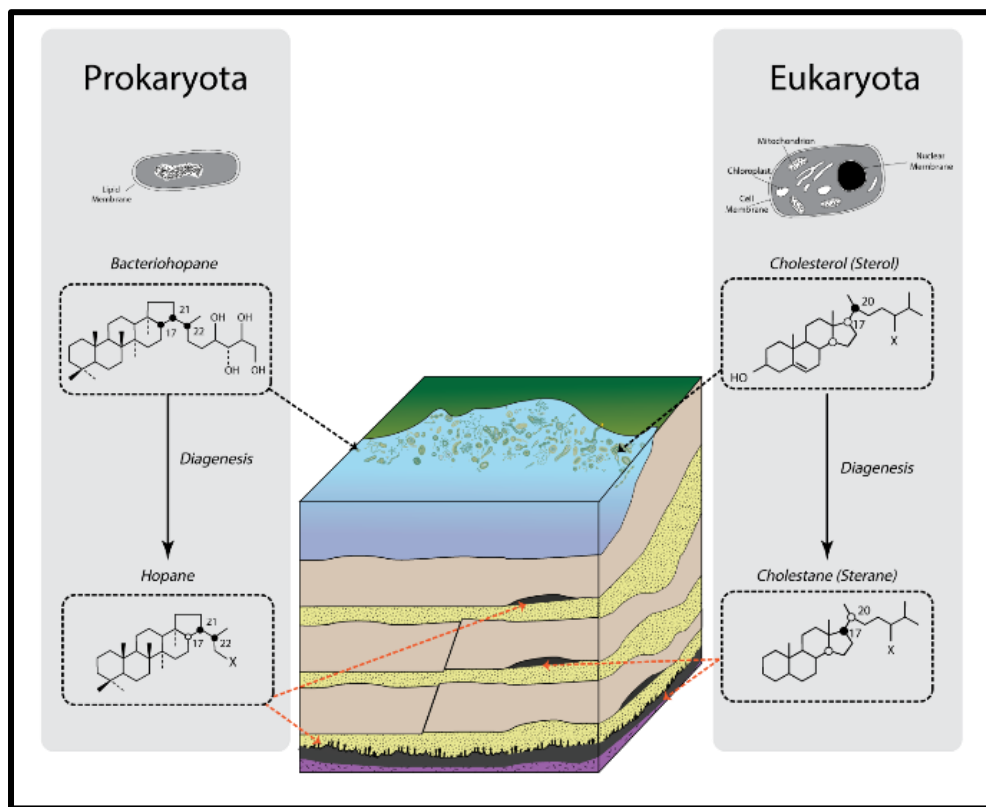
Figure 18: Generalized model showing origin of the dominant biomarkers in petroleum, which are sterane and hopane series. The bacteriohopanes are found in prokaryota lipid membranes, which are believed to be a precursor of the ubiquitous hopane biomarkers found in crude oil. Similarly, sterols found in most eukaryota cell membranes are precursors of sterane biomarkers. Modified from (Peters et al., 2005d).

eukaryotic organisms (Figure 18) (Peters et al., 2005d). Moreover, different biomarker classes can be sensitive to conditions during sediment deposition and post-deposition, such as depositional environment, paleoclimate settings, the extent of biodegradation and thermal maturation, among others (Eglinton and Eglinton, 2008; Hunt, 1996). These biomarker attributes provide geoscientists with a unique interpretation tool applied to different geoscientific disciplines. For example, in the petroleum industry, biomarkers are usually used for petroleum exploration and production assessment; more specifically, biomarkers are used in oil–oil and oil–source-rock correlation, to predict potential hydrocarbon migration pathways (Peters and Fowler, 2002; Philp and Mansuy, 1997). Another example of the application of biomarkers is in the understanding of the evolution of climate through geological time (e.g., alkenone biomarkers which are biosynthesized by unicellular haptophyte marine algae), where they are used as a proxy for past sea-surface temperature (Brassell et al., 1986). These analytical techniques are critical for reconstructing past climatic regimes.

Normal Alkanes and Acyclic Isoprenoids

Normal alkanes are straight-chain and most abundant hydrocarbon compounds ranging in oil samples from $n\text{C}_3$–$n\text{C}_{40+}$ while in rock extracts from $n\text{C}_{10}$–$n\text{C}_{40+}$. In rock extract, the lack of light and short straight-chain normal alkanes is due to evaporation loss during sample preparation. Acyclic isoprenoids are branched hydrocarbons composed of subunits of isoprene that can be linked head-to-tail or tail-to-tail. Distribution of both acyclic isoprenoids and normal alkane—also known as the normal alkane envelope—is used to interpret different parameters of the crude-oil and bitumen extracts, including source-identification, oil–oil correlation, maturity assessment and biodegradation evaluation.

Normal alkanes are organic compounds biosynthesized by different organisms, resulting in a moderately source-specific normal-alkane envelope. For example, certain algae of aquatic origin are observed to feature an abundance of normal alkanes in the range of nC_{15}–nC_{24} and maximizing at nC_{17} (Gelpi et al., 1970; Tissot and Welte, 1984). Furthermore, algal taxa associated with a lacustrine depositional environment, such as *Botryococcus braunii*, showed an abundance of *n*-alkanes in the range of nC_{17}–nC_{33}, maximizing at nC_{29} and nC_{31} (Gelpi et al., 1970). By contrast, terrigenous depositional environment that is usually associated with higher-plant organic-matter input contains normal alkanes

Aside from absolute abundance, relative ratios of certain n-alkanes compounds have been proposed as a tool for correlation proposes, including terrigenous/aquatic ratio (TAR), carbon preference index (CPI) and odd-to-even preference (OEP) (Bourbonniere and Meyers, 1996; Bray and Evans, 1961; Scalan and Smith, 1970). However, n-alkanes' absolute abundance and relative ratios can be subjected to alteration due to thermal maturation or microbial degradation, hence hindering the original source-specific geochemical signature (Peters et al., 2005d). For example, normal alkanes are among the first compounds preferentially attacked by microbes, which usually results in heavy crudes lacking n-alkane envelope and having an unresolved complex mixture (UCM) hump in the gas chromatogram (Al Atwah et al., 2018a). Thermal maturity results in the cracking of the long-chain hydrocarbons (nC_{15+}) to form short-chain light hydrocarbons, such as in condensates; this results in masking the initial kerogen n-alkane fingerprint. Because of their dominant abundance in sediments extract and crude oil, n-alkanes can be quickly measured using gas-chromatography techniques, which making them a convenient compound for hydrocarbon screening and fluid typing analysis.

Acyclic isoprenoids including regular "head-to-tail" and irregular "head-to-head" isoprenoids have been reported to reflect different microbial organic-matter input, such as methanogens archaea and phototrophic organisms. Pristane (C_{19}) and phytane (C_{20}) are one of the ubiquitous and readily measured acyclic isoprenoids in crude-oil and bitumen extracts. The source of pristane and phytane is primarily the cleavage of a phytol side chain of bacteriochlorophyll a and b in purple sulfur bacteria and chlorophyll-a in phototrophic organisms (Brooks et al., 1969; Powell and McKirdy, 1973). Figure 19 exemplifies the relationship between pristane and phytane biomarkers and their
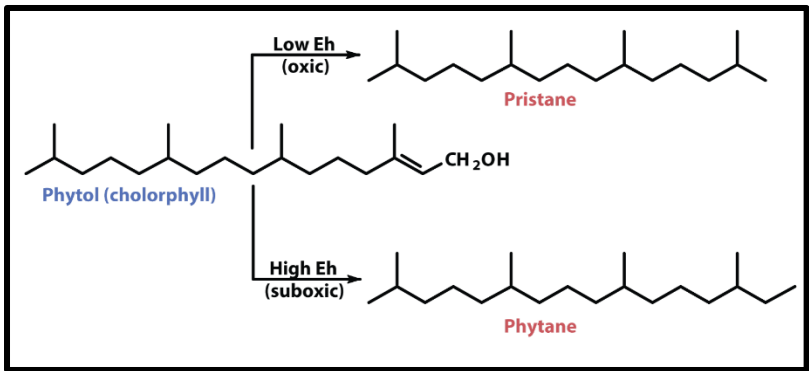
Figure 19: An example of diagenetic pathway of pristane and phytane from phytol, consisting of cleavage of chlorophyll side chain (Peters et al., 2005d).

phytol precursor from the chlorophyll a side chain, with suboxic deposition settings favoring the formation of phytane by reducing phytol to dihydrophytol then to phytane, while oxic redox conditions would promote the enrichment of a pristane biomarker (Peters et al., 2005d). Using this relationship, a number of researchers have used ratios of pristane/phytane (Pr/Ph) to infer source-rock redox condition from related crude oils, where Pr/Ph < 1, suggesting anoxic, and Pr/Ph > 1, indicating oxic source-rock deposition settings (Alexander et al., 1981; Didyk et al., 1978; Sofer, 1984). Other sources for the formation of pristane and phytane biomarkers suggest a much more complex origin than being a diagenetic byproduct of the phytol. For example, Chappe et al. (1982) proposed that dihydrophytol is a constituent in archaeal cell membranes and associated kerogen. A more recent review by Rotani and Bonin (2011) summarizes all the potential sources for pristane and phytane biomarkers. Briefly, in addition to the origins listed above, the authors suggest that

prokaryotes can contribute to the formation of pristane during invertebrate feeding, also during convert trimeric of α-tocopherol to pristane, together with the maturation effect of isoprenyl glyceryl ethers as another source of pristane and phytane (Rontani and Bonin, 2011). Another challenge with pristane and phytane biomarkers is analytical; other biomarkers, such as crocetane, can coelute with phytane and are unresolvable under the normal gas-chromatography conditions, due to similarities in their molecular mass (Greenwood and Summons, 2003).

Therefore, caution must be taken when interpreting pristane and phytane ratio by examining multiple biomarkers before drawing final conclusions. Pristane and phytane biomarkers are low in specificity compared to other diagnostic biomarkers. Overall, it has been suggested to use the following guideline when interpreting pristane and phytane ratio; if Pr/Ph ranges from 0.8 to 3.0, interpretation is not encouraged, while Pr/Ph > 3.0 suggests a terrigenous organic-matter input under oxic to suboxic conditions, and Pr/Ph < 0.8 indicates saline and hypersaline settings associated with carbonate and evaporite (Peters et al., 2005d).

Terpanes

Terpanes represent a broad compound class of saturated hydrocarbon with branched and cyclic structures. Terpanes are one of the ubiquitous biomarkers found in crude oil and rock extract (bitumen), which include tricyclic and tetracyclic terpanes and pentacyclic terpanes (hopanes). Most terpanes are measured by monitoring for m/z 191 mass chromatogram, while some need to be measured using multiple reaction monitoring (MRM) for a diagnostic precursor to product transition, such as m/z 414→191 for extended tricyclic terpane. Table 2 list all terpane biomarkers examined in this study.

Tricyclic terpanes are pervasive biomarkers with the backbone structure of three six-member rings with a side chain of regular isoprenoid at C-14 (Figure 20) (Aquino Neto, 1982). Tricyclic terpanes, also known as "cheilanthanes," were first reported from Green River extracts (Anders and Robinson, 1971). The series of tricyclic terpanes range from C_{19} to C_{54}, with C_{23} usually being the most abundant. Extended tricyclic terpanes ($>C_{24}$) feature a long regular isoprenoid side chain, which resulting in a lack of abundance of C_{22}, C_{27}, C_{32}, C_{37} and C_{42} homologs (Moldowan et al., 1983) In the m/z191 fragmentogram, extended tricyclic terpanes occur as diastereomeric doublet epimers as a result of the stereochemical difference in the carbon at position 22 of the isoprenoid side chain (Peters, 2000). Measurement of extended tricyclic terpanes ranging between C_{33} to C_{39} is unresolvable using classic single-quadrupole mass-spectrometer (GC-MS) techniques because C_{33} to C_{39} tricyclic terpanes co-elute with pentacyclic terpanes (also known as "the homohopanes series") due to the similarities in their molecular masses. However,
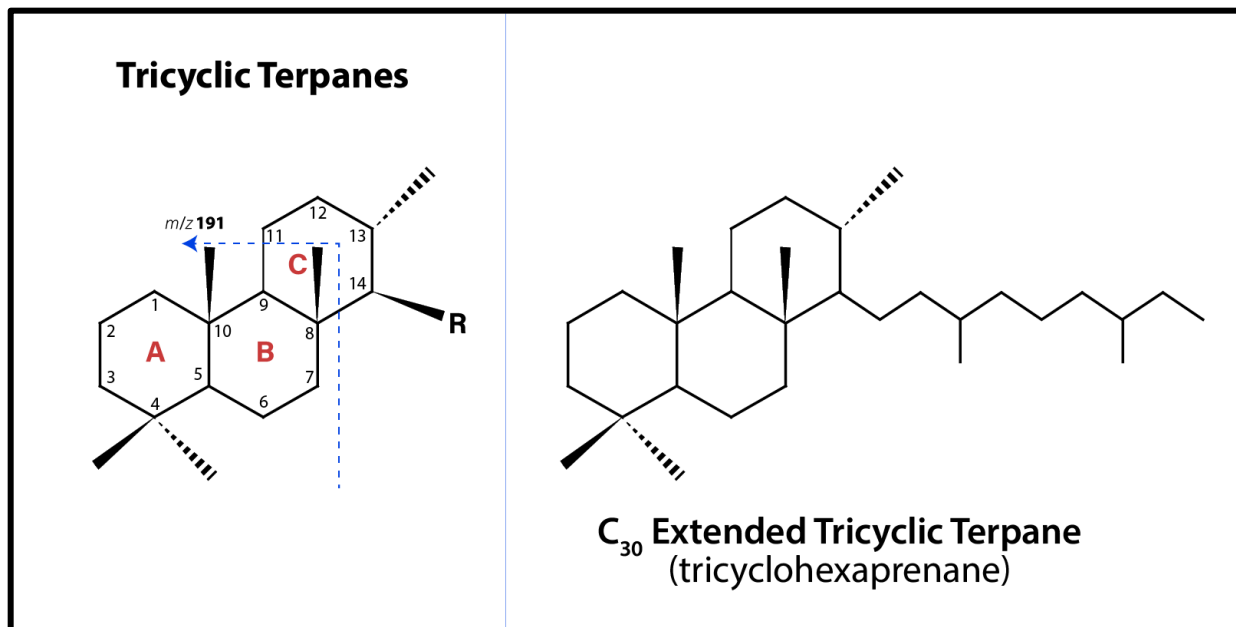
Figure 20: Back-bone carbon skeleton of tricyclic terpane biomarkers with the main diagnostic mass-fragment m/z 191 with an example of the C_{30} extended tricyclic terpane, showing the major carbon structure with a long isoprenoid side chain, which is characteristic of extended tricyclic terpane biomarkers.

this challenge can be overcome by utilizing the triple quadrupole mass spectrometer (GC-MS/MS) with MRM selectivity, which detects extended tricyclic terpanes as doublets based on the carbon number following relationship for precursor ion ($262 + (n \times 14)$, were n ranges from 0 to 17, and the main product ion is m/z 191 (Atwah et al., 2018; Philp et al., 1988).

The biological precursor related to biosynthesizing tricyclic terpanes is not clearly defined, with both algal and bacterial sources having been proposed (Aquino Neto, 1982; Behrens et al., 1999; Ourisson et al., 1982). Moreover, due to diagenetic alteration for sedimentary organic matter after deposition and burial, the tricyclic terpane skeleton structure is believed to represent a degraded fragment of tricyclohexaprenol (Ourisson et al., 1982). According to Ourisson et al. (1982), tricyclohexaprenol is predicted to be a constituent of prokaryote membranes, with the main mechanism possibly being biosynthesizing by cyclization of squalene. However, correlation of enrichment in tricyclic terpane and their aromatics counterparts with *Tasmanite*-rich kerogens is observed and interpreted to reflect high paleolatitude settings (Azevedo et al., 1998; Greenwood et al., 2000). This correlation of *Tasmanite*-related tricyclic terpane is postulated to originate from cyclization of octaprenol in the *Tasmanites* algae (Azevedo et al., 1998). It remains unclear what biological precursor extended tricyclic terpanes ($>C_{24}$) are related to. Extended tricyclic terpanes are reported from the Brazilian basins occurring in the Upper Cretaceous marl and calcareous organic-rich shales, together with Lower Cretaceous lacustrine freshwater black shales (De Grande et al., 1993). Water salinity and deposition of organic matter within shallow water-settings are believed to be associated with enrichment in extended tricyclic terpanes, suggesting that organisms that survive in saline and shallow water settings might be related to extended tricyclic terpanes. Petrographic examination of macerals of Mississippian organic-rich rocks within the Cherokee

Platform of Oklahoma shows a predominance of lamalginite associated with an abundance of extended tricyclic terpanes (Atwah et al., 2018).

Tricyclic terpane biomarkers have been used as a tool for source-rock quality prediction, oil–source and oil–oil correlation, and biodegradation assessment (Peters and Moldowan, 1993; Seifert and Moldowan, 1981; Seifert et al., 1980; Zumberge, 1987). For example, the relationship of tricyclic terpanes to 17 α-hopanes can be used as an organic-matter source parameter, which in theory represents different prokaryotic species—more specifically, the sum of C_{28} and C_{29} divided by hopane or C_{23} divided by hopane (Peters et al., 2005a). Moreover, cross-plot comparing two different ratios (C_{24}/C_{23} vs. C_{22}/C_{21}) of tricyclic terpanes can be used to infer source-rock lithology from crude-oil samples, with carbonate source rock exhibiting a high C_{22}/C_{21} ratio (>0.4) relative to the C_{24}/C_{23} ratio, with lacustrine-sourced oils exhibiting high C_{26}/C_{25} (>1.2) tricyclic terpane (Peters et al., 2005a). Tricyclic terpanes are resistant to biodegradation, and hence can be used for correlation application in heavily biodegraded oils (Seifert and Moldowan, 1979). Holba et al. (2001) used the ratio of tricyclic terpane to C_{27} hopane; more specifically, they examined extended tricyclic doublets C_{28} and C_{29} with Ts (terpane stable) C_{27} (18-α [H]-trisnorhopane) to discriminate between crude-oil source-rock age of Triassic (enriched in tricyclic terpanes) versus Jurassic (depleted in tricyclic terpanes) oils (Holba et al., 2001). Additionally, the sum of the C_{26} tricyclic terpane doublets (S+R) relative to Ts C_{27} (18-α [H]-trisnorhopane) as a marker for crude oil originated from source rock deposited during paleo-oceanic upwelling events (Hill et al., 2007; Holba et al., 2003).

Tetracyclic terpane biomarkers include saturated hydrocarbon featuring a backbone structure of four six-member rings ranging in total carbon number from C_{24} to C_{27} (Figure 21) (Aquino Neto, 1983; Trendel et al., 1982). Measurement of tetracyclic terpanes typically uses a

m/z 191 mass chromatogram with the mass-spectrometer running in single-ion monitoring (SIM) mode. The most abundant compound of these biomarker classes in crude oil and rock extract (bitumen) is the C_{24} tetracyclic terpane, usually expressed as C_{24}tet (Peters et al., 2005a).

Due to structural similarities between tetracyclic terpanes and hopane, it is suggested that origin of tetracyclic terpane biomarkers represents a thermally or diagenetically altered version of hopane, forming by a rupture in the E-ring of a hopanoid precursor (Trendel et al., 1982). Even though a biosynthesized pathway is possible for the formation of tetracyclic terpanes, it is yet to be documented. If the presumption of hopanoid origin is true, then tetracyclic terpanes can be used as a signature of prokaryotic input. Since it is a diagenetically altered compound, it reflects source-rock lithology or thermal maturity, or both.

Application of tetracyclic terpanes in petroleum geochemistry is primarily used as a source-rock lithology and thermal maturity parameter. A number of ratios are thought to indicate
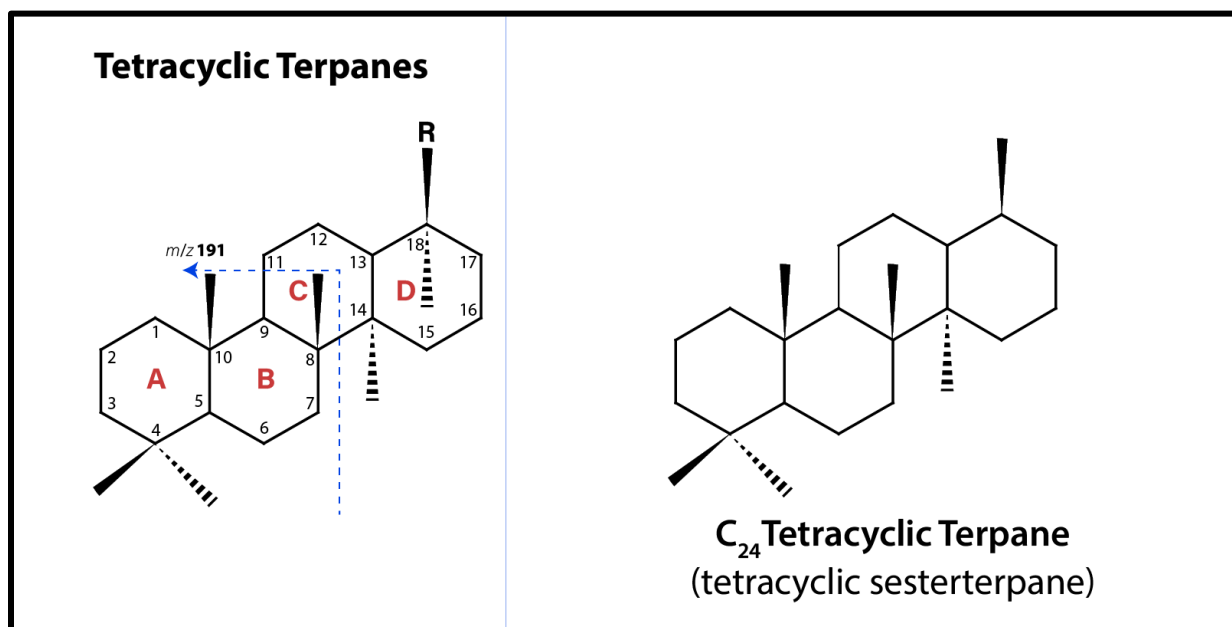
Figure 21: Backbone carbon skeleton of tetracyclic terpane biomarkers and their diagnostic mass fragment is m/z 191, with an example of the C_{24} tetracyclic terpane (Tet.24), which is the most abundant biomarker in its homologues series.

49

carbonate and evaporite sourced oils, with an abundance of C_{24}tet relative to C_{23} tricyclic terpane.

For instance, anhydrite sabkha-type source rocks and associated oils from the Aquitaine Basin were differentiated from carbonate-derived oils by examining a suite of molecular signatures; among them are the tetracyclic terpane biomarkers. (Connan et al., 1986) interpret this fingerprint as resulting from halophilic bacteria. A similar study examined rock extracts and oils from the Black Creek Basin, Alberta, and the prevalence of C24tet was observed as a biomarker for the hypersaline environment with an evaporite-carbonate depositional system (Clark and Philp, 1987). However, other studies have reported enrichment of C_{24}tet in crude oil sourced from terrigenous organic matter (Philp and Gilbert, 1986; Zhang and Huang, 2005). Moreover, coal extracts from the Sydney Basin feature the presence of C_{24} tetracyclic terpane, with the absence of tricyclic terpanes (Philp and Gilbert, 1986). Like the tricyclic terpane, the tetracyclic terpanes are resistant to biodegradation and, hence, constitute a useful correlation tool for altered oils (Seifert and Moldowan, 1979).

Hopanes are series C_{27} to C_{35} pentacyclic triterpene biomarkers. The main structure is composed of four six-member cyclohexane rings (A, B, C) and one five-member cyclopentane ring (D) (Figure 22). Hopanes exhibit different isomeric series, including diahopanes, neohopanes, moretane, demethylated hopanes and homohopanes (Peters et al., 2005a). Chromatographically, most of the hopanes are resolved by running GC-MS on SIM for ion *m/z*191. However, homohopanes can co-elute with extended tricyclic terpanes; therefore, in samples enriched in extended tricyclic terpanes, homohopanes can be accurately measured using GC-MSMS running on MRM mode, and more specifically by monitoring for precursors to product transitions as

50

showing the following relationship for the precursor ion: $370 + (n \times 14)$, where n ranges from 0 to 10, and main product ion is m/z 191 (Philp et al., 1988).
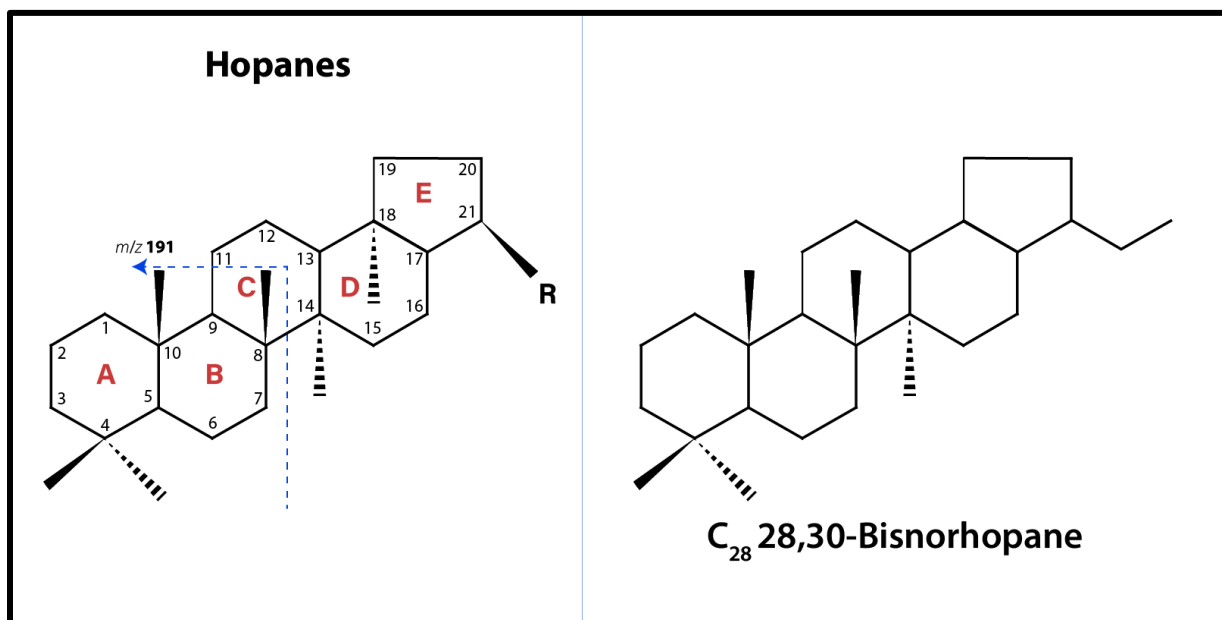
Figure 22: Backbone carbon skeleton of hopane biomarkers and their diagnostic mass fragment m/z 191, with an example of the C_{28} 28,30-bisnorhopane which is missing methylation groups at carbon positions 28 and 30.

The origin of hopane biomarkers found in petroleum source rocks and crude oil is related to the bacteriohopanetetrol compound found in the bacterial (prokaryotic) membrane (Ourisson et al., 1984). Moreover, in the hopanes family, pentacyclic triterpenoids were observed in diverse taxonomic groups of prokaryotic organisms, such as cyanobacteria, purple non-sulfur bacteria and chemoheterotrophs (Rohmer et al., 1984). For example, the compound bacteriohopanepolyols (BHPs), a biological precursor for the geological compound series of hopanes, have been found and isolated from thermoacidophile *Bacillus acidocaldarius* (Langworthy et al., 1976). Hopanoids have been detected in minor amounts from fungi, mosses and ferns, while they are absent in archaea and animals (Mahato and Sen, 1997; Ourisson et al., 1987). Interestingly, Ourisson et al. (1987) suggest that hopanoids were discovered initially in eukaryotes in two distinct families,

51

differentiated based on the presence or absence of oxygen atoms in carbon at position number 3, with the former forming from cyclization of squalene, while the latter formed from squalene itself. Further, hopanoids are found in few higher-plants; one example is hopanoids found in dammar resin from *Hopea*. Those hopanoids exhibit unique structures, containing an oxygen atom at carbon potion number 3 and the absence of a side chain (Ourisson et al., 1987).

Hopanes are one of the classic biomarkers used routinely in petroleum geochemistry studies, with applications for oil–oil and oil–source correlation, deposition environment, biodegradation and maturity assessment. Some of the key hopane ratios include 28,30-bisnorhopane/25, 28,30-trisnorhopane (BNH/TNH), C_{35} homohopane index, 30 norhopane/hopane and gammacerane index (Peters et al., 2005a). BNH and TNH are biomarkers indicative of bacterial signature that is associated with anoxic redox condition during source rock deposition, with low clay-content (Katz and Elrod, 1983). The biomarkers BNH and TNH are indicative of a bacterial signature associated with anoxic redox condition during source-rock deposition, with low clay-content (Katz and Elrod, 1983). Moreover, Mello et al. (1988) used the bisnorhopane index among other molecular signatures to typify offshore Brazilian oils; BNH and TNH were associated with oils sourced from marine carbonate and evaporite source rocks (Mello et al., 1988). Homohopanes distribution and C_{35} homohopane index biomarkers are source-specific signatures. Homohopanes distribution, particularly enrichment in C_{35} relative to C_{34} homohopanes, is considered a proxy for highly reducing marine settings (Peters and Moldowan, 1993). Homophones distribution has been used to characterize crude oils produced from the Vienna Basin, and source rocks were inferred to be Jurassic and Paleogene organic-rich rocks (Picha and Peters, 1998). The ratio of norhopane to hopane is widely used as a marker for anoxic marl and carbonate source rocks. Hopane and C_{29} 17 α-norhopane are the most abundant compounds in

bitumen and crude oils in the *m/z* 191 trace, while the norhopane-to-hopane ratio is >1, which reflects a signature of anoxic carbonate or marl source rock (Peters et al., 2005a). The gammacerane biomarker is a highly specific compound for water-column stratification during

deposition of source rock. However, the cause of water-column stratification remains a subject of debate, particularly if gammacerane is a marker for water-column stratification due to hypersalinity (halocline) or due to the temperature gradient (thermocline) (Peters and Moldowan, 1993). The carbon skeleton of gammacerane suggests it originated as a diagenetic product from tetrahymanol, which is a polycyclic triterpenoid lipid widely distributed in a variety of sedimentary environments, including marine sediments, fresh-water and bacterivorous marine ciliates (Harvey and McManus, 1991; Holz and Conner, 1973; Ten Haven et al., 1989). Sinninghe Damsté et al. (1995) summarize gammacerane geochemistry and provide evidence for why gammacerane is found in hypersaline but also can be found in marine and lacustrine settings. The gammacerane index is usually calculated using the following formula: $10 \times$ gammacerane/(gammacerane + C_{30} hopane). Due to gammacerane's specificity, it has been used as an oil to source-rock correlation

Table 2 List of major terpane biomarkers and their diagnostic precursor-product transitions

Compounds	MRM Precursor-Product Transition *m/z*	Compound Abbreviation
Tricyclic and Tetracyclic Terpenes (*m/z* 191)		
C_{20} Tricyclic terpane	*m/z* 276→191	C20TT
C_{21} Tricyclic terpane	*m/z* 290→191	C21TT
C_{22} Tricyclic terpane	*m/z* 304→191	C22TT
C_{23} Tricyclic terpane	*m/z* 318→191	C23TT
C_{24} Tricyclic terpane	*m/z* 332→191	C24TT
C_{25} Tricyclic terpane (S+R)	*m/z* 346→191	C25TT(S+R)
C_{24} Tetracyclic terpane (TET)	*m/z* 330→191	C24TET

Table 2 continued

Compounds	MRM Precursor Product Transtion *m/z*	Compound abbreviation
C26 Tricyclic terpane (S+R)	*m/z* 360→191	C26TT(S+R)
C28 Extended tricyclic terpane (S+R)	*m/z* 388→191	C28ETT(S+R)
C29 Extended tricyclic terpane (S+R)	*m/z* 402→191	C29ETT(S+R)
C30 Extended tricyclic terpane (S+R)	*m/z* 416→191	C30ETT(S+R)
C31 Extended tricyclic terpane (S+R)	*m/z* 430→191	C31ETT(S+R)
C33 Extended tricyclic terpane (S+R)	*m/z* 458→191	C33ETT(S+R)
C34 Extended tricyclic terpane (S+R)	*m/z* 472→191	C34ETT(S+R)
C35 Extended tricyclic terpane (S+R)	*m/z* 486→191	C35ETT(S+R)
C36 Extended tricyclic terpane (S+R)	*m/z* 500→191	C36ETT(S+R)
C38 Extended tricyclic terpane (S+R)	*m/z* 528→191	C38ETT(S+R)
C39 Extended tricyclic terpane (S+R)	*m/z* 542→191	C39ETT(S+R)
Hopanes (*m/z* 191)		
C27 Ts 18α(H)-trisnorhopane	*m/z* 370→191	C27Ts
C27 Tm 17α(H)-trisnorhopane	*m/z* 370→191	C27Tm
C28 17α18α21 β (H)-bisnorhopane	*m/z* 384→191	BisHop
C29 Tm 17 α (H)21 β (H)-norhopane	*m/z* 398→191	C29Tm
C29 Ts 18α(H)-norneohopane	*m/z* 398→191	C29Ts
C29 normoretane	*m/z* 398→191	C29Mor
C30 17α(H)-hopane	*m/z* 412→191	Hop
C30 moretane	*m/z* 412→191	C30Mor
C31 22S+R 17α(H) homohopane	*m/z* 426→191	C31HHop S+R
Gammacerane	*m/z* 412→191	Gamm
C32 22S+R 17α(H) bishomohopane	*m/z* 440→191	C32HHop S+R
C33 22S+R 17α(H) trishomohopane	*m/z* 454→191	C33HHop S+R
C34 22S+R 17α(H) extended hopane	*m/z* 468→191	C34HHop S+R
C35 22S+R 17α(H) extended hopane	*m/z* 482→191	C34HHop S+R

hopane). Due to gammacerane's specificity, it has been used as an oil to source-rock correlation marker, for example, oil samples from the Fulin Basin in East China were grouped to originate from carbonate-evaporite source rock, with gammacerane index >0.3 (Chen et al., 1996a). Similarly, gammacerane was used to identify Tertiary age crude oils produced from Great Basin, which were correlated to the lacustrine Elko Formation (F.G. Poole and Claypool, 1984).

Diterpanes

Tricyclic diterpanes are saturated hydrocarbon biomarkers featuring three six-member rings with multiple methylation sites. Some of the commonly used tricyclic diterpanes include rimuane, pimarane, rosane, isopimarane (Figure 23) and phyllocladane. Measurement of tricyclic diterpanes in crude oil and rock extracts can partially be archived using GC-M S(Table 3)(Gough, 1964). The diagnostic ion for tricyclic diterpanes is m/z123. A comprehensive measurement of tricyclic and tetracyclic diterpanes is possible with using GC-MS/MS operated on MRM, specificallymonitoring different precursor-to-product transitions, such as m/z 276 →123, m/z 278→123 and m/z 276→247.(Table 3) (Peters et al., 2005a; Zinniker, 2005).

The origin of tricyclic diterpanes is attributed to higher plants, including both gymnosperm and angiosperm input (Noble et al., 1986; Shan-Tan and Kaplan, 1992; Weston et al., 1989). Moreover, tricyclic diterpenoid biomarkers were first measured in coniferous trees, particularly the southern-hemisphere families of *Araucariaceae* and *Podocarpaceae* (Gough, 1964; Thomas, 1969). Resinous higher plants from the present day to the Jurassic age are another source of tricyclic diterpanes, with the proposed association of resins and admixed mucilages as the primary maceral source (Simoneit et al., 1986). While the marine algal source of diterpenoid is possible

and has been observed in present-day marine biota, the relationship between tricyclic diterpanes and a clear marine precursor is yet to be defined in the geological record (Schever, 2012; Simoneit et al., 1986). Therefore, tricyclic diterpanes exhibit high specificity proxy for higher plant contribution into kerogens and crude oils (Peters et al., 2005a).

Tricyclic diterpanes have been used in a number of studies for oil–oil and oil–source-rock correlation. In a study of waxy bitumen from the southern Australian coastline, tricyclic diterpanes were observed to indicate higher-plant input and served as a signature to correlate these bitumens to Cenozoic lacustrine shales (Edwards et al., 2018). Similarly, in the Qaidam Basin, tricyclic
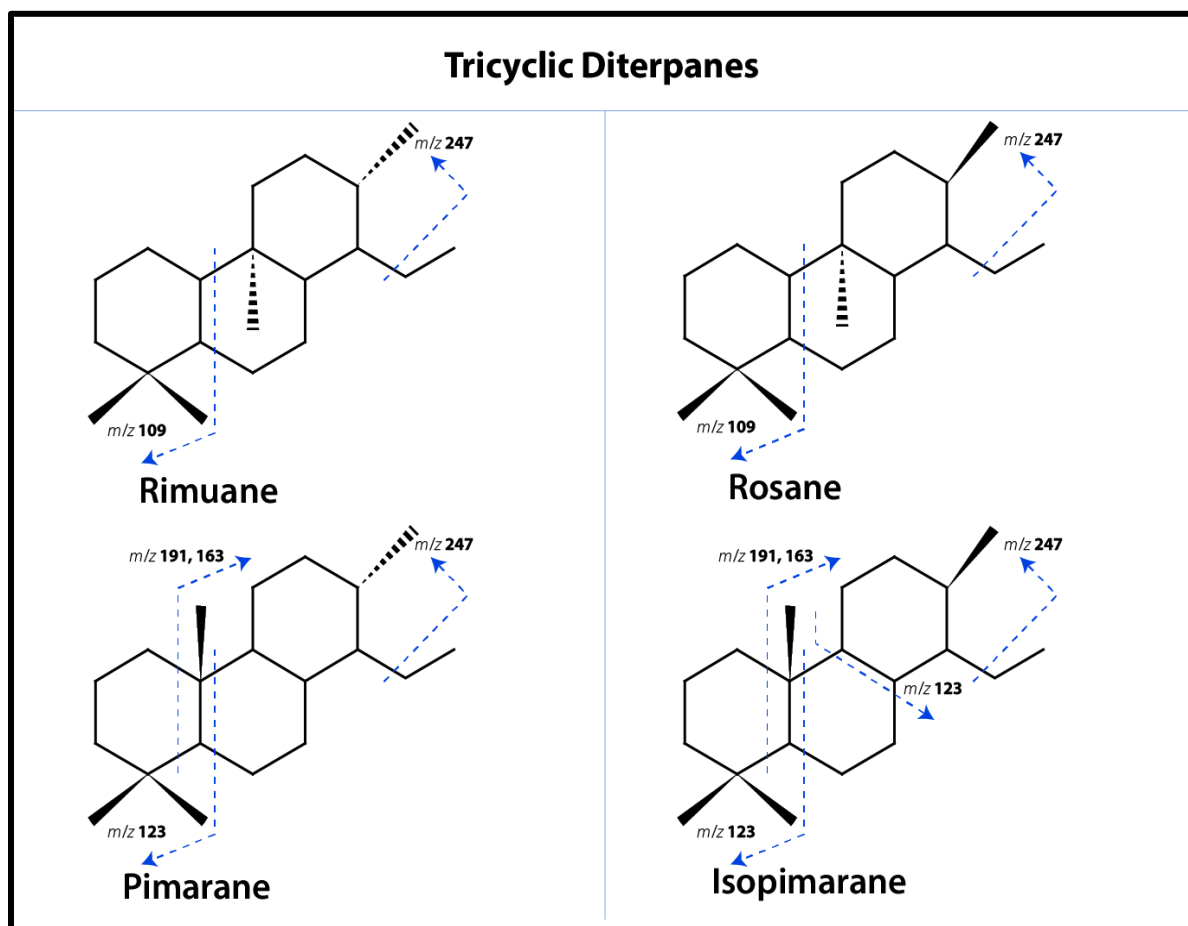
Figure 23: Backbone carbon skeleton of tricyclic diterpane biomarkers and their diagnostic precursor product transition is m/z 276→247, with an example of the major four biomarker analyzed in this study, including Rimuane, Rosane, Pimarane and Isopimarane

diterpanes were documented in Jurassic source rocks and related oils, indicating contribution from higher plants; more specifically, the authors observed clustering in the oil and rock extracts when they compared ratios of 4 β (H)-19-norisopimarane to regular and rearranged C_{27} sterane biomarkers (Hanson, 2001). Dzou et al. (1999) utilized tricyclic diterpanes by monitoring for *m/z* 123 mass chromatogram as a diagnostic chemical fossil for Tertiary-sourced oils within the central of Llanos Basin.

Tetracyclic diterpanes consist of a four-ring carbon-skeleton system (Figure 24), including beyerane, 16β phyllocladane, 6β kaurane, atisane, 16α phyllocladane and 16α kaurane (Table 3) (Zinniker, 2005). Tetracyclic diterpanes are measured by monitoring for diagnostic ions such as *m/z*123, 231, 245, 259 and 274; however, if present in trace amounts, the use of GC-MSMS (with MRM) is sometimes required for their detection, with the diagnostic precursor to product transition at *m/z* 274→123 (Table 3) (Peters et al., 2005a; Zinniker, 2005).

Tetracyclic diterpanes, like their tricyclic diterpane counterpart, are compounds of the diterpanoid class, and hence their origin is closely related to terrigenous organic matter. In nature and in biological samples, diterpenoids and particularly tetracyclic diterpanes (parent compounds of tetracyclic diterpanes) are found in the leaf resin of conifers, particularly related to *Podocarpaceae*, *Araucariaceae* and *Cupressaceae* families (Noble et al., 1985; Noble et al., 1986). Tetracyclic diterpanes are found in conifers restricted to the southern hemisphere, such as *Agathis* and *Podocarpus.* Moreover*, Agathis*— a species of *Araucariaceae*—is observed to be enriched in the biomarker kaurane, while the biomarker phyllocladane is detected in *Podocarpus* and *Dacrydium*, species of *Podocarpaceae* (Noble et al., 1985). Tetracyclic diterpanes are believed to be a paleobotanical biomarker for Upper Triassic to Tertiary plants; however, work by Schulze and Michaelis (1990) documented the presence of tetracyclic diterpanes in Carboniferous coals,

and they propose a link between tetracyclic diterpanes and their Upper Carboniferous ancestors—

the *Voltziale*. Another source for tetracyclic diterpane is the plant hormone Gibberellin, which

belongs to the diterpenoid compound class and shares a backbone structure similar to the

tetracyclic diterpane biomarkers. Gibberellin is a crucial hormone for land plants, as it controls

plant growth and development (Graebe et al., 1965). A marine origin of tetracyclic diterpane is

possible, since some marine algae biosynthesize diterpenoids, but it is not clear which of those

tetracyclic diterpane isomers would be associated with marine input as opposed to plant input
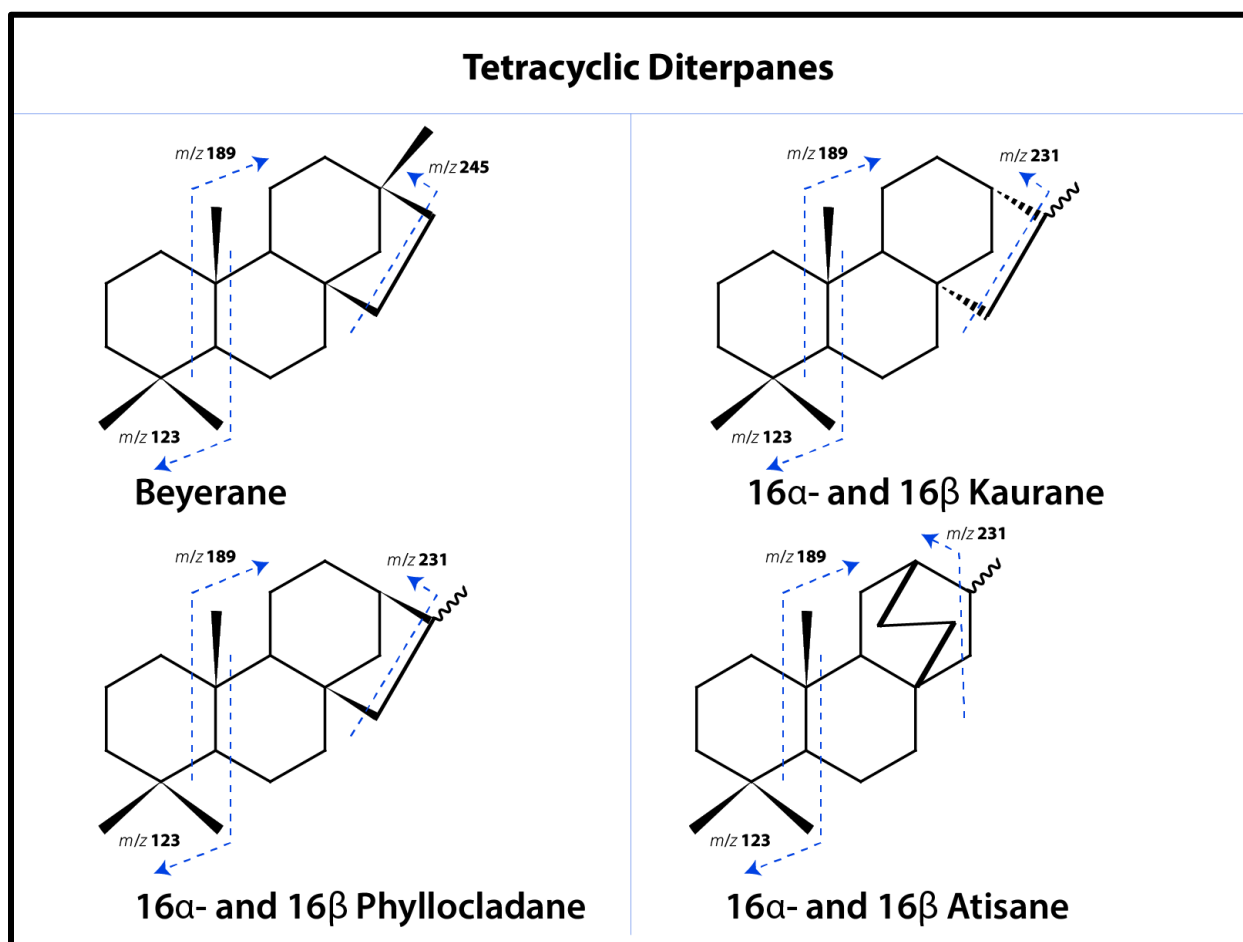
Figure 24: Backbone carbon skeleton of tetracyclic diterpane biomarkers and their diagnostic precursor product transition is m/z 274→123, with an example of the major four biomarkers analyzed in this study, including Beyerane, 16β-Phyllocladane, 6β-Kaurane, Atisane, 16α-Phyllocladane and 16α-Kurane

(Peters et al., 2005a; Simoneit et al., 1986). Specificity of tetracyclic diterpane is therefore high for terrigenous organic-matter input.

Due to their specificity, tetracyclic diterpanes are mainly used as a source parameter in geochemical and petroleum system analysis studies. Nobel et al. (1985) correlated oils produced from Gippsland Basin in southern Australia to coal and shale extracts, utilizing a collection of tetracyclic diterpane biomarkers. Weston et al. (1989), reported the presence of 16 β (H)-phyllocladane ent-16 β (H)-kaurane with oils associated with New Plymouth oil-field within the Taranaki Basin of New Zealand. In a similar study within the Taranaki Basin, tetracyclic diterpanes, particularly beyerane, phyllocladanes and kauranes, were found in rock-cuttings, and along with other biomarkers, they helped mark the flora evolution in a transition during Mesozoic and Tertiary, from gymnosperms to angiosperms during the Eocene (Killops et al., 1995).

Table 3 List of major diterpane biomarkers and their diagnostic precursor-product transitions.

Compounds	MRM Precursor-Product Transition m/z	Compound Abbreviation
Tricyclic Diterpanes		
C_{20} Rimuane	m/z 276→247	Rimuane
C_{20} Rosane	m/z 276→247	Rosane
C_{20} Pimarane	m/z 276→247	Pimarane
C_{20} Isopimarane	m/z 276→247	Isopimarane
Tetracyclic Diterpanes		
C_{20} Beyerane,	m/z 247→123	Beyerane
C_{20} 16β Phyllocladane	m/z 247→123	β Phyllocladane
C_{20}, 6β Kaurane	m/z 247→123	β Kaurane
C_{20} Atisane	m/z 247→123	Atisane
C_{20} 16α Phyllocladane	m/z 247→123	α Phyllocladane
C_{20} 16α Kaurane	m/z 247→123	α Kaurane

Steranes are a broad class of biomarkers with six isoprene subunits composing the main carbon skeleton of three cyclohexane rings and one cyclopentane ring, with a major side chain at carbon position number 7 (Figure 25). Steranes range from C_{20} to C_{30}, which are subdivided into regular-sterane and rearrange-steranes (diasterane), with the latter exhibiting the migration of C-10 and C-13 methyl groups to C-5 and C-14 as a diagenetic byproduct of an acidic condition, clay-catalysis and thermal maturation (Peters et al., 2005a). Detection of steranes is usually performed by monitoring for m/z 217 and 218 ions using GC-MS on SIM mode. Steranes exhibit structural asymmetric centers due to hydrogen and methyl groups resulting in a number of isomers and
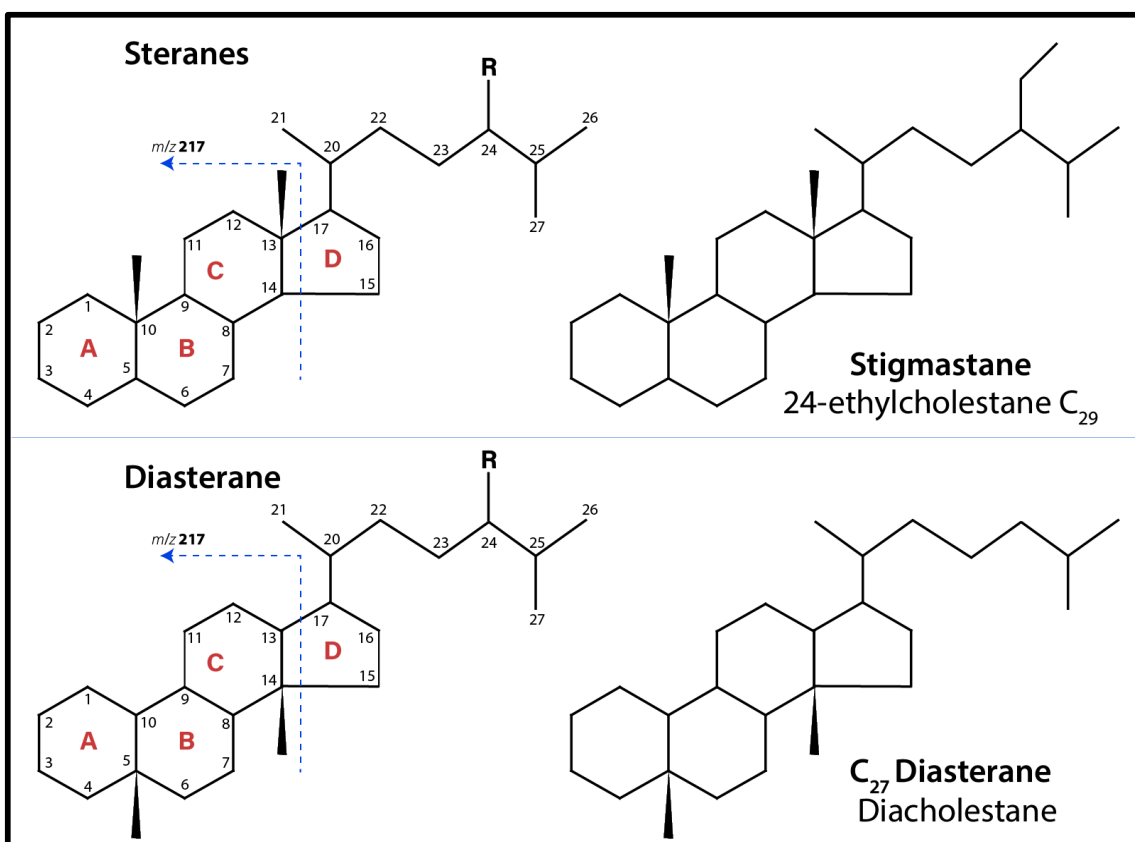
Figure 25: Backbone carbon skeleton of sterane and disterane biomarkers and their diagnostic mass fragment is *m/z* 217, with an example of C_{29} regular sterane (stigmastane) and an example of rearranged sterane C_{27} diasterane.

epimers. More specifically, methylation occurs in steranes at carbon positions of C-5, C-14, C-17, and C-20, resulting in the possibility of complex isomeric structures. However, due to steranes isomeric and epimeric character, with similar molecular masses resulting in co-elution, steranes are only partially resolved with the GC-MS technique. Therefore, regular and rearranged steranes are fully resolved with use of GC-MSMS run on MRM, by monitoring for diagnostic precursor product transitions following this formula: $372 + (n \times 14)$, where n range from 0 to 3 and the main product ion is m/z 217(Table 4) (Philp et al., 1988).

Sterane compounds originate from the biological precursor sterols, which are found in eukaryotic organisms' cell membranes and hormones as phospholipids (Mackenzie et al., 1982a). Phospholipids play an essential role in the physiology of eukaryotes, particularly in membrane fluidity (Ourisson et al., 1987) Sterols are found in a number of different biota classes, including phytoplankton (e.g., diatoms, dinoflagellates), terrigenous plants and higher organisms (e.g. coelenterates and sponges) (Mackenzie et al., 1982a and reference therein). Moreover, sterols are produced in different forms including cholesterol in animals, sitosterol and stigmasterol in higher land plants, and ergosterol is produced by fungi (Huang and Meinschein, 1979). This relationship is used to distinguish the biotic input of sedimentary organic matter, however, marine algae have been observed to synthesize all sterol types; particularly, C_{30} sterols are synthesized in abundance (Volkman et al., 1998). The geological counterpart compounds to sterols are cholestane (C_{27} regular sterane), ergostane (C_{28} regular sterane), and stigmastane (C_{29}), and from the sterol relationship it is postulated that steranes would follow a similar trend, with C_{27} cholestane indicating marine algal organic matter, while C_{28} ergostane suggests lacustrine algae and C_{29} stigmastane marks higher plant input, usually reported in a ternary diagram (Mackenzie et al., 1982a; Moldowan et al., 1985). Enrichment of C_{29} stigmastane is not strictly the result of a

61

terrigenous organic-matter input, as stigmastanes are reported in marine shale, particularly marine Paleozoic source rocks, such as the Woodford Shale (Miceli Romero and Philp, 2012; Moldowan et al., 1985). Overall, the sterane versus hopane abundance is used as a proxy to estimate bacterial organic matter's contribution versus that of marine algae and higher plants (eukaryotes) (Peters et al., 2005a). Short-chain steranes (pregnanes) together with rearranged steranes (diasteranes) are compounds that are altered byproducts of sterols, occurring as a function of thermal-maturity methylation cleavage and clay catalysis reactions (Rubinstein et al., 1975; Wang et al., 2015a). Additionally, the enrichment of pregnanes and their homologues was first reported to associate with hypersaline (Ten Haven et al., 1985), marine carbonates (Requejo et al., 1997) and sulfur-rich settings (Lu et al., 2011). A more comprehensive study on the origin of pregnanes and their homologues postulates that enrichment of those biomarkers is due to diagenesis and catagenesis of a sterol precursor bounded to the macromolecule of kerogen, in conjunction with clastic-starved water columns and carbonate-rich depositional environments. Collectively, sterane compounds sensitive to source-rock lithology and thermal maturity allow the inference of source-rock properties through analysis of cured oils.

Application of sterane biomarkers in petroleum geochemistry studies is used for oil–oil and oil–source correlation, determination of source-rock depositional environment, together with assessments of biodegradation and maturity. A ternary diagram of regular steranes comparing the sum of 5α, 14α, 17α ; (20S) + (20R) plus 5α, 14β,17β (20S) + (20R) steranes for C_{27}, C_{28} and C_{29} represents a relationship used to infer source-rock lithology. Moldowan et al. (1985) examined a wide range of crude oils from different basins ranging in age from Late Miocene to Precambrian.

Table 4 List of major sterane biomarkers and their diagnostic precursor-product transitions

Compounds	MRM Precursor-Product Transition *m/z*	Compound Abbreviation
Steranes (*m/z* 217)		
C26 13β 17α -24 -20S Diasterane	*m/z* 358→217	C26αβ24S
C26 13β 17α -24 -20R Diasterane	*m/z* 358→217	C26αβ24R
C26 13β 17α -27 -20S Diasterane	*m/z* 358→217	C26αβ27S
C26 13β 17α -27-20R Diasterane	*m/z* 358→217	C26αβ27R
C26 ααα -24-nor-20S Sterane	*m/z* 358→217	C26ααα20S
C26 αββ-24-nor-20R Sterane	*m/z* 358→217	C26αββ20R
C26 αββ -24-nor-20S Sterane	*m/z* 358→217	C26αββ20R
C26 ααα -24-nor-20R Sterane	*m/z* 358→217	C26ααα20R
C26 21-nor ααα+ αββ Sterane	*m/z* 358→217	C26nor21
C27 13β 17α 20S Diacholestane	*m/z* 372→217	C27βα20S Dia
C27 13β 17α 20R Diacholestane	*m/z* 372→217	C27βα20R Dia
C27 13α 17β 20S Diacholestane	*m/z* 372→217	C27αβ20S Dia
C27 13α 17β 20R Diacholestane	*m/z* 372→217	C27αβ20R Dia
C27 ααα 20S Cholestane	*m/z* 372→217	C27ααα20S
C27 αββ 20R Cholestane	*m/z* 372→217	C27αββ20R
C27 αββ 20S Cholestane	*m/z* 372→217	C27αββ20S
C27 ααα 20R Cholestane	*m/z* 372→217	C27ααα20R
C28 13β 17α dia 20S (24S+24R)	*m/z* 386→217	C28βα20S Dia
C28 13β 17α dia 20R (24S+24R)	*m/z* 386→217	C28βα20R Dia

Table 4 continued.

Compounds	MRM Precursor-Product Transition m/z	Compound Abbreviation
C$_{28}$ ααα 20S Ergostane	*m/z* 386→217	C28ααα 20S
C$_{28}$ αββ 20R Ergostane	*m/z* 386→217	C28αββ20R
C$_{28}$ αββ 20S Ergostane	*m/z* 386→217	C28αββ20S
C$_{28}$ ααα 20R Ergostane	*m/z* 386→217	C28ααα 20R
C$_{28}$ 21-nor Ergostane	*m/z* 386→217	C28nor21
C$_{29}$ 13β 17α dia 20S	*m/z* 400→217	C29βα20S Dia
C$_{29}$ 13β 17α dia 20R	*m/z* 400→217	C29βα20R Dia
C$_{29}$ ααα 20S Stigmastane	*m/z* 400→217	C29ααα20S
C$_{29}$ αββ 20R Stigmastane	*m/z* 400→217	C29αββ20R
C$_{29}$ αββ 20S Stigmastane	*m/z* 400→217	C29αββ20S
C$_{29}$ ααα 20R Stigmastane	*m/z* 400→217	C29ααα20R
C$_{30}$ 13β 17α 20S Diasterane	*m/z* 414→217	C30βα20S Dia
C$_{30}$ 13β 17α 20R Diasterane	*m/z* 414→217	C30βα20R Dia
C$_{30}$ ααα 20S Sterane	*m/z* 414→217	C30ααα20S
C$_{30}$ αββ 20R Sterane	*m/z* 414→217	C30αββ20R
C$_{30}$ αββ 20S Sterane	*m/z* 414→217	C30αββ20S
C$_{30}$ ααα 20R Sterane	*m/z* 414→217	C30ααα20R

In this study, the authors established relationships of regular steranes and associated source-rock

application of pregnane biomarkers is to fingerprint sulfur-rich heavy crude oils produced from

lithology, which provides a tool for correlation purposes (Moldowan et al., 1985). Moreover, crude

oil produced from Jurassic sandstone reservoirs in the Inner Moray Firth Basin was correlated with both contribution from Jurassic Kimmeridge Clay and Middle Devonian lacustrine sources, this correlation was achieved by utilizing a number of molecular markers, among them regular steranes, and their relation to diasteranes, with bitumen extracts from Kimmeridge Clay exhibiting an enriched fingerprint of C_{28} regular sterane relative to C_{29} and C_{27} (Peters et al., 1989). Another the Bohai Bay Basin of East China; these oils have been identified as sourced from Eocene lacustrine carbonate source rocks (Wang et al., 2010).

Diamondoids

Diamondoids are a broad compound-class also known as polymantanes, which are saturated hydrocarbons with a fused cage-like structure, with adamantane constituting the smallest single cage member. Adamantane ($C_{10}H_{16}$) is the building block unit within a diamond lattice structure. The nomenclature comes from the Greek word for "diamond gemstone," which is *adamas* (Αδάμας). By definition, diamondoid molecules are hydrocarbons possessing one adamantane unit or more, which can be superimposed on the diamond lattice (Balaban and Ragé Schleyer, 1978) (Figure 26). In addition to adamantanes, diamondoids as compounds can include two cages (diamantanes), three cages (triamantane), and extended diamondoids of four cages (tetramantanes), five cages (pentamantane) six-cages (hexamantanes) and so on. Listed in Table 5 are some physical properties of lower and higher diamondoids. Diamondoids are normally measured using GC-MS operated on SIM mode, and quantification is achieved using deuterated-diamantane. Care must be taken to achieve a representative diamondoids analysis, especially for those compounds that are susceptible to evaporation loss and occur in trace amounts. Therefore, unique and careful segregation methods for sample preparation is crucial (Moldowan, personal

communication). Some of the diagnostic ions include (*m/z* 135, 136, 149) for adamantanes and alkylated counterparts (*m/z* 188, 201) for diamantanes. The use of GC-MSMS run on MRM can be used for the measurement of diamondoids, especially with samples with trace amounts of diamondoids, such as black oils and rock extracts. However, GC-MSMS is reported to be useful only in measurement of adamantanes and diamantanes, while extended polymantanes require sample preparation prior to analysis. Some of the diagnostic precursors to product transitions are *m/z* 136→93 for adamantane, and *m/z* 188→131 for diamantane (Liang et al., 2012).

Unlike biomarkers, the origin of diamondoids is not clearly related to a biological precursor capable of synthesizing a cage-like carbon skeleton compounds. This lack of capability is partly because diamondoids are not observed to be produced in modern sediments, and occur only in
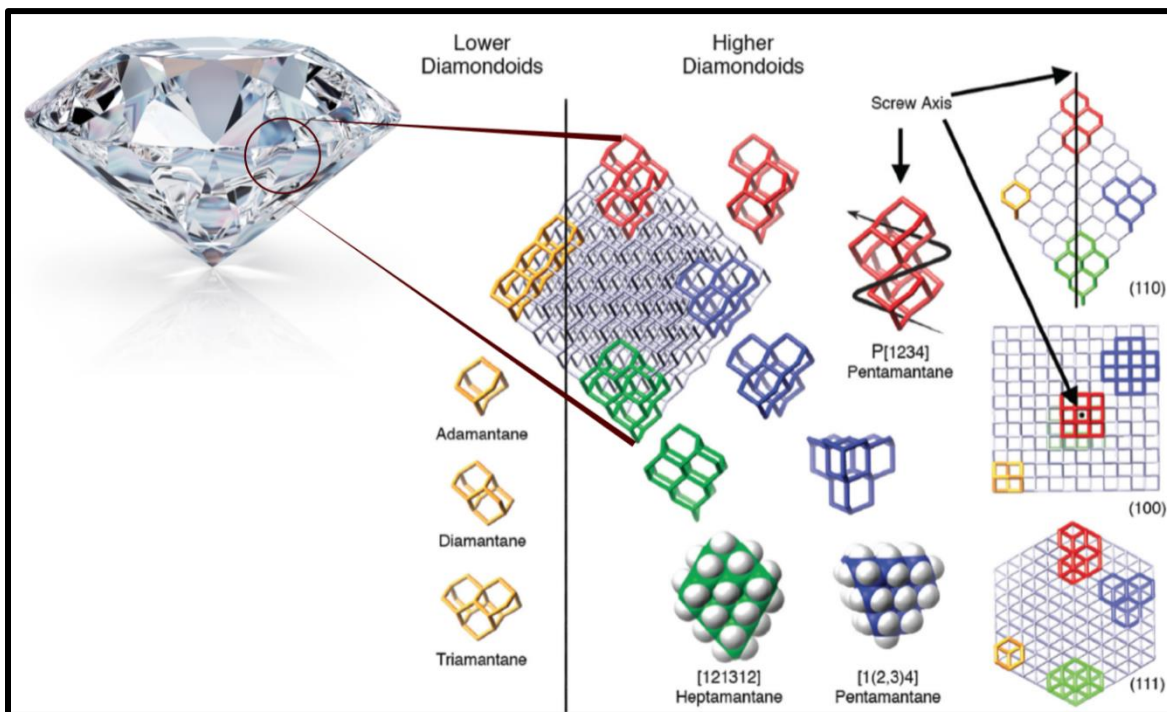
Figure 26: Diamondoids structure relative to diamond lattice. Showing in yellow are the lower diamondoids, including adamantane, diamantane and trimantane, with most predominant occurrence in crude-oil and rock extracts. Higher diamondoids (extended diamondoids) include diamondoids with four or more cages. Modified from (Dahl et al., 2003).

trace amounts in association with thermogenic petroleum seepages. It has been suggested that diamondoids originate within the framework of complex kerogen as a function of clay catalysis and thermal maturation, particularly due to carbonium ion mechanisms resulting from Lewis acid sites during interaction between rock minerology and kerogen matter (Wei et al., 2006). Moreover, Wei et al. (2006) conducted hydrous pyrolysis experiments of different types of pure kerogen with the presence of different types of clay minerals. These authors suggested that diamondoids are observed to form in abundance as a function of maturation, surface acidity and clay minerology. Additionally, montmorillonite (K10) and acidic aluminosilicate (MS-25) were reported to have the largest yield of diamondoid, while calcium carbonate hindered the yield of diamondoids during an artificial maturation experiment using hydrous pyrolysis technique (Wei et al., 2006). Beyond the natural occurrence of diamondoids, the first successful artificial synthesis of adamantine was achieved by Prelog and Seiwerth in 1941, with limited yield percentage. Further improvement in diamondoid synthesis methods and yield percentage has since been achieved, primarily by carbocation equilibration reactions, which are adequate only for synthesis of lower diamondoids, up to tetramantanes, with a four-cages structure (Hartmut et al., 2008). Synthesis of higher diamondoids remains challenging and requires further research, but Dhal et al. (2003) were able to isolate higher diamondoids from condensates, which sparked the impetus among chemists for synthesizing higher diamondoids through unconventional methods such as electric discharge microplasmas in supercritical fluids (Oshima et al., 2012), pulsed laser ablation plasma (Nakahara et al., 2011), and atmospheric-pressure microplasmas (Sven et al., 2014).

Due to diamondoids' exceptional thermal stability, application of diamondoids in petroleum geochemistry is usually associated with thermally mature hydrocarbons. In 1999, Dahl et al. introduced the concept of assessing the extent of natural petroleum cracking. This assessment

is achieved by comparing a set of diamantane isomers with stigmastane biomarker as a molecular indictor to detect uncracked black oils, cracked petroleum (i.e. condensates) and mixed fluids of cracked and uncracked hydrocarbons (Dahl et al., 1999b). Schulz et al. (2001) used diamondoids to infer source-rock facies by comparing the relative abundance of three isomers of dimethyl diamantanes to distinguish different kerogens' contributions (e.g. II-carbonate, Type-II marl and Type-III) (Schulz et al., 2001). Moreover, the authors examined 64 oil and condensate samples from an offshore Norway Province and extracted rock bitumen ranging in age from Carboniferous to Upper Jurassic. They observed a unique enrichment in 3,4-dimethyldiamantane (3,4DMD) relative to 4,8-dimethyldiamantane (4,8DMD) and 4,9-dimethyldiamantane (4,9DMD) in Type-III kerogens, while carbonate Type-II source rocks exhibited enrichment in 4,8DMD relative to the rest of the dimethyldiamantane isomers (Schulz et al., 2001). Another use of diamondoid to identify oil-sourcing has been introduced by Moldowan et al. (2017), who used quantitative extended diamondoid analysis (QEDA) and CSIA of diamondoids (CSIA-D). Quantitative extended diamondoid analysis is essentially a fingerprint reflecting the abundance of extended diamondoids relative to triamantane; these extended diamondoids include different isomers of tetramantanes and pentamantanes together with cyclohexamantane (Moldowan et al., 2015). Quantitative extended diamondoid analysis was utilized to correlate cracked and uncracked marine sourced oils from the Santos Basin, Brazil (Moldowan, 2014). Compound-specific isotope analysis of diamondoids is another approach using diamondoids for correlation purposes, achieved through the isolation of adamantanes, diamantanes, triamantanes and their alkylated counterparts, to measure stable carbon isotopes (δ^{13}C) for individual diamondoid compounds. Compound-specific isotope analysis of diamondoids was applied successfully to a collection of fluid samples, which were grouped based on CSIA-D fingerprint into two petroleum systems in the West Siberian Basin.

Those two petroleum systems were sourced from the Middle-Lower Jurassic Tyumen Formation, and the Upper Jurassic Bazhenov Formation. Tyumen soured fluids were cracked hydrocarbons, which are impossible to geochemically correlate due to the absence of biomarkers at such elevated thermal maturity. With the use of CSIA-D, Tyumen fluid exhibited an isotopically heavier diamondoid fingerprint than that of Bazhenov-sourced hydrocarbons (Moldowan, 2011; Moldowan et al., 2015). The application of diamondoids analysis proved to be insightful on a number of crude-oil samples from the Timan-Pechora Basin, Russia. Diamondoid analysis helped to classify cracked hydrocarbons, and with the identification of a hydrocarbon mixture originating from low and high thermal maturity levels (Schever, 2012). Overall, diamondoids are exceptionally useful geochemical tools for source maturity assessment. . This is usually attributed to the stability of the cage-carbon structure, which exhibits thermal and kinetic stabilities. Even though they are considered one of the underutilized geochemical tools in petroleum- and basin-modeling studies, their future use holds great potential, especially with the emerging unconventional hydrocarbon systems, where light hydrocarbons are produced (Moldowan et al., 2015).

In addition to the application of diamondoids in petroleum geochemistry, they are also used in different industries, such as nanotechnology, material and biomedical sciences. In nanotechnology, diamondoids can be used for purposes related to self-assembly, positional assembly and nanofabrication (Ramezani and Mansoori, 2007). In material science, diamondoids play an important role in the modification of polymers, copolymers, nanocomposites and crystal

Table 5 Lower and higher diamondoids and key physical properties, after (Mansoori et al., 2014)
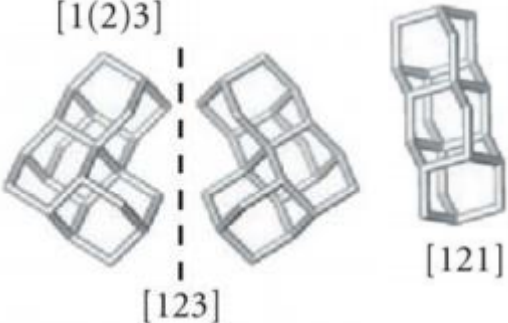
Diamondoid Chemical Formula	Molecular Structure	Molecular Weight	Melting Point [C °]	Normal Density [g/cc]	Crystal Structure
Adamantane $C_{10}H_{16}$		136.240	269	1.07	Cubic, fee
Diamantane $C_{14}H_{24}$		188.314	236.5	1.21	Cubic, Pa_3
Triamantane $C_{18}H_{24}$		240.390	221.5	1.24	Orithorhombic, Fddd
Tetramantanes $C_{22}H_{28}$		292.466	[1(2)3]:NA [123]: NA [121]:174	[1(2)3]:NA [123]: 1.32 [121]:1.27	[1(2)3]: NA [123]: Triclinia, [121]: Monoclinic, $P2_1/n$

[1(2)3]

[123]

[121]

Table 5 continued.

Diamondoid Chemical Formula	Molecular Structure	Molecular Weight	Melting Point		Diamondoid Chemical Formula
Pentamantanes $C_{26}H_{32}$	[12(3)4] [1(2,3)4] [1213] [1212] [12(1)3] [1234]	344.543	NA	[1212]:1.26 [1234]:1.30 [1(2,3)4]:1.33 [12131]:1.36	[1212]: Orthorhombic, $P2_12_12_1$ [12(3)4]: Monoclinic, $P2_1/n$ [1(2,3)4]: Triclinic, P-1

Table 5 continued.

Diamondoid Chemical Formula	Molecular Structure	Molecular Weight	Melting Point		Diamondoid Chemical Formula
Cyclohexamantane C$_{26}$H$_{30}$	Top Side [12312]	342.528	>314	1.38	Orthorhombic, Pnma
Heptamantanes C$_{30}$H$_{34}$	[121321] [123124]	394.602	NA	1.35	[121321]: Monoclinic, C2/m (#12)

engineering, among other applications within the field of material science. For example, the thermal stability of polymers has been achieved by incorporating polymer with acetylene-terminated adamantanes (Burnham et al., 2006). Biomedical application of diamondoids represents a major industry for diamondoid technology, as marked by number of patents filed, with 11–23% of total patents filed for biomedical application (Mansoori et al., 2014). Diamondoid application in biomedical science is primarily focused on drug delivery. Moreover, an adamantane-based drug commercially known as SQ109 is used in treating advanced stages of re-emerging tuberculosis, caused by exposure to *Mycobacterium tuberculosis*. The drug SQ109 is composed of an adamantane carbon backbone with a side chain containing amine monomers, myrtanylamine and isopinocamphylamine and isoprenoid structures (2-adamantyl; ethane-1,2-diamine) (Sacksteder et al., 2012). Adamantane molecules are also used in oncology, particularly the adamantly ester of tyrphostin (adaphostin), which experimentally showed great potential for treating both myelogenous leukemia and chronic lymphoblastic leukemia (Figure 27) (Shanafelt et al., 2005; Svingen et al., 2000).
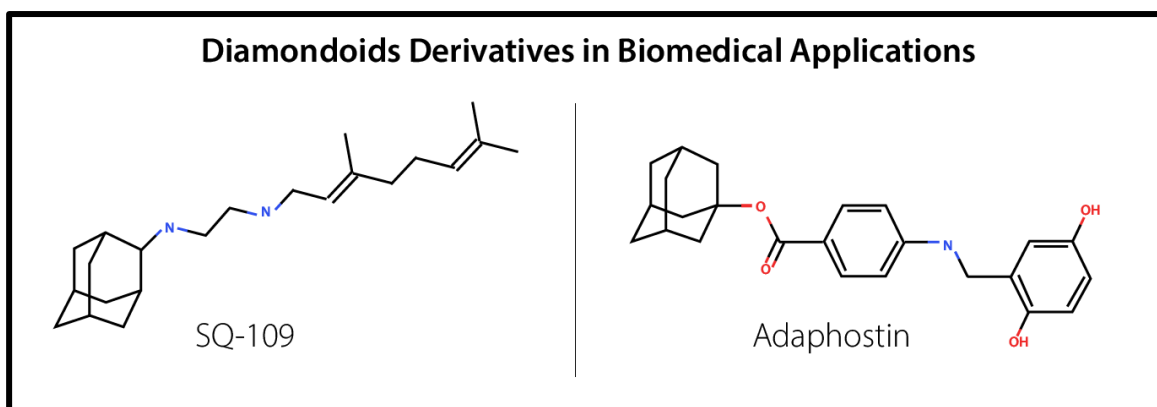
Figure 27: Example of adamantane-based compound structures. Left is (2-adamantyl)ethane-1,2-diamine, known as SQ-109 used to treat tuberculosis (Sacksteder et al., 2012). Right is (1-Adamantyl) ethylenediamine known as Adaphostin, which showed potential for targeted treatment in different leukemia types (Svingen et al., 2000).

Aromatic Hydrocarbons

Aromatic hydrocarbons represent a compound class that is found in abundance in both crude-oil and rock extract, with a chemical structure containing one or more benzene rings. Aromatic hydrocarbon fraction includes, benzene, naphthalene, polycyclic aromatic hydrocarbon and cycloalkanoaromatics (i.g. mono- and triaromatic steroids). Additionally, organo-sulfur compounds such as benzothiophenes, and porphyrins can also be classified as aromatic hydrocarbons. Measurement of aromatic hydrocarbons is done by running GC-MS on SIM mode and monitoring for diagnostic mass-chromatograms like m/z142 for naphthalenes, and m/z192 for phenanthrenes (Peters et al., 2005d). Figure 28 shows different classes of aromatic hydrocarbons that are routinely measured in petroleum geochemistry studies, including naphthalenes, phenanthrenes and dibenzothiophenes.

Aromatic hydrocarbons are formed by diagenetic transformations of natural hydrocarbon product as a function of thermal maturation; such alteration can be manifested as ring opening, alkylation, dealkylation and isomerization (Peters et al., 2005d and references therin). Moreover, living organisms do not biosynthesize aromatic hydrocarbons in adequate abundance to be accounted as aromatic compounds found in petroleum. Therefore, most aromatic compounds are believed to be a byproduct of thermal alteration as opposed to being biologically derived. However, aromatization of certain compounds can still hold value in determining organic-matter sources. For example, aromatic hopanoids are indicative of bacterial organic-matter contribution, while aromatized terpenoids such as retene are indicative of terrigenous organic matter (Alexander et al., 1992; Killops, 1991). Similarly, triaromatic dinosteroids are believed to coincide with the fossil record of dinoflagellate cyst diversity; therefore, triaromatic steroids are considered an age-biomarker indicating marine pre-Triassic source-rock contribution (Moldowan et al., 2001).

Moreover, aromatic steroids have also been utilized as indicators of source-rock lithology and
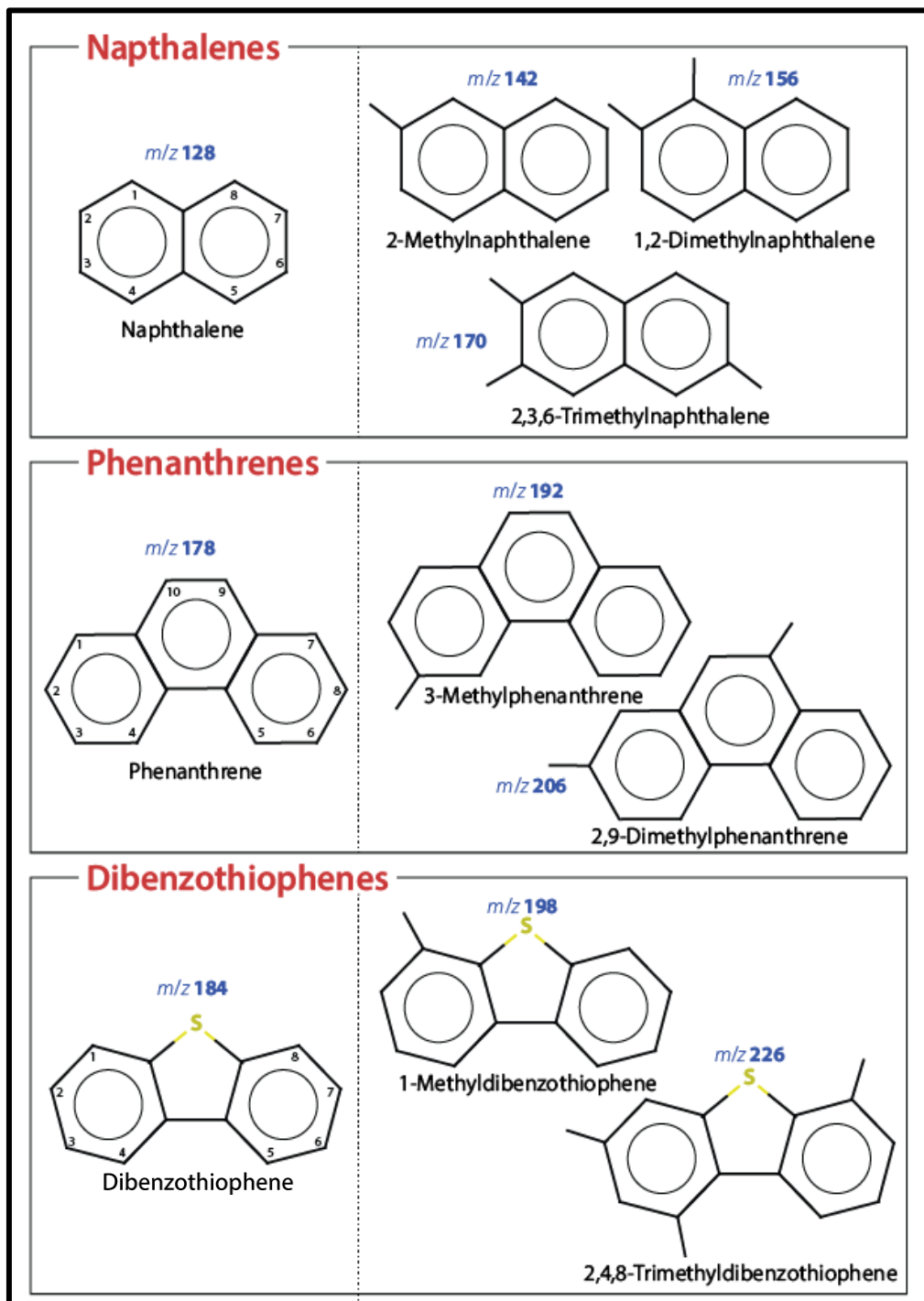
Figure 28: Examples of aromatic hydrocarbons that are routinely measured in petroleum geochemistry including napthalenes, phenanthrenes and dibenzothiophenes. Napthalenes and phenanthrenes are usually used for maturity assessment, whereas dibenzothiopenes are usually used in defining source-rock

depositional environment settings, in an fashion analogous to regular sterane ternary diagrams (Moldowan et al., 1985). Hughes (1984) introduced the concept of comparing a different set of aromatic compounds (i.e., phenanthrene and dibenzothiophene) in conjunction with pristane and phytane ratio to predict source-rock depositional environment, with carbonate source rocks associated with enrichment in organosulfur compounds such as dibenzothiophenes. Aside from organosulfur aromatic compounds, fluorenes and dibenzofurans together with other aromatic compounds have been examined and can reflect the disparity of organic-matter input, primarily depicting marine versus terrigenous (Pu et al., 1990). Most importantly, kerogen aromaticity as a mechanism is sensitive to thermal maturation, so aromatic hydrocarbons are useful indicator in the
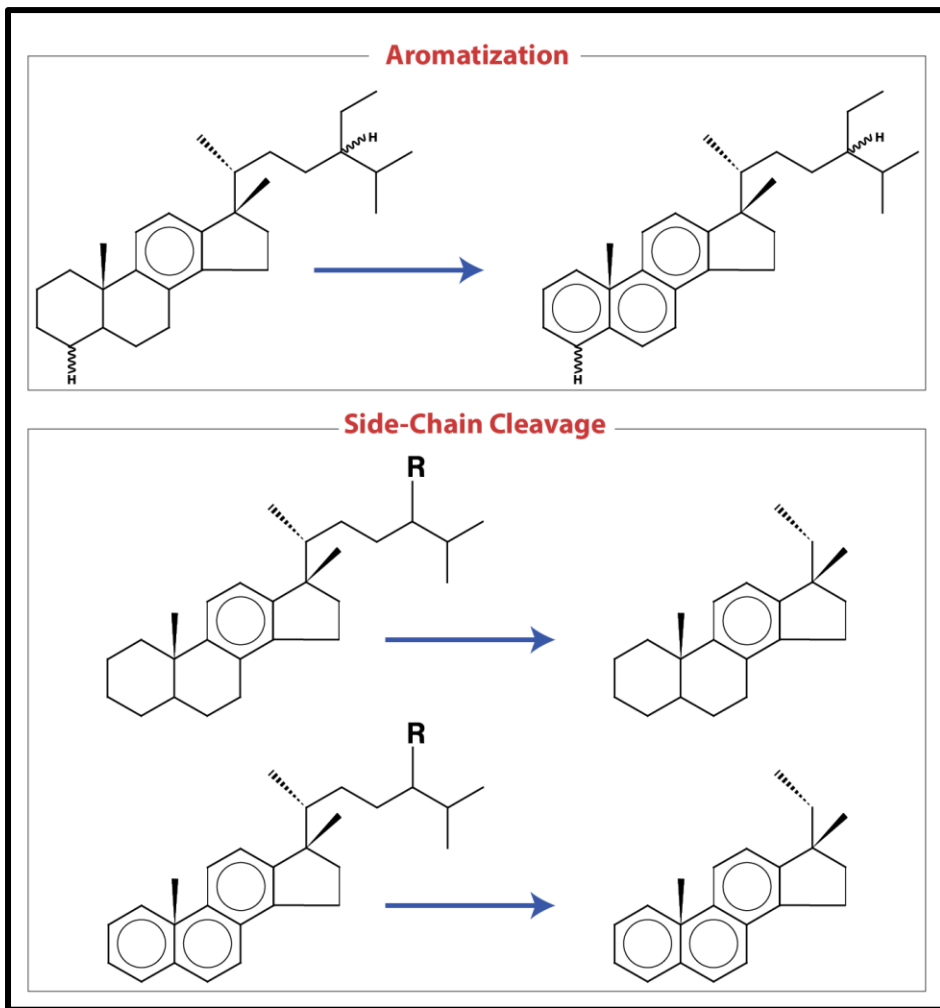
Figure 29: Proposed destructive alteration on aromatic steroids as a function of thermal maturation including aromatization and side chain cleavage. R = H, CH3, C2H5. Proposed side chain cleavage includes monoaromatic steroid and triaromatic steroid (Beach et al., 1989; Mackenzie et al., 1982b).

evaluation of fluid maturity (Radke et al., 1982a). A number of studies have investigated different aromatic maturity indicators, such as the methylphenanthrene index or a set of alkylated naphthalenes ratios (Alexander et al., 1985; Alexander et al., 1983; Radke et al., 1982a). Additionally, aromatic steroid biomarkers are used in evaluating thermal maturity, which can be achieved with two approaches. First, by comparing the relative abundance of mono-aromatic steroids relative to the triaromatic steroids, with the concept of increasing maturity, aromaticity will increase from one benzene ring to three benzene rings (Mackenzie et al., 1982b). The second approach compares relative abundance of short-chain aromatic steroid to the long-chained counterparts, with the rationale that increasing thermal maturity will result in the cleavage of the side chain, producing dominance of the short-chained aromatic steroids (Beach et al., 1989) (Figure 29).

Application of aromatic hydrocarbons is crucial in petroleum systems studies for both source and maturity assessment. Aromatic hydrocarbons have been used as a tool to identify hydrocarbon mixing to discriminate between two different petroleum systems within the Eromanga Basin, Australia (Arouri and McKirdy, 2005). More specifically, the examined aromatic compounds included 1,2,5-trimethylnaphthalene, 1-methylphenanthrene, 1,7 dimethylphenanthrene and retene; all collectively proved served as a useful tool to differentiate between Cretaceous- and Permian-sourced oils (Al-Arouri et al., 1998; Arouri and McKirdy, 2005). Another study within the Williston Basin utilized aromatic and saturated hydrocarbon to differentiate between Bakken and Lodgepole bitumen extracts, with Lodgepole rocks showing an abundance of benzohopanes together with monoaromatic tetracyclic hydrocarbons; such fingerprints were assessed by identifying petroleum systems within the Williston Basin (Jiang et al., 2001). Furthermore, the authors extended work done on rock extracts to oils produced from

the Winston Basin on both the Canadian and the American sides. Bakken petroleum systems were evidenced to extend to Madison-reservoired oils; the authors were able to refine the Bakken oil fingerprint utilizing a collection of molecular markers, some of which included aromatics compounds such as alkylbenzenes, biphenyls, diphenylmethanes, tetramethylnaphthalenes and dibenzothiophenes. As for maturity assessment, the triaromatic steroid ratio (TAS) was used at the Fort Worth Basin, north-central Texas, for a group of crude oil, core and cuttings from marine Mississippian Barnett Shale. Because of the effect that thermal maturity can induce on source-related biomarkers, Hill et al. (2007) utilized triaromatic steroid as a qualifier for screening for thermally unaltered oils, for more accurate oil–source correlation. Thiophenic compounds are used to assess the thermal maturity of different oil and rock extracts from the Trim and Liaohe Basins in China (Li et al., 2013; Zhang et al., 2005). Such ratios compared dibenzothiophenes with their alkylated counterparts, which showed a linear relationship with other aromatic parameters such as the methylphenanthrene index, and therefore were used to infer vitrinite reflectance values for crude oils. Overall, aromatic hydrocarbons are useful tools in petroleum geochemistry and petroleum systems analysis, due to their sensitivity to organic-matter type and to thermal maturity.

Petroleum Migration Milometers

Petroleum migration is one of the more complex processes in petroleum systems analysis, as it is associated with many factors through geological time that are difficult to predict and measure accurately (England et al., 1987). However, a number of models have been proposed in petroleum systems and basin modeling software packages (e.g. PetroMod) in which a deterministic and mathematical models are constructed based on physical principles (Hantschel and Kauerauf, 2009). Another approach in estimating petroleum migration is the measurement of certain compounds in crude oil that are sensitive to migration distance. Geochemists have proposed a

number of different oil tracers to estimate both primary and secondary petroleum migration. In 1980, Espitalie et al. first documented the retention of heavy hydrocarbon in clay minerals as petroleum interacts with rocks. Since then, a number of geochemical studies have aimed to understand this phenomenon of petroleum-compositional change as function of migration distance. For example, crude oils and bitumen from Japan and Sumatra were investigated with particular focus on nitrogen-containing organic compounds. Yamamoto (1992) observed a selective removal of specific compounds as petroleum interacted with clay or water. Neon and argon isotopes partitioned from groundwater and migrating petroleum, and based on mass-balance calculation volumes of interacting oil during secondary petroleum migration, were estimated for the Magnus oilfield, within Shetland Basin in the North Sea (Ballentine et al., 1996). Larter et al. (1996) conceived petroleum chemical odometers (milometers), in which they proposed certain carbazole ratios to estimate petroleum secondary migration.

Carbazoles

Carbazoles are a class of hydrocarbons composed of two benzene rings fused into cyclopentane-ring containing nitrogen (Figure 30). The general formula for the main carbazole compound is $C_{12}H_9N$, which naturally occurs in petroleum and rock extracts. Furthermore, a series of alkylated carbazoles are found to extend from C1 to C7, with diagnostic ions ranging from *m/z* 167 to 265 (Li et al., 1992). Moreover, benzocarbazoles are another subclass of carbazoles compounds consisting of the main carbazole skeleton with an extra benzene ring, resulting in three benzene rings bounded to a five-membered nitrogen-containing ring, with a formula of $C_{16}H_{11}N$ (Figure 30). Benzocarbazoles occur in three isomers, including benzo [a] carbazole, benzo[b]carbazole and benzo[c]carbazole, with benzo[a] and benzo[c] carbazole isomers prevailing in fluid and geological samples. Measurement of carbazole compounds is achieved

using GC-MS running in SIM mode, but samples require specialized sample preparation prior to GC-MS analysis. Due to carbazole polarity, those compounds are usually eluting with resins (NSO) compounds during liquid-chromatography separation for saturate, aromatic resins and asphaltene analysis (SARA). Therefore, samples require solid-phase extraction (SPE) for selectively isolating carbazoles from crude oil and rock extracts (see Chapter III for further detail).

The first documentation of nitrogen compounds in petroleum is recorded in a study by Lotchte and Littmann (1955). In particular, carbazole compounds were observed in petroleum samples in early 1980s (Dorbon et al., 1982; Dorbon et al., 1984). In general, the origin of nitrogen-containing organic compounds in petroleum and rock extracts can be explained in three possible ways, according to Shmitter and Arpino (1983): first, the alteration of biologically synthesized
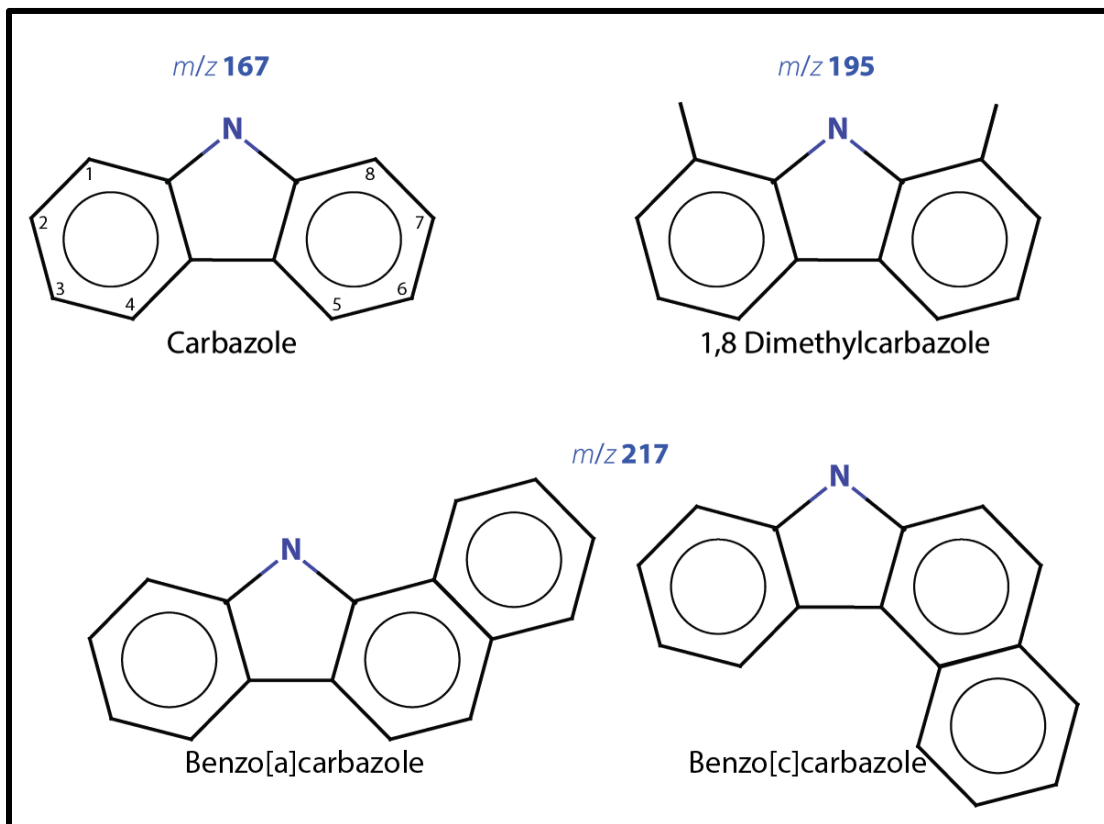
Figure 30: Main carbazole skeleton structure, with some example, alkylated carbazole compound and most abundant benzocarbozoles found in petroleum and rock extracts.

compounds containing pyridine rings such as alkaloids, which are produced by higher plants;

80

second, through alteration of other ring systems such as pyrrole; and third, cyclization of acyclic compounds and incorporation of nitrogen through the reaction of ammonia with a dioxo group (Brody and Ruby, 1960; Schmitter and Arpino, 1983). Another source of nitrogen-containing organic compounds is the breakdown of peptide groups into sediments and subsequent diagenetic degradation, and ultimately the incorporation of these sediments into nitrogen heterocyclic structures bounded to the kerogen matrix (Tissot and Welte, 1984). Overall, a clear biological precursor relationship for carbazoles remains unclear, so the carbazole specificity for organic input is poor. It is postulated, however, that carbazoles are formed during petroleum generation, are sensitive to source-rock lithology and are affected by thermal maturation. For example, crude oil and pyrolysate of Phosphoria Shales are observed to contain higher quinolines, benzoquinolines and carbazoles than those of oils originating from limestone source rocks (Bakel and Philp, 1990).

The application of carbazoles in petroleum systems studies is critical as an oil migration distance estimator (milometer). A collection of marine and non-marine crude oils from Japan and Indonesia was observed to vary in alkylquinolines and alkylcarbazoles relative to the oils' isomers homologues, interpreted to indicate petroleum-migration direction and distance (Yamamoto, 1992). However, in this study, differentiation of primary migration and secondary migration was not clearly defined, together with the influence of thermal maturation on masking alkylquinoline and alkylcarbazole ratios. Therefore, benzocarbazole ratio (BC ratio) was proposed to be sensitive to secondary petroleum migration and minimally influenced by thermal maturity (Larter et al., 1996). The BC ratio is calculated by the following relationship: benzo[a]carbazole/(benzo[a]carbazole+benzo[c]carbazole (BC ratio). Larter et al. (1996) used the BC ratio to estimate petroleum-migration distance in two petroleum systems of in Western Canada and three petroleum systems from the North Sea Province. In this study, crude-oil samples were

of different maturities, with estimated migration distances reaching up to 900 km. Authors argue that non-alkylated benzocarbazoles isomers are more stable than alkylated counterparts, making benzocarbazoles a maturity-independent parameter. During secondary migration of petroleum, it is suggested that selective removal of rod-shaped benzo[a]carbazole relative to sub-spherical benzo[c]carbazole takes place by means of sorption of benzocarbazole into clay minerals and kerogen contained in carrier beds (Larter et al., 1996). In a recent study, the petroleum-filling sequence of different oil fields has been achieved utilizing BC ratios of crude oils within the Jurassic Hanifa and Tuwaiq Mountain petroleum system, Saudi Arabia (Yang and Arouri, 2016). Authors examined oil samples from five different oil fields within the Gotnia Basin, previously thought of to have resulted from the spill-and-fill sequence, from north to south, of a single petroleum-migration pathway. However, after utilizing the BC ratio, the authors suggested multiple migration pathways, which improved petroleum-migration modeling, and increased petroleum prospectivity in unexplored regions by lowering hydrocarbon-charge risk (Yang and Arouri, 2016).

Phenols

Phenols are broad class of aromatic hydrocarbons containing a hydroxyl group, with phenol as the simplest compound in this class, consisting of a benzene-ring bounded to a hydroxyl group (Figure 31). Alkylated counterparts are found to occur naturally in petroleum and in sedimentary organic matter. Of particular interest to our study are cresols (also known as hydroxytoluenes), which exhibit a similar structure to phenol, with an additional methyl group. Cresols are found in three main isomers: *o*-cresol, *m*-cresol and *p*-cresol. Overall, phenol exhibits higher solubility in water, due to the benzene and the hydroxyl group. Measurement of phenols are not normally performed by traditional petroleum geochemistry analysis, and just like carbazole measurement of

phenol, such investigation requires specialized sample preparation prior to analysis on GC-MS. One approach for sample preparation suggests derivatization of crude oils prior to analysis. Derivatization is achieved by heating the sample in sealed vials with the presence of derivatizing agent, catalyst and other additives to facilitate the reaction (Galimberti et al., 2000). This analytical approach requires elaborate sample preparation and is time consuming, with 3 h treatment time per sample. However, a more rapid and chromatography-based analytical procedure has been proven more efficient in the preparation of crude-oil and rock-extract samples for phenol measurement (Bastow et al., 2003). After sample preparation, quantitative measurement of phenols is achieved by operating GC-MS in SIM mode and monitoring for diagnostic ions such as *m/z* 94 and *m/z* 108.

Phenols are observed in different biological and geological samples. For example, phenols are biosynthesized by lower and higher plants together with algae (Cheynier et al., 2013). Phenols are also observed in the sedimentary organic matter of different ages and depositional settings (Bastow et al., 2003; Derenne et al., 1990). Phenolic compounds also occur in higher abundance
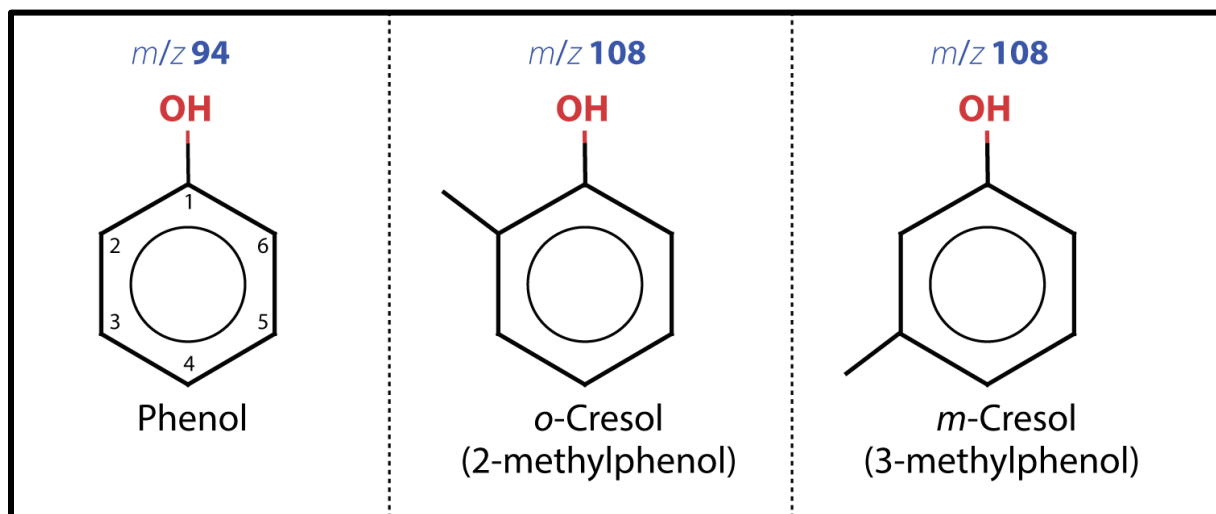
Figure 31: Main phenol skeleton structure, with the major alkylated phenol compounds and most abundant in petroleum and rock extracts including *o*-cresol and *m*-cersol.

than do bituminous coals (Levine et al., 1982). In crude oil, phenols can be source related, or can be enriched due to secondary oil alteration processes. Work done by Ioppolo et al. (1992) identified a series of phenols in crude-oil samples obtained from number of Australian basins ranging in age from Ordovician to Cretaceous. The oils included coaly, marine and lacustrine organic-matter-derived oils, with phenols being enriched in coaly sourced oils followed by marine oils, with trace amounts in lacustrine derived oils (Ioppolo et al., 1992). Furthermore, phenol can be enriched due to secondary oil alteration processes such as biodegradation, water washing and petroleum secondary migration (Meredith et al., 2000; Taylor et al., 1997). Therefore, the ubiquitous occurrence of phenols from different kerogens together with secondary alteration of petroleum together make phenols a poor organic-matter-specific indicator, and hence are used in this study only as a petroleum-migration tracer and, particularly, as water-washing tool.

Application of phenols in petroleum system studies is focused on tracing oil migration direction, together with water washing. It has been suggested that phenols partitioning between oil and water occur in petroleum systems during petroleum's secondary migration through carrier beds (Taylor et al., 1997). Therefore, phenols tend to decrease in concentration in petroleum masses that have traveled 10s of kilometers. Unlike carbazoles, research on phenols as milometers remains in its early-stages, so the ratio of specific distances to phenols has not been investigated (Larter and Aplin, 1995). Moreover, phenols exhibit high aqueous solubility and a low partitioning coefficient, as evidenced by formation of water associated with active petroleum systems (Dale et al., 1995). In the North Sea, phenols have been used to delineate petroleum-migration paths from the kitchen province by examining the relative abundance of phenol to alkyl phenols (Galimberti et al., 2000). The molecular migration index (MMI) is a ratio calculated by comparing concentrations of *o*-cresol to phenol, tending to increase with increasing migration distance

(Galimberti et al., 2000). An experimental study of water-washing experiments of crude-oil under controlled lab conditions found that water washing of petroleum can be traced by the relationship of phenol to cresol, calculated by comparing the concentration of phenol relative to the sum of cresols (Peters et al., 2018).

CHAPTER III

SAMPLING AND ANALYTICAL PROCEDURES

Rock and Crude-Oil Sampling

The study area is located in North-Central Oklahoma covering eastern-edge of the Anadarko Basin and Shelf, together with the Nemaha Uplift province and the western-edge of the Cherokee Platform (Figure 32). Three type of samples were examined in this study, including rocks, crude-oils and fluid inclusions. The analytical workflow used for all sample types in this study is illustrated in more detail in Figure 33.
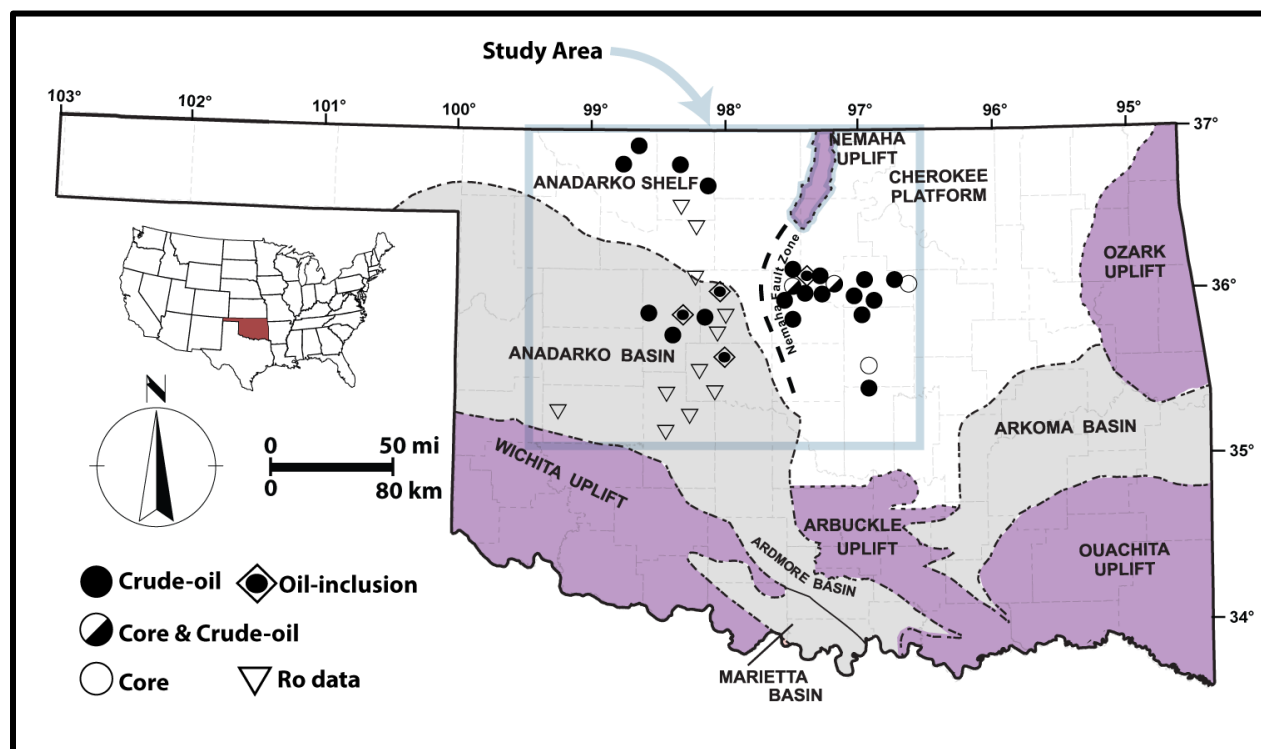
Figure 32: Study area map showing sample's location. The study area includes Anadarko Basin and Shelf, together with Nemaha-uplift and Cherokee Platform. Geographic distribution of sampled oils, rocks and oil incisions can broadly divided into three provinces: the Sooner Trend Anadarko Basin Canadian and Kingfisher Counties (STACK) play, the Anadarko Shelf and central Oklahoma. Vitrinite reflectance values are taken from published literature (Pawlewicz, 1990)
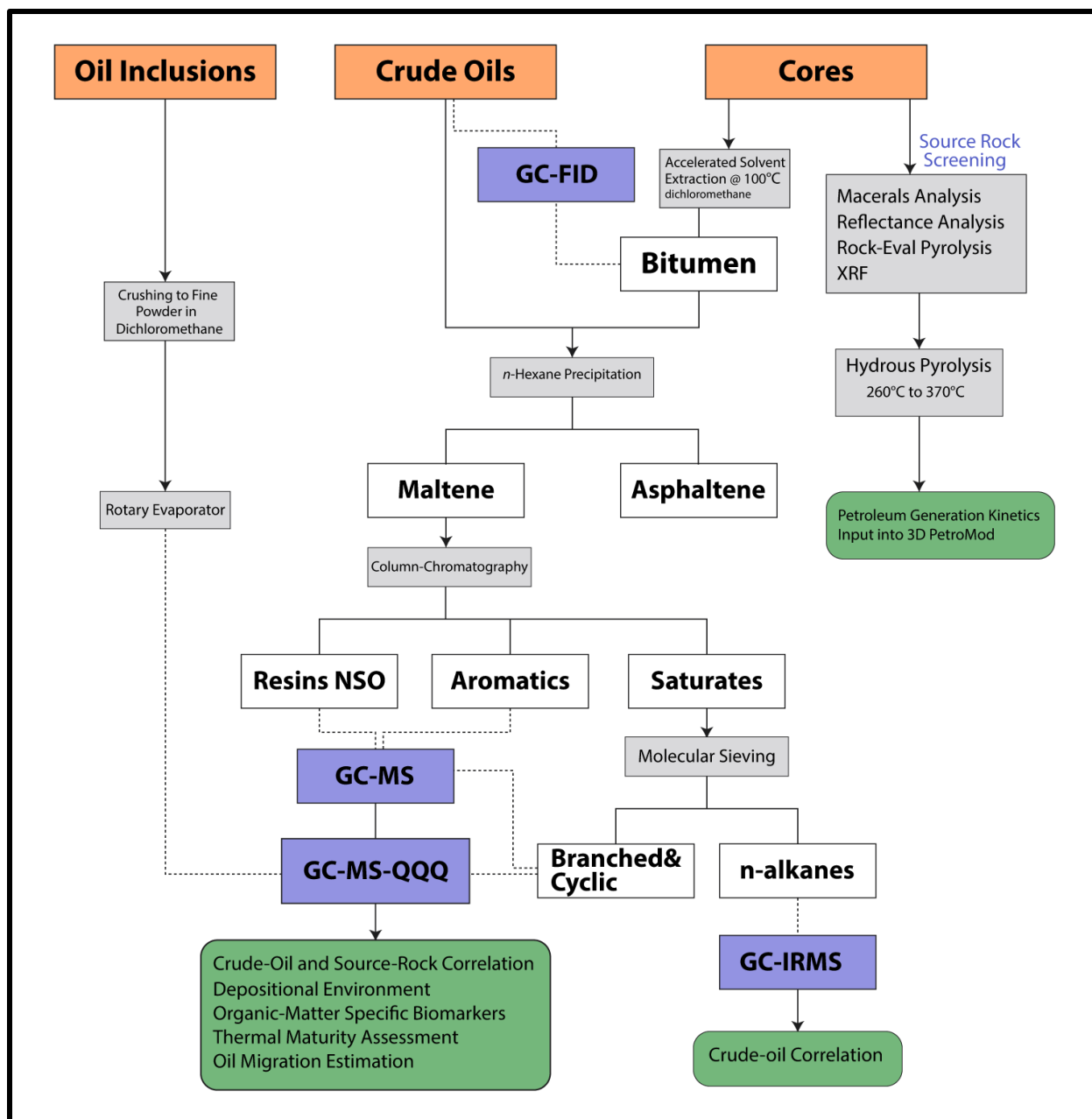
Figure 33: Schematic of this study's analytical lab workflow. Blue rectangules indicate instruments including GC-FID: gas chromatograph equipped with flame ionization detector (FID); GC-MS: gas chromatograph equipped with mass spectrometer; GC-MS-QQQ: gas chromatograph equipped with triple quadrupole mass spectrometer (also known as GC-MS/MS); and GC-IRMS: gas chromatograph equipped with Isotope-ratio mass spectrometry. Gray rectanglues mark sample-preperation process, and green rouded rectangule indicate results application, XRF: X-ray fluorescence.

Rock samples were collected from five different cores, with a total of 98 rock samples. Since rocks were collected from cores, this eliminates the possibility of any contamination effect normally associated with cutting samples drilled with oil-based drilling mud. Detailed information about the studied core samples is shown in Table 6. The key core for this study is located in Lincoln County (LNK), which contains a complete core of the Mississippian carbonate and Woodford Shale sections. Additionally, the LNK core is located (Figure 34) in a marginally mature (0.49%R_o) province (Cardott, 2012), ensuring that any kerogen alteration due to thermal maturation is minimal. Therefore, LNK was selected for further maceral examination, together with core description and minerology analysis. The other cores, located in Payne and Logan counties, were sampled to evaluate organic richness and kerogen type in the Mississippian and Woodford.

Stratigraphic intervals samples included mudrock intervals within the lower section of the Mississippian carbonates and upper and middle Woodford Shale. Mississippian rocks encompass late Kinderhookian to early Chesterian; it is referred to the sampled section as the lower Mississippian mudrocks. This adapted nomenclature is used primarily for two reasons: first, the lack of a well-established biostratigraphic framework, and second, the lack of regionally correlatable biostratigraphically constrained electrofacies markers (Harris, 1975a; Hunt, 2017). Based on sparse conodont data, the Mississippian section in LNK is mostly Chesterian, whereas the sections in LGN, PYN-1 and PYN-2 include Osagean through early Chesterian strata. As a result, the stratigraphic interval of the Lower Mississippian could be equivalent to the Caney Shale, Sycamore Limestone, and Welden Limestone on the Arbuckle Uplift and Boone Group, Mayes Group, Fayetteville Shale and Pitkin Limestone in the Ozarks (Braun, 1961b; Chenoweth et al., 1959; Coffey, 2001; Godwin et al., 2017; Harris, 1975a; Peace, 1994)

88

Table 6 Key information about studied core samples

Core Code	Sampled Formation	County	Total Sample Number	Top Core Depth(ft)	Bottom Core Depth (ft)	Sampled Thickness (ft)
LGN	Lower Mississippian	Logan	27	5518	5801	283
PYN-1	Lower Mississippian	Payne	22	5144	5302	158
PYN-2	Lower Mississippian	Payne	6	4363	4481	118
PYN-3	Woodford	Payne	7	3360	3381	21
LNK	Lower Mississippian and Woodford	Lincoln	36	4968	5262	218

.
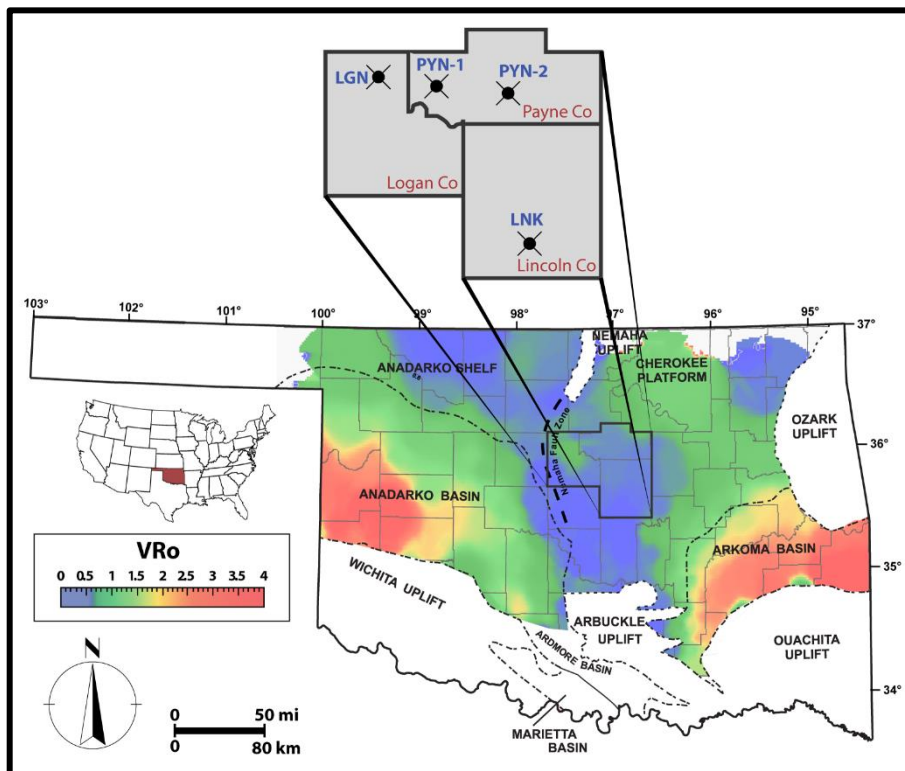
Figure 34 Map showing study area, boundaries for selected counties in Oklahoma and locations of sampled cores. Color overlay is a map of vitrinite reflectance constructed using published data, color scale with blue represent immature and red is dry-gas (Cardott, 2012; Cardott and Lambert, 1985

89

Crude-oil samples were obtained from the well-head and were collected in 30-ml glass bottles, then stored in a samples freezer (Figure 35). A total of 34 crude-oil samples were studied from seven different counties (Figure 32). Crude oils were produced from both, Mississippian and Woodford formations, and detailed information on crude-oil samples are shown in Table 7. Crude oils are classed into three broad groups, based on geographical location, including

Figure 35: Examined crude oil samples produced from Mississippian and Woodford Shale Reservoirs ranging from heave to light crude oils and condensates

STACK play, Anadarko Shelf and Central Oklahoma oils. The STACK play samples include oils from Blaine, Canadian and Kingfisher counties. Anadarko Shelf oils include samples at Alfalfa, Kay and Woods counties; and Central Oklahoma oils are from Garfield, Payne, Logan and Lincoln

Table 7 List of crude-oil samples and analyses performed.

Sample ID	County	Reservoir	Analysis		
			Gasoline HC	Biomarkers	Isotopes
Alf-01-M	Alfalfa	Middle Miss	✓	✓	
Alf-02-M	Alfalfa	Miss(Meramec)	✓	✓	✓
Bla-01-M	Blaine	Mississippian			✓
Can-01-M	Canadian	Mississippian	✓	✓	✓
Can-02-M	Canadian	Mississippian		✓	✓
Can-03-M	Canadian	Mississippian	✓	✓	✓

Table 8 continued.

Sample ID	County	Reservoir	Gasoline HC	Biomarkers	Isotopes
Can-04-M	Canadian	Mississippian		✓	
Gar-01-M	Garfield	Miss-Chat	✓	✓	✓
Kay-01-M	Kay	Mississippian	✓	✓	✓
Kin-01-N	Kingfisher	NA	✓	✓	✓
Kin-02-M	Kingfisher	Miss-Chat	✓		✓
Kin-03-M	Kingfisher	Mississippian	✓	✓	✓
Kin-04-M	Kingfisher	Miss-Chat	✓	✓	
Lin-01-M	Lincoln	Mississippian		✓	✓
Lin-02-M	Lincoln	Mississippian		✓	✓
Lin-03-M	Lincoln	Mississippian	✓	✓	✓
Lin-04-W	Lincoln	Woodford	✓	✓	✓
Log-01-M	Logan	Mississippian	✓	✓	✓
Log-02-M	Logan	Mississippian	✓	✓	✓
Log-03-M	Logan	Miss	✓	✓	✓
Log-04-W	Logan	Woodford	✓	✓	✓
Log-05-W	Logan	Woodford		✓	✓
Log-06-W	Logan	Woodford		✓	✓
Log-07-W	Logan	Woodford	✓	✓	✓
Pay-01-M	Payne	Mississippian		✓	✓
Pay-02-M	Payne	Mississippian	✓	✓	✓
Pay-03-M	Payne	Mississippian		✓	✓
Pay-04-M	Payne	Mississippian	✓	✓	✓
Pay-05-M	Payne	Mississippian	✓	✓	✓
Pay-06-M	Payne	Mississippian	✓	✓	✓
Pay-07-W	Payne	Woodford	✓	✓	✓
Pay-08-W	Payne	Woodford	✓	✓	✓
Woo-01-M	Woods	Miss(Meramec)	✓	✓	✓
Woo-02-M	Woods	Miss(Osage)	✓	✓	✓

counties. Prior to crude-oil compositional analysis, for each oil sample an aliquot of approximately

0.75 mg of crude oil was spiked with a standard mix of different deuterated compounds with

known concentration for quantitative analysis. Reservoir production is based on perforation depth reported by the operator or as listed by the Oklahoma Corporation Commission. Therefore, the reservoir indicated in Table 7 is not conclusive, especially when oil is produced from horizontal wells that have been hydraulically stimulated, which can result in commingled production from different reservoir zones.

Oil-bearing fluid inclusion samples were collected from four different cores of the Mississippian Limestone Formation. Fluid inclusions are observed to occur in calcite cements filling fractures, breccia and vug (Mohammadi et al., 2017). Petrographic examination and screening for oil-bearing fluid inclusions was done as part of a PhD dissertation by Sahar Mohammadi. Samples containing oil inclusions were shipped in glass vials for further compositional analysis of the petroleum inclusion. A collection of four oil-inclusion samples was examined in this study (Table 8) (Figure 32). One of the samples was located east of the Nemaha Uplift (SMD-2216), and the other three samples were located west of the Nemaha Uplift (CA-99336-B, AM-8371 and GS-9698). Microthermometry and isotope geochemistry data of aqueous inclusions were used in this study from work done by Mohammadi et al. (2017).

Table 9 Oil-bearing fluid inclusion samples (Mohammadi et al., 2017)

Sample ID	County	Type/Open Space Type
CA-99336-B	Canadian	Primary, calcite/Vertical, shear
SMD-2216&2217	Payne	Primary, calcite/Vertical
AM-8371	Kingfisher	Primary, calcite/Ptygmatic
GS-9698	Blaine	Secondary, calcite/Breccia

Rock-Eval Pyrolysis

Approximately 50–60 mg of grinded rock samples were screened using a Rock-Eval 6 instrument running on the Source Rock evaluation mode. The instrument is equipped with two micro-ovens for pyrolysis and oxidation. Initially, the sample was introduced in the pyrolysis oven. At this phase, the free hydrocarbons were measured (S1 peak) by heating (pyrolyzing) the sample at 300^0C for 3 min, followed by a programmed pyrolysis stage, with the temperature ramping at a rate of 25^0C/min to 550^0C to acquire the thermally cracked hydrocarbons (S2 peak). Then, the sample was introduced into the oxidation oven and heated up to 850^0C to measure for CO and CO_2 content to determine mineral carbon. The Rock-Eval 6 was calibrated after each run to the IFP160000 standard. This pyrolysis technique is used as a quick tool to screen for organic richness, maturity and type of kerogen. Since the Rock-Eval 6 approach comprises an open non-isothermal pyrolysis, the technique heats kerogen quickly and is not suitable for simulating petroleum generation. Therefore, we used a hydrous pyrolysis technique for further kinetic parameters determination.

Hydrous Pyrolysis

Organic-rich rock chips (1–4 mm; 30g) were placed in a 250 ml T316 vessel, together with about 33 ml of distilled water (Figure 36). The vessel was then tightly sealed and purged with nitrogen gas followed by argon gas. The vessel then was placed into the heater module at isothermal interval ranging from 260°C to 370°C for 72 h. Warm-up time of the reaction vessel ranged from 0.5 to 1 h, then the reaction vessel was kept at a single temperature for 72 h. After the reaction, the vessel was cooled, and expelled oil was recovered. The vessel's inner walls were

93
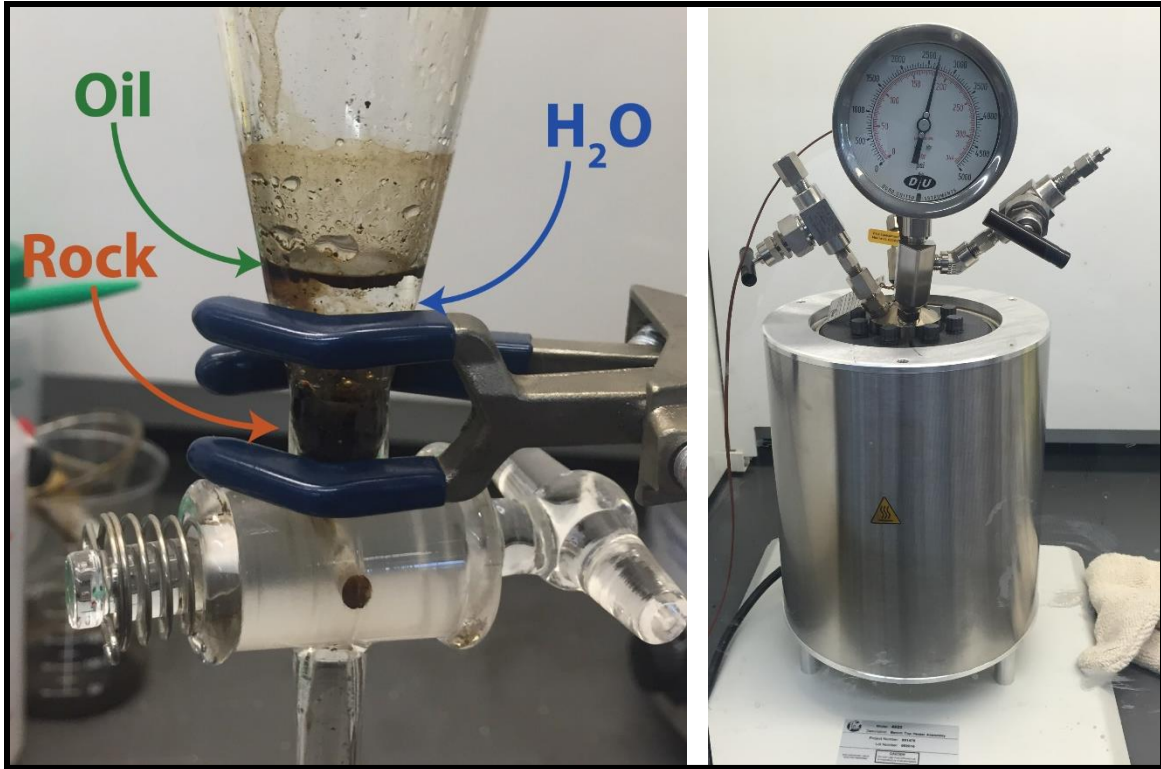
Figure 36: Hydrous pyrolysis Parr reactor showing the reaction vessel and the heater. Left: example of collected products after hydrous pyrolysis experiment showing expelled oil.

washed using dichloromethane and then dewatered using sodium sulfate. The generated oil was used to derive the reaction kinetic parameters using Arrhenius's first-order reaction equation:

$$\mathbf{k} = \mathbf{A}\mathbf{e}^{\frac{-Ea}{(RK)}} \qquad \text{[Eq 1]}$$

where **k** is the rate constant, **K** is the absolute temperature (in degrees Kelvin), **A** is the pre-exponential factor (i.e., a constant for each chemical reaction that defines the rate due to frequency of collisions in the correct orientation), **Ea** is the activation energy for the reaction, and **R** is the universal gas constant. Moreover, for petroleum generation, the Arrhenius equation can be rearranged as a function of oil-generation extent [$f(\mathcal{E})$]:

$$\boldsymbol{f}(\mathcal{E}) := \left(\boldsymbol{A}\boldsymbol{e}^{\frac{-Ea}{(RT)}}\right) \times \boldsymbol{t} \qquad \text{[Eq 2]}$$

where **t** is the heating time during hydrous pyrolysis (*t*=72 h). By the use of a series of hydrous pyrolysis experiments and by assuming that petroleum generation is a first-order function it can be expressed as

$$f(\varepsilon) := Ln(^1/_{(1-X)})$$ **[Eq 3]**

Were **X** is the fraction of generated oil at a specific temperature during hydrous pyrolysis, more specifically, maximum yield of oil during each hydrous pyrolysis experiment. Using this relationship, the rate constants (*k*T) for each experiment temperature can be expressed as:

$$k\text{T}:= Ln(\frac{1}{(1-Xt)})/t$$ **[Eq 4]**

where **t** is experiment time (72 h), and **Xt** is the generated oil during a specific temperature experiment. By combining Eq 2 and Eq 4,

$$k\text{T}:= Ln(\frac{1}{(1-Xt)})/t = Ae^{\frac{-Ea}{(RK)}}$$ **[Eq 5]**

Kinetic parameters including activation energy (*E$_a$*) and frequency factor (*A*) can be determined by plotting the natural logarithm of rate constant (Ln k) versus the reciprocal of temperature (1/*K*). From this plot, the activation energy (*E$_a$*) is defined as the slope, and the frequency factor is calculated from the intercept (Lewan and Ruble, 2002).

Organic Petrography and Vitrinite Analysis

Organic-rich rock samples (TOC >2%) were selected for organic petrography and vitrine reflectance analysis. Rock pellets were prepared for the characterization of organic macerals. Whole rock chips (1–2 cm) were mounted in 1-inch epoxy resin pellets. Pellets were then prepared for grinding and polishing using silicon carbide paper ranging in grit size from 220 to 1200 with the presence of deionized water, followed by polishing cloths using alumina polishing suspensions

with 0.3 µm and 0.05 µm. Rock pellets were examined using a Leica microscope equipped with a CRAIC 508 PV™ Microscope Spectrophotometer to characterize fluorescence and petrography. Macerals were counted (approximately 500 point count) and classified using the guidelines from the International Committee for Coal Petrology (ICCP) with a more detailed classification for the submaceral liptinite group (Pickel et al., 2017).

Reflectance analyses was performed on vitrinite ($VR_o\%$) and solid bitumen ($BR_o\%$) by taking an average of around 25 reflectance measurements per sample. Vitrinite was identified, and reflectance measurements were made on a random-mean basis. Solid bitumen reflectance was also measured and then corrected to the vitrinite equivalent reflectance values using a relationship published by Landis and Castaño (1995). Glass standards (i.e. *Spinel, Strontium-Titanate, Yttrium-Aluminium-Garnet*) were used to calibrate the reflected-light microscope.

Core Description and XRF Rock Mineralogy

The Mississippian limestone sections in cores LNK, PYN-1 and PYN-2 were examined and described at the hand-specimen scale and sampled for thin sections and geochemical analyses. Each core was described to identify depositional facies and document significant stratigraphic surfaces, biogenic features, and sedimentary structures. Depositionally significant surfaces such as flooding surfaces were noted to delineate stacking patterns and develop a sense of cycle hierarchy. Carbonate facies were named using the Dunham's (1962) classification scheme. Siliciclastic facies were named based on grain size and mineralogy, texture, sedimentary structures and the degree of bioturbation (Bann et al., 2008). Colors were determined using the Geological Society of America Rock Color Chart. A composite section of carbonate and siliciclastic facies was constructed for each core to illustrate facies thickness, frequency and stacking patterns, which were the basis of establishing cycle hierarchy and the sequence stratigraphic framework (Hill,

2017; LeBlanc, 2014). Petrographic thin sections were obtained from the Mississippian section. All thin sections were blue-epoxy impregnated to identify open pores and stained with alizarin red and potassium ferricyanide to identify calcite and dolomite, respectively. Thin-section petrography was crucial to identifying features and describing variations within fine-grained rocks that were not apparent in hand sample, including types and abundances of detrital grains and cement, relative abundance and morphology of bioclasts, pore characteristics and detailed textural relationships. Mineralogical composition was determined using powder X-ray diffraction (XRD) measurements of the selected intervals sampled for thin sections. X-ray diffraction analyses included whole rock bulk mineralogy to identify framework grain and cement mineralogy. Abundances of common mineral components in sedimentary rocks were quantified. X-ray-diffraction-derived composition, augmented by thin-section petrography and whole-core analysis, was used to identify changes in mineralogy over short lengths of the core. Sampling for XRD and thin sections of targeted textural and color differences in cored strata appear to reflect changes in depositional energy and water depth. These textural and compositional changes were used to define facies, depositional cycles or sequences and sequence boundaries (Hill, 2017; LeBlanc, 2014).

Bitumen Extraction

Organic-rich rock samples (TOC > 2%) were finely grounded and subjected to bitumen extraction. A range of 10g to 30g of rock powder was used for extraction. The extracted sample's weight was based on sample organic-richness. Rock powder was packed into a 34-ml stainless steel sample cell, then tightened with end caps by hand. The filled cells were then loaded into a Dionex accelerated solvent extractor (ASE 350 by Thermo Scientific). After the cell with sample was loaded into the ASE, the pump fully filled the cell with dichloromethane solvent. The filled cell with the solvent was pressurized at 1500 psi, and the oven set to 100°C for 5 min. The static

time was set at 5 min, with rinse volume set at 50% of the cell volume. Following the final solvent rinse, the solvent was purged with nitrogen out of the cell at 150 psi for 90 s, with a total extraction time of 15 min per sample. The bitumen was delivered into 60-ml collection vials, and solvent volume was reduced to 2 ml, using evaporation under a low-flow stream of nitrogen. The concentrated bitumen was then spiked with a standard contaning deuterated compounds of known concentration for quantitative analysis.

Silica-Gel Chromatography

T.J. BAKER Silica Gel 40 µm flash chromatography packing was activated at 260°C, for 24 h. Treated silica gel was packed in disposable serological pipettes fitted with glass wool. Packed columns were stored in an oven at 130°C. An aliquot of 0.75 mg of spiked crude-oil and bitumen samples were placed at the top of the silica-gel columns. Saturated hydrocarbons were eluted with hexane, and around 8 ml of solvent was collected. Aromatics eluted with dichloromethane with 30 ml of solvent was collected.

Further purification and removal of *n*-alkanes was performed on the saturated hydrocarbon fraction using zeolite. Silicalite ZSM-5 zeolite powder was combusted at 400°C for 24 h. Treated silicalite was packed into Pasteur pipettes fitted with glass wool. The saturate fraction in hexane was reduced in volume to 1 ml using evaporation under a stream of nitrogen. The saturate fraction was then placed on the silicalite column and eluted with iso-octane solvent, with a total volume of 4 ml of solvent, and the sample was collected. Finally, the sample was concentrated by evaporation under a low-flow stream of nitrogen. Saturate and aromatic hydrocarbons were then run

Solid-Phase Extraction (SPE)

Solid phase extraction is another technique used for sample preparation prior to GC-MS analysis. Solid phase is particularly useful in selectively separating polar compounds from a complex matrix such as crude oil. In this study, SPE was used to selectively isolate polar compounds of interest, including carbazoles, benzocarbazoles and phenols. This was achieved by utilizing normal phase SPE procedure, in which a C18 stationary phase was used. C18 is a sorbent material consisting of hydrophobic-bonded silica, which is a retentive phase for non-polar to moderately polar compounds. This allows for the removal of non-polar compounds found in crude-oil samples (i.e. saturate and aromatic hydrocarbons), which leave the polar compounds bounded into the stationary-phase. Then, the polar compounds can be liberated by eluting with polar solvent, resulting in a purified polar fraction from complex crude-oil matrix.

In this procedure, ISOLUTE cartridges were applied, which are manufactured pre-packed with 100mg of C18, and with a reservoir capacity of 3ml. An aliquot of 100mg of crude oil was spiked with 9-phenylcarbazole standard. For the heavy and viscous oils, an additional hexane was added to dilute the sample in a GC-vial for easier sample handling. Cartridges were securely tightened into a column rack and then placed into the vacuum manifold. Cartridges were first conditioned with 5ml of hexane, then the spiked oil aliquot was added to the top of the cartridge top packing. The sample was first eluted into two fractions, saturate and aromatic fraction, and NSO fraction. The saturate and aromatic hydrocarbons were eluted with 5ml of hexane, while the NSO compounds were eluted with 6ml of dichloromethane. The elution process was further enhanced by applying a vacuum of 5psi. The collected NSO fraction in 6ml dichloromethane was further concentrated by evaporating dichloromethane under a low stream of nitrogen down to 1ml.

The NSO fraction was then analyzed on the GC-MS for quantitative analysis of carbazoles and phenols.

Gas-Chromatography Flame Ionization Detector (GC-FID)

Crude oil and rock bitumen, together with hydrous-pyrolysis oil, were analyzed using an Agilent 7890B gas chromatograph (GC) equipped with a flame ionization detector (FID). The GC has a DB-1 fused silica 60 m $\times$ 0.25 mm $\times$ 0.25 µm column, with a flow of He at 1.3 ml/min, and a temperature program from 35°C to 375°C with a temperature ramp of 2°C/min. The analysis was performed under split injection mode with a split ratio of 50:1 carrier gas to sample mixture for crude oil and hydrous-pyrolysis oil, whereas rock bitumen was injected under splitless mode. This analysis provides light hydrocarbons, *n*-alkanes and isoprenoids composition.

Gas-Chromatography Mass-Spectrometry (GC-MS)

The GC-MS analysis was performed using two different instrument methods and column configurations. The first configuration was suitable for diamondoids and biomarkers of the saturate fraction, while the second configuration was used to measure aromatic hydrocarbons, together with the NSO fraction.

The first GC-MS configuration consisted of an Agilent 7890 GC interfaced to an Agilent 5975C mass selective detector (GC-MS). The GC-MS is equipped with a DB-1 fused silica 60 m $\times$ 0.25 mm $\times$ 0.25 µm column with helium as a carrier gas at a flow rate of 1.2 ml/min, a pressure of 19.93 psi and an average velocity of 20.538 cm/sec. Moreover, the GC-MS is operated on splitless injection, with the oven programmed at an initial temperature of 35°C for 2 min, and increased at a rate of 2°C/min to 80°C, then 3°C/min from 80°C to 320°C, followed by 15 min at

320°C. The analysis was carried out using 70 eV ionization potential. The GC-MS data were acquired in SIM mode with 50–100 msec dwell times for ions of interest..

The second GC-MS configuration consisted of an Agilent 7890 GC interfaced to an Agilent 5975C mass selective detector (GC-MS). The GC-MS is equipped with a DB-5 fused silica 60 m × 0.25 mm × 0.25 µm column with helium as a carrier gas at a flow rate of 1.4 mL/min, a pressure of 10.71 psi and an average velocity of 42.795 cm/sec. Moreover, the GC-MS was operated on splitless injection, with the oven programmed at an initial temperature of 60°C for 2 min and increased at a rate of 2°C/min to 320°C, followed by 15 min at 320°C. The analysis was carried out using 70 eV ionization potential. The GC-MS data were acquired in SIM mode with 50–100 msec dwell times for ions of interest.

Gas-Chromatography Mass-Spectrometry Triple Quadrupole (GC-MS-QQQ)

Biomarkers in the saturate fraction extracted from the rock's bitumen and crude oils, together with oil inclusions, were further analyzed using an Agilent 7890-7010B triple quadrupole (GC-MS-QQQ; also known as GC-MS/MS). The instrument is equipped with a DB-1 fused-silica column (60 m × 0.25 mm × 0.25 µm) and the oven programmed for an initial temperature of 80°C for 1 min, then increased 2°C/min to 320°C, followed by 5 min at 320°C. Helium was used as a carrier gas with a flow rate of 1.3 mL/min, and in the second quadrupole, nitrogen was used as collision gas. The GC-MS/MS was run in precursor-product ion mode for MRM. The Agilent 7010 GC-MS/MS system features a triple quadrupole mass spectrometer that resolves complex biomarkers using the specific precursor to product ion relationships. In this study, we monitored for C_{26} up to C_{30} of regular and rearranged steranes (i.e., m/z $358 \rightarrow 217$, $372 \rightarrow 164\ 217$, $386 \rightarrow 217$, $400 \rightarrow 217$, and $414 \rightarrow 217$), methyl steranes (i.e., m/z $414 \rightarrow 231$), extended tricyclics terpanes from C_{29} to C_{39} (i.e., m/z $402 \rightarrow 191$, $416 \rightarrow 191$, $430 \rightarrow 191$, $458 \rightarrow 191$, $472 \rightarrow 191$,

486 → 191, 500 → 191, 528 → 191, and 542 → 191), tricyclic diterpanes (i.e. m/z 276 → 247), and tetracyclic diterpanes (i.e. m/z 247 → 123). Compound ratios were calculated directly from peak areas or peak heights of targeted markers and compared with internal standards.

Not all biomarkers are resolvable with the classical GC-MS techniques, due to the close similarity in biomarkers molecular masses; therefore, diagnostic MRM approach using the GC-MS-QQQ provides further detailed and robust biomarkers analysis. Additionally, due to small quantity of oil inclusions, sample preparation is not possible, so direct injection on the GC-MS-QQQ allow for detailed biomarkers analysis without the need for sample preparation.

Gas-Chromatography Isotope Ratio Mass Spectrometry (GC-IRMS)

Crude oils were analyzed on an Agilent 7890B GC interfaced with GC5 combustion furnace and isoprime precisION stable isotope ratio mass spectrometer (GC-IRMS). Samples were injected into the GC on split mode at 40:1 carrier gas to sample mixture. The GC is equipped with a DB-1 fused-silica column 60 m × 0.25 mm × 0.25 μm. The GC oven was programmed from 39°C to 350°C at 1°C /min up to 60°C, then 7°C /min up to 350°C for 35 min. Helium was used as a carrier gas at 1 ml/min. The carbon isotopic composition of targeted compounds was identified using mass spectrometer signal at *m/z* 44 (12C16O16O) and *m/z* 45 (13C16O16O). The combustion furnace was used for oxidation of chemicals to eluent conversion into CO_2 by setting temperature at 865°C, and using a microbore 0.7 mm (I.D.) of quartz tube packed with CuO pellets. During each crude-oil run, two reference gas peaks were injected into the mass spectrometer. All isotopic results were calibrated to a certified B4 mix from Indiana University (Bloomington, IN, USA; http://mypage.iu.edu/~aschimme/hc.html). All $\delta^{13}C$ isotopic values of *n*-alkanes in the B4 mix standard are certified relative to the Vienna Pee Dee Belemnite (VPDB) isotope scale. Carbon isotope ratios of individual compounds provide another dimension to examine the relationship

between crude oils and their sources. Additionally, CSIA of individual diamondoid species allowed fingerprinting crude oils with condensate when biomarkers were absent due to thermal alteration.

CHAPTER IV

SOURCE ROCK PETROGRAPHY, GEOCHEMISTRY AND

PETROLEUM GENERATION KINETICS

Organic Richness and Kerogen Type

The cored Mississippian organic-rich intervals ranged from 50 ft (15.24 m) to 100 ft (30.48 m) of gross thickness. In general, the Mississippian organic-rich sections are characterized by high TOC (>2%) and high HI values (>200). Table 9 shows results of Rock-Eval pyrolysis of selected samples with good generation potential. Additionally, Figure 37 summarizes major Rock-Eval parameters for source-rock evaluation based on kerogen quality and quantity. Hydrogen index (HI) varied the most across the samples. The richest samples in HI are from the LNK core, while core LGN exhibited the lowest HI values. Oxygen index (OI), however, varied most in the
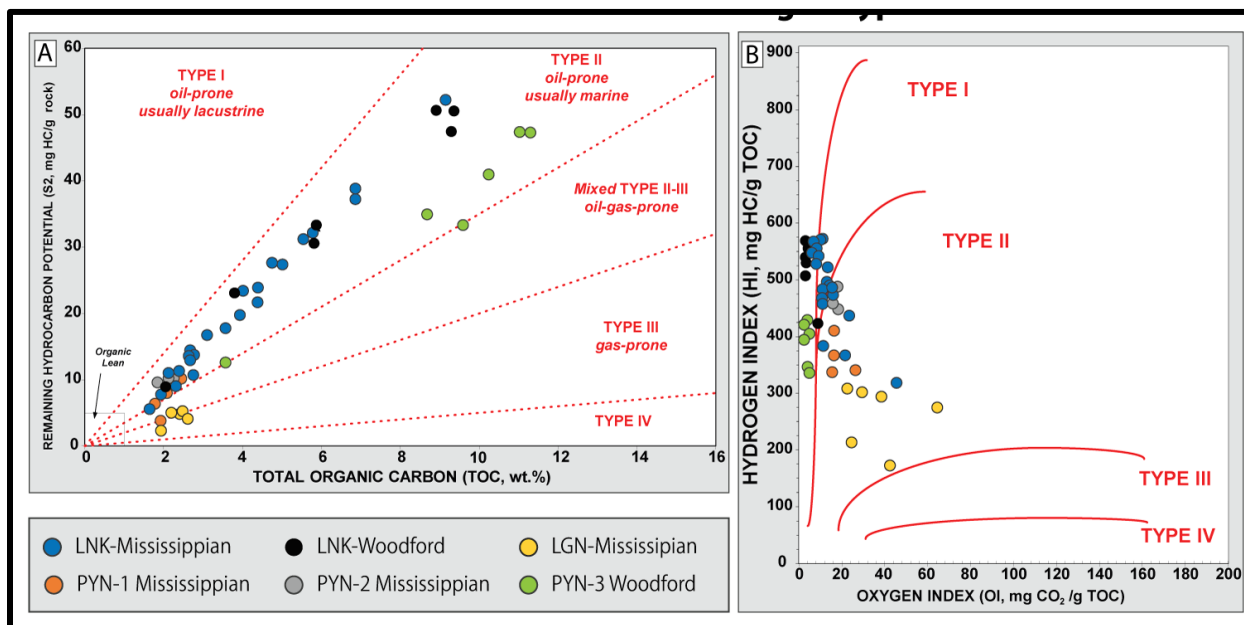
Figure 37: Rock-Eval-derived parameters for study samples. (A) Available hydrocarbons (S2) vs. total organic carbon content (TOC) for each kerogen type. (B) Van Krevelen diagram for the study samples comparing hydrogen index (HI) with oxygen index (OI). Note the variation between the two diagrams even though the organic material is predominantly Type-I and Type-II kerogens.

Mississippian carbonate samples, whereas Woodford samples had low values. Variation in oxygen index is expected, especially in rocks containing carbonate minerals, as they can release CO_2 that masks the oxygen signal generated from the kerogen (Katz, 1983). As shown in Figure 39-B, most Woodford Shale samples plot within Type I, which is a result of the hydrogen-rich *Tasmanites* (Al Atwah et al., 2019) and references therein). However, most Woodford Shale kerogen is primarily marine Type II, as evidenced from maceral composition.

The observed variability in HI of Mississippian samples could be influenced either by thermal maturation, or by initial depositional settings: that is, organic matter productivity and preservation. Since the examined samples come from marginally mature rocks as indicated by the vitrinite reflectance map in Figure 34, it is unlikely that the variability in HI is due to thermal maturity. Hence, it is possible the HI difference is caused by the paleobathymetry settings during Mississippian time exhibiting a drastic change in the paleo-shoreline effecting water depth. Therefore, organic-matter richness is likely influenced by both the organic matter productivity and preservation.

Table 10 Rock-Eval pyrolysis data of sampled cores and key pyrolysis ratios

Core Code	Formation	Depth (ft)	S1 (mg/g)	S2 (mg/g)	S3 (mg/g)	T_{max}(°C)	HI	OI	TOC(%)
LGN	Lower Mississippian	5568	1.01	4.83	0.34	442	310	22	2.34
		5570	1.04	4.58	0.44	434	305	29	2.25
		5574	1.23	4.85	0.63	430	294	38	2.475
		5576	0.8	4.55	1.06	432	276	64	2.475
		5701	0.75	3.76	0.43	437	214	24	2.64
		5757	0.76	2.31	0.56	432	172	42	2.01
PYN-1	Lower Mississippian	5144	0.69	7.79	0.34	447	369	16	2.11
		5280	1.05	3.59	0.27	443	342	26	2
		5156	0.88	6.17	0.27	444	339	15	1.82
		5157	1.24	10.13	0.4	443	413	16	2.45

Table 9 continued.

Core Code	Formation	Depth (ft)	S1 (mg/g	S2 (mg/g	S3 (mg/g)	T_{max}(°C)	HI	OI	TOC(%
PYN-2	Lower Mississippian	4363	0.72	10.2	0.39	439	453	17	2.25
		4365	0.73	9.46	0.31	439	490	16	1.93
		4367	0.66	10.16	0.33	438	464	15	2.19
PYN-3	Woodford	3360	2.13	12.3	0.13	448	336	4	3.66
		3367	2.76	32.76	0.37	438	341	4	9.61
		3371	2.21	35.03	0.27	442	404	3	8.68
		3376	3.1	47.28	0.24	439	420	2	11.27
		3377	3.05	47.36	0.31	446	428	3	11.06
		3381	2.83	41.01	0.14	442	403	1	10.17
LNK	Lower Mississippian	4968.5	0.72	9.58	0.5	437	441	23	2.17
		4972	0.35	7.64	0.44	439	367	21	2.08
		4973	0.29	5.56	0.79	442	320	45	1.74
		4975	1.24	19.75	0.48	439	500	12	3.95
		4983	2.65	51.72	0.59	439	569	6	9.09
		4992	1.31	21.48	0.46	432	490	11	4.38
		5033	1.18	14.25	0.36	439	526	13	2.71
		5044	1.62	23.07	0.39	437	575	10	4.01
		5050	1.62	37.23	0.55	439	543	8	6.86
		5055	0.6	13.18	0.4	441	490	15	2.69
		5059	0.75	10.7	0.31	431	385	11	2.78
		5075	1.59	27.37	0.43	436	546	9	5.01
		5108	0.65	10.54	0.33	439	475	15	2.22
		5112	0.79	17.92	0.46	441	498	13	3.6
		5117	0.69	11.1	0.25	437	464	10	2.39
		5137	2.29	31.7	0.21	438	548	4	5.78
		5138	3.13	38.36	0.21	433	560	3	6.85
		5156	1.26	23.89	0.25	435	544	6	4.39
		5160	0.82	12.75	0.27	440	472	10	2.7
		5171	1.47	31.06	0.39	431	561	7	5.54
		5184	1.17	27.55	0.42	434	574	9	4.8
		5195	1.04	13.54	0.29	434	492	11	2.75
	Woodford	5201	1.32	32.96	0.23	439	561	4	5.87
		5210	0.71	9.03	0.17	446	426	8	2.12
		5224	2.3	31.07	0.19	440	535	3	5.81
		5248	3.57	51.19	0.26	441	572	3	8.95
		5253	3.37	47.44	0.25	435	511	3	9.29

Thermal Maturity

Examined source rock maturity ranged from immature to early-stages of oil generation with values ranging from 0.49–0.75%R_o. The data for vitrinite reflectance and calculated vitrinite refelctance from Tmax is shown in Table 9; only selected measurement were made on most organic-rich samples. Measured vitrinite reflectance was performed on two samples per core, covering the top and the base of the core interval. It is clear that the overall trend in the measured reflectance values decreases to the east and to the north. In Logan County core, the highest measured reflectance at 0.86%R_o, while lowest values are observed at Logan County at 0.47%R_o. This trend coincides with measured vitrinite reflectance values published by Cardott (2012), as shown in Figure 34. Table 10 depicts is a general trend with measured vitrinite reflectance values and depth, with deepest samples, from LGN core with the highest reflectance values. However, one exception is the LNK core, with samples at depths of 4968 ft to 5262 ft, while exhibiting the lowest reflectance values. This phenomenon can be due to that LNK core is farthest away from the main the Nemaha Uplift fault-system, and the Nemaha Province has the possibility of been affected by hydrothermal fluid movements that caused both, temporal and lateral variation in the geothermal gradient (Higley, 2014a; Mohammadi et al., 2017).

In general, vitrinite reflectance values that are derived from T_{max} using the formula proposed by Jarvie et al. (2001) does not correlate well with measured values (Table 10). The calculated vitrinite reflectance coincide well with measured values around 0.7%; however, maturity is underestimated at 0.8% and higher, as shown in the LGN sample (Table 10). Calculated values also overestimated vitrinite reflectance at very low reflectance values (<0.6%), such as with LNK samples (Table 10). Therefore, care must be taken when evaluating maturity by deriving vitrinite reflectance equivalent value from T_{max}, as there are multiple sources of error. One source

of error could be the presence of an S_2 peak shoulder due to the carry-over effect caused by the presence of heavy hydrocarbon (bitumen) in the sample. This problem can be overcome by extracting bitumen from the rock with organic solvent and rerunning extracted sediments on a Rock-Eval instrument.

Table 11 Thermal maturity parameters on selected core samples

Core Code	Depth (ft)	TOC (wt %)	Measured %R_o	T_{max} (°C)	Calculated %R_o
LGN	5574	2.47	0.84	430	0.58
	5757	2.64	0.86	432	0.62
PYN-1	5156	1.80	0.75	444	0.83
	5280	2.00	0.81	443	0.81
PYN-2	4363	2.25	0.74	438	0.72
	4367	2.19	0.73	439	0.74
PYN-3	3360	3.66	0.71	448	0.90
	3377	11.06	0.71	446	0.87
LNK	5050	6.80	0.47	441	0.78
	5248	8.95	0.49	441	0.78

Macerals Characterization

Examined kerogen macerals exhibited different distributions between Mississippian and Woodford Shale samples. Figures 38 and 39 are photomicrographs showing major macerals observed in Mississippian and Woodford kerogens. In Mississippian samples, macerals are dominantly composed of lamalginites occurring as thin wispy lamellae of planktonic origin. Furthermore, bituminite is a dominant maceral occurring as amorphous organic matter fused with the mineral matrix. A unique organic structure that was observed in the Mississippian samples is

the presence of spore-like bodies of acritarchs. Acritarchs can be classified based on their unique morphology as herkomorph acritarchs. Those spore-like structures could have an affinity to dinoflagellate cysts and prasinophyta phycomas (Al Atwah and Jacobi, 2017; Arouri et al., 1999; Moldowan and Talyzina, 1998). A recent study by Kaźmierczak and Kremer (2009) suggests that Paleozoic herkomorphs could be related to vegetative green algal cells, a conclusion based on similar morphological features between Silurian herkomorphs and modern chlorococcalean microalgae (Kaźmierczak and Kremer, 2009)

Table 12 Maceral composition of Mississippian and Woodford samples represented as relative percentage

Depth (ft)	TOC%	%Telalg[a].	%Lamalg.[b]	%AOM[c]	% Vit.[d]	%Inert.[e]	%SB[f]
Mississippian Formation							
4983	9.09	0.00	12.70	53.17	0.00	9.52	24.60
5050	6.86	15.25	18.64	42.37	0.00	5.93	17.80
5075	5.01	3.28	29.51	36.07	0.00	4.92	26.23
5137	5.78	13.92	22.15	36.08	0.63	6.33	20.89
5156	4.39	0.00	15.79	61.40	0.00	1.75	21.05
5171	5.54	2.48	19.83	52.89	0.00	0.83	23.97
5184	2.8	1.65	11.57	61.16	0.00	0.00	25.62
Woodford Formation							
5201	5.87	23.33	30.83	17.50	0.00	13.33	15.00
5224	5.81	15.83	45.00	18.33	0.00	7.50	13.33

[a] Telalginite, [B] Lamalginite, [C] amorphous organic matter (bituminite and amorphinite), [d] vitrinite, [e] inertinite, f solid bitumen
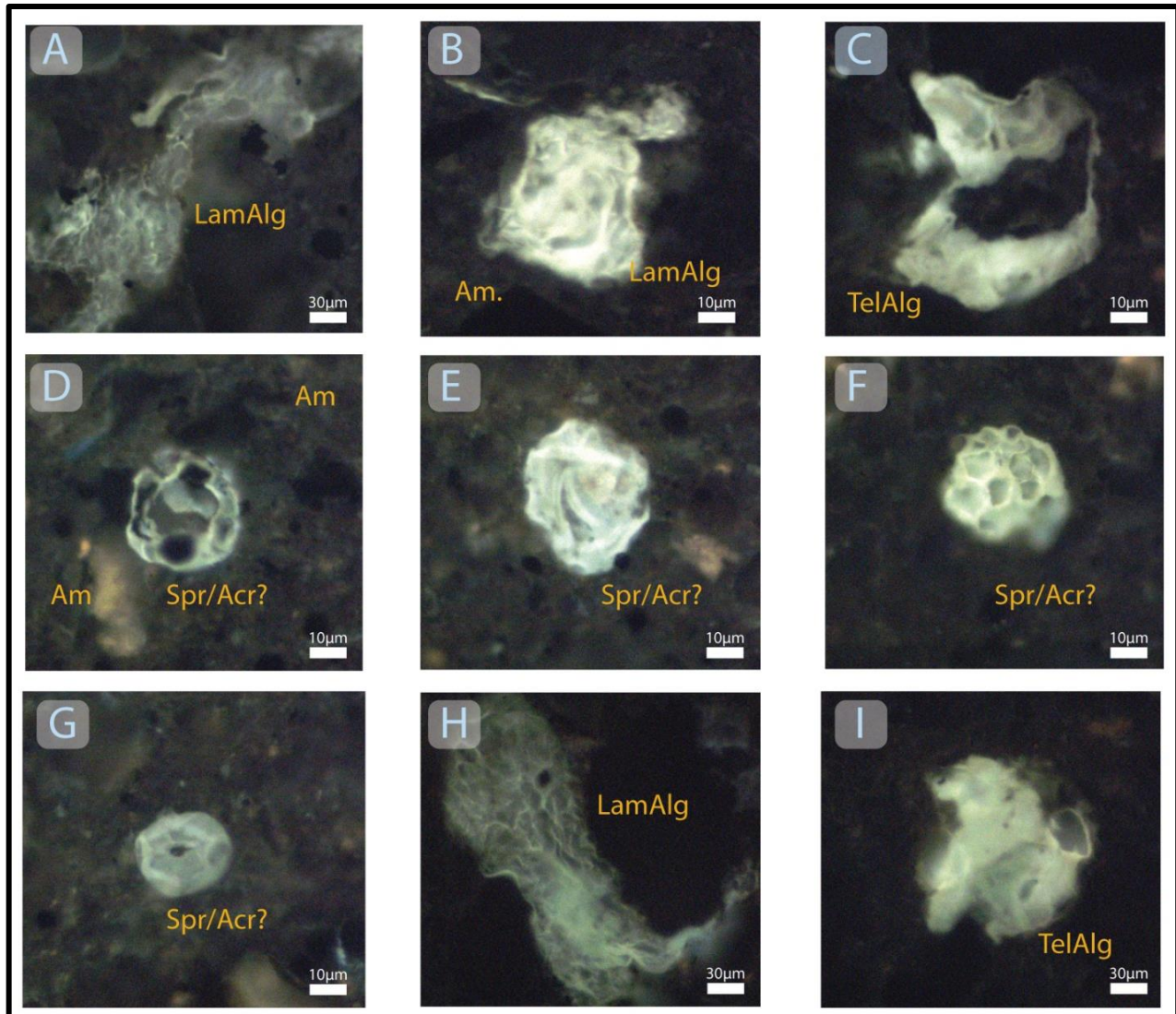
Figure 38: Photomicrographs of macerals in organic-rich Lower Mississippian carbonate from LNK core, examined under reflected white-light and ultraviolet (UV) light with oil immersion. (A) LamAlg: lamalginite; (B) LamAlg: lamalginite showing thin laminated structures, Am: amorphous organic matter; (C) TelAlg: telalginite that has been distorted; (D, E, F and G) Am: amorphous organic matter, Spr/Acr: spore-like acritarchs (*Dictyotidium sp*?); (H) LamAlg: lamalginite with transparent and thinly laminated wispy structure; (I) TelAlg: telalginite.

Woodford samples had different macerals than those of Mississippian samples. The most dominant maceral in the Woodford is telalginite, particularly *Tasmanites and leiospheres*. Furthermore, few acritarchs were observed. However, unlike Mississippian acritarchs, Woodford acritarchs are spine-bearing bodies (acanthomorphs; Figure 39-D). Limited occurrence of

110

lamalginite was observed in the Woodford samples. Overall, Woodford alginites feature preserved morphology, and the alginite clast size increased with increasing depth. In contrast, Mississippian alginites are laminated, lacking distinct structures and amalgamated with the mineral matrix.
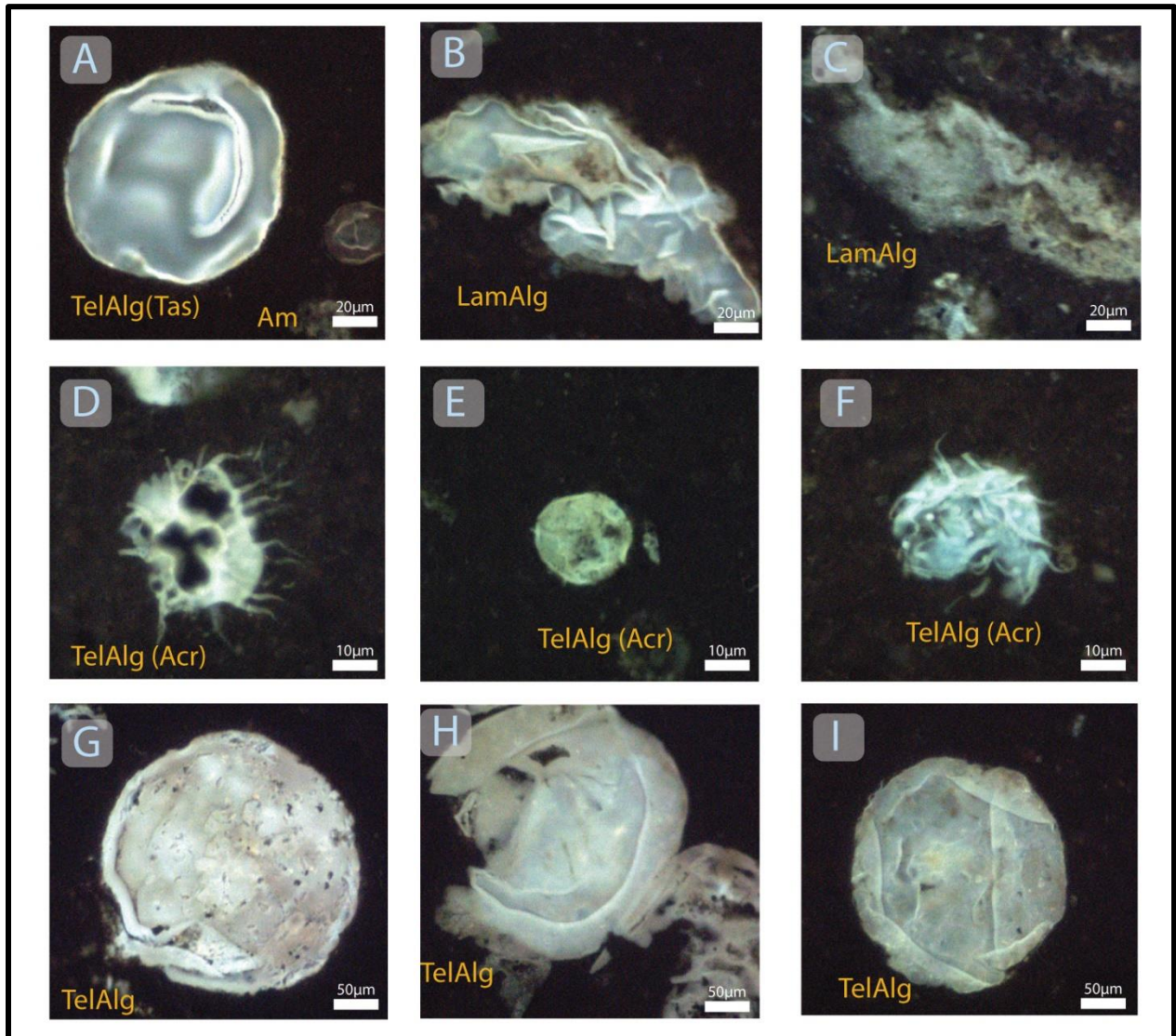
Figure 39: Photomicrographs of macerals in the Woodford Shale from LNK core. Examined under UV light,(A) TelAlg (Tas): telalginite (Tasmanites) of about 60um in diameter; (B and C) TelAlg: telalginite with thinly laminated structure; (D,E and F) TelAlg Acr: Telalginite showing different species of acritarchs; (G) TelAlg: telalginite (*Tasmanites*) of about 200um in diameter, (H and I) TelAlg: telalginite of prasinophyte alginite (leiospheres).

solid-bitumen clast under reflected white-light, while solid bitumen is exhibiting a dark-gray color (Figure 40). As evidenced from hydrous-pyrolysis experiments, it is well established that the transformation of kerogen into expelled hydrocarbons follows the sequence of kerogen, to polar-rich bitumen, and then ultimately to petroleum (Lewan, 1985). Therefore, the presence of pre-oil solid bitumen at LNK samples indicate that those kerogens are immature for generating petroleum, which supports the low reflectance values measurement presented in Table 10 for LNK samples.
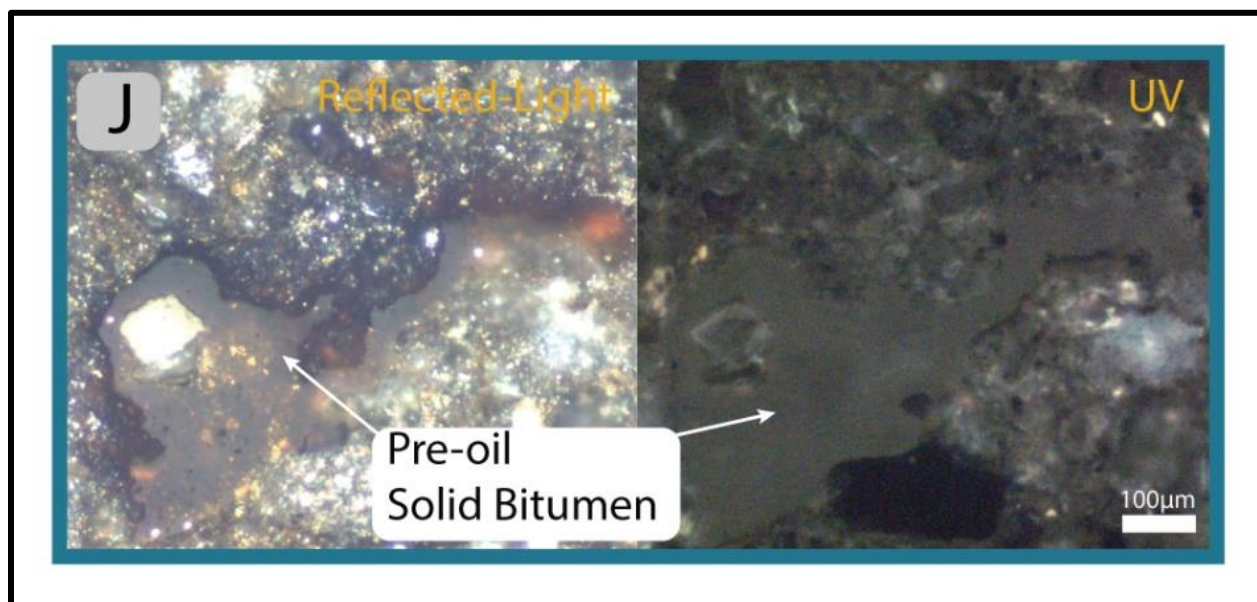
Figure 40: Pre-oil solid bitumen showing dark gray color under reflected white light and a very weak fluorescence under UV light; which is marking one of the first thermal transformation stages from kerogen to polar-rich solid bitumen.

LNK Core Description and Mineralogy

Six Mississippian depositional facies were identified in the LNK core (Hill, 2017). The stacking patterns of these facies are consistent with shallowing- or shoaling-upward sequences identified by LeBlanc (2014), Flinton (2016) and Hill (2017), who interpreted the depositional setting as a gently sloping carbonate ramp that was likely distally steepened. Carbonate-dominated facies types range from lower-energy mudstones and wackestones to higher-energy packstones

112

and grainstones (Figure 41). Siliciclastic facies range from clay- and silt-rich mudrocks and shales to silty sandstones. The six depositional facies observed in the LNK core (Table 12) are Facies 1 (glauconitic sandstone), Facies 2 (clay-rich siltstone), Facies 3 (sandy calcareous siltstone), Facies 4 (silty argillaceous sandstone), Facies 5 (silty burrowed mudstone-wackestone), and Facies 6 (silty peloidal-packstone-grainstone). Facies 1 is fine-medium sand-sized glauconite (50–60%), silt- to sand-sized quartz (35–40%), clay minerals (20–45%) and lesser amounts of dolomite (3–10%), pyrite (5–6%) and phosphate grains, including conodonts and bone fragments (2–3%). Though Facies 1 is thin (<1.0 feet, 0.3 m) and not volumetrically significant, it is recognized in cores and bit cuttings across much of northern Oklahoma (Hill, 2017) and is interpreted as the initial stage of a transgressive event that flooded the post-Woodford Shale surface. Facies 2 is dark dusky green to grayish black clay-rich siltstone with commonly preserved laminae. Facies 2 is 40–50% silt-sized quartz, 20–30% clay minerals, principally illite, 10–17% calcite and 10–20% other grains including feldspar, pyrite or marcasite, and apatite. Skeletal debris are relatively sparse and bioturbation scarce compared to other facies. Facies 2 is interpreted to represent continued transgression following Facies 1 and deposition in calm, poorly oxygenated waters. Facies 3 is sandy calcareous siltstone that is commonly bioturbated and olive-gray to dark-gray color. Facies 3 is dominated by silt through very fine sand-sized quartz (37–49%), calcite (37–49%) and clay minerals (12–18%). Facies 3 contains 15% other minerals, including feldspar and pyrite. Skeletal debris includes small unidentifiable grains and larger brachiopod and crinoid fragments. Facies 3 was interpreted by Hill (2017) as more oxygenated than Facies 2 with abundant millimeter-scale horizontal burrows and the appearance of thin-shelled brachiopods. Facies 4 is silty argillaceous sandstone that occurs in the upper 30 m (98 feet) of the core. Facies 4 is dusky green to moderate olive brown color and contains very fine to fine sand-sized quartz (50–61%), clay minerals –

113

mainly illite (15–27%), calcite (7–21%) and 12–15% other minerals including feldspar, pyrite, and apatite. Facies 4 contains parallel laminae, low-angle planar crossbedding, and abundant bioturbation. Hill (2017) has attributed the occurrence of current features, as well as bioturbation, to increased circulation and oxygenation. Facies 5 is silty burrowed mudstone-wackestone that is light olive gray to grayish black color. It is commonly bioturbated with vertical and horizontal burrows that are millimeter to centimeter scale. Mineralogically, Facies 5 is silt-sized carbonate grains and carbonate mud (35–48%), very fine sand-sized quartz (20–35%), clay minerals (12–15%) and other grains (<10%) including feldspar and pyrite. Bioclasts include brachiopods and crinoids, but most carbonate grains are unidentifiable. Facies 5 contains intervals of bioturbated and laminated beds interpreted as deposition under alternating oxygenated and dysoxic conditions (Hill, 2017). Facies 6 is silty peloidal packstone-grainstone that is medium gray to moderate yellow-brown color and massively bedded. Facies 6 contains silt to sand-sized carbonate grains (45–71%), silt-sized quartz (22–35%) and 7% other minerals including clay minerals, feldspar, pyrite and apatite. Peloids are up to 50% of carbonate grains and bioclasts, including brachiopods, crinoids, and lesser amounts of sponge spicules, and unidentified micritized grains make up the rest. The increase in skeletal grains reflects more oxygenated water, though the absence of current features suggests deposition below fair-weather wave base (LeBlanc, 2014; Hill, 2017).
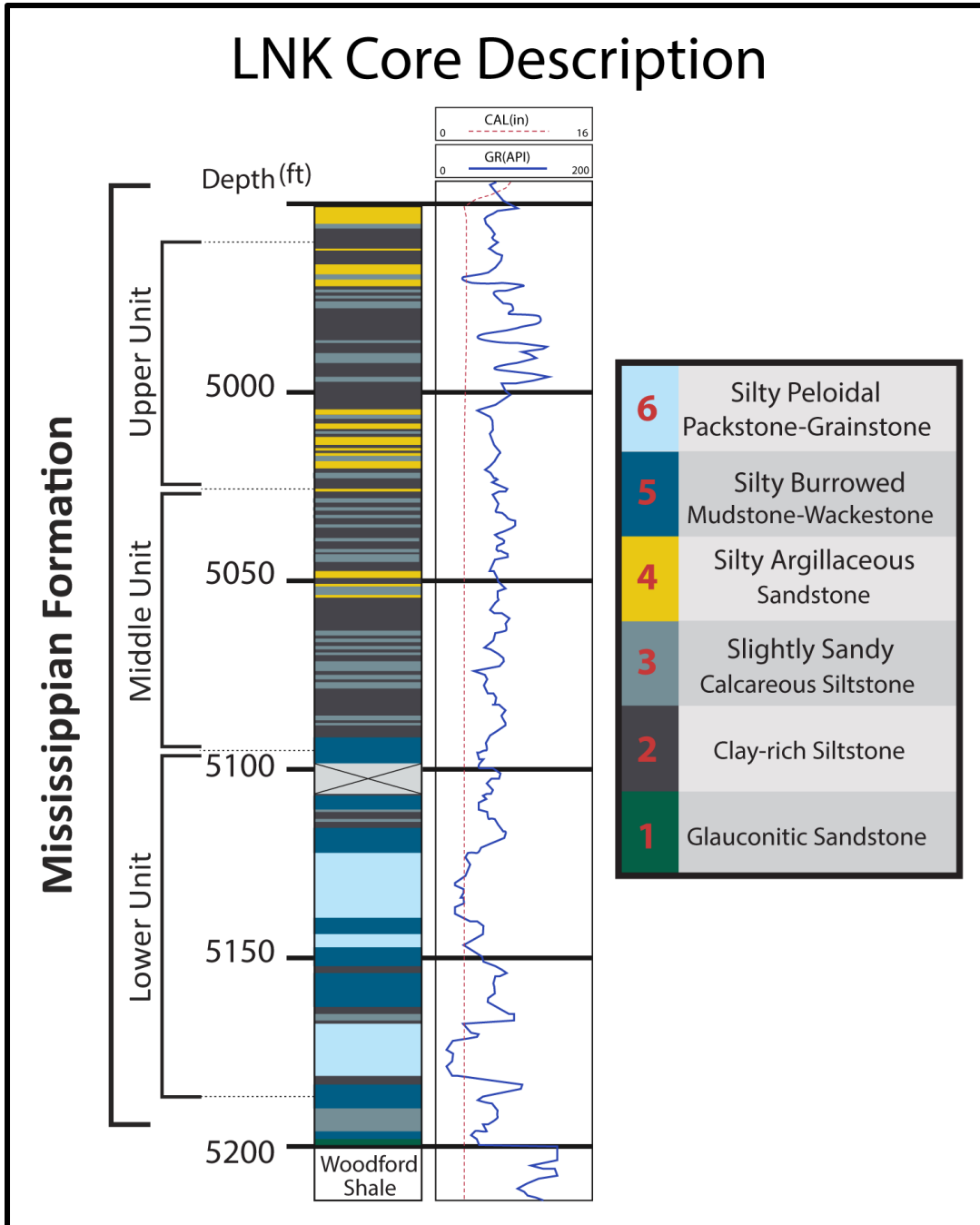
Figure 41: Mississippian depositional facies from LNK core with gamma-ray log of the Woodford, Mississippian and part of the Pennsylvanian sections, Lincoln County, Oklahoma. Six principal facies were determined using sedimentological features and composition from XRD and thin-section petrography (Table 11)(Hill, 2017).

Table 13 Description of principal Mississippian facies, LNK core (Hill, 2017).

Facies	Color	Minerology (Ave %)			Sedimentological Character	Primary Grain Constituent
		Quartz	Carbonate	Clays		
6-Silty Poloidal Packstone-Grainstone	Very light gray to medium gray & moderate yellowish brown	29.4	56.6	4.4	Massive Bedded, Mineralized Fractures	Peloids, crinoids, brachiopods, and minor bryozoan fragments
5- Silty Burrowed Mudstone-Wackestone	Light olive gray & greenish black to grayish black	30.5	46.2	15.0	Burrowed, Mineralized Fractures	Brachiopods, crinoid fragments, indistinguishable skeletal debris
4-Silty Argillaceous Sandstone-2	Dark greenish gray to dusky yellow green & moderate olive brown	56.0	8.4	18.8	Burrowed and Bioturbated to Laminated parallel to bedding	Brachiopods, very fine sand, and silt-sized quartz grains
3-Slightly Sandy Calcareous Siltstone	Olive-gray to dark gray	47.0	19.3	15.7	Bioturbated and Burrowed, Mineralized Fractures	Brachiopods, silt, and sized quartz grains
2-Clay-rich Siltstone	Dusky green, greenish black & grayish black	43.5	11.8	24.6	Planar Laminae, Locally-Thinly Bedded	Brachiopods, silt, and sized quartz grains
1-Glauconitic Sandstone	Dusky yellowish green to grayish green	45.0	3.0	37.0	Massive Bedded, Burrowed	Conodonts, Brachiopod fragments, glauconitic; quartz grains

Normal Alkanes and Acyclic Isoprenoids

Normal alkanes and acyclic isoprenoids of LNK core samples varied with depth, particularly within the Mississippian section. Figure 42 compares rock extract chromatograms of the major subunits in the Mississippian and the Woodford Shale. Overall, most chromatograms show a unimodal distribution of normal alkanes, maximizing at around n-C_{13} to n-C_{15}. Such n-alkane envelopes are documented in marine phytoplankton and hence considered evidence supporting the inference that Mississippian and Woodford kerogens are of marine origin (Blumer et al., 1971). However, some samples from the upper and middle Mississippian units are enriched in isoprenoids, particularly phytane. Isoprenoid enrichment could be due to isoprenoid resistance to biodegradation and maturity, together with enrichment due to kerogen source (Alexander et al., 1981; Didyk et al., 1978). Biodegradation effect is unlikely to be the cause of enrichment of isoprenoids in the Mississippian samples because n-alkanes are still intact and aerobic microbes preferentially attack n-alkanes prior to the rest of hydrocarbons (Peters et al., 2005c). Since these core samples are within the immature oil-window as indicated in Figure 34, the enrichment of isoprenoids is unlikely caused by maturity, and hence the Mississippian sample predominance in pristane and phytane is unlikely due thermal maturation of glyceryl ethers (Rontani and Bonin, 2011). It is possible that the enrichment of isoprenoids in the Mississippian sample is caused either by the source of organic matter or the redox conditions during sediments deposition. However, the specificity of n-alkanes and isoprenoids is poor for the reasons discussed in Chapter II; pristane and phytane exhibit multiple origins. Another relationship of pristane and phytane to their normal alkanes counterpart is observed to reflect kerogen type and redox settings, more specifically, the ratio of pristane to n-C_{17} compared the ratio of phytane to n-C_{18}. Figure 43 compares those ratios in a cross-plot, with superimposed kerogen type and redox conditions. Clearly, the Woodford
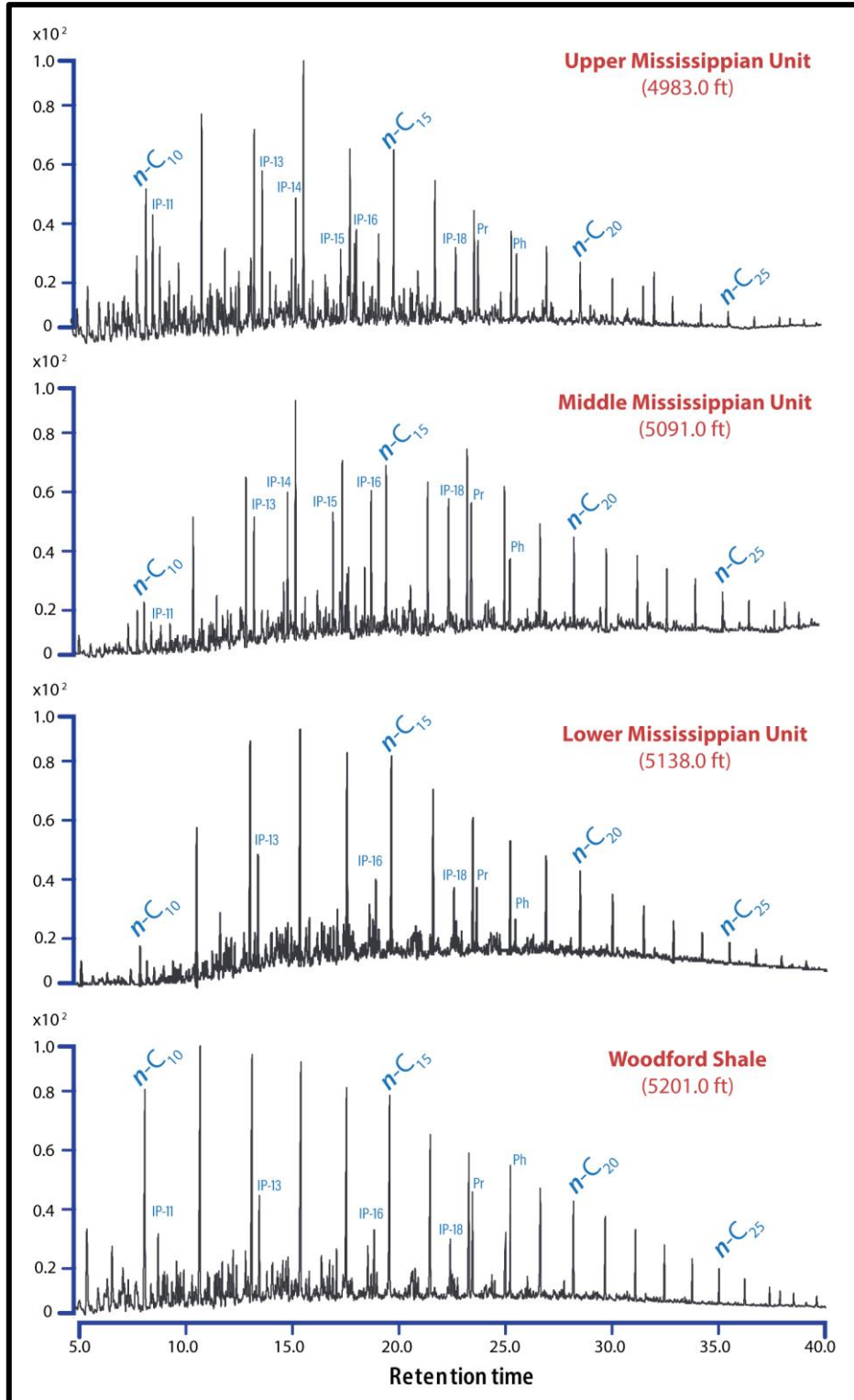
Figure 42: Chromatograms of extracted bitumen showing overall *n*-alkane envelope distribution. LNK core samples are from organic-rich mudrocks from upper, middle and lower units of the Mississippian and the Woodford Shale.

118

Shale sample plot is within Type II with primarily marine Type-II kerogen, which is also supported by visual petrographic evidence shown in the photomicrographs of Figure 37. Moreover, Mississippian samples overall varied between Type-II marine, and Types II and III kerogens (Figure 43). The Lower Mississippian unit shows the most reducing and marine organic-matter contribution compared to the Middle and Lower Mississippian units. This shift in redox conditions was also observed in other parameters, which are discussed in further details in the depositional model section.
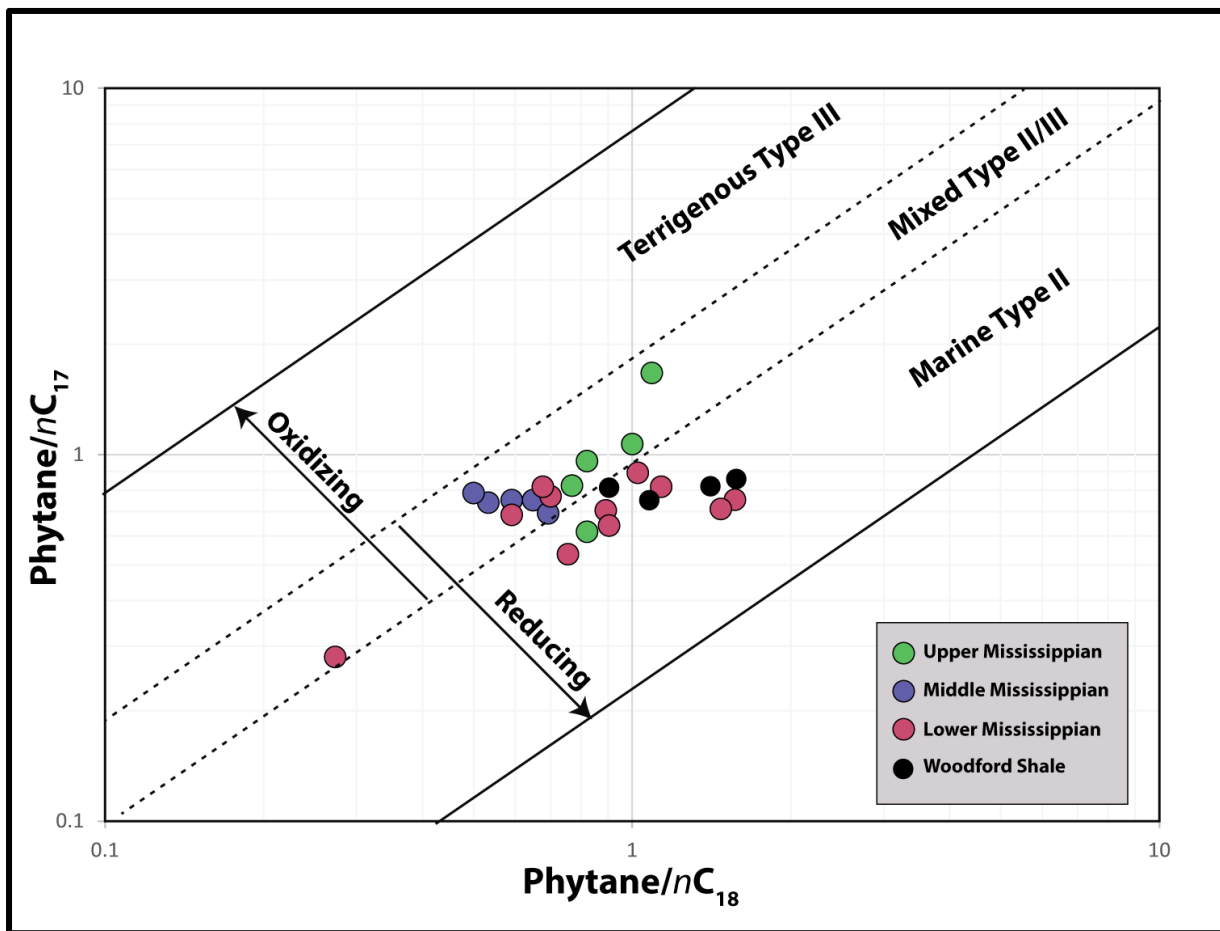
Figure 43: Cross-plot comparing ratios of pristane to heptadecane (n-C_{17}) and the ratio of phytane to octadecane (n-C_{18}).

Biomarkers

In the terpane biomarkers class, Mississippian samples are uniquely enriched in extended tricyclic terpanes ranging up to C_{39}. This observation coincides with previous geochemical studies that examined crude oil and rock extracts from Mississippian rocks . Previous studies used single-quadrupole mass-spectrometer (GC-MS) techniques to detect theses terpane biomarkers, particularly through interpreting the fragmentogram of m/z 191. Figure 44 shows multiple mass chromatograms of extracted bitumen from organic-rich Mississippian and Woodford samples (Al Atwah et al., 2019; Wang and Philp, 1997a). A clear difference in terpane biomarkers can be observed between Mississippian and Woodford rock extracts. This difference is reflected in the presence and absence of extended tricyclic terpanes, together with the relative abundance of tricyclic terpane to hopane biomarkers (Figure 44). However, the challenge with extended tricyclic terpanes, especially those ranging between C_{33-39}, is that they co-elute with the pentacyclic terpanes (also known as the homohopanes series) due to the similarities in their molecular masses (Figure 44). The m/z191 mass chromatograms illustrate the challenge of quantifying extended tricyclic terpanes in Mississippian samples. Therefore, in this study, we overcome this co-elution problem by utilizing the triple quadrupole mass spectrometer (GC-MS/MS) with MRM selectivity, which detects extended tricyclic terpanes as doublets based on the carbon number (Figure 45).

In the Mississippian samples, both lower and extended tricyclic terpane biomarkers are more abundant than hopanes, and they are different than the Woodford Shale. Moreover, extended tricyclic terpanes ranging from C_{30} to C_{39} in Mississippian samples exhibited an average absolute concentration of 30 ppm, whereas Woodford samples contain an average absolute concentration of only 3 ppm extended tricyclic terpanes ranging from C_{30} to C_{35}, with the absence of C_{36} to C_{39} tricyclic terpanes. The overall hopanes distribution also varied across the examined rock extracts,

with hopane and homohopanes prevailing in the Woodford Shale extracts (Figure 44). Particularly, Woodford extracts are characterized by an abundance of hopane and C_{29} norhopane together with the C_{31} to C_{35} homohopane series. In the Mississippian extracts, the extended tricyclic terpanes dominated and coeluted with homohopanes. Additionally, the C_{23} tricyclic terpane relative to hopane is higher in Mississippian extracts, while lower in Woodford extracts. This ratio increased with increasing depth within the Mississippian sample and is reversed in the Woodford Shale, the hopane dominate over the C_{23} tricyclic terpane (Figure 44).

The biological precursor of the extended tricyclic terpanes is not clearly defined. It has been suggested that *Tasmanites* could be a source for the tricyclic terpanes (Greenwood et al., 2000). An abundance of tricyclic terpanes ranging from C_{19} to C_{54} was observed in crude oil and rock extracts of Early to Late Cretaceous age from Brazilian marginal basins (De Grande et al., 1993; Mello et al., 1988). In these studies, the enrichment of extended tricyclic terpanes is believed to reflect water salinity conditions during deposition, with their enrichment associated to marine carbonate and lacustrine environments (De Grande et al., 1993). In the studied Mississippian carbonates, the origin of extended tricyclic terpanes is related to the biota that survived at the littoral zone, associated with shallow and clear waters within a carbonate-ramp depositional setting. For the Woodford Shale samples that contain *Tasmanites* (Figure 39), their presence did not coincide with the enrichment of extended tricyclic terpanes (Table 13), which are only found in trace amounts. From Figure 47, we observe a correlation between the dominance of bituminite and the increase in extended tricyclic terpane concentration. However, this is not adequately clear evidence to suggest that the correlation is causal between bituminite and extended tricyclic terpanes.
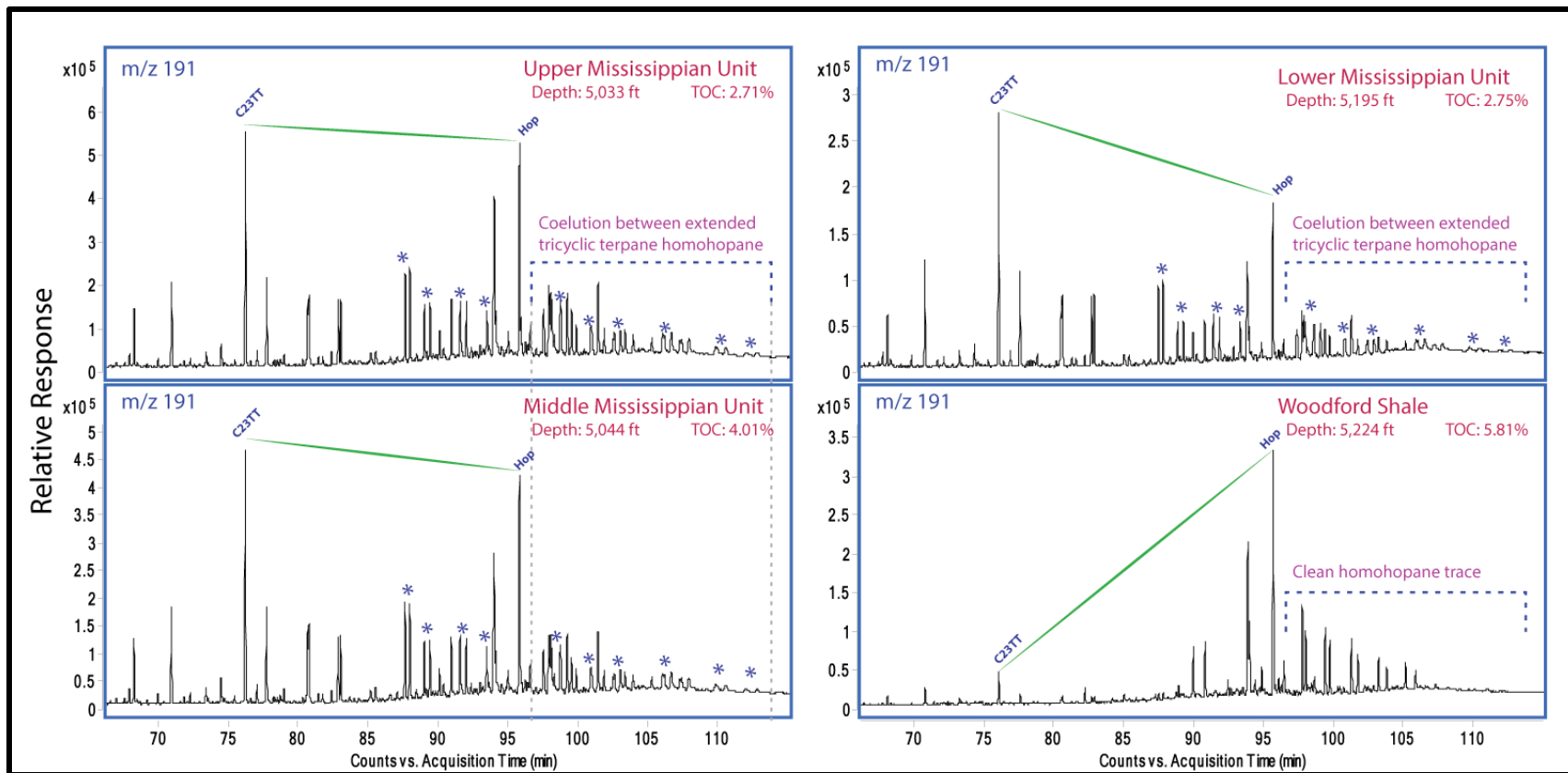
Figure 44: Mass chromatograms of extracted bitumens showing overall terpane biomarkers distribution. Samples are from organic-rich mudrocks from the upper, middle and lower units of the Mississippian, and the Woodford Shale. $C_{23}TT$: C_{23} tricyclic terpane, Hop: hopane. Peaks marked by * are series of extended tricyclic terpanes ranging from C_{28} to C_{39}, peaks are listed in Table 2. Note how extended tricyclic terpanes co-elute with homohopanes in Mississippian samples, and are absent from Woodford Shale.
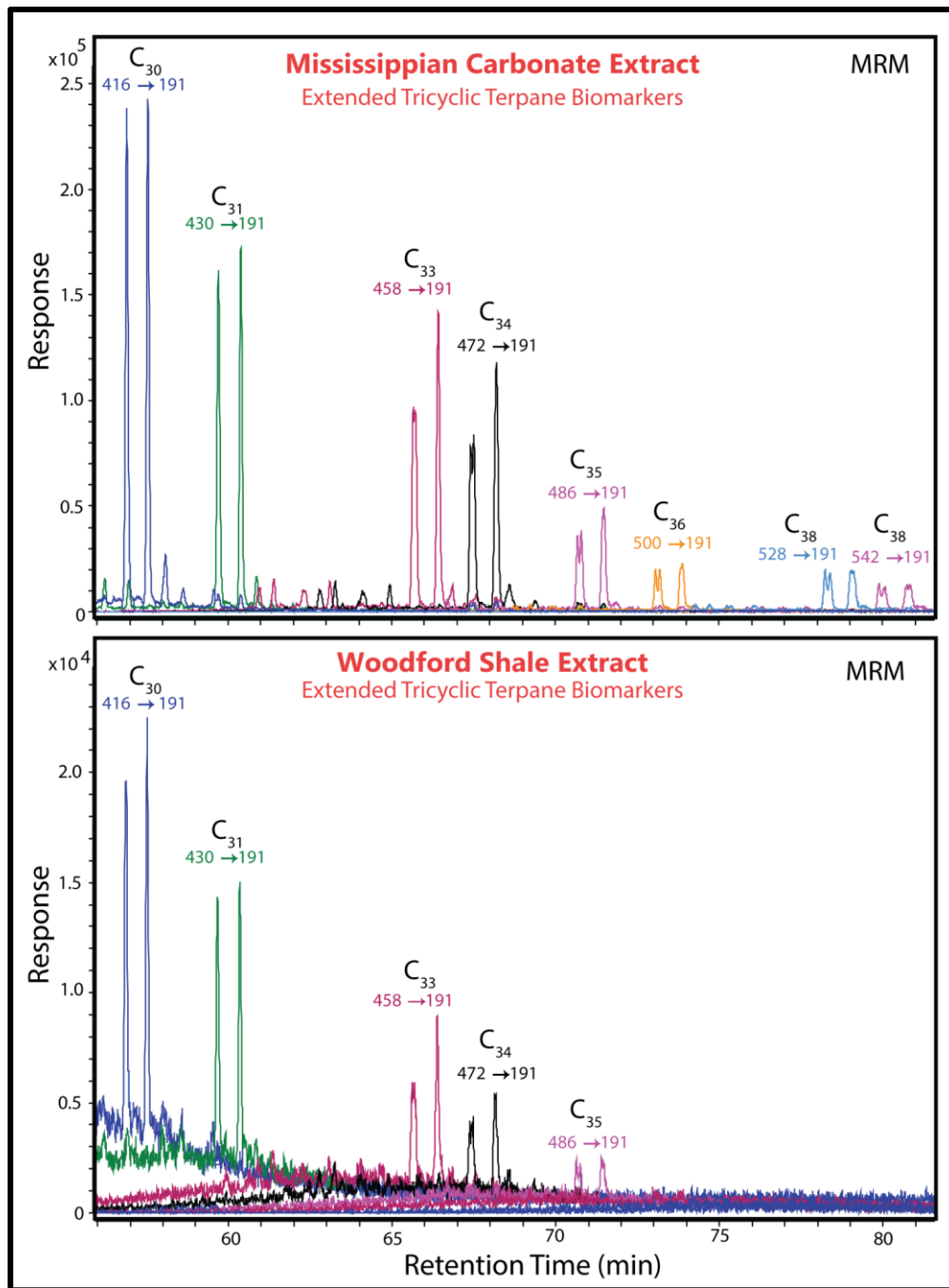
Figure 45: Mass fragmentograms showing diagnostic precursor-product transitions of extended tricyclic terpane biomarkers. The series of extended tricyclic terpanes are enriched in Mississippian mudrocks and depleted in Woodford Shale. (MRM: Multiple Reaction Monitoring).

As for the sterane biomarker class, Figure 46 shows the classic ternary diagram comparing regular steranes. The relative concentration of C_{29} sterane is the highest in the Woodford Shale, whereas the highest C_{28} and C_{27} values occur in Mississippian samples. However, there is a large overlap between the samples in their regular steranes content. This overlap could be because samples are of marine origin, and therefore share a similar eukaryotic sterol signature.

Notably, 4-methylsterane biomarkers are found in higher concentrations in samples from the Woodford Shale and lower Mississippian than in other samples (Figure 47). The 4-methylsteranes maximize in the Woodford Shale at about 1.35 ppm, followed by 1.13 ppm in the
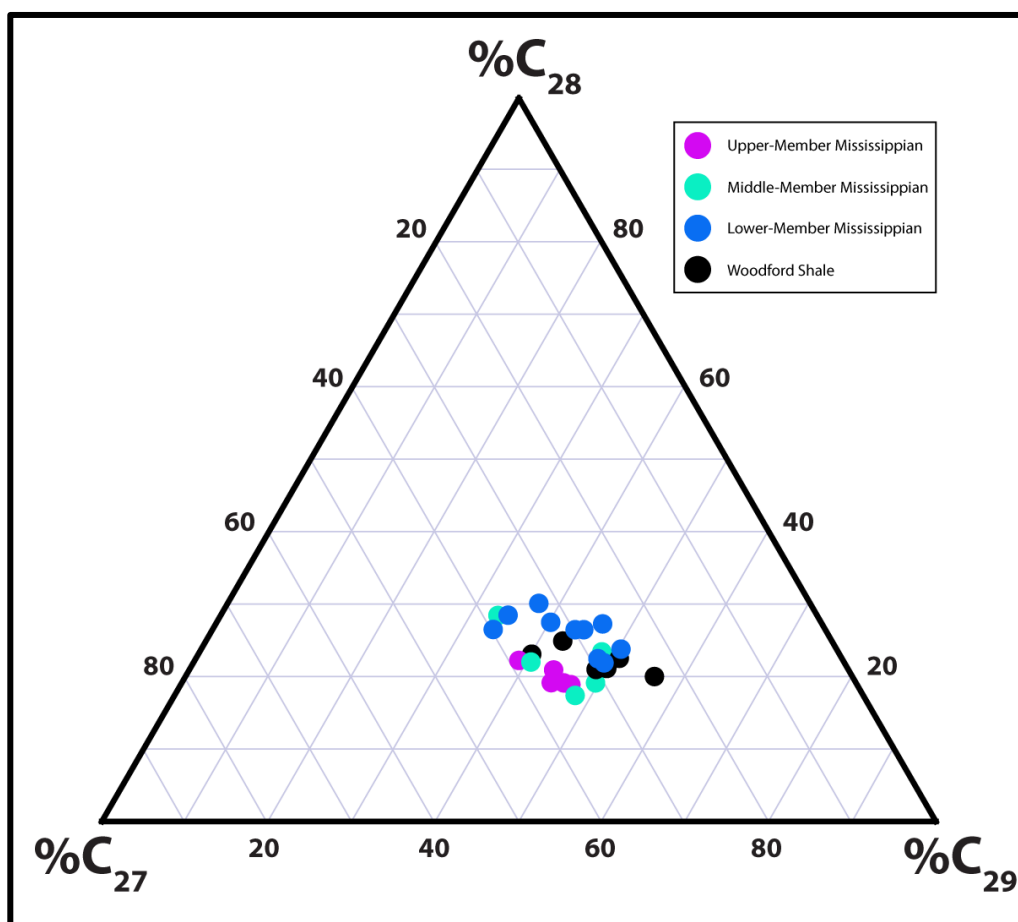
Figure 46: Classic ternary diagram comparing relative concentrations of ααα-C_{27}, C_{28} and C_{29} regular steranes of Woodford Shale samples and different members of Mississippian mudrocks as measured by GC-MS/MS.

lower unit of the Mississippian. This observation could be related to the presence of acritarchs in the Woodford Shale, where they were preserved (Figure 39). A number of studies investigating the occurrence of methylsterane biomarkers suggest its link to acritarchs as ancestors for dinoflagellates (Al Atwah and Jacobi, 2017; Moldowan and Talyzina, 1998; Talyzina et al., 2000).

Diterpanoid biomarkers are usually linked to terrigenous organic matter and crude oil generated from terrigenous kerogens (Noble et al., 1986). Moreover, the occurrence of diterpenoid has been suggested to originate from conifer resins (Gough, 1964). Table 13 shows key diterpanoids measured for the studied samples. Clearly, rock extracts from the Mississippian interval showed trace amounts of diterpanoid biomarkers, particularly tetracyclic and tricyclic (Figure 44). However, Woodford Shale extracts did not contain diterpanoid biomarkers. Furthermore, Mississippian extracts are higher in tetracyclic diterpanes than tricyclic diterpanes,
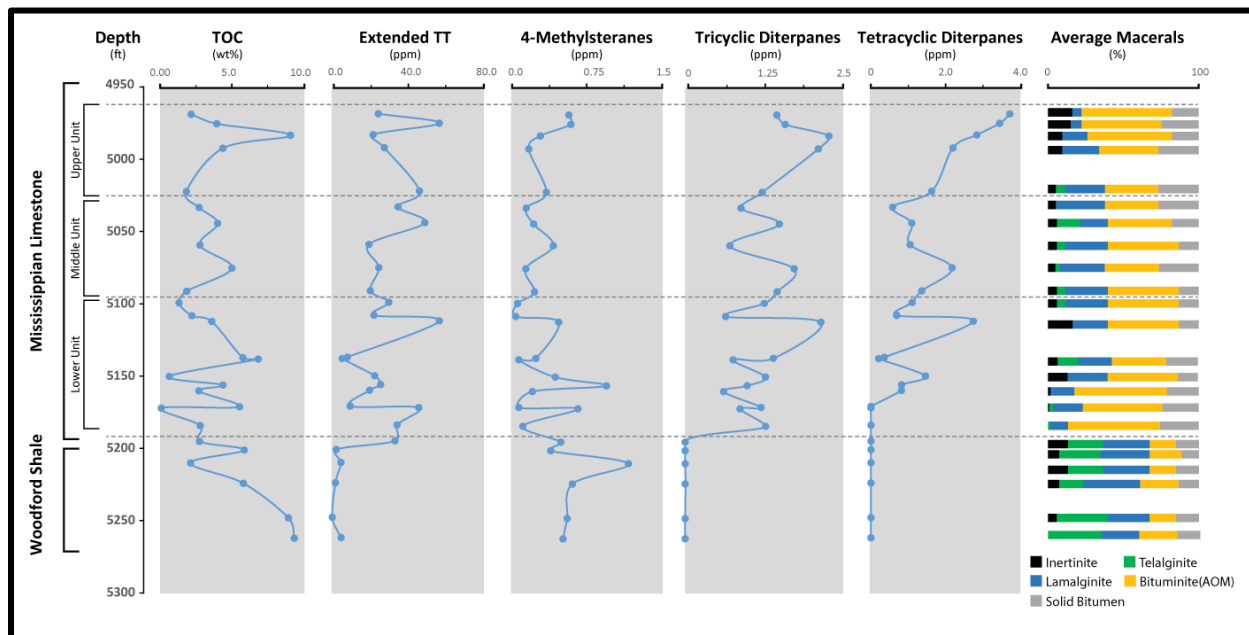
Figure 47: Depth profiles across the Woodford Shale and Mississippian limestone comparing concentrations of total organic carbon, key selected biomarker ratios (Extended TT [tricyclic terpanes], 4-methylsteranes, Tricyclic Diterpenes, and Tetracyclic Diterpenes), and average maceral distribution.

125

more specifically, the sum of tetracyclic diterpanes (Beyerane, 16β Phyllocladane, 6β Kaurane, Atisane, 16α Phyllocladane, and 16α Kaurane) (Table 13). It is apparent also from Figure 47 that concentrations of diterpanoid biomarkers decrease with depth, suggesting a higher terrigenous organic input in the upper unit of the Mississippian. It is furthermore important to note that the Mississippian carbonate mudrock kerogen is primarily of marine origin, as evidenced from the macerals; however, the occurrence of diterpenoids suggests minor input of terrestrial organics that otherwise might be overlooked.

Table 14 Key biomarker ratios of extracted bitumens, Mississippian limestone and Woodford Shale, LNK core.

Formation			Depth (ft)	Pr/n-C$_{17}$ *	Ph/n-C$_{18}$ ×	4-MeStern +	ETT ∘	TriDi ±	TetraDi [Δ]
Lower Mississippian	Upper Unit		4,968.5	0.70	0.89	0.75	25.02	1.33	3.50
			4,975.0	0.62	0.85	0.77	57.34	1.47	3.19
			4,983.0	1.67	1.09	0.46	22.22	2.20	2.55
			4,992.0	0.96	0.83	0.35	28.16	2.00	1.99
			5,022.0	0.91	1.02	0.52	46.77	1.15	1.51
	Middle Unit		5,033.0	0.70	0.69	0.32	35.44	0.85	0.52
			5,044.0	0.82	1.13	0.39	49.66	1.50	0.97
			5,059.0	0.80	0.75	0.59	20.03	0.70	0.83
			5,075.0	0.73	0.59	0.31	25.29	1.61	1.88
			5,091.0	0.74	0.53	0.40	20.77	1.31	1.19
			5,099.0	0.78	0.50	0.23	30.60	1.13	0.95
			5,108.0	0.69	0.70	0.21	22.63	0.56	0.57
	Lower Unit		5,112.0	0.71	1.47	0.65	57.29	1.30	1.35
			5,137.0	0.75	1.56	0.42	8.63	1.10	0.36
			5,138.0	0.71	0.59	0.24	5.89	0.65	0.19

| | 5,150.0 | 0.82 | 0.67 | 0.61 | 23.12 | 1.10 | 1.30 |

Table 13 continued.

Formation	Depth (ft)	Pr/n-C$_{17}$ *	Ph/n-C$_{18}$ ×	4-MeStern +	ETT ∘	TriDi ±	TetraDi Δ
	5,156.0	0.74	0.65	1.13	26.27	0.85	0.72
	5,160.0	0.64	0.90	0.38	20.33	0.53	0.64
	5,171.0	1.04	1.01	0.24	10.10	1.20	0.00
	5,172.0	0.54	0.75	0.84	46.43	0.86	0.00
	5,184.0	0.79	0.69	0.28	34.99	1.27	0.00
	5,195.0	0.29	0.27	0.67	33.85	0.99	0.00
Woodford Shale	5,201.0	0.86	1.56	0.57	2.72	0.00	0.00
	5,210.0	0.81	1.40	1.35	5.22	0.00	0.00
	5,224.0	0.82	0.90	0.78	2.30	0.00	0.00
	5,248.0	0.76	1.08	0.73	0.67	0.00	0.00
	5,262.0	0.78	1.01	0.69	5.30	0.00	0.00

*Pristane/n-C$_{17}$

×Phytane/ n-C$_{18}$

+4-MeStern: Sum of 4-methylsteranes (4α-Methyl-24-ethylcholestane20S+4α-Methyl-24-ethylcholestane14,17β(H)20R+4α-Methyl-24-ethylcholestane20R)

∘ETT: Sum of extended tricyclic terpanes C$_{30}$ to C$_{39}$ in PPM

±TriDi: Sum of tricyclic diterpanes (Rimuane, Pimarane, Rosane, Isopimarane and Phyllocladane) in PPM

ΔTetraDi: Sum of tetracyclic diterpanes (Beyerane, 16β Phyllocladane, 6β Kaurane, Atisane, 16α Phyllocladane, and 16α Kaurane)

□ETT/HH: Sum of extended tricyclic terpanes C$_{30}$ to C$_{39}$ / sum of homohopanes C$_{31}$ to C$_{35}$

Diamondoids

Diamondoids distribution of LNK samples showed relatively slight variations than those observed in biomarkers. The lower units of Mississippian, together with Woodford Shale, showed the relative higher abundance of diamondoids. However, the absolute concentrations of diamondoids in all samples are considered very low compared to the diamondoids presence in mature source rock or cracked hydrocarbons (i.e., condensates). Upper and middle units within Mississippian rocks range in total diamondoid concentration from 25 to 30 ppm, and with 4-

methyldiamantane and 3-methyldiamantane of 1.4 to 2.2 ppm. Moreover, the Lower Mississippian unit together with Woodford Shale exhibited total diamondoid concentration of 28–36 ppm, and particularly 4-methyldiamantane and 3-methyldiamantane ranging from 2.5–2.8 ppm (Table 14). Diamondoid concentration of immature rock extracts are critical to establish the diamondoid baseline. The diamondoid baseline is used as a tool to evaluate the extent of hydrocarbon cracking and unravel petroleum mixing of various maturities (Dahl et al., 1999b). Based on examining crude oils from different source rocks and basin settings, Moldowan et al. (2016) observed that the diamondoid baseline can vary depending on the source-rock type. For example, the diamondoid baseline for oil samples correlated to the Kreyenhagen Formation within the San Joaquin Basin Province is 2 ppm, while oils from the Smackover Formation within the Gulf of Mexico exceeds 10 ppm (Moldowan et al., 2015). Therefore, it is crucial to establishing the baseline for each petroleum system defined by its source rock. From the results documented in Table 14, it is clear that the baseline for Mississippian-Devonian source rocks is within approximately 2 ppm.

The origin of diamondoids as discussed in Chapter II is closely related to the kerogen type and the type of clays present during petroleum generation from the source rock. Therefore, it is very likely that the difference of diamondoid concentration observed in Table 14 is influenced by clay content. However, even though the clay content is higher in the Upper and Middle units of the Mississippian formation containing Facies 3 (slightly sandy calcareous siltstone) and Facies 2 (clay-rich siltstone), it is unclear why they contain lower concentration of diamondoid than the Lower Mississippian unit. Nevertheless, the overall absolute concentrations of diamondoid in the LNK core are relatively low, which support the evidence previously presented that the LNK core is thermally immature, and that the Mississippian-Devonian source rocks exhibit a lower

diamondoid baseline than that of other source rocks examined by other authors (Moldowan et al., 2015).

Table 15 Diamondoids concentration of extracted bitumen from LNK core

Formation		Depth (ft)	Adamantane[a]	Diamantanes[b]	Total Diamondoids[c]	4-+3-Methyldiamantane °
Lower Mississippian	Upper member	4,968.5	4,968.50	24.21	4.27	28.48
		4,975.0	4,975.00	28.35	2.02	30.37
		4,983.0	4,983.00	20.51	8.18	28.69
		4,992.0	4,992.00	19.10	5.80	24.90
		5,022.0	5,022.00	22.57	3.95	26.52
		5,033.0	5,033.00	17.99	8.21	26.2
	Middle member	5,044.0	5,044.00	22.58	2.88	25.46
		5,059.0	5,059.00	23.36	5.85	29.21
		5,075.0	5,075.00	25.92	2.41	28.33
		5,091.0	5,091.00	27.21	3.54	30.75
		5,099.0	5,099.00	23.22	6.88	30.1
		5,108.0	5,108.00	19.36	3.95	23.31
	Lower member	5,112.0	5,112.00	31.17	4.15	35.32
		5,137.0	5,137.00	27.21	7.01	34.22
		5,138.0	5,138.00	19.63	8.66	28.29
		5,150.0	5,150.00	28.36	5.05	33.41
		5,156.0	5,156.00	22.83	7.02	29.85
		5,160.0	5,160.00	29.11	6.14	35.25
		5,171.0	5,171.00	25.74	4.57	30.31
		5,172.0	5,172.00	26.33	4.08	30.41
		5,184.0	5,184.00	27.12	8.94	36.06
		5,195.0	5,195.00	22.75	5.41	28.16
Woodford Shale		5,201.0	5,201.00	24.36	5.22	29.58
		5,210.0	5,210.00	27.22	5.99	33.21
		5,224.0	5,224.00	26.88	8.27	35.15
		5,248.0	5,248.00	27.25	7.03	34.28
		5,262.0	5,262.00	29.22	4.11	33.33

[a] Adamantanes=sum of adamantane and its alkylated counterparts (*m/z:*135, 136, 149, 177)
[b] Diamantanes=sum of diamantanes and its alkylated counter parts (*m/z:* 187, 188, 201)
[c] Total Diamondoids=Sum of a+b

Organofacies Depositional Model

The general depositional setting of the Oklahoma Basin during Late Cambrian through Mississippian time was dominantly an epeiric sea that resulted in thick carbonate deposits interbedded with shales and coarser siliciclastic sediments (Johnson, 1989a). Our results more specifically capture the transition from Late Devonian to Mississippian time. Sedimentological and organic-matter evidence suggest that depositional settings shifted from deeper, low-energy, and poorly oxygenated water (Woodford Shale) to shallower more-oxygenated waters (Upper Mississippian). The presence of diterpanoid biomarkers, spore-like acritarchs, and the increase in both, carbonate mineral content and the increase in skeletal grains in the Middle and Upper units of the Mississippian support the interpretation of somewhat restricted shallower waters during deposition. In contrast, the Woodford Shale depositional settings and to some extent the Lower unit of the Mississippian carbonate mudrocks contain acritarch spines and *Tasmanites.* The enrichment in 4-methylsteranes, together with the lack of any terrigenous biomarkers, are more characteristic of distal to shoreline, low-energy deposition. Figure 48 summarizes the overall maceral and biomarker signatures along with the inferred associated depositional settings.

Across the stratigraphic column, Mississippian units show clear trends that can be observed in Figure 41. With shallowing or shoaling-upward sequences, the Lower unit contains mudstone to packstones and is dominantly Facies 5 and 6, with limited occurrences of Facies 2. This unit is also characterized by the presence of diterpenoids and relatively enriched in 4-methylsteranes, which are interpreted to indicate that the Lower unit marks the deepest water settings reached during Mississippian carbonate deposition. In contrast, facies of the Middle and Upper units are dominantly clay-rich siltstones, with a mixture of sandy calcareous siltstone and silty argillaceous sandstones (Figure 40). Additionally, biomarkers such as diterpenoids increase in concentration

with decreasing depth, maximizing in the upper unit. This geochemical trend coincides with a relative increase in inertinite macerals (Figure 47). Collectively, all are multiple lines of evidence that Mississippian rocks represent a prograding shoaling-upward sequence in close proximity to the shoreline.
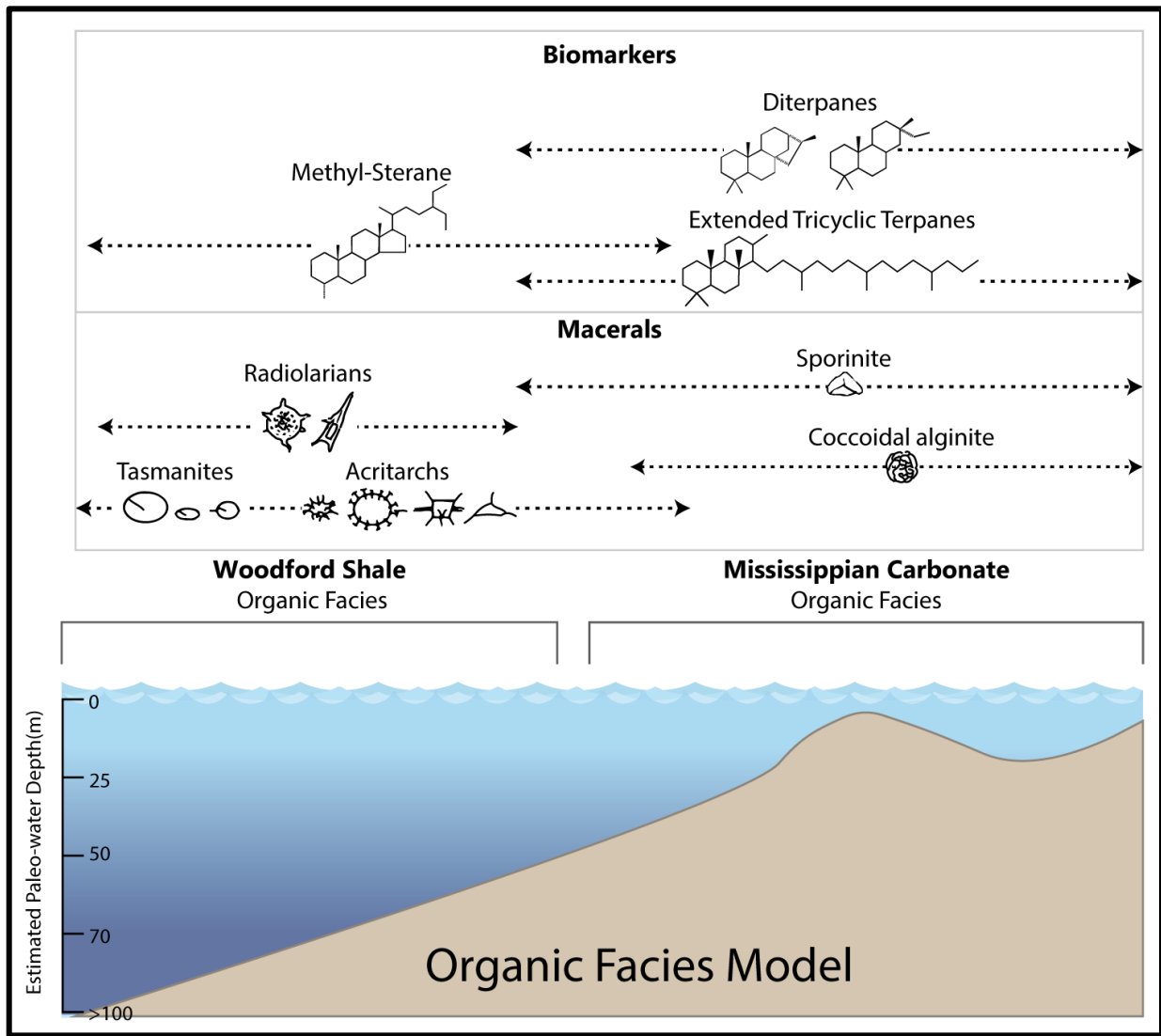
Figure 48: Proposed organic facies model during the transition from Late-Devonian to Early-Mississippian in central-Oklahoma. The model is supported by distinct maceral morphologies and biomarker compositions. Modified from (Stasiuk and Fowler, 2004).

The process of petroleum generation and expulsion from source-rocks are referred to as primary migration, whereas secondary migration is the movement of petroleum through carrier beds into conventional hydrocarbon accumulations (Hunt, 1996). Petroleum generation and expulsion is primarily controlled by source-rock kinetics, that is, the interaction of source-rock kerogen and mineralogy. Among geochemists, two main different schools of thought exist with regards to deriving source-rock kinetics, which primarily vary in the experimental setup. These schools include closed isothermal hydrous pyrolysis and open non-isothermal non-hydrous pyrolysis approaches. Each analytical approach has its advantages and disadvantages. For
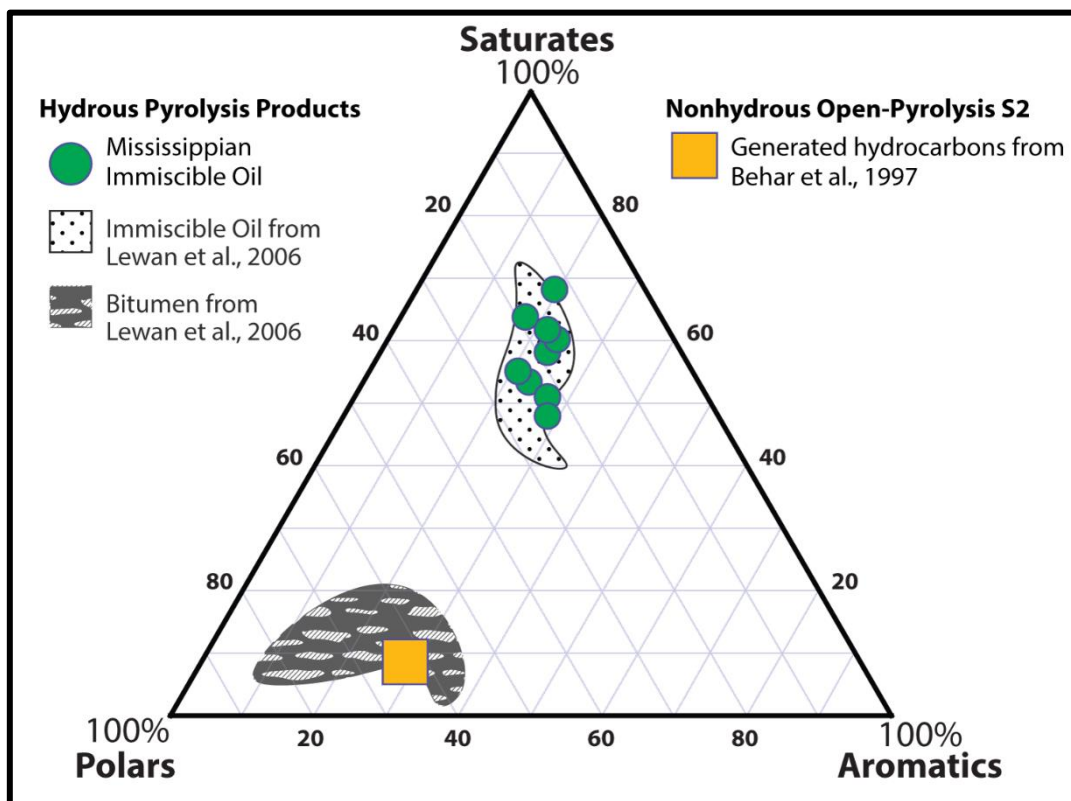
Figure 49: Ternary diagram of the relative abundance of saturates, aromatics and polars (resins and asphaltens) of immiscible oil generated from hydrous pyrolysis experiment of composite Mississippian source rock. Shaded polygons are results published in the literature experiments (Behar et al., 1997; Lewan et al., 2006).

example, the isothermal hydrous pyrolysis approach's advantage is the ability to generate oil under laboratory conditions, with oil-pyrolysis can be quantified with a very close composition to natural crude oil. However, hydrous pyrolysis requires a large quantity of sample (>30g) and takes three days to conduct the experiment. In contrast, the advantage of non-isothermal non-hydrous pyrolysis is that it requires small sample size (<100 mg) and can be quickly completed with a number of experiments conducted within a few hours. However, non-isothermal non-hydrous pyrolysis generates hydrocarbons that usually include artifacts caused by the quick temperature ramping and the inability to differentiate between generated oil and bitumen. Without a doubt, petroleum generation under geological conditions is a complex phenomenon to simulate under laboratory conditions. Therefore, it remains a subject of debate among geochemists as to which approach provides robust kinetic parameters. For the purpose of our study, we selected the hydrous pyrolysis approach for the main advantage of its ability to generate oil closely related to produced crude-oil composition, and due to the samples' availability (Lewan, 1985; Lewan and Ruble, 2002).

Generated oil from hydrous pyrolysis experiments of Mississippian composite source rock are enriched in saturated hydrocarbons and contain fewer polar components such as resins (NSOs) and asphaltenes (Figure 49). This also coincides with published literature on the immiscible oil that is usually generated during hydrous pyrolysis, which is compositionally similar to geological crude oils (Lewan et al., 2006; Lewan and Ruble, 2002). This similarity is due to the presence of water, with its role of differentiating between kerogen converting into polar-rich bitumen and cracking into immiscible oil that would flow on the surface of the water. Non-hydrous open-pyrolysis experiments lack this differentiation, with a composition of generated products being enriched in polar components (Figure 49) (Behar et al., 1997). Table 15 summarizes the parameters

133

Table 16 Key result of hydrous pyrolysis parameters.

Experiment No.	Temperature (°C)	Warm-up time (minutes)	Sample Weight (g)	Immiscible oil (mg/gTOC)	Fraction of reaction[a] (X)
HP-Miss-1	230.2	61.2	30.63	8.63	0.028
HP-Miss-2	280.1	57.3	31.06	25.16	0.082
HP-Miss-3	290.3	54.0	30.81	56.94	0.185
HP-Miss-4	300.0	68.8	31.21	71.84	0.234
HP-Miss-5	310.1	66.3	31.01	262.77	0.856
HP-Miss-6	320.6	58.9	30.81	289.18	0.945
HP-Miss-7	330.2	55.7	30.20	307.00	1.000
HP-Miss-8	340.1	64.3	30.38	296.26	0.965
HP-Miss-9	350.0	64.0	30.65	241.34	0.782

[a] X=immiscible oil yield/342.3

and results of the hydrous pyrolysis temperature-series experiments of the composite Mississippian

s The maximum yield of immiscible oil was observed at experiment No. HP-Miss-7 with a

temperature of 330°C, and a total of 307.00 mg of generated oil per gram of rock total organic

carbon, which is followed by experiment HP-Miss-8 at a temperature of 340°C with generated oil

of 296.26 mg of oil per gram of total organic carbon (Table 15). If assuming a first-order reaction

$f(x)$ of oil generation and maximum expelled-oil yield will mark the complete set of reactions with

the fraction of reactions set at 1, which is marked by experiment HP-Miss-7. The lowest yield of

oil is in experiment HP-Miss-1, with a temperature of 230°C and 8.63 mg of oil per gram of rock

total organic carbon and only 0.028 fraction of the reaction took place. Most notably, in experiment

No. HP-Miss-5, generated-oil abruptly increases almost threefold at 310°C to that of HP-Miss-4

experiment at 300°C. This increase could very likely mark the beginning of the oil window at the Mississippian source rocks. For comparison with the Woodford Shale, according to the hydrous pyrolysis experiments conducted by Lewan and Ruble (2002), the Woodford maximum yield of immiscible oil took place at a temperature of 350°C at around 240mg of oil per gram total organic carbon (Lewan and Ruble, 2002). Shown in Figure 50 are comparative curves representing oil yields of temperature-series hydrous pyrolysis experiments. A clear observation is the maximum yield of Mississippian rocks occurring at 330°C, while the Woodford Shale is at 350°C, which clearly reflects the difference in petroleum generation kinetics between the two source rocks. In addition, the absolute amount of oil generated is higher in Mississippian source rocks as compared
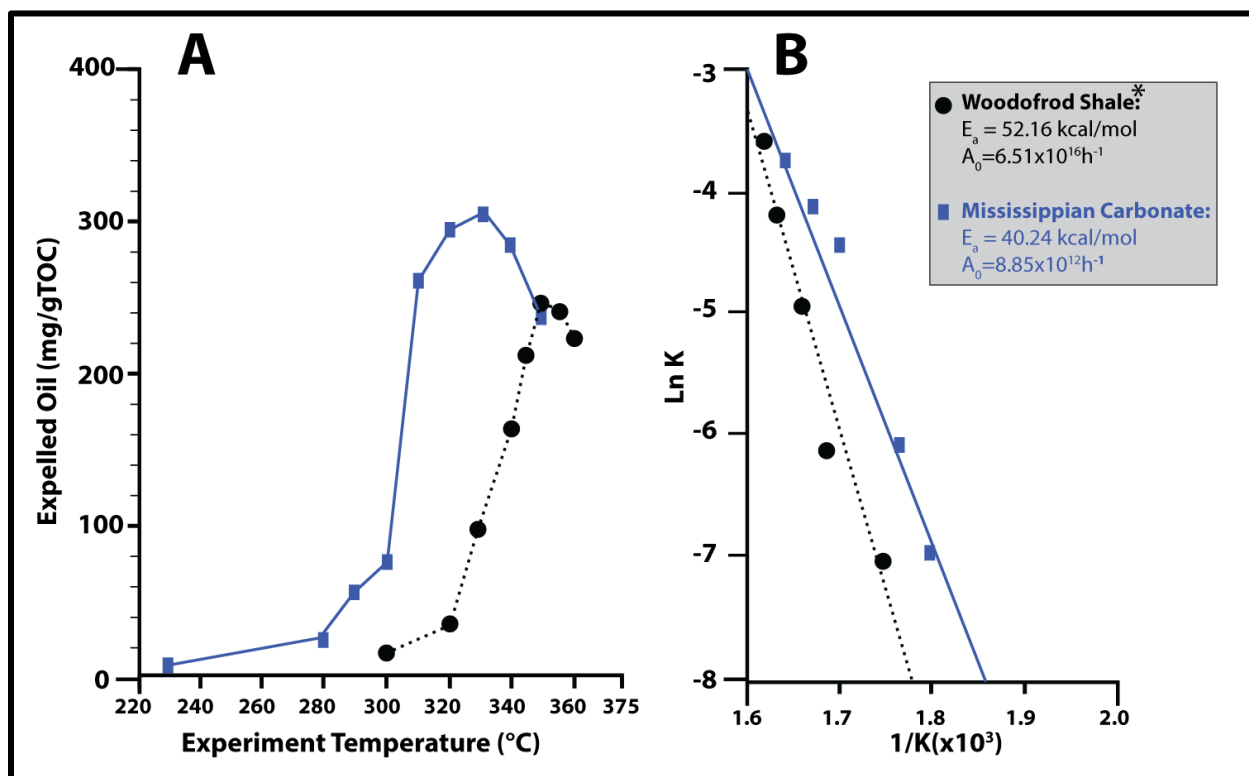
Figure 50: A) Cross plot comparing on the x-axis hydrous pyrolysis experiment temperature, and on the y-axis is weight of $C_{15}+$ hydrocarbons generated after the reaction is complete with a unit of mg of oil per gram of rock % TOC. B) Arrhenius plot comparing derived from hydrous pyrolysis temperature-series assuming a first-order reaction rate, Woodford data is from Lewan and Ruble (2002).

with Woodford Shale, with a maximum immiscible-oil yields for the former at 307 mg/gTOC and the latter at around 250 mg/gTOC (Table 15) (Lewan and Ruble, 2002). Such a difference in oil yield can be controlled by organic-matter type and its interaction with the mineral matrix.

Petroleum generation kinetic parameters can be derived from linear Arrhenius relationship from measured immiscible oil from hydrous pyrolysis experiments. More specifically, the activation energy (E_a) and frequency factor (A_0) of Mississippian and Woodford source rocks are shown in Figure 50-B. Those parameters are derived by plotting the natural logarithm of determined reaction rate constants at each experiment versus the reciprocal of their temperature. Hence, from this linear relationship, E_a is defined as the slope, and A_0 is derived from the intercept. From the Arrhenius plots, the derived activation energy (E_a) of Mississippian source rock is 40.24 kcal/mol, and the frequency factor (A_0) is $8.85 \times 10^{12} h^{-1}$ (Figure 50-B). The Woodford Shale activation energy is 52.16 kcal/mol, and the frequency factor is $6.51 \times 10^{16} h^{-1}$ (Lewan and Ruble, 2002). The Mississippian source rocks exhibit a lower activation energy than that of Woodford Shale, about 12 kal/mol difference between the two different source rocks. This observation is crucial and indicates that the Mississippian source rocks will start generating petroleum at lower thermal maturity than that of Woodford Shale source rock. This also dictates the amount of liquid versus gas hydrocarbons generated, and the timing of the onset of petroleum generation within the Anadarko Basin and Cherokee Platform

The differences in the kinetic parameters of petroleum generation between Mississippian and Woodford source rocks can be controlled by different factors that range from kerogen composition to the mineral matrix of the source rock. From the kerogen perspective, Type-II sulfur-rich kerogens have been reported to have lower activation energy than that of marine Type-II kerogen. For example, the Monterey Shale is composed of Type-II-S kerogen, with an activation

energy of 34.32 kcal/mol and a frequency factor of $7.59 \times 10^{10} h^{-1}$ (Lewan and Ruble, 2002).

However, it is unlikely that the lower kinetic parameter values of the Mississippian rocks are due

to the presence of sulfur-rich kerogen, for two main reasons: First, most of the produced oils from

both Woodford and Mississippian reservoirs are sweet crude oils with only trace amounts of sulfur;

therefore, it is unlikely that those oils have been generated from sulfur-rich kerogens. Second,

when examining the composition of generated oils during hydrous pyrolysis experiments, together

with composition of extracted bitumen from Mississippian and Woodford samples, both exhibit

trace amounts of organosulfur compounds, indicating the unlikelihood of the presence of any

Type-II-S kerogen in these source rocks. Moreover, Figure 51 compares the relationship between

dibenzothiophene (DBT) to phenanthrene (Phen) ratio vs pristane to phytane ratio; which can be

used to infer the depositional setting of the source rock, using dibenzothiophene as the proxy for

the enrichment for organosulfur compounds (Hughes, 1984). Both Mississippian and Woodford
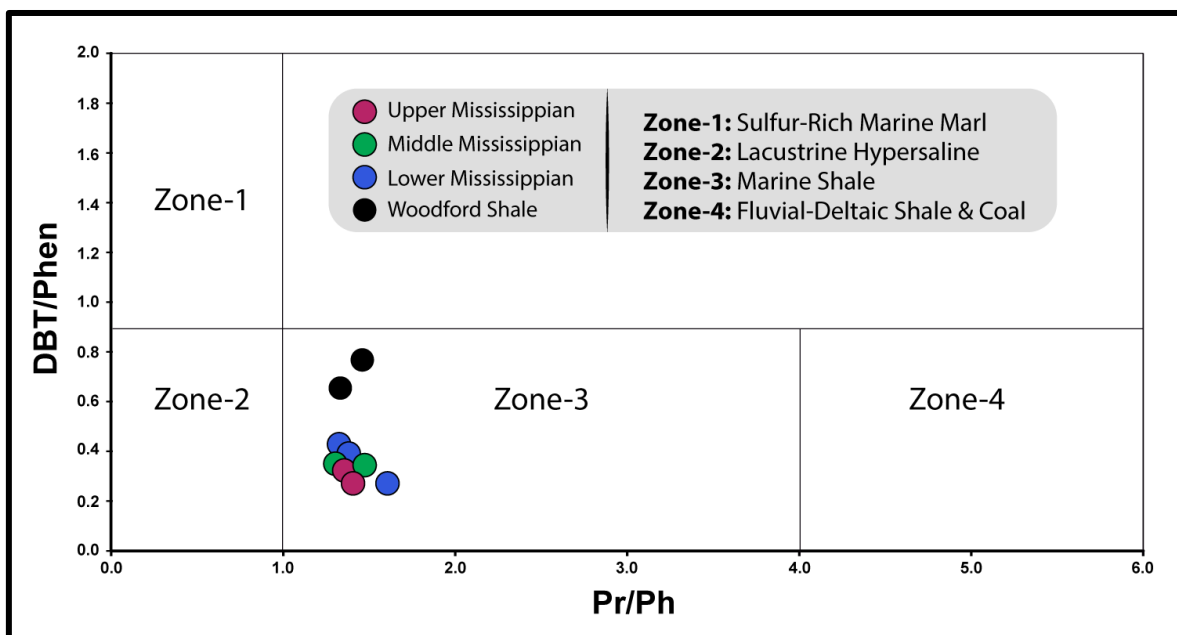
Figure 51: Cross plot of Mississippian and Woodford bitumen extracts comparing on the x-axis the ratio of pristane (Pr) to phytane (Ph) and on the y-axis is the ratio of dibenzothiophene (DBT) to phenanthrene (Phen). This graph is used to infer source rock depositional setting. Graph is modified from Hughes (1984).

samples plot within Zone 3, suggesting that they were deposited in marine shale settings, which supports the absence of Type-II-S kerogen within the Mississippian source rock. Therefore, the lower kinetic parameters of Mississippian source rock can be attributed to the kerogen structure and its interaction with the mineral matrix. Mississippian macerals can be observed in Figure 38 and Table 11 are the dominated by amorphinite, which is a submaceral group of liptinite (also known as bituminite). The morphology of amorphinite and its infusion through the mineral matrix increases the surface area for the reaction between the kerogen and the mineral matter, thereby facilitating the catalytic effect of minerals on the kerogen. This ultimately influences the reaction rates associated with the thermal conversion of kerogen into petroleum.

CHAPTER V

PETROLEUM GEOCHEMISTRY AND SOURCE-ROCK–OIL

CORRELATION*

Crude-Oil SARA

Crude-oil compound-class characterization also known as SARA analysis is listed in Table 16 together with API gravity. Overall, API gravity values varied the most within oil samples from the Anadarko Shelf, followed by oils from the STACK play. More specifically, Anadarko Shelf oils are produced from Mississippian reservoirs with API gravity ranging from 22° to 49° indicating medium, black oils and condensates, while STACK oils exhibited API gravity range of 32° to 50° (Table 16). Such API gravity variations within the Anadarko Shelf coincides with the trend of GOR within the Anadarko Shelf, which shows a wide range of fluid types ranging from black oil to dry gas (Figure 8). Oil samples from central Oklahoma situated on the eastern side of the Nemaha Uplift showed a narrower API gravity range of 33°–38° with primarily medium gravity oils.

Overall the crude-oil compound class followed a similar distribution trend with regards to percentage weight of the SARA components. Moreover, the most abundant fraction is the saturated hydrocarbons, followed by aromatics, then resin and asphaltenes. Such distribution of crude oil is also observed from the hydrous pyrolysis oils shown in Figure 50. Saturated hydrocarbons tend to increase with lighter hydrocarbons, such as in the condensate Bla-01-M with an API gravity of 49° and 87.5 wt. % of saturated hydrocarbons; however, relatively heavier fluids in some cases could also exhibit high saturated hydrocarbons such as Log-02-M (Table 16), a medium oil with 81 wt.

% saturates. As mentioned in the general trends, aromatic hydrocarbons varied most remarkably in oils located in the Anadarko Shelf and STACK play. These oils exhibited a wider range and higher abundance of aromatic hydrocarbons compared with oils from central Oklahoma. Aromatic hydrocarbons in oils located within the Anadarko Shelf ranged from 14–29 wt.% and 11–30wt.% for oils within the STACK. Theoretically, thermal maturity is a major factor for the increase of aromaticity observed in kerogens and coals; therefore, it is likely that the variation of aromatic hydrocarbons in these oils is a reflection of thermal maturity (Faulon et al., 1993; Tissot et al., 1987). However, to confirm the thermal maturity effect, further molecular evidence is needed, such as maturity-sensitive biomarker ratios.

Table 17 Bulk compositional and physical characteristics of selected crude oil samples.

Sample ID	Reservoir	API°	%SAT.[a]	%ARO.[b]	%POL[c]	%ASP[d]	Oil Type
Anadarko Shelf							
Alf-01-M	Mississippian	36.12	78.2	14.3	5.4	2.1	Medium Oil
Alf-02-M	Mississippian	37.39	63.4	28.7	3.4	4.5	Medium Oil
Woo-01-M	Mississippian	28.10	58.1	21.7	11.1	9.1	Black Oil
Woo-02-M	Mississippian	21.73	50.5	24.2	14.8	10.5	Black Oil
Kay-01-M	Mississippian	48.91	69.1	29.2	0.9	0.8	Condensate
Central OK							
Lin-03-W	Woodford	38.45	77	14.2	4.5	4.3	Medium Oil
Lin-02-M	Mississippian	33.24	78.3	11.2	7.7	2.8	Medium Oil

Sample ID	Reservoir	API°	%SAT.[a]	%ARO.[b]	%POL[c]	%ASP.[d]	Oil Type
Log-01-M	Mississippian	38.12	75.5	18.9	3.5	2.1	Medium Oil

Table 16 continued.

Sample ID	Reservoir	API°	%SAT.[a]	%ARO.[b]	%POL[c]	%ASP.[d]	Oil Type
Log-02-M	Mississippian	38.14	81.2	13.5	4.2	1.1	Medium Oil
Pay-01-M	Mississippian	38.27	66.6	17.8	8.4	7.2	Medium Oil
Pay-07-W	Woodford	34.21	75.7	18.7	3.8	1.8	Medium Oil
STACK Play							
Can-02-M	Mississippian	32.54	70.8	21.4	5.2	2.6	Medium Oil
Can-03-M	Mississippian	33.38	61.8	30.1	3.3	4.8	Medium Oil
Kin-02-M	Mississippian	35.6	64.5	28.7	5.0	1.8	Medium Oil
Kin-03-M	Mississippian	33.71	68.8	22.1	4.7	4.4	Medium Oil
Bla-01-M	Mississippian	49.39	87.5	10.9	1.1	0.5	Condensate

[a] SAT.: Weight percentage of saturate hydrocarbons
[b] ARO.: Weight percentage of aromatic hydrocarbons
[c] POL: Weight percentage of polar resin compounds (NSO)
[d] ASP.: weight percentage of asphaltenes

Gasoline-Range Hydrocarbons

Gasoline-range hydrocarbons encompass hydrocarbons with carbon numbers ranging from C_4 to C_{10}. Such compounds are a useful geochemical tool for oil-oil correlations, and for assessing oil alterations (e.g. water washing, biodegradation, thermal maturity, etc.) (Halpern, 1995; Thompson, 1983). Meanwhile, the inherent volatility of gasoline makes them vulnerable to evaporation loss; therefore, black oils and rock extracts sometimes lack these compounds. In this study, a selective sampling was performed for gasoline-range hydrocarbons, while the rest of the oil samples lacked the presence of adequate gasoline range hydrocarbons. Overall, of the 35 crude oils listed in Table 7, a total of 25 crude samples contained enough light hydrocarbons. Listed in Table 7 are analyzed samples, while Figure 52 shows the key ratios of the gasoline range hydrocarbons, which particularly focuses on heptanes and their alkylated counterparts.

Overall heptanes (C_7) results vary based on the geographic location of the samples. Samples located within the Anadarko Shelf exhibited a unique fingerprint of the C_7 star diagram (Figure 52). Particularly, these oils were enriched in the 3,3-dimethylpentane isomer relative to the rest of heptane isomers. Similarly, enrichment in 2,2-dimethylpentane and 2 4-dimethylpentane is observed within Mississippian oils located on the Anadarko Shelf. Additionally, within these oils the highest variance occurred at 2,2-dimethylpentane, followed by 3,3-dimethylpentane isomers (Figure 52). However, even with those variations, the overall star-diagram fingerprint is unique of Mississippian oils produced from the Anadarko Shelf compared to oils from Central Oklahoma and the STACK play (Figure 52). Most notably, oils located in central Oklahoma showed a narrow variation of the oil correlation star diagram, with a relatively moderate variance at the 3,3-dimethylpentane followed by 2,4-dimethylpentane isomers (Figure 52). Those subtle variations can group central-Oklahoma oils into two subgroups; the first group is enriched in 3,3-

142

dimethylpentane and lower in by 2,4-dimethylpentane isomers, while the second group is enriched in 2,4-dimethylpentane isomers and depleted in 3,3-dimethylpentane isomers. Crude oil from the STACK play showed a similar fingerprint to that of central-Oklahoma oils, with a wider variance of the star-diagram fingerprint.

The distribution of heptanes and its alkylated isomer compounds of the light hydrocarbons is believed to be sensitive to the crude-oil origin, with the rationale that each source rock producing a unique star-diagram fingerprint (Halpern, 1995). Moreover, the concept of using light hydrocarbons for oil correlation purposes was popularized by Mango (1987). Mango proposed that the origin of light hydrocarbons in crude oils from via metal-catalyzed steady-state kinetic reaction. Furthermore, Mango observed that while the concentration of light hydrocarbons from the same source varied by orders of magnitude, certain ratios of light hydrocarbons remained invariable, such as the sum of 2-methylhexane and 2,3-dimethylpentane relative to the sum of 3-methylhexane and 2,4-dimethylpentane (K_1) (Mango, 1987). To explain the invariance of the C_6-C_7 hydrocarbons, Mango postulated that light hydrocarbons originate from a higher saturated hydrocarbon with the presence of metal catalysis, resulting in a similar rate of reaction for homologous series. For example, the reaction that produces *n*-hexane and methylpentane should be similar to the yield of *n*-heptane and methylhexanes (Mango, 1987). While Mango's theory provides an attractive rationale to explain the formation of light hydrocarbons within the oil window's thermal stage, many aspects with regards to Mango's ring closure reactions remain unproven. For example, Mango's reaching scheme for the formation of light hydrocarbon requires the presence of olefinic bonds and hydrogen formed by kerogen precursor to yield the metal-catalyzed ring closure (Peters et al., 2005c). Following Mango's theory on the invariance of the

light hydrocarbons relative abundance of the same source rock, Halpern (1995) developed the star diagram for oil-oil correlation and oil transformation assessment.

The observed variation of star-diagram fingerprints in Mississippian and Woodford oils we suggest are related to the source-rock and evaporative fractionation. Crude oils located within the Anadarko Shelf are the farthest oils from the kitchen area of the Anadarko Basin. Therefore, these oils exhibit a unique fingerprint due to the influence of evaporative fractionation. Evaporative fractionation is a secondary alteration process by which an oil becomes enriched in light aromatic and naphthenic hydrocarbons relative to straight-chain and branched hydrocarbons (Thompson, 1987). Therefore, the oils within the Anadarko Shelf are a result of different hydrocarbon charges into the Mississippian reservoirs, in which these hydrocarbon charges are mostly affected by evaporative fractionation, and hence resulted in a unique star-diagram fingerprint. Crude oils within the STACK and central Oklahoma share an overall similar C_7 fingerprint, even though those oils are of different sources, as confirmed by biomarkers. The C_7 fingerprint does not appear to be an effective geochemical tool for identifying Mississippian-sourced oils from Woodford-sourced oils.

Light hydrocarbons can also be used to assess secondary crude-oil alteration such as biodegradation, water-washing and thermal maturity. The oil transformation star diagram is a multivariate plot in polar coordinates developed by Halpern (1995) to combine different ratios based on C_4-C_7 hydrocarbons (Halpern, 1995). These parameters include ratios such as the abundance of toluene relative to 1,1-dimethylcyclopeneante, labeled in Figure 52 as Tr1. This parameter is sensitive to water-washing effect, the Tr1 ratio decreases as the function of water-washing alteration. Such a ratio, for example, utilizes the solubility of toluene in water, which is

144

known to be around 520 ppm in distilled water, relative to the solubility of 24 ppm of 1,1-dimethylcyclopentane (Halpern, 1995)

The results of the Mississippian and Woodford oil transformation star diagrams share a common characteristic (Figure 52). First, most of the oils showed a low concentration of toluene, and hence, low Tr1 ratio, which is indicative of water washing. Such observation is not uncommon, especially for crude oils produced from the Mississippian Lime Play, like oils located in the Anadarko Shelf and central Oklahoma. One of the common observations of oil production from

the conventional Mississippian reservoir is the associated saline water production, and such.
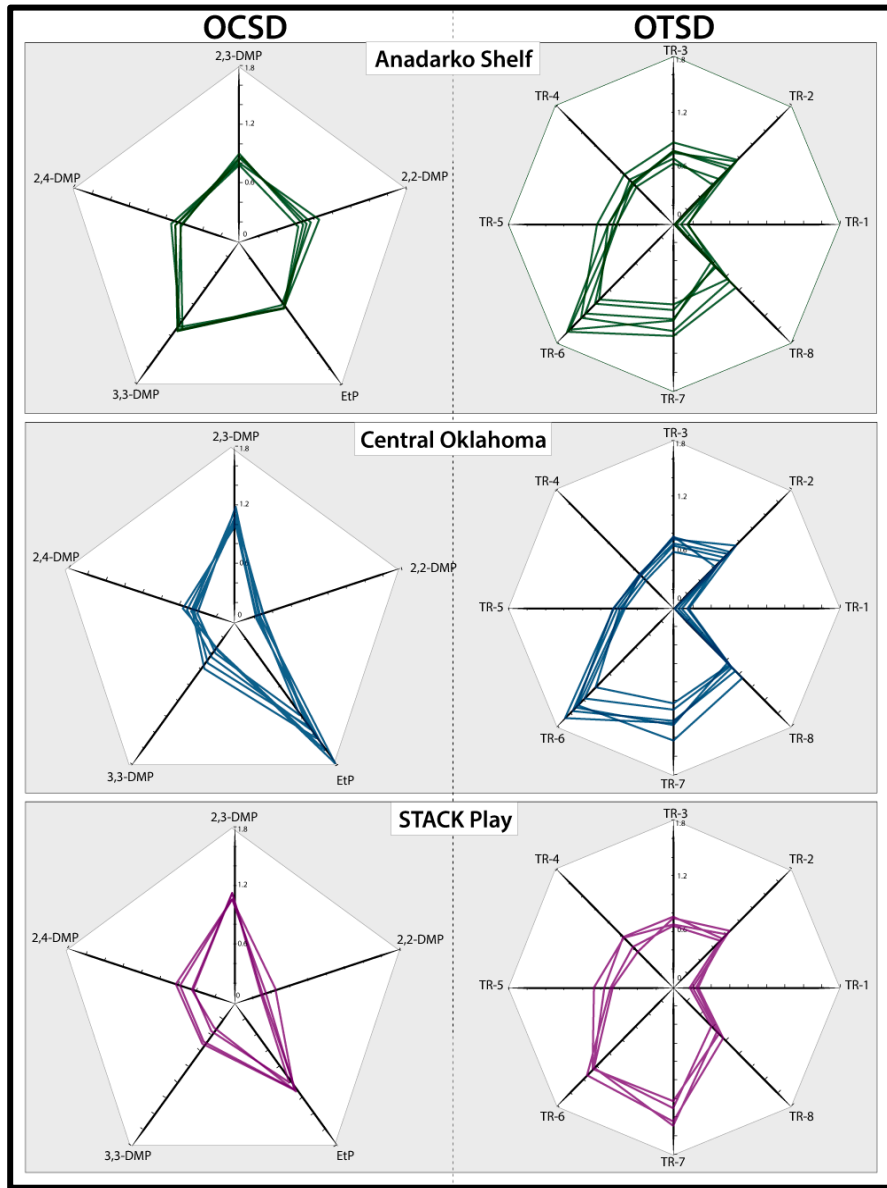
Figure 52: Star diagrams of oil correlation (OCSD; left) and oil transformation (OTSD; right). P1: = 2,2-dimethylpentane + 2,3-dimethylpentane + 2,4-dimethylpentane + 3,3-dimethylpentane + 3-ethylpentane.C1: 2,2-dimethylpentane/P1, C2: 2,3-dimethylpentane/P1, C3: 2,4-dimethylpentane/P1, C4: 3,3-dimethylpentane/P1, C5: 3-ethylpentane/P1. X = 1,1 dimethylcyclopentane, P2 = 2-methylhexane + 3-methylhexane. TR1: Toluene/X, TR2: nC7/X, TR3: 3-methylhexane/X, TR4: 2-methylhexane/X, TR5: P2/X, TR6: 1-cis-2-dimethylcyclopentane/X, TR7: 1-trans-3-dimethylcyclopentane/X, TR8: P1/P2 (Atwah et al., 2019; Halpern, 1995).

processes could result in the depletion of toluene from Mississippian crude oils. The Tr1 ratio is also low for oils produced from unconventional the Woodford Shale, however, as well as tight Mississippian carbonates oils produced within the STACK play. This depletion of toluene could be due to hydraulic fracturing fluids, where highly water-soluble hydrocarbons preferentially removed from the produced crude oils. Furthermore, toluene was observed to decrease in abundance consistently, with increasing distance from the Anadarko Basin depocenter (Burruss and Hatch, 1989b). These authors concluded that since the studied oils are not biodegraded, the toluene depletion is not related to water washing (which is usually due to meteoric-water aquifer recharge), they attributed the systematic depletion of toluene in crude oil to migration distance. The likelihood of crude oil interaction with the formation water increase as the distance of oil migration increases, which reduces toluene (Burruss and Hatch, 1989b). Another alteration parameter is the Tr6 ratio, which is sensitive to light hydrocarbon evaporation loss. The Tr6 ratio is calculated by dividing 1-cis-2-dimethylcyclopentane over 1,1-dimethylcyclopentane, which essentially utilizes the large difference in boiling points between those two compounds, so as the value of Tr6 ratio decreases, the effect of evaporation loss of light hydrocarbon increases (Halpern, 1995). Crude oils from central Oklahoma exhibit relatively high Tr6 ratio with a narrower variation compared to the rest of the oil samples, suggesting a minimum effect of evaporation loss (Figure 52). The most oils with evaporation loss were observed at Mississippian oils of the Anadarko Shelf, as expected, since those oils as indicated by diamondoids and other migration-sensitive tracers are a result of long-distance migration, which could result in hydrocarbon migration loss via solution and diffusion mechanisms (Al Atwah et al., 2019; Schowalter, 1979).

Light hydrocarbons are a useful to evaluate hydrocarbon fluid thermal maturity. A number of light hydrocarbon (C_6-C_7) based maturity parameters have been published in the literature, with a first attempt by Hunt et al. (1980b). These authors observed that certain ratios of light hydrocarbons such as 2,2-dimethylbutane/2,3-dimethylbutane tend to increase with increasing depth. Similarly, Thompson (1983) introduced the heptane ratio as a maturity parameter, which is calculated by dividing *n*-heptane by the sum of different heptane isomers (Thompson, 1983) (Figure 53). Thompson (1983) defined stages for maturity assessment of oils based on heptane
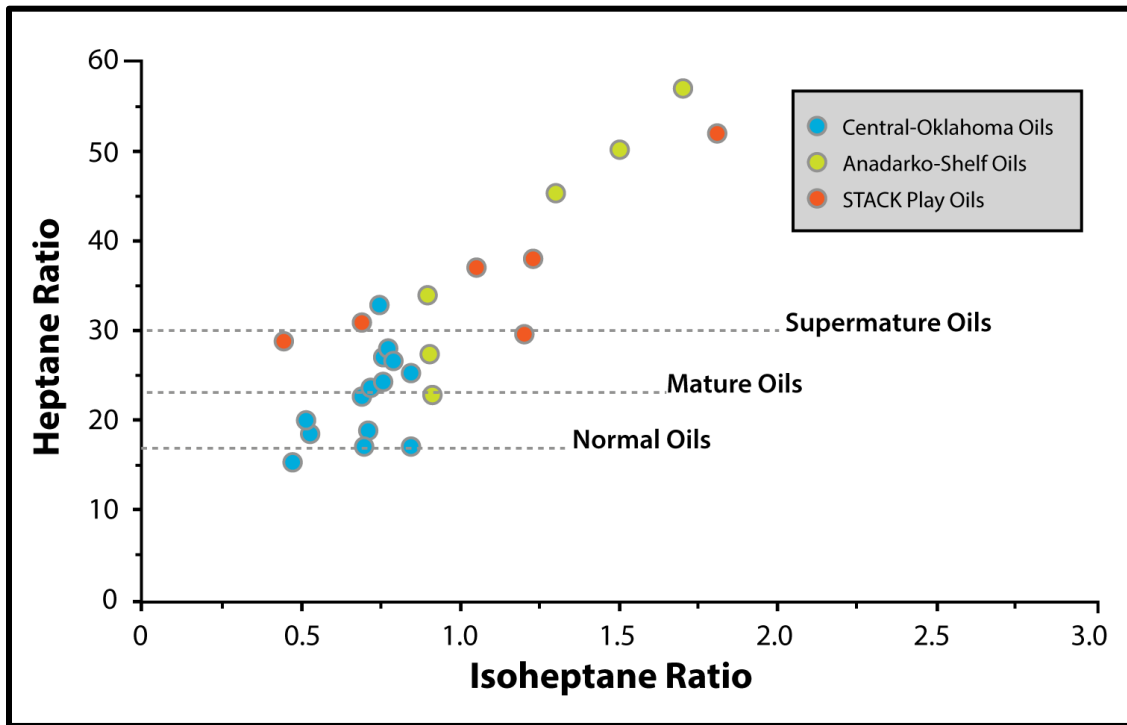
Figure 53: Cross plot of heptane versus isoheptane ratios to assess crude oils maturity from Mississippian and Woodford zones of three major areas: the Anadarko Shelf, central Oklahoma and Sooner Trend Anadarko Basin Canadian and Kingfisher Counties (STACK) play oils. Heptane ratio: (100*n-heptane)/(cyclohexane + 2-methylhexane + 1,1-dimethylcyclopentane (DMCP) + 3-methylhexane + 1-cis-3-DMCP + 1-trans-3DMCP + 1-trans-2-DMCP + n-heptane+methylcyclohexane); Isoheptane ratio: (2-methylhexane + 3-methylhexane)/(1-cis-3-DMCP + 1-trans-3DMCP + 1-trans-2-DMCP).

ratio as follows: Isoheptane ratios from 18 to 22 represent normal uncracked oil, 22 to 30 represent mature oil, and heptane ratio >30 represent supermature oil (Thompson, 1983).

The heptane ratio of crude oils examined in this study is shown in Figure 53; a clear variation of heptane ratio is observed for oils within the Anadarko Shelf and STACK Province. Oils within the Anadarko Shelf exhibit a range of isoheptane ratios: 1.0–2.0 and 22.0–59.0 (Figure 53). Oils of the STACK play showed a slightly wider variation in isoheptane ratio, ranging from 0.5–2.0, while the heptane ratio ranging from 30.0–50.0 (Figure 53). The majority of the samples located west of the Nemaha Uplift plot within the mature to supermature oils zone as defined by Thompson's heptane maturity parameters (Thompson, 1983). However, oils located east of the Nemaha Uplift in the central Oklahoma cluster together within the normal oil classification, with few samples plotting within the mature oil zone based on the heptane ratio. However, they can still be classified as normal paraffinic oils, based on the isoheptane values (Thompson, 1983). Oils from central Oklahoma showed one oil sample plotting below the normal oil cutoff. According to Thompson (1983), both heptane and isoheptane decrease as a function of biodegradation, with heptane and isoheptane values ranging from 0–18 and 0–0.8, respectively. While this observation is valid and while normal alkanes are one of the hydrocarbons readily degraded by microbes, other factors can result in low heptane and isoheptane ratios. The heptane and isoheptane ratios can be influenced by the crude oil source-rock type. Type II-S kerogen and aliphatic-rich source rocks are observed to yield high heptane and isoheptane ratios, while other types of kerogen yielded low values of heptane ratio (~12), this has been observed in non-biodegraded low maturity crude oils from the offshore Oligocene-Miocene shale of the Niger Delta (Peters et al., 2005c). Since most of the Mississippian and Devonian oils in our study are of marine origin, the variation of heptane and isoheptane ratios due to source-rock type is likely. However, the lower values observed in

central Oklahoma oil samples have likely resulted from low thermal maturity. Nevertheless, heptane and isoheptane provided a useful tool for broad crude-oil maturity classification, as supported with additional maturity ratios.

Normal Alkanes and Acyclic Isoprenoids

The overall *n*-alkane envelope of crude oils showed a unimodal distribution and, in some cases, a bimodal distribution. Oils located in central Oklahoma all showed a unimodal *n*-alkane envelope, maximizing at *n*-C_{10} to *n*-C_{12}, with some samples containing normal alkanes up to *n*-C_{40} (*n*-tetracontane) (Figure 54). In addition to the unimodal *n*-alkane profile, some oils at the Anadarko Shelf and within the STACK play exhibit a bimodal distribution maximizing at the light-end including *n*-C_6 to *n*-C_9 and another maximum at *n*-C_{13} to *n*-C_{15} (Figure 54). The first interpretation of the examined oils is that they are non-biodegraded or possibly slightly biodegraded. This interpretation is evidenced by the presence of unaltered *n*-alkane with stable baseline chromatograms lacking any UCM hump, which is usually associated with weathered oils (Al Atwah et al., 2018a). While *n*-alkanes are not specific to organic matter, they can give general information about the oil source (e.g. marine, non-marine), biodegradation, thermal maturity, oil contamination and evaporation loss (Peters et al., 2005b). In our samples, variation in normal alkanes is attributed to reservoirs with different hydrocarbon charges, with unimodal receiving single hydrocarbon charge, while bimodal receive multiple hydrocarbon charges with various degrees of thermal maturity (Al Atwah et al., 2019). Since most of the examined oils are sourced from Devonian and Mississippian marine source rocks, an *n*-alkane profile alone is not sensitive enough to discriminate between these marine source rocks.

150

The relative abundance of odd-to-even *n*-alkane carbon number is another geochemical signature we examined the crude-oil samples. The abundance of *n*-alkanes odd-over-even carbon number relationship is attributed to thermal maturity. With both *n*-alkanes, odd and even carbon number preference indicated low thermal maturity. A number of ratios have been proposed to calculate the odd over even ratio. Bary and Evans (1961) introduced the CPI, which captures the odd-over-even preference of *n*-alkanes in the range of *n*-C$_{24}$ to *n*-C$_{34}$. In 1970, Scalan and Smith published an improved OEP ratio. Unlike the CPI, the OEP is easier to calculate because it uses a narrow range of *n*-alkanes from *n*-C$_{25}$ to *n*-C$_{28}$ or *n*-C$_{21}$ to *n*-C$_{25}$. Most of the crude oil samples showed values close to 1.0, indicating that most of the samples are mature fluids, with some exceptions for crude oils
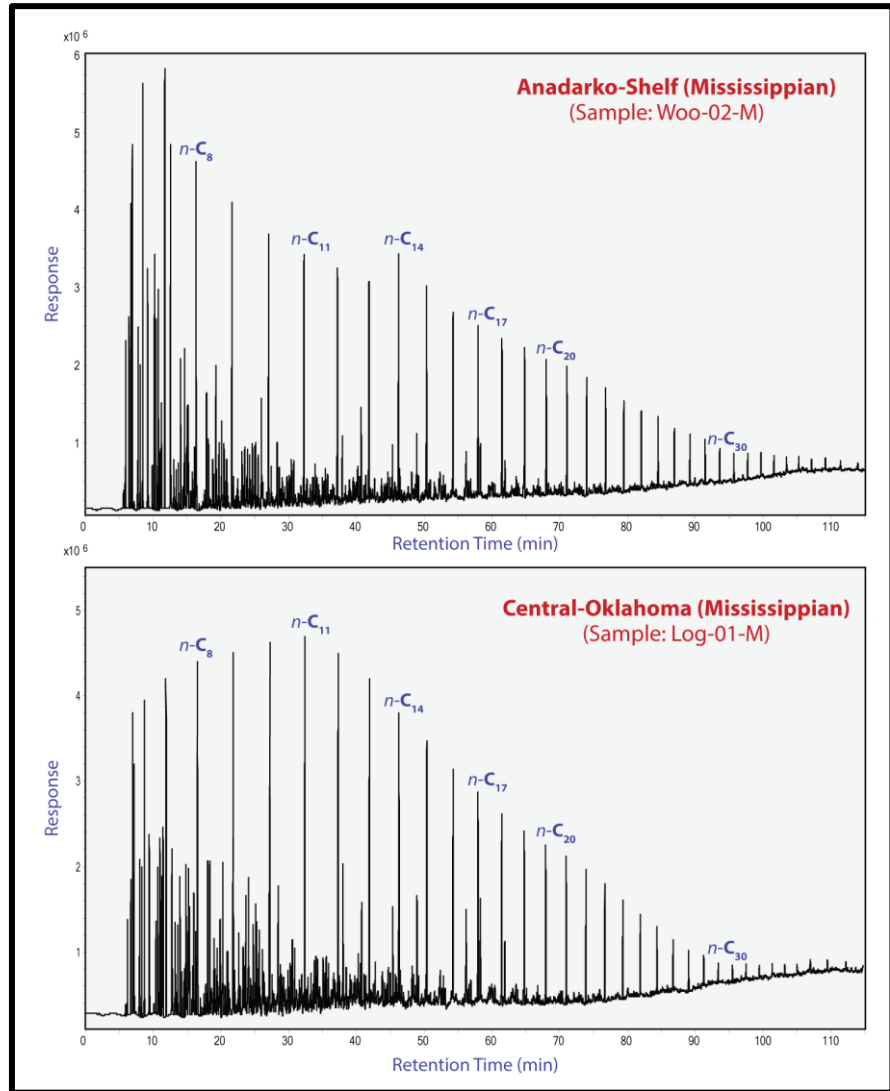
Figure 54: oil chromatogram for sample Woo-02-M and Log-01-M. Note the bimodal distribution of *n*-alkanes in the sample located west of the Nemaha Uplift and the unimodal distribution of *n*-alkanes in sample east of the Nemaha Uplift (Al Atwah et al., 2017a).

from central Oklahoma. Both, Lin-02-M and Lin-03-W samples exhibited odd-over-even preference ratio of 0.91 for CPI and 0.87 for OEP. These relatively low ratios suggest a slightly odd *n*-alkane carbon number preference over even *n*-alkanes, and those oils are located where the Woodford Shale and overlying Mississippian Formation are immature, with values ranging from 0.47–0.49%R_o. Therefore, this slightly odd *n*-alkane preference could be due to low thermal maturity. Most notably, none of the examined crude oils showed a strong preference of odd-numbered *n*-alkanes in the range of *n*-C_{10} to *n*-C_{20}, whose signature is associated with Ordovician-sourced crude oil. For example, oils reservoired in the Ordovician Viola limestone are mainly sourced from Simpson source rock with a unique odd-preference maximizing at *n*-C_{15} and *n*-C_{17}
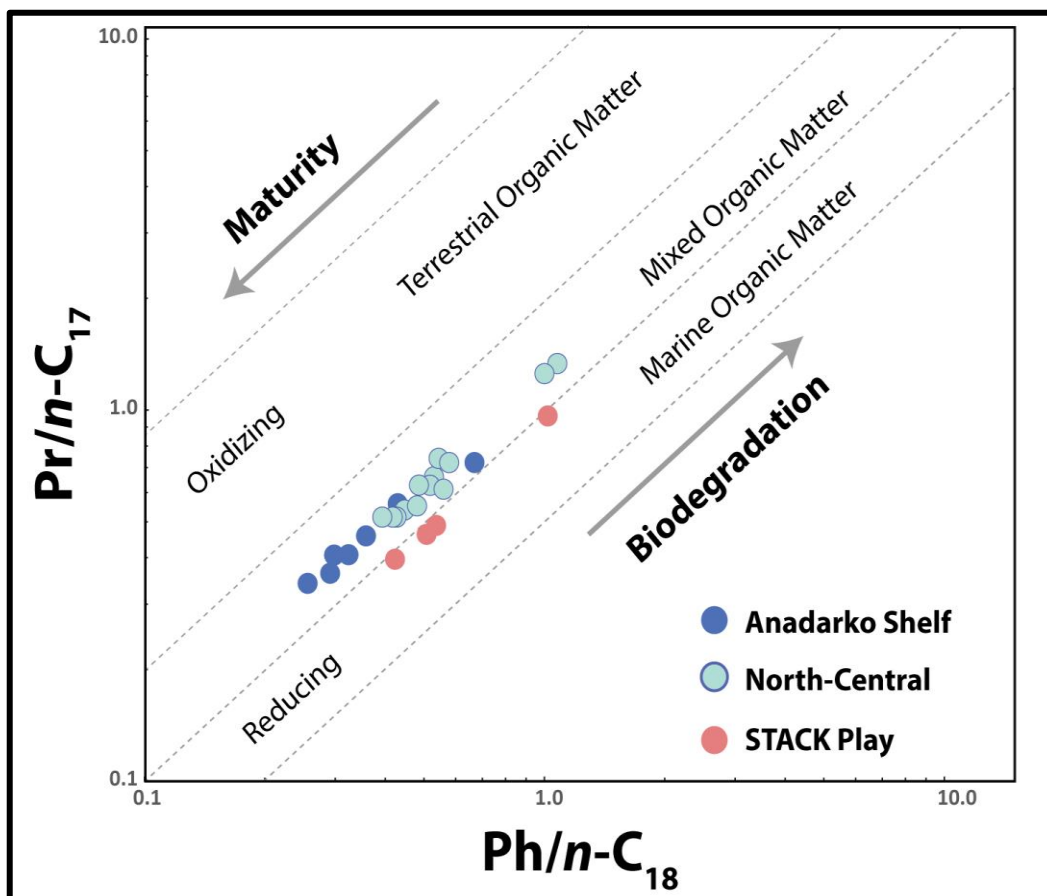
Figure 55: Cross-plot comparing Mississippian and Woodford crude-oils ratio of pristane to heptadecane (*n*-C_{17}) and the ratio of phytane to octadecane (*n*-C_{18}).

(Burruss and Hatch, 1989b). This signature of Ordovician oils is mainly observed in the Anadarko Basin, but it persists over different basins, and it has been observed in Forest City, Kansas, and in the Williston Basin, North Dakota (Longman and Palmer, 1987).

Crude oils were examined for the relationship of acyclic isoprenoid that is pristane and phytane to n-C_{17} and n-C_{18}. As indicated in Chapter II, acyclic isoprenoids are sometimes useful to infer source-rock depositional settings and organic-matter type. Shown in the cross plot of Figure 55 is the relationship of pristane to n-C_{17} versus phytane to n-C_{18}. Most crude oils from Anadarko Shelf and central Oklahoma plot within the Type-II or -III mixture kerogens, while all of oils from the STACK play plotting within a marine Type-II source, with a stronger signature of reducing depositional settinsg than oils from central Oklahoma and the Anadarko Shelf. Most of the Mississippian and Woodford Shale source rocks are of marine origin, as confirmed from maceral composition, together with mineralogical and sedimentological characteristics presented in Chapter IV. Therefore, the contribution of Type-III organic matter is unlikely to be significant in these dominantly marine source rock. However, if Type-III organic matter is present, it would be in a trace amounts and likely overprinted by the dominant marine geochemical signature. While it is not clear why these oils exhibit relatively high Ph/n-C_{17} ratios, one possible explanation is that this finding could be due to less reducing conditions during the deposition of source rocks that generated those oils (Figure 55). A close examination of the redox-sensitive biomarker would help to validate this interpretation.

Biomarkers

Biomarkers of the saturated hydrocarbons showed a variable compositional change between Woodford and Mississippian crude oils. Biomarkers of the examined crudes are broadly

153

divided into terpane and sterane biomarker classes. Shown in Table 17 are some of the key biomarker ratios of terpane and sterane biomarker classes. Based on biomarker fingerprints, oils overall showed two major source-rock contributions from the Woodford Shale and Mississippian mudrocks. Biomarker singtures are discussed in details based on biomarker classes.

In the terpane biomarker class, Mississippian crude oils showed a unique signature, differing from that of Woodford oils. The prevalence of lower and extended tricyclic terpanes is a diagnostic biomarker signature of Mississippian-sourced oils. This crude-oil fingerprint was first recognized in 1997 and observed in crude oils produced from the Anadarko Basin (Wang and Philp, 1997a). Extended tricyclic terpanes occur in abundance in oils located within Logan County and within the STACK play. Utilizing the distribution of extended tricyclic terpanes, an index to capture the contribution of Mississippian-sourced oils was developed by comparing the sum of extended tricyclic terpanes to the sum of homohopanes. Extended tricyclic terpanes index (ETT/HH) values of 2 and higher indicating a Mississippian source-rock contribution. In Mississippian oils, both lower and extended tricyclic terpanes dominate over hopanes on the m/z191 mass fragmentogram (Table 17). The overall distribution of these tricyclic terpane biomarkers is consistent across the Mississippian-sourced oils, with C23 as the dominant lower tricyclic terpane and C_{28} as the dominant compound in the extended tricyclic terpanes. Some of the tricyclic terpanes such as C_{22}, C_{27}, C_{32} are present in trace quantities. This is because of the regular head-to-tail side chain with a methyl group at the even number carbon portions. The series of extended tricyclic terpane

154

Table 18 Key biomarker ratios of terpane and sterane biomarkers of selected crude oils

Biomarker ratio	Alf-01-M	Woo-01-M	Log-01-M	Pay-04-M	Gar-01-M	Log-01-W	Log-07-W	Pay-06-M	Lin-01-M	Pay-08-W	Can-03-M
$(C_{21}+C_{22})/(C_{27}+C_{28}+C_{29})$ [a]	0.09	0.09	0.11	0.11	0.15	0.12	0.07	0.07	0.07	0.10	0.10
C_{27}/C_{29} ($\alpha\alpha\alpha$ R)[b] (217)	0.38	0.30	0.74	0.89	0.85	0.67	0.66	0.77	0.83	0.64	0.81
C_{27}/C_{29} ($\alpha\beta\beta$ S+R)[c] (218)	0.58	0.50	0.60	0.60	0.55	0.70	0.55	0.49	0.54	0.49	0.54
Gammacerane/Hopane [d]	0.07	0.06	0.12	0.16	0.13	0.12	0.07	0.10	0.08	0.08	0.18
C_{29}/C_{30} Hopane [e]	0.55	0.60	0.77	0.72	0.64	0.59	0.54	0.56	0.51	0.49	0.47
C_{24} Tetracyclic/C_{26} Tricyclics [f]	0.39	0.45	0.15	0.16	0.11	0.15	0.27	0.17	0.16	0.22	0.19
Homohopane index (HHI)[g]	0.01	0.09	0.14	0.15	0.12	0.17	0.10	0.10	0.10	0.10	0.10
Diahopane/(Diahopane +Hopane)	0.06	0.04	0.13	0.11	0.14	0.18	0.04	0.05	0.05	0.08	0.09
C_{24}Tetra/C_{23}TT[h]	0.23	0.28	0.11	0.11	0.16	0.09	0.17	0.11	0.09	0.15	0.12
C_{24}TT/C_{23}TT[i]	0.70	0.66	0.78	0.73	0.78	0.76	0.68	0.58	0.51	0.68	0.77
Hop31R/HopC$_{30}$[j]	0.35	0.37	0.27	0.25	0.26	0.18	0.29	0.28	0.28	0.28	0.25
C_{23}TT/Hop[k]	0.45	0.35	0.68	1.10	0.74	0.75	0.53	0.64	0.58	0.54	0.62
ETT/HH[l]	0.14	0.31	4.25	8.34	3.62	2.60	1.01	1.65	0.89	1.56	1.71

a: sum of C_{21} and C_{22} sterane over sum of C_{27} $\alpha\alpha$ 20R, C_{28} $\alpha\alpha$ 20R and C_{27} $\alpha\alpha$ 20R C_{29} steranes; b: C_{27} $\alpha\alpha$ 20R cholestane over C_{29} $\alpha\alpha$ 20R stigmastane; c: C_{27} $\beta\beta$20R+S cholestane over C_{27} $\beta\beta$ 20R+S stigmastane. c: gammacerane over C_{30} 17α hopane; C_{29} 17α 21β – norhopane over C_{30} 17α hopane; f: C_{24}tetracyclic terpane over C_{26} tricyclic terpane; g : C_{35} (22 S+R) homohopane over sum of $C_{31\ to\ 35}$ (22 S+R) homohopanes; h: C_{24} tetracyclic terpane over C_{23} tricyclic terpane; i: C_{24} tricyclic terpane over C_{23} tricyclic terpane; j: C_{31} 22R homohopane over C_{30} 17α hopane; k: C_{23} tricyclic terpane over C_{30} 17α hopane ; l: sum of extended tricyclic terpanes $C_{28\ to\ 45}$ (R+S) divided by sum of C_{31} to $_{35}$ (22 S+R) homohopan

biomarkers reaches up to C_{45} in oils located in central Oklahoma and the STACK play. Other crude oils, such as Alf-01-M and Woo-01-M contained some of the lower tricyclic terpanes, and a limited occurrence of extended tricyclic terpanes up to C_{29}, with ETT/HH lower than 1 (Table 17).

While tricyclic terpanes are one of the most resistant to biodegradation and maturity alteration, the relative enrichment of tricyclic terpanes can often indicate a thermally mature or microbially degraded oil (Peters and Moldowan, 1993). In the examined Devonian and Mississippian oils, none of the oils showed any evidence of biodegradation, with the majority of oils within the early-middle oil window. Hence, the enrichment of tricyclic terpane in the Mississippian oils has two possible causes. First, the tricyclic terpane biomarker source is related to the organic matter that is to suggest a specific biota of a Mississippian age that preferentially biosynthesized a tricyclic terpane carbon skeleton with a long isoprenoid side chain. The second possibility is related to the depositional environment, in that enrichment of tricyclic terpane is caused by early stages of diagenetic transformations either caused by a biological agent or due to mineral catalysis reactions.

Across the terpane biomarker class, the C_{24} tetracyclic terpane is observed to be relatively higher in samples from the Anadarko Shelf, such as the four crude samples from Alfalfa and Woods counties (Table 17). These oils are produced from different zones of the Mississippian limestone Formation, with relatively high C_{24} tetracyclic terpane compared to oils produced from Central-Oklahoma. For example, the ratio of C_{24} tetracyclic terpanes relative to C_{26} tricyclic terpane of sample Woo-01-M is 0.45, while the ratio in sample Gar-01-M is 0.11, which is located in central Oklahoma (Table 17). Even absolute concentrations of C_{24} tetracyclic terpane are higher in some samples than others. Sample Alf-01-M (Anadarko Shelf), exhibits a concentration of 29.82 ppm while Log-01-M (central Oklahoma) has a concentration of 7.39 ppm.

The C_{24} tetracyclic terpane biomarker has been used to infer source-rock lithology, with its enrichment suggesting carbonate source rock. Particularly, the ratio of C_{24} relative to C_{23} tricyclic terpane was used to indicate carbonate and evaporite source-rock contribution (Connan et al., 1986). However, in our crude oil samples, the enrichment of C_{24} tetracyclic is not as high as reported in the literature. Therefore, it is unlikely that our oils are carbonate and evaporite sourced. The enrichment of C_{24} tetracyclic terpane is likely related to an alteration process caused by a rupture in the E-ring of a hopanoid precursor (Trendel et al., 1982). This is supported by the fact that the oils with higher C_{24} tetracyclic terpanes are also enriched in hopane biomarkers.

Hopanes are a major series of the terpane biomarker class and are ubiquitous in recent and ancient sedimentary organic matter (Ourisson et al., 1987). In examined crude oils, hopanes varied drastically, especially for oils located in central Oklahoma together with the STACK Province. Crude oils that are enriched in tricyclic terpanes showed an unusual depletion of the hopane biomarkers; for instance, sample Log-01-M had higher abundance of thfe C_{23} tricyclic terpane relative to C_{30} hopane biomarker with a ratio of 1.10. In contrast, the C_{23}TT/Hop ranged from 0.35–0.45, in the Anadarko Shelf oils. Moreover, the C_{29} norhopane was observed to be higher in some of the oil samples located in central Oklahoma and STACK region. For example, the C_{29} norhopane to C_{30} hopane ratio is slightly high in sample Log-01-M at 0.77 and low in sample Can-03-M. Normally, the abundance of C_{29} norhopane over C_{30} hopane (<1) indicates a carbonate or evaporite source-rock signature (Clark and Philp, 1987). In our oil samples, this trend could suggest a carbonate source-rock contribution. This supposition is also supported by the homohopanes distribution, which are a series of extended hopanes that reflect carbonate source-rock contribution to the oils (Connan and Dessort, 1987). Sample Alf-01-M has a low homohopane index value of 0.1, and similar ratios are also observed for oils in the Anadarko Shelf (Appendix).

157

Some samples, but not all, showed higher homohopane index with values ranging from 0.13–0.21, which could also be an indication of carbonate-sourced oils. An important observation that occurred within the homohopane biomarkers is the unusual abundance of the C_{33} 22S homohopane. This abundance is mainly observed in samples with high abundance of extended tricyclic terpanes. This abnormal enrichment of C_{33} 22S homohopane is due to the co-elution with C_{35} 22R extended tricyclic terpane. This is crucial to identify because it can alter some of the biomarker ratios. The best approach to overcome this co-elution is by running the samples on GC-MS-QQQ for MRM, which allows for selective separation.

Group of the oil samples showed the C_{30} 17α diahopane biomarker in higher concentration than other oils. In particular, the ratio of C_{30} 17α diahopane relative to C_{30} 17α hopane reflects the difference of this biomarker distribution. Ratios of C_{30} 17α diahopane relative to C_{30} 17α hopane for all examined crude oils ranged from 0.02 to 0.22. The C_{30} 17α diahopane is observed to be relatively high in samples located in central Oklahoma and STACK areas. For example, Log-01-M, a central Oklahoma sample, shows a ratio of 0.13, while Anadarko Shelf samples, such as Woo-01-M, show 0.06. The C_{30} 17α diahopane biomarker has been observed in different crude oils and source-rock types from terrigenous to marine sources (Moldowan et al., 1991; Philp and Gilbert, 1986). The C_{30} 17α diahopane originates by rearrangement of the base structure of hopanoids exhibiting a functionality on the D-ring (Corbett and Smith, 1969). Therefore, the source of diahopane is related to bacterial organic sources, and particularly it is related to the bacteriohopanetetrol biosynthetic pathway. Aside from its biological origin, diahopane's structural rearrangement is suggested to be facilitated by the presence of clay. Diahopane was first documented in coals and oils derived from a terrigenous origin, where rocks are usually clay-rich and deposited in oxygenated water columns; hence, it has been deduced that presence of diahopane

is linked to source rocks with considerable amounts of clay depositing under oxic to suboxic conditions (Peters et al., 2005c). The relatively high abundance of diahopane in some of the oil samples suggests that these oils are derived from clay-rich rocks deposited in oxygenated conditions. However, the enrichment of diahopane in those oils is not comparable to the abudance of diahopane in oils derived from terrigenous sources reported in the literature(Philp and Gilbert, 1986).

Other compounds of the hopanoid biomarkers were observed but in minor concentrations Gammacerane, a biomarker usually associated with hypersaline depositional settings or a stratified water column was present in most of the samples (Peters and Moldowan, 1993). Overall, crude oils showed low absolute concentrations of gammacerane, and low ratios of gammacerane relative to C_{30} hopane ranging at 0.07–0.18. Additionally, samples with high abundance extended tricyclic terpanes obscured the signature of gammacerane. This is interpreted as partial co-elution of C_{33} 22R extended tricyclic terpane with gammacerane. Another compound that is present in low amounts in the majority of the oil sample is the C_{29} nor-25-hopane. In general, C_{29} nor-25 hopane is an altered version of the hopane, which is normally used as a proxy for assessing crude-oil biodegradation. Enrichment of C_{29} nor-25-hopane usually indicates severe stages of biodegradation (Peters and Moldowan, 1993). Therefore, the absence of C_{29} nor-25-hopane of the examined oils provides another line of evidence suggesting that none of the studied oils are biodegraded.

Terpane biomarkers that are sensitive to crude-oil maturity were examined in detail. The terpane-based maturity parameters include homohopane isomerization, hopane to moretane, tricyclic terpane to hopane and Ts/Tm ratios (Ts: terpane stable, Tm: terpane maturable). Table 18 shows key oil samples and a list of maturity parameters based on terpane biomarkers. In general,

159

most of the terpane ratios indicate peak-oil maturity for the oils, with few exceptions on samples in central Oklahoma. Moretane divided by C_{30} hopane is used as a maturity ratio, especially for oils within early stages of the oil window. The biological configuration of hopanoid biomarkers usually exhibits a 17β, 21β(H) structural orientation, which is readily converted into its geological isomer 17β, 21α (H) moretane, and with further burial and thermally induced alteration of its configuration to 17α, 21β (H) hopane, which is a much more stable isomer (Seifert et al., 1980). Therefore, the relation of moretane to hopane is a useful molecular tool for assessing thermal maturity, with a decrease in this ratio indicates an increase in thermal maturity. In the examined crude oils, moretane to hopane ratios ranged from 0.07 to 0.28, with an average of 0.11. Such values indicate that most of these oils are from mature source rocks within early-to peak-oil with the least mature oils located in Lincoln County, such as sample Lin-03-W. Another terpane-based maturity ratio is the Ts/Ts+Tm, which is calculated by dividing C_{27} Ts 18 α (H)-trisnorhopane (Ts) by the sum of C_{27} Tm 17 α (H)-trisnorhopane(Tm) and C_{27} Ts 18 α (H)-trisnorhopane (Ts). Results of Ts/Ts +Tm ratios also support the moretane and hopane ratios indicating early-oil to peak-oil maturity level for most of the crude oils. Values of Ts/Ts+Tm range from 0.23 to 0.72 with an average of 0.51. A consistent level of maturity for the oils is observed on the rest of the terpane-based maturity ratios in Table 18. However, the tricyclic terpane maturity ratio indicates a drastically different level of maturity than the rest of the terpane-based maturity ratios, ranging from 0.10 to 0.90 with an average of 0.79, suggesting that oils are at peak-oil and slightly beyond the peak-oil maturity level, corresponding to a range of 0.8 to 1.0%Ro equivalent (Peters et al., 2005c). These slightly higher values of the tricyclic terpane ratio are likely influenced by the source of organics rather than due only to a maturity effect. Overall, terpane-based maturity ratios are highly affected by the source of the initial organic matter. In the examined crude oils, the initial

enrichment of tricyclic terpanes hindered the maturity signal of the sum of C_{28} and C_{29} tricyclic terpanes divided by sum of C_{28} and C_{29} tricyclic terpanes and C_{29} Ts 18α (H)-norneohopane. Additionally, maturity terpane ratios are useful for immature to peak-oil stages of petroleum generation. Beyond this stage, terpanes are thermally and chemically unstable at elevated temperatures, due to the inherent structural framework of the cyclic carbon backbone skeleton, which tends to fragment at high maturity levels (Peters et al., 2005c).

Steranes are another important class of biomarkers sensitive to many variables that can help unravel the crude-oil source of organic matter, maturity level and source-rock lithology. In the examined crude oils we focused on different groups of steranes, including short-chain steranes, ranging from C_{21}-C_{22} also known as pregnanes, rearranged steranes also known as diasteranes and regular steranes ranging from C_{26} to C_{30}. All groups of steranes will be discussed in terms of organic-matter input, source-rock lithology, and maturity assessment.

Table 19 Key terpane-based maturity ratios of Mississippian and Woodford crude oils

Sample ID	Mor/Hop [a]	Ts/(Ts+Tm) [b]	H32S/HH (S+R) [c]	H35/(H34+H35) HH [d]	$(C_{28}+C_{29}$ TT)/Ts+C_{28}+C_{29} TT) [e]
Alf-01-M	0.10	0.44	0.59	0.54	0.78
Alf-02-M	0.09	0.38	0.59	0.47	0.84
Woo-01-M	0.10	0.28	0.58	0.47	0.83
Woo-02-M	0.10	0.23	0.58	0.46	0.82
Pay-01-M	0.10	0.45	0.58	0.45	0.86
Pay-05-M	0.10	0.47	0.59	0.44	0.83
Pay-07-W	0.09	0.53	0.60	0.47	0.81
Lin-03-W	0.28	0.24	0.22	0.56	0.10
Log-01-M	0.07	0.69	0.60	0.50	0.89
Gar-01-M	0.08	0.70	0.59	0.47	0.82
Kin-02-M	0.08	0.62	0.59	0.31	0.90
Pay-04-M	0.08	0.65	0.61	0.51	0.87

Table 18 continued.

Sample ID	Mor/Hop [a]	Ts/(Ts+Tm) [b]	H32S/HH (S+R) [c]	H35/(H34+ H35) HH [d]	$(C_{28}+C_{29}$ TT)/Ts+C_{28}+ C_{29} TT) [e]
Pay-09-W	0.13	0.32	0.66	0.65	0.19
Kay-01-M	0.08	0.64	0.59	0.48	0.83
Log-05-W	0.04	0.72	0.57	0.50	0.85
Log-06-W	0.04	0.72	0.60	0.49	0.88
Kin-01-N	0.09	0.62	0.60	0.43	0.85
Can-01-M	0.11	0.56	0.58	0.45	0.85
Log-02-M	0.10	0.44	0.59	0.40	0.85
Pay-02-M	0.11	0.46	0.59	0.44	0.84
Log-07-W	0.10	0.42	0.58	0.45	0.86
Pay-06-M	0.12	0.43	0.58	0.46	0.87
Log-02-W	0.09	0.64	0.58	0.53	0.87
Kin-04-M	0.08	0.53	0.57	0.44	0.84
Can-03-M	0.10	0.54	0.60	0.46	0.84
Kin-03-M	0.10	0.48	0.59	0.47	0.87
Lin-02-M	0.13	0.59	0.58	0.46	0.84

a: C_{30} moretane/ C_{30} 17α hopane; b: C_{27} Ts 18 α (H)-trisnorhopane divided by C_{27} Tm 17 α (H)-trisnorhopane+ C_{27} Ts 18 α (H)-trisnorhopane ; c: C_{32} 22S 17 α (H) bishomohopane divided by C_{32} 22S+R 17 α (H) bishomohopane ;d: C_{34} 22R+S17 α (H) homohopane divided by $C_{34 + 35}$ 22R+S17 α (H) homohopanes; e: sum of C_{28} and C_{29} tricyclic terpanes divided by sum of C_{28} and C_{29} tricyclic terpanes and C_{29} Ts 18α (H)-norneohopane

Pregnane and homopregnane biomarkers of 21 and 22 carbon atoms are generally observed in different sedimentary rocks and petroleum samples. Overall, they consist of the main carbon-skeleton structure of steranes which has three cyclohexane rings and one cyclopentane ring with a methyl or dimethyl group at the carbon position C-20. Pregnanes are geologically stable compounds believed to be related to an altered version of steroids bounded to the kerogen matrix. Furthermore, pregnanes and homopregnanes have been suggested to form by a catalysis effect of carbon or carbonate minerals, resulting in the preferential cleavage of pregnanes from kerogen at carbon position of C-20 and C-22 (Wang et al., 2015b). Pregnanes were observed in higher

proportion relative to the regular steranes in some oils located in central Oklahoma and within the STACK play. Table 19 shows the ratio comparing pregnanes to steranes ranging from 0.15 to 0.07, with an average in some oils from central Oklahoma of 0.13. The higher ratios of pregnanes are observed to suggest carbonate-sourced oils, whereas relatively low values are associated with crude oils derived from clay-rich shales (Wang et al., 2015b). The variation in pregnanes ratio in the examined oils suggests different source-rock contributions.

Regular and rearranged steranes biomarkers are crucial for delineating crude oils organic-matter type and source-rock lithology. Regular steranes, particularly the relative abundance of stigmastane (C_{29}), ergostane (C_{28}), and cholestane (C_{27}), varied across the crude oil samples with an apparent prevalence of stigmastane. Some oils in central Oklahoma and STACK play showed a slight enrichment in cholestane such as Log-01-M and Kin-02-M, while others exhibited lower cholestane such as Pay-01-M and Alf-02-M (Table 19). This trend is also observed in both, the αββ 20S and ααα 20R steranes. Enrichment in stigmastane can indicate different types of organic-matter contribution. Theoretically, stigmastane is usually related to stigmasterol, which is an unsaturated phytosterol found in living higher plants (Huang and Meinschein, 1979). Therefore, source rocks and crude oils with higher concentrations of stigmastane would suggest terrigenous organic matter contribution. However, the suggestion is not conclusive, and in practice, some marine source rocks and related crude oils can exhibit high stigmastane relative to ergostane and cholestane. This observation in particular, is observed to be strictly for Paleozoic marine shales and their derived petroleum. The high abundance of stigmastane in Paleozoic shales and oils is postulated to result from the biosynthesis of stigmasterol by ancient microorganisms, which might have preceded the biological ability to produce other forms of sterols (Moldowan et al., 1985). Therefore, such distribution of regular steranes in the examined crude oils is expected, since all

the crude oils analyzed have generated by Paleozoic source rocks. Besides the abundance of stigmastane, the slight abundance of cholestane over ergostane could suggest varying degrees of marine planktonic organic matter input which is associated with marine carbonate source rocks (Moldowan et al., 1985).

Rearranged sterane biomarkers are another important set of compounds regarded as sensitive to both, rock mineralogy and thermal maturity. During diagenesis, clays acid sites alter the conversation of sterol to form diasteranes (Rubinstein et al., 1975). Hence, diasteranes are used to infer source rock lithology from crude oil, with the ratio of diasteranes to regular steranes mainly used as a parameter to differentiate between carbonate- versus shale-sourced oils. Theoretically, the depletion of diasteranes in carbonate rocks is related to increased water alkalinity caused by bicarbonate and ammonium ions formed by bacterial activity during early-diagenetic stages in a carbonate system (Berner et al., 1970). However, due to similar molecular masses between different steranes and diasteranes, co-elution under GC-MS conditions is a common problem, which can be overcome by using the MRM of GC-MS-QQQ. Diasterane concentration did not vary as significantly across the oil samples, with the highest diasterane content in oils located in the central Oklahoma, produced from Mississippian and Woodford intervals. Moreover, the ratio of diasterane to sterane ranged from 0.39 to 0.20, with an average of 0.28. Overall, this range suggests the majority of the oils were sourced from rocks that contained clay minerals. Such an interpretation is not conclusive, however, as thermal maturity can also increase the abundance of diasterane (Peters et al., 2005b).

Methyl steranes are biota-specific biomarkers that are linked to dinoflagellates and acritarchs (Al Atwah and Jacobi, 2017; Moldowan and Talyzina, 1998). More specifically, 4α-methyl sterols are found in living dinoflagellates (Wolff et al., 1986). Other sources for 4α-methyl

164

sterols are also observed in prymnesiophyte microalgae and some methanotrophic bacteria of the

species of *M. capsulatus* (Bird et al., 1971; Volkman et al., 1990). The distribution of methyl

Table 20 Key steranes biomarker ratios of selected Mississippian and Woodford oils.

Sample ID	%C$_{27}$ abbS (218)	%C$_{28}$ abbS (218)	%C$_{29}$ abbS (218)	%C$_{27}$ aaaR (217)	%C$_{28}$ aaaR (217)	%C$_{29}$ aaaR (217)	S/(S+R) (C$_{29}$ aaa) (217)	bbS/(bbS+ aaR) (C$_{29}$) (217)	(C$_{21+22}$)/(C$_{27+28+29}$) (217)	C$_{27}$/C$_{29}$ (abbS) (218)	C$_{28}$/C$_{29}$ (abbS) (218)	Diast/(Di ast+ster) (217)
Alf-01-M	0.20	0.22	0.50	0.24	0.15	0.62	0.49	0.56	0.09	0.58	0.44	0.23
Alf-02-M	0.26	0.22	0.52	0.19	0.13	0.68	0.45	0.57	0.11	0.50	0.43	0.29
Woo-01-M	0.27	0.21	0.53	0.19	0.15	0.66	0.48	0.53	0.09	0.50	0.39	0.27
Woo-02-M	0.24	0.20	0.53	0.26	0.16	0.58	0.50	0.51	0.07	0.51	0.38	0.22
Pay-01-M	0.21	0.22	0.50	0.26	0.23	0.49	0.52	0.50	0.11	0.66	0.48	0.26
Log-01-M	0.38	0.26	0.46	0.31	0.27	0.42	0.59	0.63	0.11	0.60	0.57	0.30
Gar-01-M	0.30	0.24	0.42	0.31	0.15	0.36	0.49	0.56	0.15	0.55	0.49	0.33
Kin-02-M	0.30	0.25	0.42	0.38	0.21	0.41	0.58	0.58	0.14	0.47	0.49	0.31
Log-05-W	0.30	0.27	0.43	0.34	0.22	0.51	0.55	0.61	0.12	0.70	0.62	0.30
Can-01-M	0.26	0.24	0.49	0.29	0.20	0.51	0.52	0.55	0.13	0.53	0.49	0.36
Log-02-M	0.26	0.24	0.50	0.35	0.14	0.51	0.54	0.54	0.07	0.53	0.47	0.27
Pay-02-M	0.26	0.23	0.51	0.30	0.17	0.53	0.51	0.50	0.08	0.51	0.45	0.25
Log-07-W	0.24	0.23	0.50	0.32	0.20	0.48	0.57	0.56	0.07	0.55	0.47	0.21
Pay-06-M	0.25	0.24	0.51	0.35	0.27	0.46	0.43	0.39	0.07	0.49	0.47	0.22
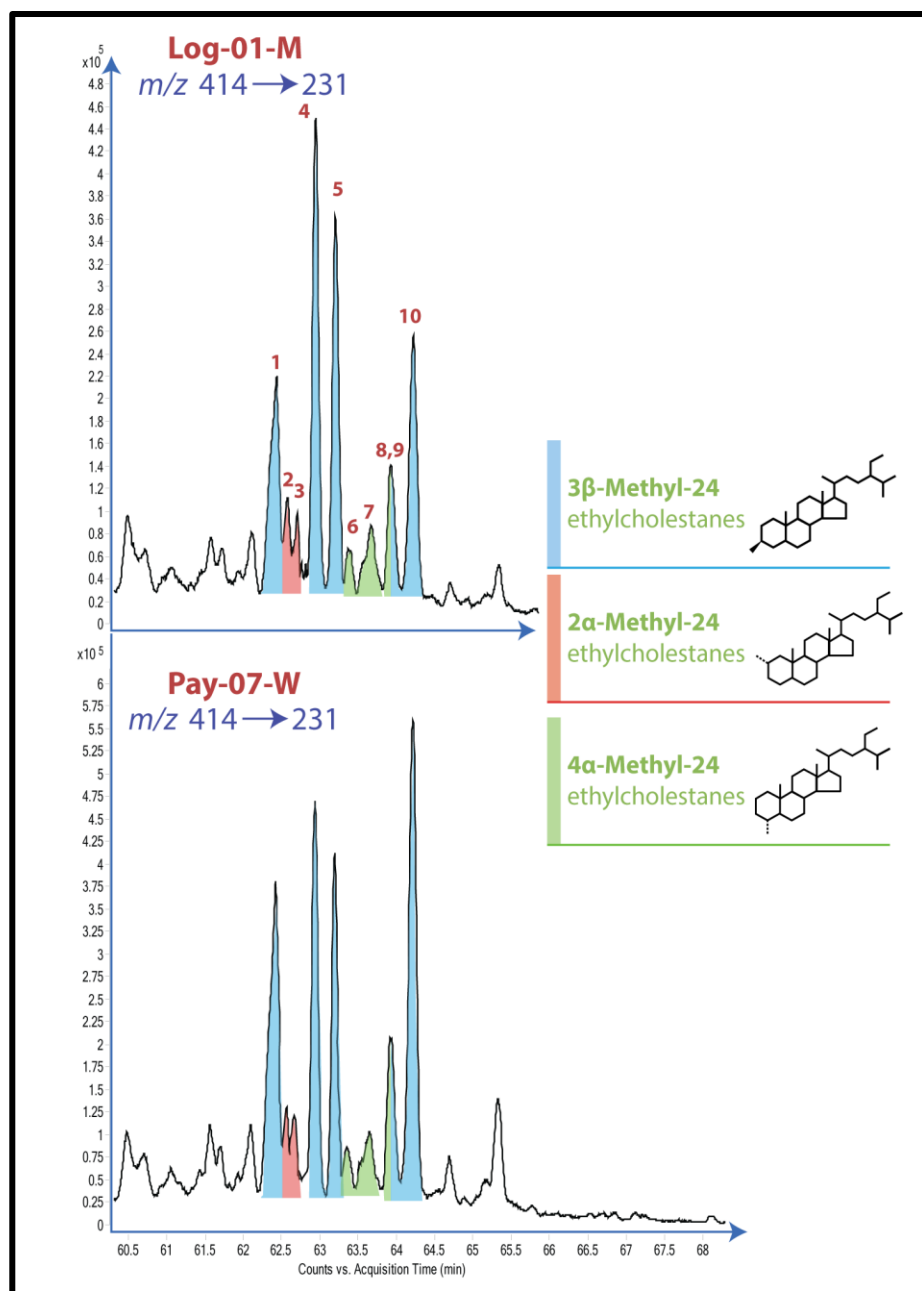
Figure 56: *m/z* 414→231 mass fragmentograms of crude oils produced from Mississippian carbonate and Woodford Shale formations, marked peaks represent series of methylsteranes, peaks identity (1) 3β-Methyl-24-ethylcholestane 20S; (2) 2α-Methyl-24-ethylcholestane 14β,17β(H) 20R; (3) 2α-Methyl-24-ethylcholestane 14β,17β(H) 20S; (4) 3β-Methyl-24-ethylcholestane 14β,17β(H) 20R; (5) 3β-Methyl-24-ethylcholestane 14β,17β(H) 20S; (6) 4α-Methyl-24-ethylcholestane 20S; (7) 4α-Methyl-24-ethylcholestane 14β,17β(H) 20R; (8,9) 2α-Methyl-24-ethylcholestane 20R + 4α-methyl-24-ethylcholestane 14β,17β(H) 20S; (10) 3β-Methyl-24-ethylcholestane 20R.

167

steranes in the crude oils showed a general trend of high abundance of three isomers of 3β-methyl-24 – ethylcholestane. The distribution of these isomers varied in the examined oil samples analyzed; for example, sample Pay-07-W showed an abundance of 3β-methyl-24-ethylcholestane 20R, relative to 3β-methyl-24-ethylcholestane 14β, 17β (H) 20R and 3β-methyl-24-ethylcholestane 14β, 17β (H) 20S. In contrast, sample Log-01-M exhibited an abundance of 3β-methyl-24-ethylcholestane 14β, 17β (H) 20R relative to the 3β-methyl-24-ethylcholestane isomers (Figure 56). Such a difference is strictly controlled by the organic-matter input, suggesting that these two crude oil samples are sourced from different source rocks, each of which exhibits a unique methyl-sterane fingerprint. The observed methyl-sterane distribution in these oils could be a result of different sources such as prymnesiophyte or acritarchs ultimately resulting distinctive methylsterols fingerprints.

Sterane isomerization ratios are the main sterane-based maturity ratios used to evaluate crude-oil maturity level. In particular, ββ/ (ββ+αα) and 20S/ (20S + 20R) C_{29} sterane ratios, with the former reaches equilibrium at the peak-oil stage, while the latter reaches equilibrium at the early oil-window (Seifert and Moldowan, 1986). The isomerization ratio of ββ/(ββ+αα) value usually increases with increasing in thermal maturity, and ultimately the ratio reaches equilibrium at a value of 0.70, equivalent to approximately 0.9% R_o indicating peak-oil generation stage (Peters et al., 2005b). The other sterane isomerization ratio is 20S/(20S + 20R) ratio, which increases from 0.0 to 0.5 and equilibrates at approximately 0.52, marking a maturity equivalent to 0.8% R_o (Seifert and Moldowan, 1986). The R structural arrangement at C-20 is observed in steroids of biological samples, while the S structural configuration is a more stable geological isomer of C_{29} sterane; therefore, during burial and maturation of sedimentary organic matter, the R isomer shifts to the S structural configuration (Beaumont et al., 1985). Under routine GC-MS conditions, these isomers

168

are not completely resolvable from the *m/z* 217 mass-chromatogram; for which, it is necessary to use GC-MSMS to accurately resolve these compounds. Otherwise, contamination from co-eluted compounds can hinder the compounds signal, resulting in an erroneous maturity evaluation. Collectively, those sterane-based maturity ratios are normally presented in a cross plot comparing the two parameters. Figure 57 shows the examined crude oil samples, which have been grouped based on geographic location to oils from the Anadarko Shelf, STACK play and central Oklahoma. Most of the central Oklahoma oils show a wide variation from immature to early oil-window maturity, while less variation is observed for oils located at the Anadarko Shelf and the STACK play. Based on the sterane maturity ratios, the STACK play oils have the highest maturity, with few samples reaching the equilibrium limit for the 20S/ (20S + 20R) ratio. The central Oklahoma oils varied the most and show a notable variation in the $\beta\beta/(\beta\beta+\alpha\alpha)$ ratio. Several studies have documented some processes that can alter the $\beta\beta/(\beta\beta+\alpha\alpha)$ maturity, such as the presence of sulfur,
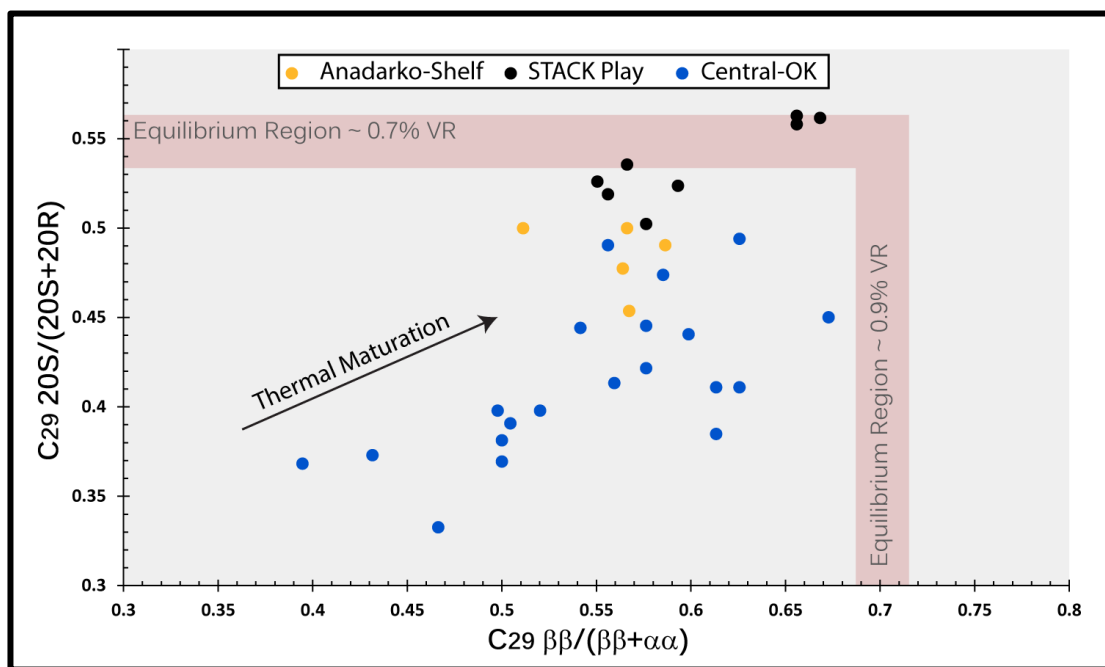
Figure 57: Crude oil steranes based maturity ratios comparing C_{29} $\beta\beta/(\beta\beta+\alpha\alpha)$ and 20S/(20S + 20R) ratios. Ratios are calculated using mass fragmentograms of GC-MS/MS run on MRM mode.

carbonate and evaporite lithologies and source-rock heating rate (Difan et al., 1990; Peters et al., 1990). While it is possible that the presence of carbonate lithology might have caused the offset the $\beta\beta/(\beta\beta+\alpha\alpha)$ ratios of central Oklahoma oils, it is likely that these oils present lower maturity than the rest of the samples, which is also supported by light hydrocarbons maturity ratios.

Diamondoids

Diamondoid hydrocarbons provide an important geochemical tool that has been used in different petroleum geochemistry applications, such as maturity assessment, oil cracking and mixing, and as a source-rock lithology proxy (Chen et al., 1996a; Dahl et al., 1999b; Schulz et al., 2001). More recently, diamondoids were applied to correlation studies, especially in fluids with various maturities, where biomarker alone fail due to their thermal instability beyond the oil window (Moldowan et al., 2015). In the examined crude oils, diamondoids were used primarily as a tool to identify the extent of hydrocarbon cracking and mixing, and we investigated different diamondoid-based maturity ratios.

By comparing diamondoids to biomarker concentrations, one could identify thermally cracked oils and unravel mixed fluids with various maturities. This concept is referred to as the extent of oil cracking, first introduced in 1999 by Dahl et al., where they compared the concentration of the sum of two diamantane isomers (i.e. 4- + 3-methyldiamantanes) to the absolute concentration of the biomarker stigmastane. The rationale for comparing these two compounds is that 4- and 3-methyldiamantanes are used as a proxy for cracked hydrocarbon due to their thermal stability and less volatility compared to adamantanes. Stigmastane is a cyclic and structurally fragile compound; therefore, with increasing maturity, the absolute concentration of stigmastane will decrease until its completely depleted at the end of the oil-window stage. On the

170

contrary, the diamantanes baseline remains constant throughout, and beyond the oil window, and they will increase in concentration due to the thermal cracking of higher hydrocarbon compounds (Peters et al., 2005c; Requejo, 1992). Figure 58 demonstrates the extent of cracking of the analyzed crude oils, color coded based on geographic locations. The first observation is the relatively low concentration of diamantanes in oils produced from central Oklahoma. Regardless of the producing reservoir, most of the oils in central Oklahoma are depleted in diamondoids with concentrations ranging from 1.2 to 4.8 parts per million (ppm). However, a fair concentration of stigmastane is still intact in these oils. The Anadarko Shelf and STACK play oils exhibit relatively high diamondoids and biomarker concentrations. The highest diamondoid concentration was

Figure 58: Extent of cracking of crude oils grouped by geographic location: Anadarko Shelf, Sooner Trend Anadarko Basin Canadian and Kingfisher Counties (STACK) play and central Oklahoma oils. The diamondoid baseline is established using immature rock extracts from the Woodford Shale and Mississippian carbonate rocks. Figure modified from Dahl et al. (1999a).
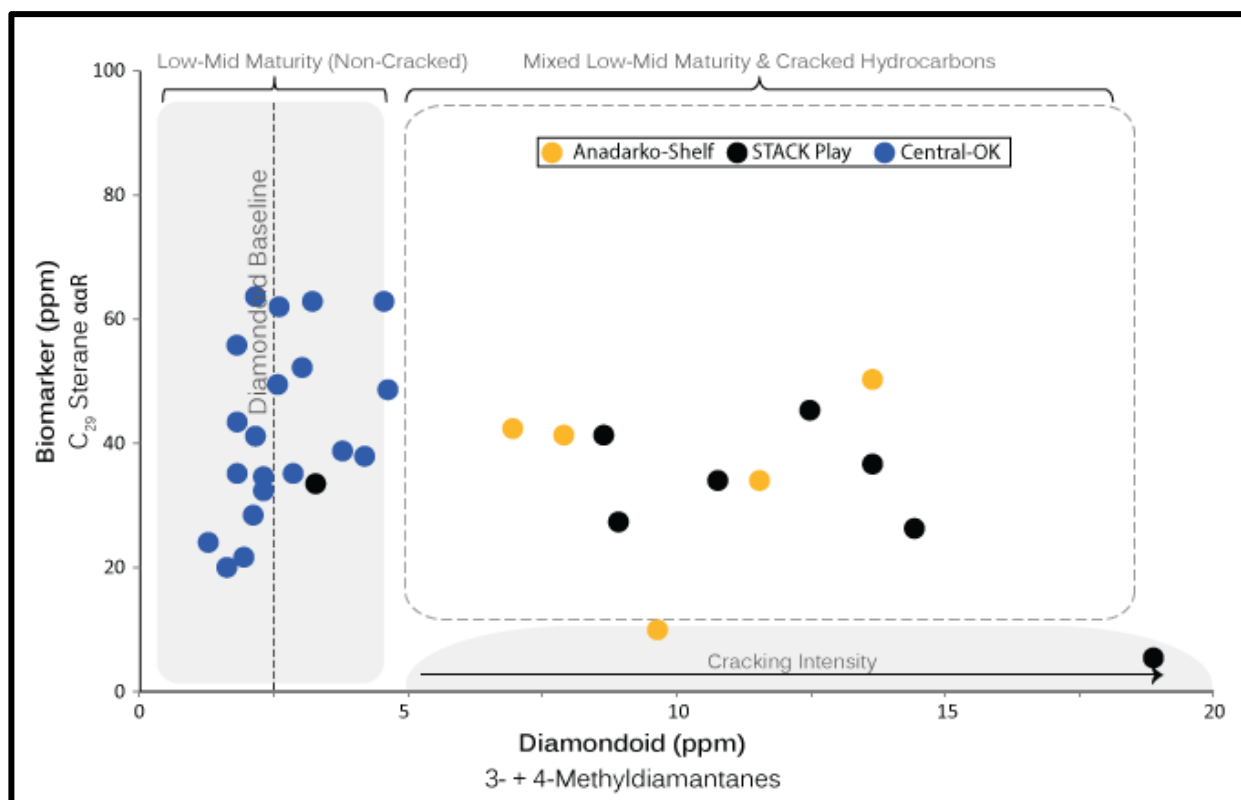
found in condensate sample Bla-01-M produced from Mississippian reservoir in Blaine County, with a sum of 4- and 3-methyldiamantanes, at 18.9 ppm. Overall, oils at the STACK play showed the widest range of diamondoid concentrations, ranging from 3.2 to 18.9 ppm, and biomarker concentration ranging from 4.0 to 41.2 ppm.

The analysis of this information suggests, that central Oklahoma oils are non-cracked hydrocarbons with intact stigmastane biomarker and diamondoids concentration near the baseline signature. In contrast, the Anadarko Shelf and STACK play oils result from a mixture of non-cracked and cracked hydrocarbons, producing dual-enrichment signals of high stigmastane together with high diamondoid concentrations (Figure 58). Another interpretation of the data could arguably be due to the presence of clay in source rocks generated oils in the STACK and Anadarko Shelf, since diamondoids are believed to generate as a result of carbonium ion interaction at acidic sited on clay minerals (Dahl et al., 1999a). In particular, clay-rich source rocks (e.g. montmorillonite) exhibit higher yield of diamondoids than source rocks with carbonate minerals; therefore, the presence of clays is clearly linked to the formation of diamondoids (Wei et al., 2006). Hence, if the source rocks that generated oils at the STACK and Anadarko Shelf are rich in clay minerals, it could explain the enrichment of diamantanes by this mechanism rather than due to petroleum secondary cracking and mixing of various maturities. While possible, this interpretation is unlikely for two main reasons. First, the quantitative measurement of diamantanes in immature rock extracts, as presented in Chapter IV, strongly suggest that the diamondoid baseline for the Woodford and Mississippian carbonate organic-rich rocks is 2 ppm ± 0.5 ppm, indicating a higher diamondoid baseline is unlikely for those rocks. Second, based on a number of studies that examined the diamondoids distribution within the Anadarko Basin, examining the diamondoids

distribution, the majority of the non-cracked oils exhibit a strong signal of 1 to 3 ppm methyldiamantanes baseline (JM. Moldowan, personal communication).

Diamondoids have also been used as a geochemical tool to infer source-rock mineralogy and to evaluate crude-oil thermal maturity. For rock mineralogy, the isomers of dimethyldiamantanes were empirically observed to be useful to discriminate between source-rock facies, including carbonate, shales, and coals (Schulz et al., 2001). This observation has been
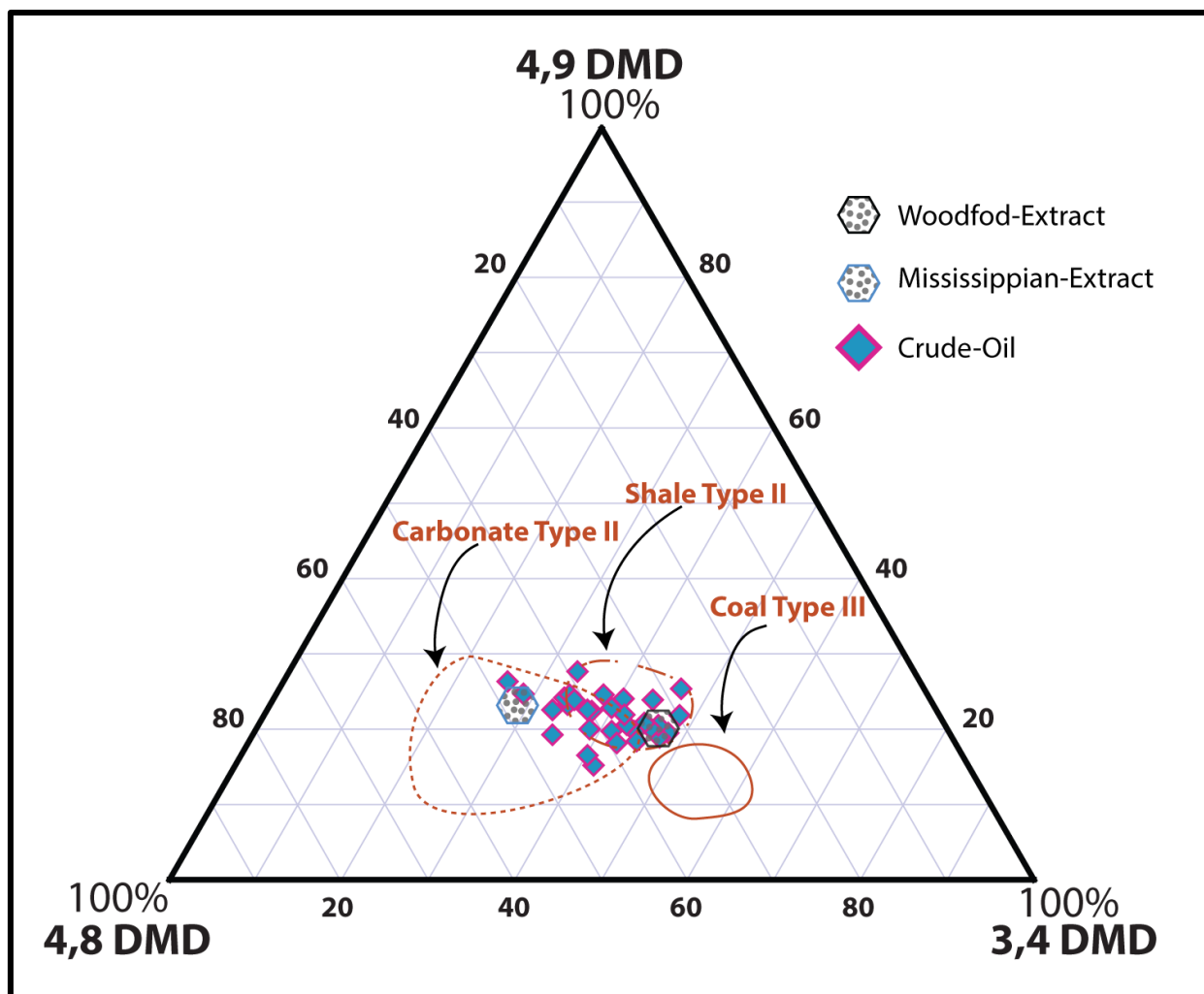
Figure 59: Ternary diamantanes diagram of crude oil and rock extracts from Mississippian carbonate and Woodford Shale samples. The diagram compares the relative abundance of three different isomers of dimethyldiamantane, including 4,9-dimethyldiamantane, 4,8-dimethyldiamantane and 3,4- dimethyldiamantane. Dimethyldiamantanes are measured from m/z 201 mass fragmentogram. Polygons of different source-rock facies are from Schulz et al. (2001).

173

further confirmed by an experimental study on different kerogen isolates in the presence of different sets of artificially-mixed mineralogies. In the experiments, an association is observed between montmorillonite and acidic aluminosilicate with a high yield of 4,8-dimethyldiamantane (Wei et al., 2006). Dimethyldiamantanes distribution in crude oils varied across the present study of crude oils, with two apparent trends. Some crude oil samples showed a dominance of 4,8-dimethyldiamantane over 3,4- and 4,9-dimethyldiamantanes, while the rest showed a stair-step distribution with a dominance of 3,4-dimethyldiamantane over the rest of dimethyldiamantane isomers. Figure 59 compares the relative abundance of the three dimethyldiamantane isomers including 3,4-, 4,8- and 4,9-dimethyldiamantanes. A spread is observed across the 3,4-dimethyldiamantane axis, which coincides with areas representing dimethyldiamantanes of extracted bitumen from Mississippian and Woodford rocks. According to Schulz et al. (2001), carbonate source rocks with Type-II kerogen showed a prevalence of 4,8 dimethyldiamantane over the rest of the dimethyldiamantane isomers, while shale siliciclastic rocks with Type-II kerogen showed a relative abundance of both, 3,4 and 4,8-dimethyldiamantane. Coal with Type-III kerogen, are commonly enriched in 3,4-dimethyldiamantane. The authors introduced a ternary diagram where they established polygons representative of each source-rock type (Schulz et al., 2001). Figure 59 depicts most of the oils plotted across the Type-II Shale and Carbonate polygons, suggesting that all the oils are of marine origin based on dimethyldiamantane isomers, with no evidence of Type-III derived oils.

Bitumens extracted from both, Mississippian and Woodford source rocks are also shown in Figure 59. Rock extracts plot within expected areas of marine shale and carbonate, which support the sensitivity of dimethyldiamantane isomers to the kerogen and rock mineralogy (Schulz et al., 2001). Crude oils from all locations show a wide range of diamantane distribution, with no

174

apparent trend associated with the geographic location. The relationship between bitumen extracts and crude oil is discussed further under the correlation of source rock to oil section.

A number of diamondoid-based ratios for maturity have been proposed in the literature (Chen et al., 1996b; Zhang et al., 2005). The basic premise of using diamondoids is that the methylated-diamondoid at bridge-head carbon-sites is thermodynamically more stable than the rest of the methylated-diamondoid series (Clark et al., 1979). Chen et al. (1996), introduced two diamondoid-based ratios for maturity, including the methyl adamantane index (MAI) and the methyl diamantane index (MDI). MAI is calculated by dividing 1-methyladamante over the sum of 1- and 2-methyladamantanes, were the methyl group at the C-1 position of an adamantane structure is representing a bridgehead methylation (thermally more stable), where methylation at C-2 is a secondary position (thermally less stable) (Chen et al., 1996b). In a subsequent study, Zhang et al. (2005), extended the use of diamondoid maturity ratios to include dimethyl diamantane. They introduced two additional ratios including the dimethyl diamantane index-1 (DMDI-1) [4,9-/(3,4- + 4,9-diemthyldiamantanes], the dimethyl diamantane index-2 (DMDI-2) [4,9-/(4,8- + 4,9-iemthyldiamantanes]. While diamondoid-based maturity parameters are in principle convincing, in practice and experimental examination they do not show a linear relationship with maturity. In particular, based on series of hydrous pyrolysis experiments, parameters such as MAI, MDI, DMDI-1, and DMDI-2 do not follow a linear trend with increasing hydrous pyrolysis temperatures, and in some instances, they showed a reversal trend for maturities below 1.3%R_o (Wei et al., 2006). In contrast, the authors proposed the use of a maturity ratio based on the three-cage diamondoid, triamantane. This ratio compares the 9-methyltrimantane relative to the sum of the rest of the methyltriamantane isomers, which appeared to systematically increase with increasing hydrous pyrolysis temperatures (Wei et al., 2006). Aside from the

methyltriamantane ratio, the adamantane and diamantane maturity ratios are also useful as maturity parameters for fluids with higher maturities $>1.3\%R_o$. Table 20 lists a number of diamondoid-based maturity ratios for crude oil samples from Oklahoma. In a careful examination of the ratios, MAI exhibits a narrow range of values ranging from 0.52 to 0.79 and an average of 0.60. Similarly, MDI did not vary much, with results averaging at 0.50. The dimethyldiamantane ratios DMDI-1 and DMDI-2 showed the least variance in the estimated maturity, with values ranging from 0.25 to 0.48, and from 0.21 to 0.45, respectively. Therefore, the adamantane- and diamantane-based ratios (i.e. MAI, MDI and DMDI), underestimate maturities, especially for condensates. For example, samples Bla-01-M and Kay-01-M which are light condensates have MAI and MDI ratios of 0.79, 0.52, and 0.50, 0.59, respectively. Such ratios do not really capture maturity as accurately as our crude oil samples at 0.6 to 1.3% vitrinite reflectance equivalent (VRE); in particular, they do not show as much variation of maturity as do other biomarker or light-hydrocarbon maturity ratios. One exception is the TMI ratio, which showed a wider range of values, from 0.09–0.68 and coincide with other maturity parameters such as the heptane and sterane ratios. Vitrinite reflectance equivalent values from diamondoids have been proposed by using a relationship based on a linear regression of absolute concentrations of 4- and 3-methyldiamantanes (Wei et al., 2006). While these type of ratios usually need to be calculated and calibrated for each source rock via hydrous pyrolysis experiments, we used a published equation for the Ordovician Vinini Limestone to estimate a vitrinite reflectance equivalent (VRE-D) for our crude oils (Table 20). Overall, VRE-D captures a similar maturity to that of the heptane and isoheptane ratios, together with biomarker maturity ratios. The maturity trend observed suggests a higher thermal maturity in STACK play and Anadarko Shelf oils, with an estimated VRE-D ranging from 0.19 to 6.88%VRE. While it is impossible to have oils at that low level of maturity, such a result emerges from using an equation

that is set for Vinini limestone, which differs in age and in organic matter from that of source rocks in Devonian-Mississippian age of Oklahoma. Despite VRE-D values do represent the real thermal maturity of the examined crude oils (oil generation commonly starts at $0.55\%R_o$), the VRE-D values obtained do separate mature fluids from black oils, as is apparent when comparing oils east of the Nemaha Uplift to oils located to the West of the uplift.

Aromatic Hydrocarbons

Aromatic hydrocarbons constitute an important fraction of the crude-oil and rock-extracts chemistry, which hold signals pertaining to kerogen type, source-rock lithology, and thermal maturity. Many investigations on the thermal and kinetic behavior of aromatic hydrocarbons are

Table 21 Selected diamondoid-based maturity ratios of crude oil samples.

Sample ID	MAI[a]	MDI[b]	MDMI-1[c]	MDMI-2[d]	MTI[e]	%VRE-D[e]
Anadarko-Shelf Oils						
Alf-01-M	0.62	0.52	0.40	0.37	0.44	2.89
Alf-02-M	0.63	0.59	0.37	0.32	0.39	5.30
Kay-01-M	0.59	0.50	0.37	0.31	0.27	4.31
Woo-01-M	0.66	0.64	0.36	0.41	0.37	6.46
Woo-02-M	0.73	0.66	0.39	0.39	0.36	3.41
STACK Play Oils						
Bla-01-M	0.79	0.30	0.35	0.38	0.62	0.95
Can-01-M	0.62	0.60	0.30	0.22	0.17	3.81
Can-02-M	0.70	0.34	0.48	0.36	0.24	4.94
Can-03-M	0.63	0.58	0.36	0.33	0.31	4.21
Can-04-M	0.63	0.50	0.41	0.45	0.48	3.94
Kin-01-N	0.61	0.64	0.27	0.23	0.35	6.88
Kin-02-M	0.53	0.50	0.33	0.35	0.37	6.44
Kin-03-M	0.60	0.63	0.34	0.33	0.09	5.86
Kin-04-M	0.62	0.57	0.34	0.40	0.17	0.19

Table 20 continued.

Sample ID	MAI[a]	MDI[b]	MDMI-1[c]	MDMI-2[d]	MTI[e]	%VRE-D[e]
Central-Oklahoma Oils						
Lin-01-M	0.57	0.53	0.35	0.57	0.20	0.32
Lin-02-M	0.56	0.43	0.43	0.56	0.12	0.61
Lin-03-W	0.53	0.25	0.27	0.53	0.24	0.39
Log-01-M	0.55	0.71	0.35	0.55	0.17	0.09
Log-02-M	0.55	0.72	0.38	0.55	0.18	0.94
Gar-01-M	0.55	0.58	0.38	0.55	0.27	0.47
Log-03-M	0.55	0.72	0.38	0.55	0.18	0.88
Log-04-W	0.55	0.70	0.36	0.55	0.17	1.24
Log-05-W	0.57	0.43	0.34	0.57	0.21	0.27
Log-06-W	0.56	0.10	0.25	0.56	0.16	0.93
Log-07-W	0.61	0.72	0.37	0.61	0.24	0.75
Pay-01-M	0.57	0.51	0.37	0.57	0.28	0.47

[a] MAI: 1-Methyladamantane/(1-+2-methyladamantanes) ; [b]MDI: 4-Methyldiamantane/(1-+3-+4-methyldiamantanes); [c] MDMI-1: 4,9-diemthyldiamantane/(3,4- + 4,9-diemthyldiamantanes); [d]MDMI-2: 4,9-diemthyldiamantane/(4,8- + 4,9-diemthyldiamantanes) ; [e]MTI: 9 Methyltriamantane/(5-+8-+9-+16-methyltriamantanes); [e] Vitrinite reflectance equivalent derived from diamondoids (3-+4-methyldiamantanes) relationship is from (Wei et al., 2006)

well documented in the literature both theoretically and in practice (Beach et al., 1989; Radke et al., 1982a). Some of the examined aromatic hydrocarbons represent an aromatized version of sterane biomarkers; those include triaromatic and monoaromatic steroids, while other compounds exhibit a small carbon-backbone structure to be considered as biomarkers such as naphthalenes, phenanthrenes and anthracene. In the presently examined oils, both classes of aromatic compounds (aromatic-biomarkers, and aromatic non-biomarkers) are discussed in detail.

Naphthalene and phenanthrenes and their alkylated homologs are primarily used in the maturity evaluation of crude oil and bitumen, and some studies have used those parameters for oil typing (Radke et al., 1986; Sivan et al., 2008). Aromatic-based maturity ratios usually compare a set of compounds to a given parent compound. This is achieved using two approaches, one that

compares the degree of methylation to the parent compound, and another that compares certain thermally-stable isomers relative to the parent compound. In both approaches, naphthalenes and phenanthrenes are crucial in supplementing other maturity parameters derived from biomarkers (Radke, 1988). Figure 60 shows a number of aromatic maturity parameters. More specifically, Figure 60-B, C and D all show ratios of naphthalenes and phenanthrenes. Dimethylnaphthalene and trimethylnaphthalene ratios did not separate oil maturity significantly; most the data cluster in the center, with few outliers such as samples Kin-02-M and Bla-01-M, with the latter being a light condensate with 49° API gravity. Similarly, the methylphnantheranes index (MPI) shown in Figure 60-B did not vary as much as the ethylnapthalene ratio (ENR), with most of the data plotting around 0.6 and 0. 8%VRE with similar samples Kin-02-M and Bla-01-M with higher values. However, ENR varied quite broadly, ranging from 0.5 to 7.5, with a lower value for outlier samples, which are the most mature samples based on other maturity parameters. With other phenanthrenes-based ratios, however, a stronger reversal trend is shown in maturation than that of other maturity indicator discussed earlier. This reversal is observed when comparing PP-1 [1-methylphenanthrene/(2-methylphenanthrene + 3-methylphenanthrene] with PPM which is another modified ratio of methylphenanthrene [1-methylphenanthrene + 9-methylphenanthrene)/(2-methylphenanthrene + 3-methylphenanthrene) (Alexander et al., 1986; Cassani et al., 1988).

It is apparent that aromatic ratios are not consistent with other maturity ratios observed from light hydrocarbons, biomarkers and diamondoids. This inconsistency can be explained according to three main points. First, most aromatic maturity ratios are source-rock- and facies-specific; that is, an ENR ratio of 2.5 is represents a reflectance value of 0.60%Rm of Type II, while the same reflectance value in a Type-III kerogen will exhibit a lower ENR ratio at 1.10 (Radke et al., 1986). Therefore, without calibration of those aromatic ratios to a specific rock facies, it is

difficult to use for drawing on conclusions about maturity. Second, some aromatic ratios also show systematic reversal-behavior with thermal maturation, which is mostly kinetically driven. This can result in a single value of MPI ratio indicating two different levels of maturities (Radke, 1983). Finally, crude oils accumulation usually results from different hydrocarbon charges, and as indicated by diamondoid evidence, some of those oils are a mixture; therefore, due to hydrocarbon mixing and migration, the aromatic maturity signal can be compromised (Radke et al., 1982b)

Aromatic biomarker ratios of monoaromatic and triaromatic steroids are among the useful maturity ratios, which span throughout the oil maturity window. Aromatic steroids are usually assessed using two ratios: one is based on monoaromatic abbreviated as MA (I) +MA (I+II), and the triaromatic steroid is abbreviated as TA (I)/TA (I+II). In these ratios, the main concept is to compare the short-chain aromatic steroid to its long-chain counterparts. The main principle is that as a function of thermal cracking, short-chain aromatic steroid will increase in abundance. The cause of the increase in short-chain steroids is well defined, as to whether they form as a result of long-chain steroid cleavage or as a result of short-chain steroid thermal stability; therefore, they do not thermally degrade or a combination of the two (Mackenzie et al., 1982b). Nevertheless, the trend of increasing short-chain homoluges is a valid trend normally observed with increasing maturity. In addition, triaromatic steroids are more stable than monoaromatic steroids and even more sensitive to higher maturities, due to the possibility of monoaromatic storied conversion to triaromatic steroid (Beach et al., 1989). For the examined oil samples, a result of TA(I)/TA(I+II) and MA(I)+MA(I+II) is shown in Figure 60-A. Overall, the data show relatively high TA(I)/TA(I+II) as compared to that of MA(I)+MA(I+II), which is unusual because triaromatic steroids are thermally more stable and therefore slightly slower in forming compared to the monoaromatic steroid. This could be due to the source of initial organic matter favoring the

formation of a triaromatic backbone structure as opposed to monoaromatic hydrocarbons. However, it is more likely that such a phenomenon is due to oil mixing in high-maturity oils, reflected in higher triaromatic steroids, with low maturity oils, reflected in monoaromatic steroids. Such a hypothesis requires further lab testing to validate, however. In general, most of the oil samples ranged from 0.05 to 0.2 in the MA(I)+MA(I+II), which is equivalent to a vitrinite reflectance range of 0.5 to 0.7%, and most of those samples are located east of the Nemaha Uplift in central Oklahoma. Moreover, TA (I)/TA (I+II) ranged mostly from 0.1 to 0.4, equivalent to a
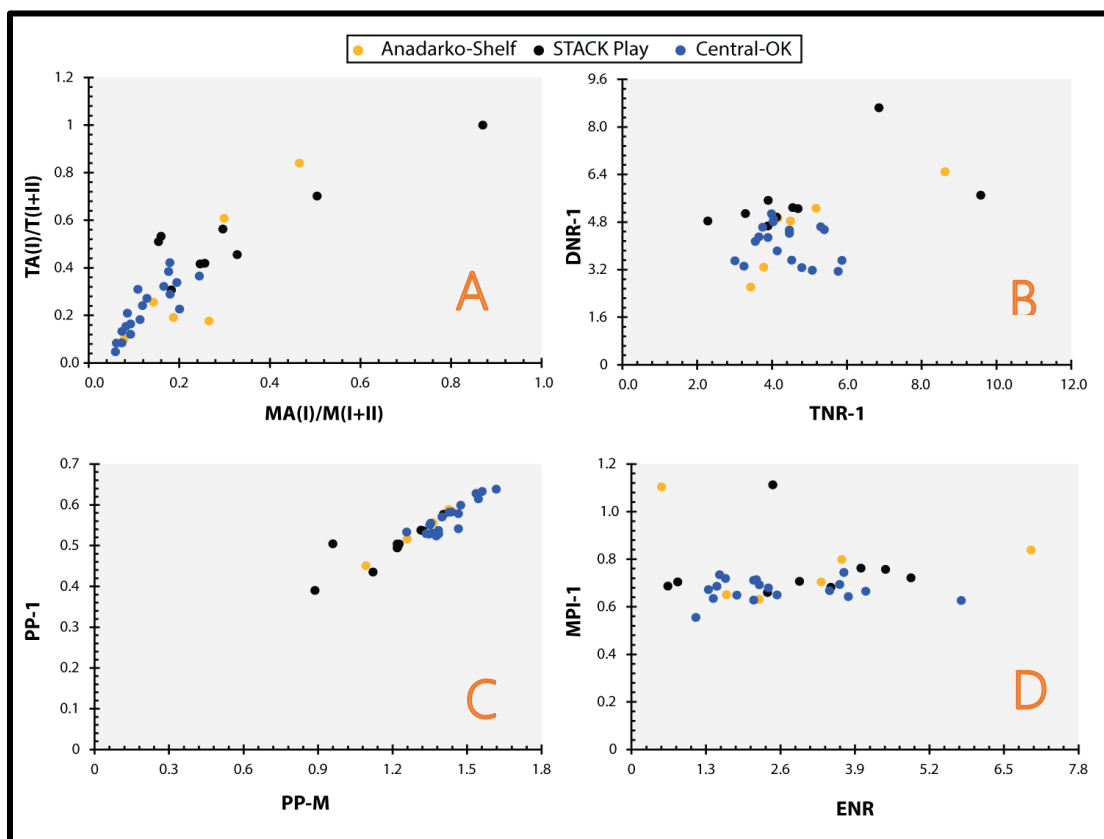
Figure 60: Cross-plots of different aromatic based maturity ratios, (A) TA(I)/TA(II): triaromatic steroid ratio (TAS) $(C_{20}+C_{21})/(C_{20}+C_{21}+C_{26}+C_{27})$; MA(I)/MA(I+II): monoaromatic steroid ratio $(C_{21}+C_{22})/(C_{21}+C_{22}+C_{27}+C_{28}+C_{29})$. (B) DNR-1: dimethylnaphthalene ratio 2,7-+3,6-dimethylnaphthalenes/1,5 dimethylnaphthalene; TNR-1:trimethylnaphthalene ratio: 1,3,7-trimethylnaphthalene/1,3,5-+1,4,6-trimethylnaphthalenes. (C) PP-1: 1-methylphenanthrene/ 3-+2-methylphenanthrenes; PP-M: 1-+9-methylphenanthrenes/ 3- + 2-methylphenanthrenes; (D) MPI-1: methylphenanthrene index: 1.5*(3-+2-methylphenanthrenes/ phenanthrene + 1- + 9-methylphenanthrenes); ENR: 2-ethylnaphthalene/1-ethylnaphthalene ratio.

range of 0.65 to 0.8%Ro, with mostly oils from central Oklahoma at this stage of maturity. Other outlier samples are observed in STACK play and Anadarko Shelf oils, particularly samples such as Bla-01-M and Kin-02-M, with an MA(I)+MA(I+II) of 0.81 and 0.55,; those are equivalent to 1.0 and 0.85%Ro, respectively (Peters et al., 2005c). Additionally, those samples exhibited slightly higher TA(I)/TA(I+II) values, at 1.0 and 0.7 corresponding to 1.3 and 0.95%Ro (Peters et al., 2005c). Anadarko Shelf oils, some of which showed higher maturity based on triaromatic steroids, such as Kay-01-M with TAS (0.84), were almost twofold higher than the monoaromatic steroids ratio (0.42), resulting in the possibility of maturity being anywhere from 0.85 to 1.2%Ro. Such discrepancy between the two maturity ratios is very likely due to the mixing of hydrocarbons, with each hydrocarbon charge bearing a different maturity level. This observation is also evident when comparing the diamondoids and biomarker concentrations of this sample, exhibiting 9.6 ppm of 4-+3-dimethyldiamantanes, an order of magnitude higher than the diamondoid baseline (Figure 58). These results suggest, indeed, that this sample has received cracked hydrocarbons; this might be the reason behind the elevated monoaromatic steroid ratio, while still showing a fair amount of stigmastane, which can be used as a proxy of low to middle maturity oil.

Aromatic hydrocarbons ratios that are sensitive to source-rock facies were examined also for the crude oil samples. More specifically, dibenzothiophene with phenanthrene aromatic compounds were compared to pristane and phytane ratios. Such a relationship has been proved to differentiate between source-rock facies such as fluvial-deltaic shale, marine shale, lacustrine and sulfur-rich marine marl (Figure 61) (Hughes, 1984; Hughes et al., 1995). Such molecular ratios are believed to reflect Eh-Ph conditions during deposition and early-diagenesis stages, together with chemical interactions induced by microbiological processes (Hughes et al., 1995). This ratio is crucial, as it supplements other biomarker-based parameters to infer source-rock lithology,

depositional environment and organic matter from crude oils. Most crude oil samples plot within Zone 3, indicating that these oils are primarily generated from marine shale petroleum source rocks. The overall abundance of dibenzothiophene is lower than that of phenanthrene, suggesting that oils are low in sulfur content. Ratios of dibenzothiophene to phenanthrene averaged at 0.65, and ranged from 0.15 to 1.35, while values of pristane-to-phytane ratio showed a narrower variance, ranging from 1.33 to 1.68 (Figure 61).
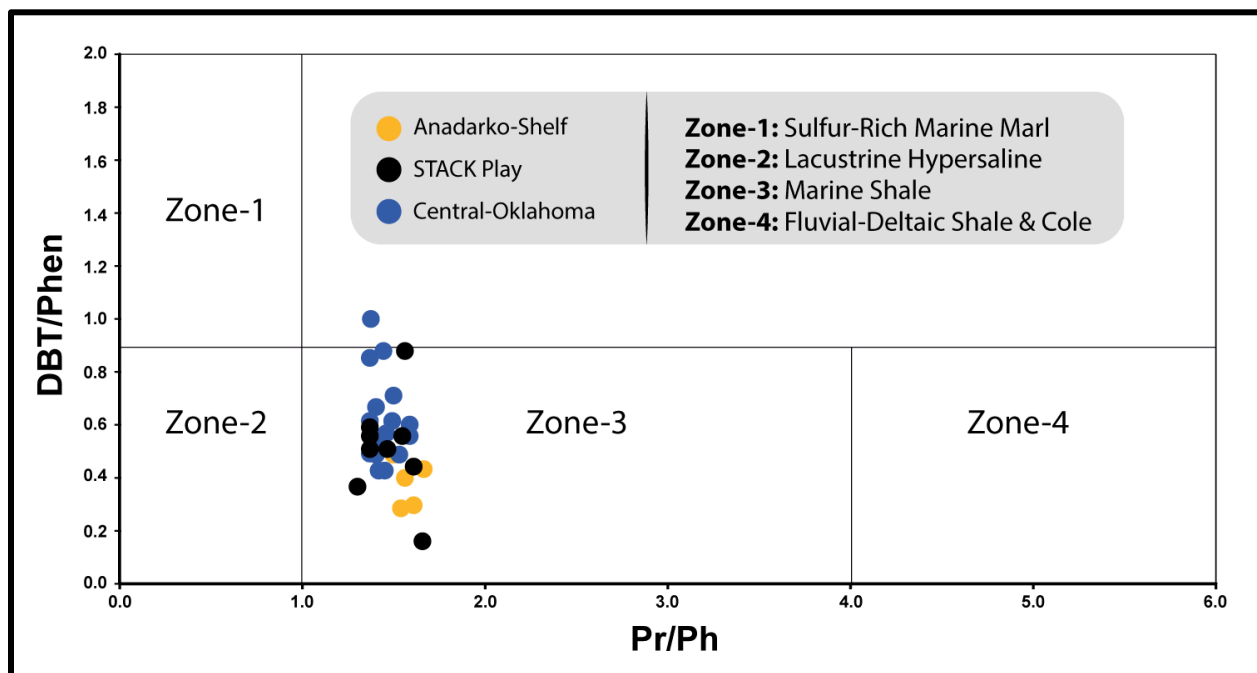
Figure 61: Cross plot of Mississippian- and Woodford-produced crude oils comparing, on the x-axis, the ratio of pristane to phytane and, on the y-axis, the ratio of dibenzothiophene to phenanthrene. This graph is used to infer source-rock depositional setting. Graph is modified from (Hughes, 1984).

Stable Carbon Isotopes

Stable carbon isotope ratio is one of the crucial geochemical tools that has been used in the application of oil–oil and oil–source-rock correlation studies. Overall, the bulk carbon isotopic composition varies based on the organic-matter source. Different stable isotope carbon signatures have been observed to associate with primary producers of the Messel Shale, where it has been

observed that eukaryotic algae and green photosynthetic bacteria exhibit a bulk carbon isotope ratio of −22‰ and −24‰, respectively (Freeman et al., 1990). Therefore, in theory, such an isotopic signature would be reflected in expelled petroleum hydrocarbons, which can be directly measured from the crude oil to infer its organic-matter source. According to Sofer (1984), the overall isotopic signature of the C_{15+} saturate and aromatic fraction of crude oils are primarily controlled by three main factors: (1) organic-matter source of the oil in terms of marine vs. terrigenous; (2) absolute crude-oil isotopic value, and to a limited extent (3) crude-oil maturity level. Moreover, it is been noted that marine sourced crude oils tend to be isotopically more positive than terrigenous sourced crude oils (Sofer, 1984). Despite the fact that a bulk C_{15+} saturate and aromatic fraction is used as a tool for oil-oil and crude-oil source identification, overlap in the isotopic signature can occur, therefore hindering any organic-matter signature. Hence, the advancement of CSIA allows for finding an improved isotopic signature for individual hydrocarbon compounds, whereby an *n*-alkane isotopic profile can be generated (Bjorøy et al., 1991; Rieley et al., 1991). The *n*-alkanes have wide-range of biological precursors, so the *n*-alkanes bear an isotopic signature distinctive in relation to the source of the organic matter. A number of studies have utilized the *n*-alkane CSIA (*n*-C-CSIA), and with the isotopic *n*-alkane profile, different sources of organic-matter types were unraveled for correlation and depositional setting reconstruction (Murray et al., 1994; Romero et al., 2017).

In this study, we measured the isotopic values of *n*-alkanes in for a total of 31 crude-oil samples. The $\delta^{13}C$ isotopic values of each normal alkane compound were calculated relative to Pee Dee Belemnite (PDB) standard. For oil samples, isotopic values were measured for 19 compounds of the normal alkanes ranging from *n*-C_{13} to n-C_{32}. Figure 62 shows the *n*-alkane isotopic profile
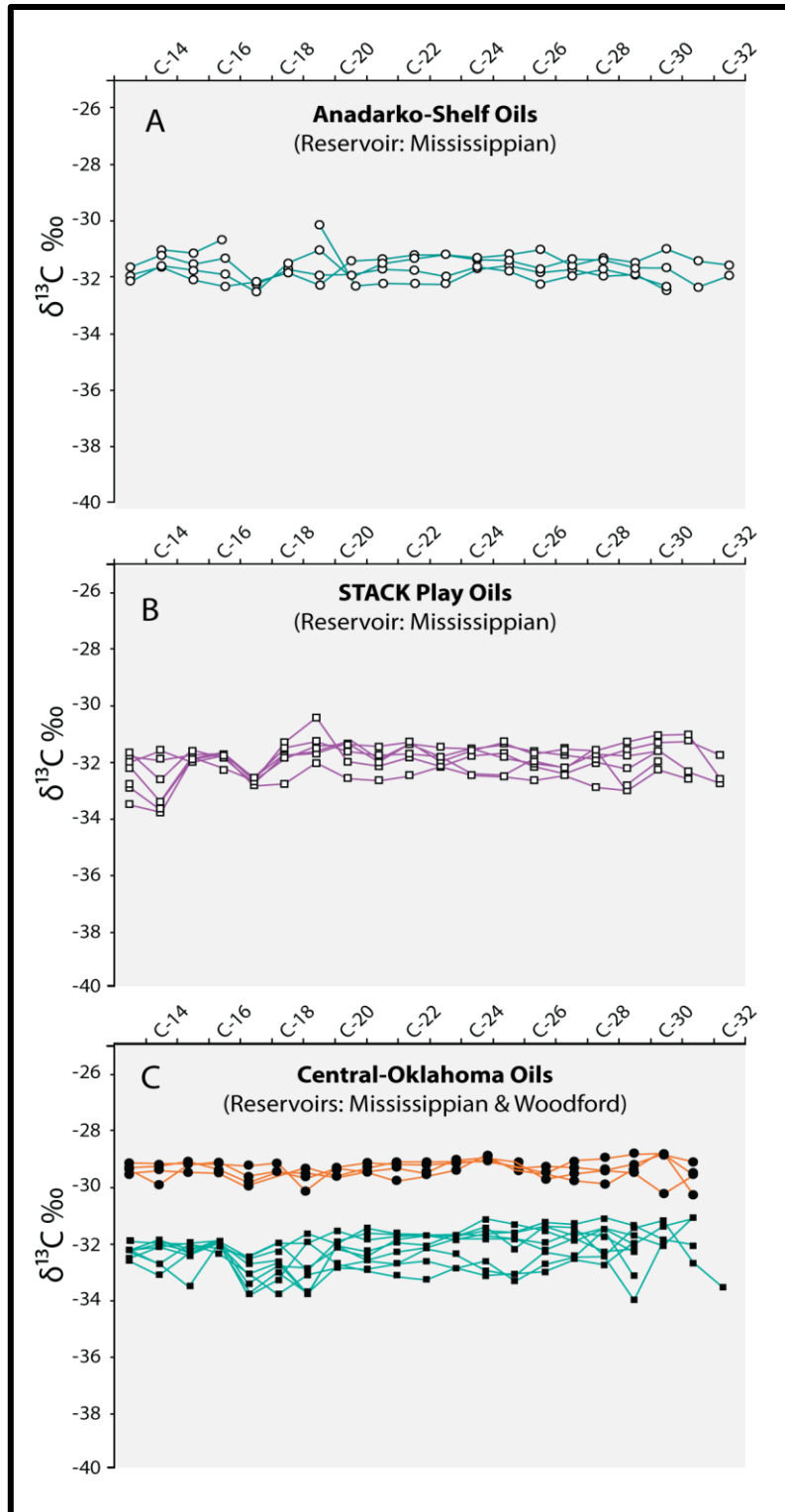
Figure 62: Normal alkanes isotopic profile of crude oils, depicting n-alkanes ranging from C_{13}-C_{32} (A) Anadarko Shelf oils, (B) Sooner Trend Anadarko Basin Canadian and Kingfisher Counties (STACK) play oils, (C) central Oklahoma oils.

of all the oil samples divided into three groups based on geographic location. Overall, the oils based on their isotopic values showed different ranges. Samples located in the Anadarko Shelf have isotopic values ranging from −32.7 to −30.0, with the highest isotopic variance between the oils occurring at n-C_{19} and the least variance at n-C_{18} (Figure 62-A). Oils at the STACK play were slightly lighter in overall isotopic signature relative to oils from the of Anadarko Shelf, ranging from −33.9 to −30.3, with isotopic variance maximizing at n-C_{13}, and isotopic variance reaching the minimum at n-C_{17}. Both oil locations the STACK play and the Anadarko Shelf oils are produced from the Mississippian reservoirs. In contrast, central-Oklahoma oils showed a unique dual isotopic trend with some Mississippian oils are isotopically heavier ranging from −30.4 to −28.6, while the other oils exhibiting an isotopically lighter signature ranging from −34.0 to −31.1. Isotopically heavier oils within central Oklahoma showed minimum variation of isotopic signature between the different normal alkane compounds, while the isotopically-lighter oil group in central Oklahoma had the maximum variance at n-C_{29}

Isotopic trends observed from the oil samples can be broadly classified into three groups with lighter, medium and heavier isotopic signatures. Most notable is the group of heavier isotopic-signature crude oils located in central Oklahoma. Those oils are produced from Mississippian carbonate reservoirs, such as Log-01-M and Log-05-M. Such higher isotopic values could be influenced primarily by organic-matter source; however, biodegradation can, in some cases, cause n-alkanes and cycloalkanes isotopic fractionation (Eglinton, 1994; Sofer, 1984). Since n-alkanes are intact in these oils, biodegradation is unlikely to be the cause of the observed isotopic values. Therefore, such negative isotopic ratios are caused by the precursor organic matter that contributed to the formation of those oils. A similar interpretation can be applied to crude oils that are lighter in their carbon isotope ratios, but some influence of maturity or migration can hinder the isotopic

186

signature. It has been as reported that maturity can cause as much as 2‰ variance in the isotopic values (Sofer, 1984). Hence, oils with that are situated in between these two end-members, such as sample Kin-03-M and Lin-03-W, exhibiting a medium isotopic value could have resulted from migration or petroleum mixing. Moreover, while maturity can influence the isotopic value for bulk saturate and aromatic fraction, as noted by Sofer (1994), the isotopic value of individual n-alkane compounds in the range of nC$_{12}$-nC$_{32}$ remains unaffected by maturity (Clayton and Bjorøy, 1994). Such an observation is further confirmed by similar nC$_{12}$-nC$_{14}$ δ13C values of a light condensate with residual oil samples; the influence of maturity on the isotopic value of normal alkane is minimal, especially given that we used nC$_{13}$ to nC$_{32}$, which are the least likely to be affected by maturity (Clayton and Bjorøy, 1994; Dzou and Hughes, 1993). The overall δ13C distribution of the n-alkanes in most of the samples followed a flat trend, with some minor zigzagging occurring at even-numbered normal alkanes. Additionally, within each oil isotopic groups, there is no difference between long and short chain n-alkanes, therefore suggesting a common organic source or depositional setting, ultimately resulting in a uniform n-alkane isotopic profile. Such an observation is also supported by a study examining different kerogen sources through flash-pyrolysis, after which pyrolysis-product isotopes were measured, revealing a ±3‰ difference from kerogens with single organic matter (Eglinton, 1994). In marine carbonate and siliciclastic sourced oils, uniform distribution of n-isotope profile is observed with minor variation in δ13C (Murray et al., 1994; Romero et al., 2017). Therefore, the isotope data further support the origin of those crude oils to be primarily of marine origin, with no contribution of terrigenous organic matter, which otherwise would result in a negatively sloping n-alkane isotopic profile (Murray et al., 1994). Additionally, oils in the Anadarko Shelf, STACK play and some in central Oklahoma share a common source based on the isotope profile, while the n-alkane isotopic profile of some oils in

central Oklahoma suggests a different source rock. Such grouping is also observed in the biomarkers of central-Oklahoma oils. The isotope data combined with biomarkers in the following section will delineate the crude-oil–source-rock relationship.

Source Rock–Oil Correlation

Source rocks examined in this study showed unique biomarker fingerprints for both Mississippian and Woodford Source rocks. Similarly, examined crude oil reflected some of the unique biomarker characteristics related to both Mississippian and Woodford Shale. In this section, compositional data will be discussed, starting with normal alkanes and isoprenoids, terpane and terpane biomarkers, and concluding with diamondoids.

Normal alkane distribution of the examined rocks lacked the light-hydrocarbons (C_4 to C_9), so using a C_7 star diagram for correlation is not possible. Normal alkanes (C_{10+}) of Mississippian and Woodford source rocks are shown in Figure 44, and some examples of oil *n*-alkane chromatograms are shown in Figure 54. Due to evaporation loss of light-hydrocarbons, it is difficult to use those chromatograms for correlation between rock extracts and oils; however, it can be concluded that both samples are derived from marine sources, as evident from the overall unimodal distribution of *n*-alkanes. Similarly, using pristane and *n*-C_{17} together with phytane and *n*-C_{18}, a general conclusion can be drawn about the marine origin of the examined kerogen and studied oils. Therefore, bulk characteristics normally measured using gas-chromatography approaches are not adequate to unravel source differences between Mississippian and Woodford source rocks. Moreover, a regional study examined a collection of crude oils from the Anadarko and Ardmore Basins together with Anadarko Shelf and Cherokee Platform, which heavily relied on *n*-alkanes, pristane, phytane and isotope and bulk parameters, grouping most of oils in the

Anadarko Basin and Shelf together to only one source. Here, we show that such general compositional data is not sufficient for distinguishing Mississippian and Woodford-sourced oils.

Terpane biomarkers represent one of the most diagnostic biomarker classes that can capture differences between Mississippian and Woodford-sourced oils. Most notably is the enrichment of lower and extended tricyclic terpane biomarker in Mississippian rock extracts and associated oils (Figure 63). Table 21 list some of the key biomarker ratios of Mississippian and Woodford source rocks and their related oils. Extended tricyclic terpanes are present in Mississippian samples up to C_{38}, with absolute concentrations of 10 ppm and higher, reaching up to 57 ppm in rock extracts and 38 ppm in crude oils. By utilizing the extended tricyclic terpanes, the following oils bear a extended tricyclic terpane fingerprint close to that of Mississippian source rocks, such as sample Log-01-M. In contrast, Woodford extracts and related crude oils exhibit trace amounts of extended tricyclic terpanes, reaching up to C_{30}, such as Alf-01-M. Using extended tricyclic terpanes, the ETT/HH ratio was developed, which compares a set of extended tricyclic terpanes to homohopane biomarkers. Both Mississippian rock extract and crude oils exhibit ETT/HH higher than 2, whereas Woodford bitumen and crude oils showed ETT/HH less than 1 (Table 21). It is important to note that the main cause of extended tricyclic terpane enrichment in Mississippian rock is highly controlled by the source of organic matter rather than thermal maturity and biodegradation. Thermal maturity as examined in both core samples and most of the oils suggests that examined rock extracts are immature with values around 0.49%R_o, while oils are ranging from early-oil to peak-oil generation stages (Figure 57). Thus, enrichment of tricyclic terpanes is not caused by elevated maturity. Enrichment of tricyclic terpane due to biodegradation effect can also be ruled out, because of the lack of any molecular signature for biodegradation. Hence, enrichment of lower

and extended tricyclic terpanes in Mississippian rocks and related oils are solely related to organic-matter source.

Hopanes are another biomarker that varied across the two end-members, with low abundance of hopane and homohopane in Mississippian extracts and oils, while they dominated all Woodford fluid samples. Additionally, some Mississippian fluids showed in the m/z191 fragmentogram higher C_{23} tricyclic terpane than C_{30} hopane (Figure 63). In contrast, Woodford oils and rocks showed a common distribution of terpane biomarkers, with an abundance of hopane and homohopane biomarkers. This abundance is clearly reflected in the ratio of $C_{23}TT/Hop$ shown in Table 21, with Mississippian end-member ranging from 0.75 to 1.01, suggesting that in some samples C_{23}, tricyclic terpane levels are higher than C_{30} hopane (Figure 63), and the Woodford end-member $C_{23}TT/Hop$ ratio ranged from 0.32 to 0.47 (Table 21). Moreover, 17α-diahopane biomarker was observed in Mississippian rock and oils in notable abundance, although unnoticeable in Woodford Shale oil and rock extracts. Such a biomarker is believed to form as a diagenetic version of C_{30} hopane in the presence of clay-catalysis, together with well-oxygenated (oxic to suboxic) water column (Moldowan et al., 1991). Such a biomarker signature coincides with sedimentological features observed in the studied Mississippian rock from LNK core, such as Facies 3, which is interpreted to be more oxygenated with millimeter-scale horizontal burrows and skeletal grains. The relative increase of 17α-diahopane is captured by the ratio of diahopane to the sum of diahopane and C_{30} hopane, with Mississippian samples averaging 0.14, and Woodford, 0.06 (Table 21). Homohopane index (HHI) values appear to be slightly higher in Mississippian samples, ranging from 0.09 to 0.16, while Woodford's range from 0.01 to 0.10. Such variation is due to the lower hopane found in Mississippian samples rather than the dominance of C_{35} homohopane. Overall, homohopanes are dominant in Woodford bitumen and oils, which.
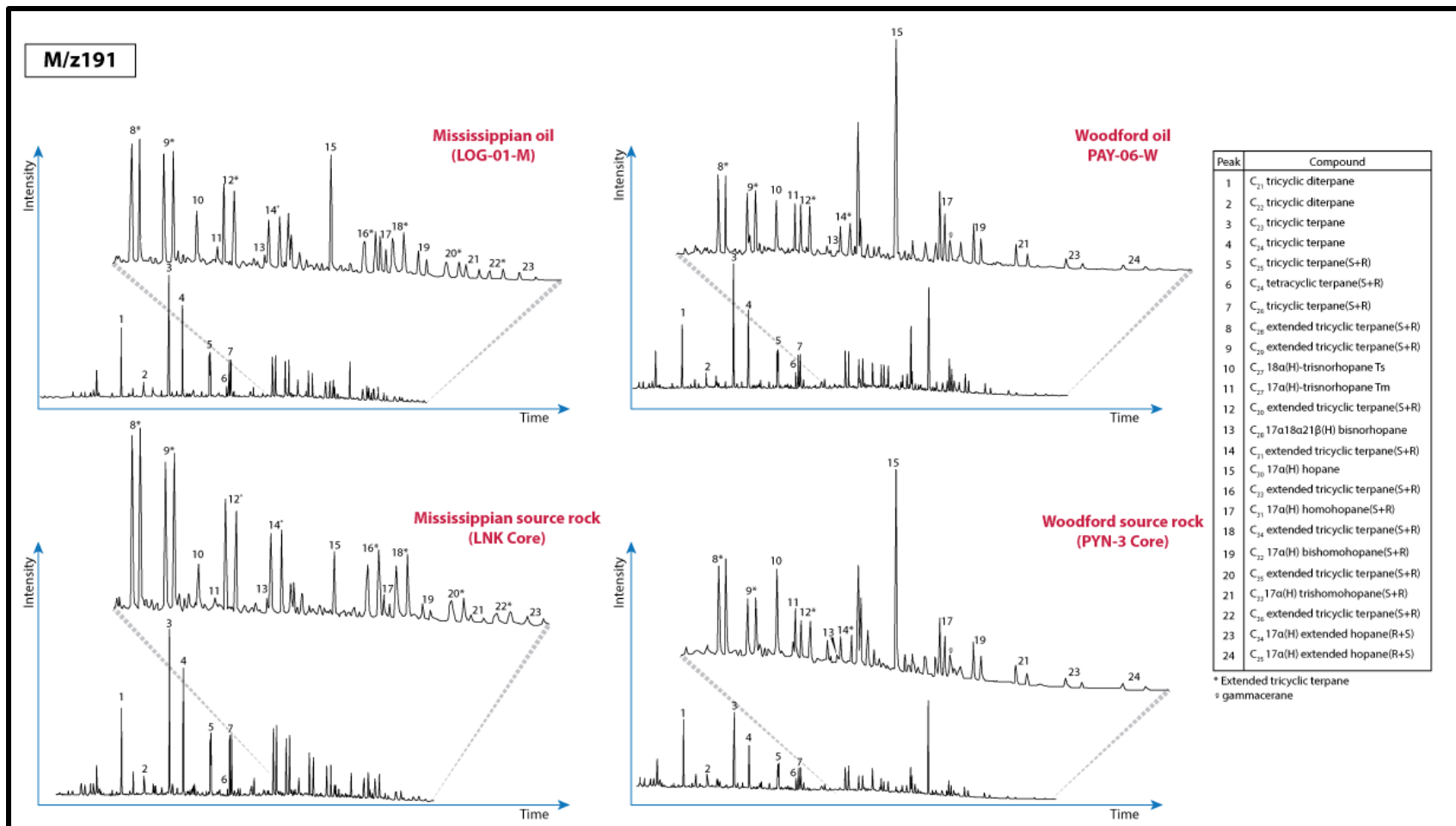
Figure 63: Mass chromatogram (*m/z* 191) of saturated hydrocarbons comparing end-members of Woodford Shale oil (Pay-05-M) and rock sample (PYN-3 Core) with Mississippian oil (Log-01-M) and rock (LNG Core). * indicates extended tricyclic terpanes.

suggest that prokaryotic organisms such as bacteriohopanetetrol largely contributed to the organic matter in the Woodford samples.

In the sterane biomarkers class, both Mississippian and Woodford end-members showed unique biomarker characteristics in pregnanes, diasteranes, and regular-steranes. Figure 64 shows the classic stack-fragmentogram of steranes ranging from C_{26} and C_{30}, with compounds and nomenclature listed in Table 21. Short-chain steranes (pregnanes) are higher in Mississippian samples, with higher C_{22} pregnanes, and this difference is also reflected in the pregnanes–regular steranes ratio, which ranges in Mississippian samples from 0.21 to 0.10, notably higher in extracted bitumen, whereas Woodford samples range from 0.10 to 0.01(Table 21). Overlap is observed in the diasterane distribution in Mississippian and Woodford samples, with an abundance of $\beta\alpha$ 20S C_{27} diasterane over $\beta\alpha$ 20S C_{29}. Moreover, in both end-members, crude-oil diasteranes are more abundant than that of diasteranes in rock extracts (Figure 64, 65). Variance of the two diasteranes isomers $\beta\alpha$ 20S and $\beta\alpha$ 20R ranging from C_{26} to C_{29} are also higher in crude oils, which decrease at C_{30} diasteranes. However, in Mississippian and Woodford rock extracts, the $\beta\alpha$ 20S and $\beta\alpha$ 20R diasterane isomers showed little variance. Since diasteranes can be sensitive to source-rock lithology, particularly in the presence of clay, in both examined source rocks, clays are present in the organic-rich Mississippian carbonate and in the Woodford Shale (Figure 64, 65). Regular steranes including cholestane (C_{27} sterane), ergostane (C_{28} sterane) and stigmastane (C_{29} sterane) can be used to distinguish Mississippian versus Woodford source-oils, with some difficulties with overlap due to mixing. Mississippian rock extracts and crude oils in general exhibit enrichment in cholestane relative to ergostane and stigmastane, while Woodford rock extracts and crude oils exhibit enrichment in stigmastane relative to cholestane and ergostane (Al Atwah et al., 2019). This distribution in regular sterane can be captured through the ratio of C_{27}/C_{29} ($\alpha\beta\beta$ S20), with

Table 22 Key biomarker ratios of terpane and sterane biomarkers for source rock to oil correlation

Biomarker ratio	Mississippian End-Member					Woodford End-Member				
	Rock-Extracts		Oil Samples			Rock-Extracts		Oil Samples		
	LNK-Core[m]	LNK-Core[n]	Log-01-M	Kin-02-M	Pay-04-M	LNK-Core[o]	LNK-Core[p]	Alf-01-M	Woo-01-M	Pay-07-W
$(C_{21}+C_{22})/(C_{27}+C_{28}+C_{29})$ [a]	0.21	0.15	0.11	0.14	0.10	0.08	0.01	0.09	0.09	0.10
C_{27}/C_{29} (abbS)[b]	0.76	0.81	0.74	0.85	0.90	0.33	0.40	0.38	0.30	0.31
C_{27}/C_{29} (abbS)[c] (218)	0.54	0.64	0.60	0.48	048	0.51	0.47	0.58	0.50	0.49
Gammacerane/Hopane [d]	0.02	0.12	0.12	0.13	0.15	0.07	0.17	0.07	0.06	0.18
C_{29}/C_{30} Hopane e	0.67	0.87	0.77	0.64	0.69	0.48	0.52	0.55	0.60	0.54
C_{24} Tetracyclic/C_{26} Tricyclics [f]	0.14\	0.11	0.15	0.11	0.13	0.33	0.57	0.39	0.45	0.19
Homohopane index (HHI)[g]	0.09	0.18	0.13	0.12	0.16	0.03	0.08	0.01	0.09	0.10
Diahopane/(Diahopane+Hopane)	0.13	0.14	0.13	0.14	0.18	0.07	0.06	0.06	0.04	0.09
C_{24}Tetra/C_{23}TT[h]	0.11	0.14	0.11	0.16	0.10	0.17	0.11	0.23	0.28	0.37
C_{24}TT/C_{23}TT[i]	0.76	0.78	0.78	0.78	0.87	0.67	0.55	0.70	0.66	0.77
Hop31R/HopC$_{30}$[j]	0.27	0.22	0.27	0.26	0.19	0.29	0.38	0.35	0.37	0.31
C_{23}TT/Hop[k]	0.75	0.68	0.68	0.74	1.01	0.32	0.44	0.45	0.35	0.47
ETT/HH[l]	8.2	6.8	4.25	3.62	2.60	0.11	0.65	0.14	0.31	0.22

a: sum of C_{21} and C_{22} sterane over sum of C_{27} αα 20R, C_{28} αα 20R and C_{27} αα 20R C_{29} steranes ; b: C_{27} αα 20R cholestane over C_{29} αα 20R stigmastane; c: C_{27} ββ20R+S cholestane over C_{27} ββ 20R+S stigmastane .c: gammacerane over C_{30} 17α hopane; C_{29} 17α 21β – norhopane over C_{30} 17α hopane; f: C_{24}tetracyclic terpane over C_{26} tricyclic terpane; g : C_{35} (22 S+R) homohopane over sum of $C_{31 to 35}$ (22 S+R) homohopanes; h: C_{24} tetracyclic terpane over C_{23} tricyclic terpane; i: C_{24} tricyclic terpane over C_{23} tricyclic terpane; j: C_{31} 22R homohopane over C_{30} 17α hopane; k: C_{23} tricyclic terpane over C_{30} 17α hopane ; l: sum of extended tricyclic terpanes $C_{28 to 45}$

Figure 64: GC-MS/MS MRM mass fragmentogram of Mississippian (Log-01-M) and Woodford (Alf-01-M) crude oils for a series of sterane biomarkers ranging from C_{26} to C_{30}; refer to Table 22 for peak number and associated compounds list.
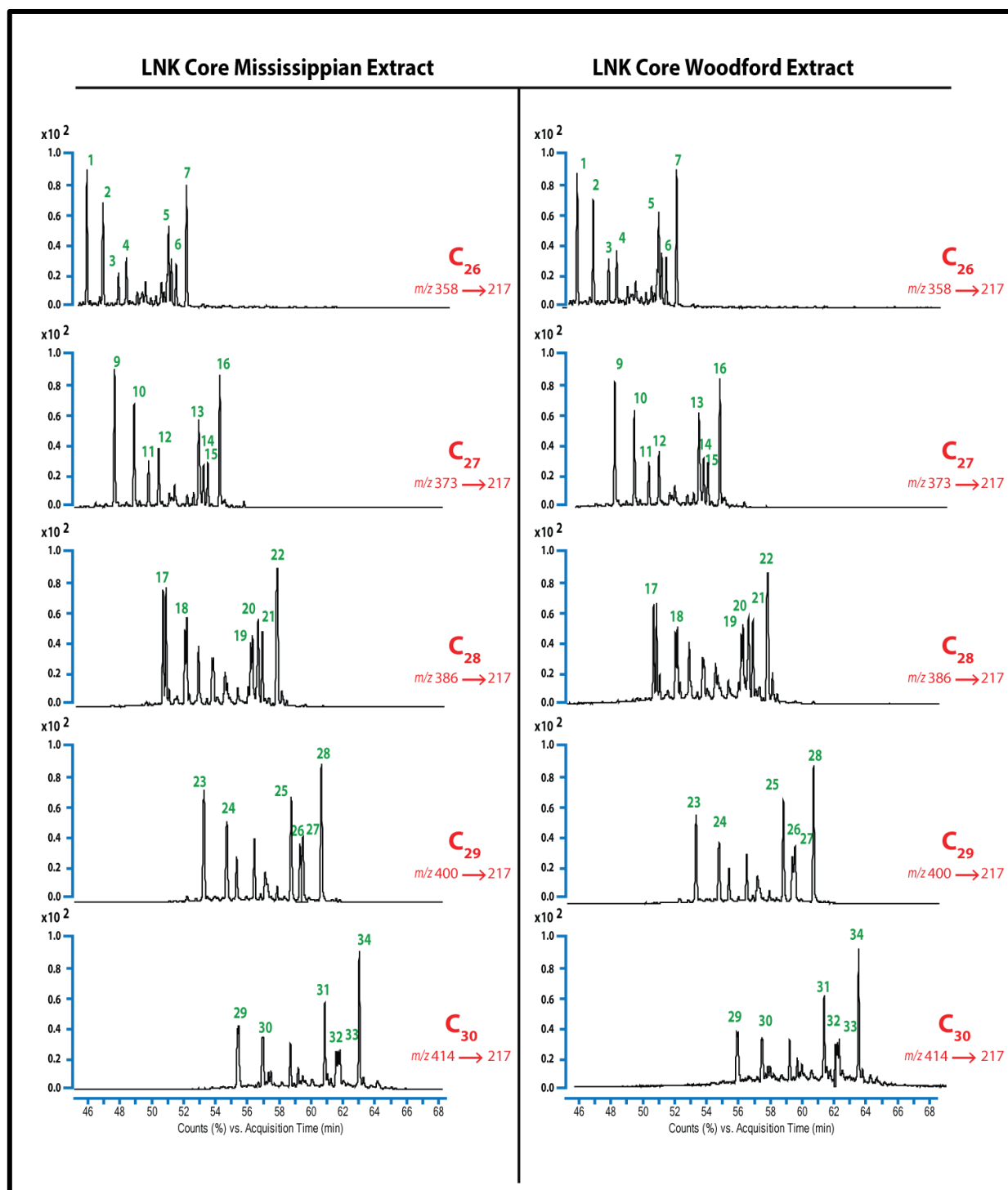
Figure 65: GC-MS/MS MRM mass fragmentogram of Mississippian (Log-01-M) and Woodford (Alf-01-M) extracted bitumen for a series of sterane biomarkers ranging C_{26} to C_{30}., refer to Table 22 for peak number and associated compounds list.

Table 23 Sterane biomarkers list of labeled peaks in figures 64 and 65.

Peak No	Compounds	Diagnostic transition
1	**C$_{26}$** 13β 17α -24 -20S Diasterane	
2	**C$_{26}$** 13β 17α -24 -20R Diasterane	
3	**C$_{26}$** 13β 17α -27 -20S Diasterane	
4	**C$_{26}$** 13β 17α -27-20R Diasterane	*m/z* 358→217
5	**C$_{26}$** ααα -24-nor-20S Sterane	
6	**C$_{26}$** αββ-24-nor-20R Sterane	
7	**C$_{26}$** αββ -24-nor-20S Sterane	
9	**C$_{27}$** 13β 17α 20S Diacholestane	
10	**C$_{27}$** 13β 17α 20R Diacholestane	
11	**C$_{27}$** 13α 17β 20S Diacholestane	
12	**C$_{27}$** 13α 17β 20R Diacholestane	*m/z* 373→217
13	**C$_{27}$** ααα 20S Cholestane	
14	**C$_{27}$** αββ 20R Cholestane	
15	**C$_{27}$** αββ 20S Cholestane	
16	**C$_{27}$** ααα 20R Cholestane	
17	**C$_{28}$** 13β 17α dia 20S (24S+24R)	
18	**C$_{28}$** 13β 17α dia 20R (24S+24R)	
19	**C$_{28}$** ααα 20S Ergostane	
20	**C$_{28}$** αββ 20R Ergostane	*m/z* 386→217
21	**C$_{28}$** αββ 20S Ergostane	
22	**C$_{28}$** ααα 20R Ergostane	
22	**C$_{28}$** 21-nor Ergostane	
23	**C$_{29}$** 13β 17α dia 20S	
24	**C$_{29}$** 13β 17α dia 20R	
25	**C$_{29}$** ααα 20S Stigmastane	
26	**C$_{29}$** αββ 20R Stigmastane	*m/z* 400→217
27	**C$_{29}$** αββ 20S Stigmastane	
28	**C$_{29}$** ααα 20R Stigmastane	
29	**C$_{30}$** 13β 17α 20S Diasterane	
30	**C$_{30}$** 13β 17α 20R Diasterane	
31	**C$_{30}$** ααα 20S Sterane	
32	**C$_{30}$** αββ 20R Sterane	*m/z* 414→217
33	**C$_{30}$** αββ 20S Sterane	
34	**C$_{30}$** ααα 20R Sterane	

Mississippian samples ranging from 0.74 to 0.80, while Woodford samples range from 0.30 to 0.40 (Table 21). The sterane ratios observed is not consistent as fingerprint to differentiate between Mississippian and Woodford sourced fluids. Unlike terpane biomarkers, steranes ratios of Mississippian samples overlapped with Woodford Shale samples. Overall, extended tricyclic terpanes appear the most diagnostic biomarker for identifying Mississippian sourced fluids, while the Woodford end-member samples lacked these biomarkers. The sterane overlap signature between the Mississippian and Woodford is likely related to a similar marin eukaryotic organic matter input .

Another set of unconventional homologous series of cholestane biomarkers was examined in Mississippian and Woodford samples (Figure 66, 67). Alkylation of those steranes occur at 3-postion, detected using GC-MSMS with a diagnostic precursor to product transitions. The 3β alkyl stigmastanes exhibit an alkyl group ranging from C1 (3β-methylstigmastane) to C7 (3β-heptylstigmastane). The origin of the 3-alkylsteroid biomarkers remains unclear; such compounds have not been observed to be directly biosynthesized in present-day organisms, but alkylsteroid is suggested to originate from the addition of a methyl group to Δ^2-sterene by microbial modification during early diagenetic interaction between sediments and organic matter (Summons and Capon, 1991). Despite the underutilization of the alkylated steranes in petroleum geochemistry applications, Dhal et al. (1994) showed the great potential of these biomarkers and documented their systematic correlation between rock extracts and related oils, ranging in age from Middle Cambrian to Tertiary—in particular, the ratio of 3β-n-pentyl steranes to 3β-isopentyl steranes together with their triaromatic counterparts including 3β-n-pentyl triaromatic steroids to 3β-isopentyl triaromatic steroids (Dahl et al., 1995). Distribution of alkyl stigmastanes was observed to vary across Mississippian and Woodford crude oils. Woodford crude oil, such as sample Pay-

07-W produced from the Woodford interval, showed a unique distribution of the different alkyl stigmastane homologous series, with a predominance of 5α, 14 α, 17α 20R, over both of 5α, 14 α, 17α 20S and 5α, 14β, 17 β 20R+S. By contrast, the majority of the Mississippian oils exhibit alkyl stigmastanes with the isomer 5α, 14β, 17 β 20R higher than the other alkyl stigmastane counterparts (Figure 66). Distribution of those isomers also changed with an increase in the alkyl group carbon number: for example, the 5α, 14β, 17 β 20R+S isomers decreased in abundance in Mississippian crude oil with increasing the alkyl group from 3β-methylstigmastanes to the 3β-pentylstigmastanes (Figure 66). Woodford crude oils, however, showed an inverse distribution to that of Mississippian oils; that is, with increasing alkyl side chain from3β-methylstigmastanes to the 3β-pentylstigmastanes, both the 5α, 14β, and 17 β 20R+S increased relative to 5α, 14 α, 17α 20S+R (Figure 66). Rock extracts were unique in their distribution of the alkyl stigmastanes, with Mississippian bitumen showing prevalence of 5α, 14 α, 17α 20R in the lower alkyl stigmastanes, particularly in 3β-methylstigmastanes, 3β-ethylstigmastanes, 3β-propylstigmastanes and 3β-butylstigmastanes, while 3β-pentylstigmastanes exhibited an abundance of 5α, 14β, 17 β 20R+S isomers over 5α, 14 α, 17α 20R+S counterparts (Figure 67). Woodford bitumen, on the other hand, showed an approximately equal abundance of 5α, 14 α, 17α 20R and 5α, 14 α, 17α 20S isomers in 3β-methylstigmastanes, 3β-ethylstigmastanes, 3β-propylstigmastanes, and 3β-butylstigmastanes, while 3β-pentylstigmastanes showing an abundance of the 5α, 14β, 17 β 20R+S. In all of the samples, the 5α, 14β, 17 β 20R+S isomer seems to be the predominant isomer, especially in 3β-pentylstigmastanes. The reported difference in the alkyl-stigmastanes could result from maturity differences, with certain isomers favoring certain thermal regimes. Moreover, according to Dhal et al. (1995), thermal maturity can greatly affect the 3β-n-pentyl steranes to 3β-isopentyl steranes ratio. More specifically, the absolute concentration of 3β-pentyl sterane decreased with increasing

oil maturity, which led to the conclusion of limited utility of these compounds for oil–source-rock correlation at high thermal maturity (Dahl et al., 1995). This result is expected, especially with the increased structural complexity of the alkyl-stigmastane, which increases the potential cleavage sites and thus the compound fragility induced by thermal stress. The use of 3-alkyl sterane as a biological marker is still at its early stages, in need of further investigation, but it can shed light on the sterol biosynthesis and its evolution (Summons and Capon, 1991). Despite the underutilization of the alkylated steranes in petroleum geochemistry application, Dhal et al (1994) showed the great potential of such biomarkers and their application oil to rock extracts correlation.

Overall, hopane and sterane biomarkers can be used to differentiate eukaryotic and prokaryotic organic-matter contribution. Mississippian samples are slightly higher in steranes and tricyclic terpanes, suggesting a more eukaryotic organic-matter input in the Mississippian carbonate. Despite the Woodford samples' content of steranes, hopane biomarkers are higher, suggesting a larger contribution of a prokaryotic source in the Woodford Shale. Additionally, tricyclic and tetracyclic diterpanes were observed in a trace amount in Mississippian rock extracts; however, none of those diterpanes were present in the Mississippian crude oils. Diterpanes are biomarkers of terrigenous origin, and since the Mississippian carbonates are of a marine ramp depositional setting, the presence of any terrigenous organic matter must be transported and is not autochthonous. Therefore, the terrigenous signature is minor, leaving a traceable fingerprint in the crude oil. Diterpanes are the only present terrigenous biomarker found in Mississippian rock extracts. None of the other biomarkers are observed, such as bicadinanes and oleananes.
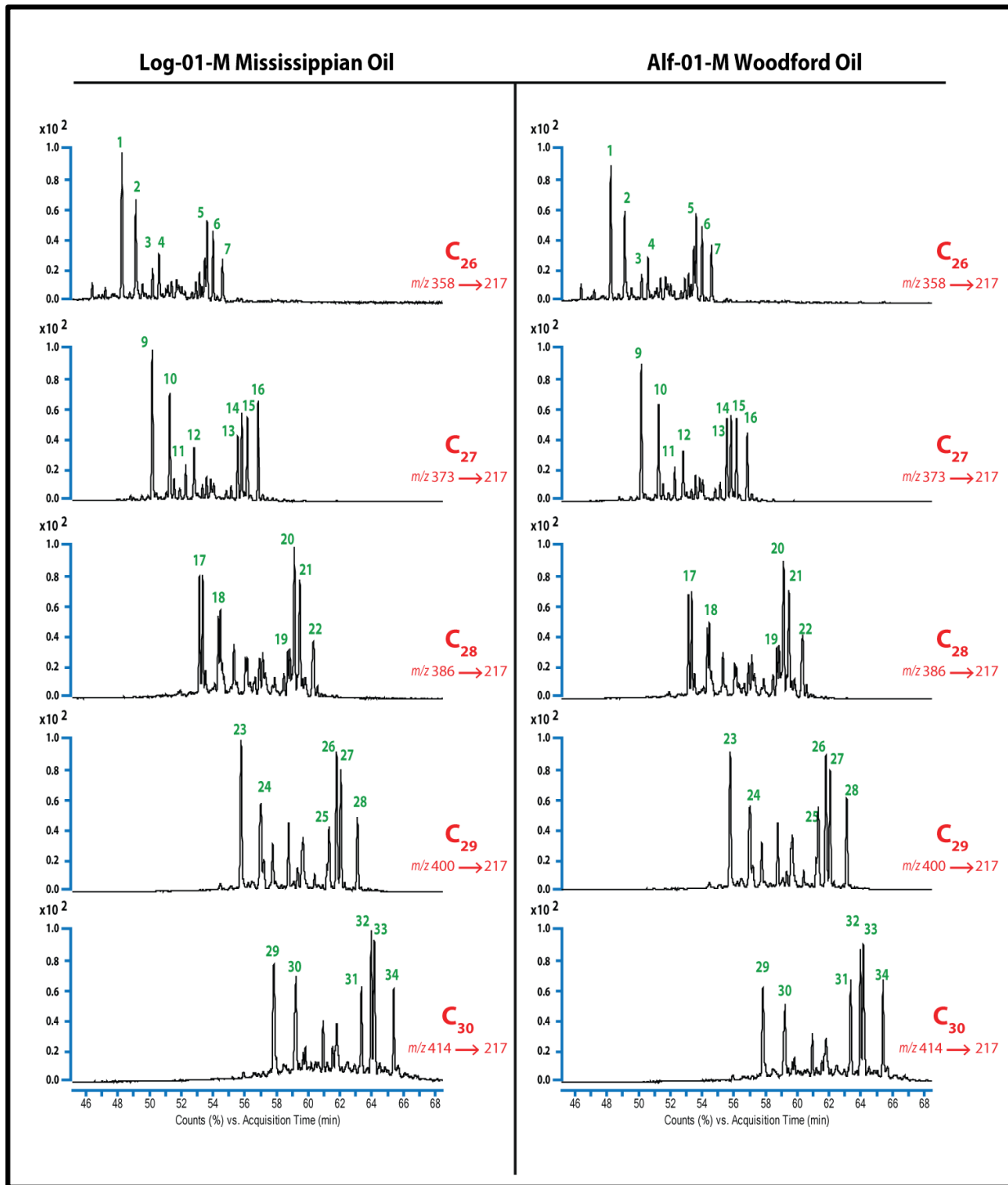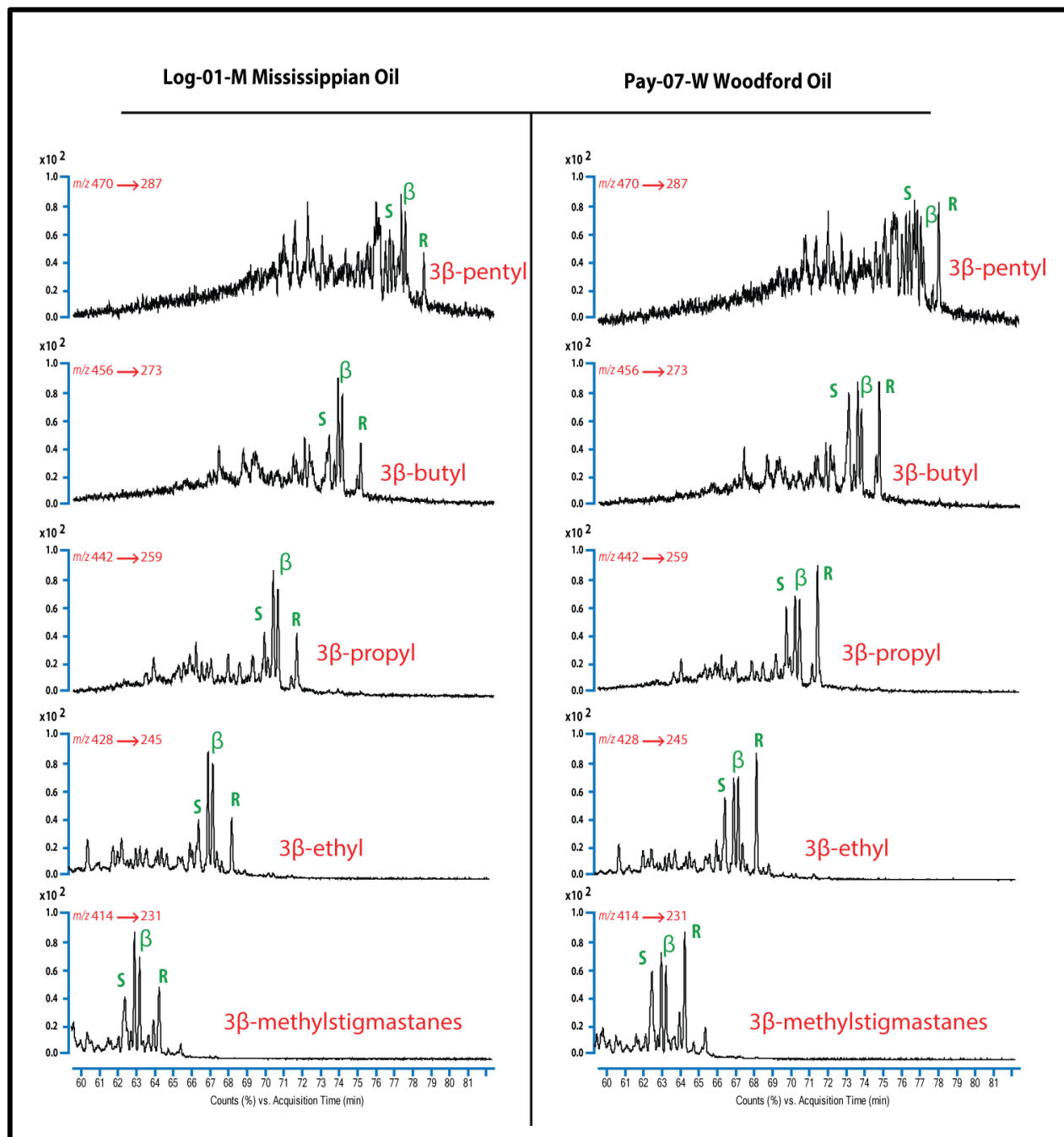
Figure 66: GC-MS/MS MRM mass fragmentogram of Mississippian (Log-01-M) and Woodford (Pay-07-W) crude oil for a series of 3-alkyl stigmastane biomarkers including 3β-methylstigmastanes (m/z 414→231), 3β-ethylstigmastanes (m/z 428→245), 3β-propylstigmastanes (m/z 442→259), 3β-butylstigmastanes (m/z 456→273) and 3β-pentylstigmastanes (m/z 470→287), peaks labeling: peak-S : of 5α, 14 α, 17α 20S, peak-R of 5α, 14 α, 17α 20R, peak- β: 5α, 14β, 17 β 20R and 5α, 14β, 17 β 20S.

200
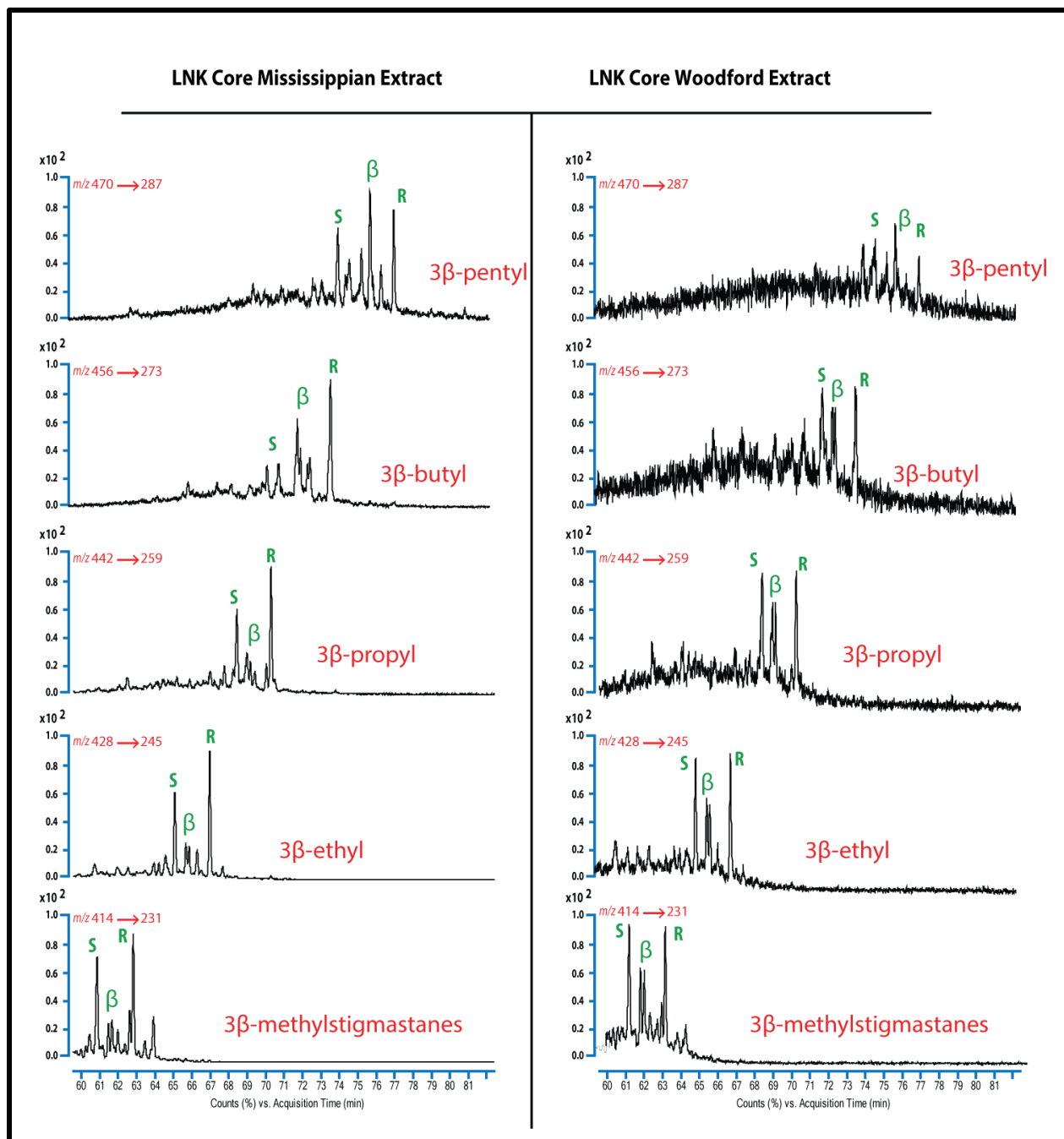
Figure 67: GC-MS/MS MRM mass fragmentogram of Mississippian and Woodford from LNK core extracted bitumen for a series of 3-alkyl stigmastane biomarkers including 3β-methylstigmastanes (m/z 414→231), 3β-ethylstigmastanes (m/z 428→245), 3β-propylstigmastanes (m/z 442→259), 3β-butylstigmastanes (m/z 456→273) and 3β-pentylstigmastanes (m/z 470→287). Peaks labelled as follows: peak-S of 5α, 14 α, 17α, 20S; peak-R of 5α, 14 α, 17α 20R; peak-β of 5α, 14β, 17 β 20R and 5α, 14β, 17 β 20S.

Based on biomarkers and compound-specific isotope compositions of crude oils and their relationship to rock extract, two petroleum systems can be defined. One is sourced by the Mississippian organic-rich carbonate, and the other by the Woodford Shale. Using these molecular and isotopic signatures, the 34 crude-oil samples were grouped into three major oil-families. Nine oil samples were fingerprinted and strongly represent the Mississippian end-member source rock (Family-1), while 8 samples showed a strong Woodford Shale fingerprint (Family-3), and the rest
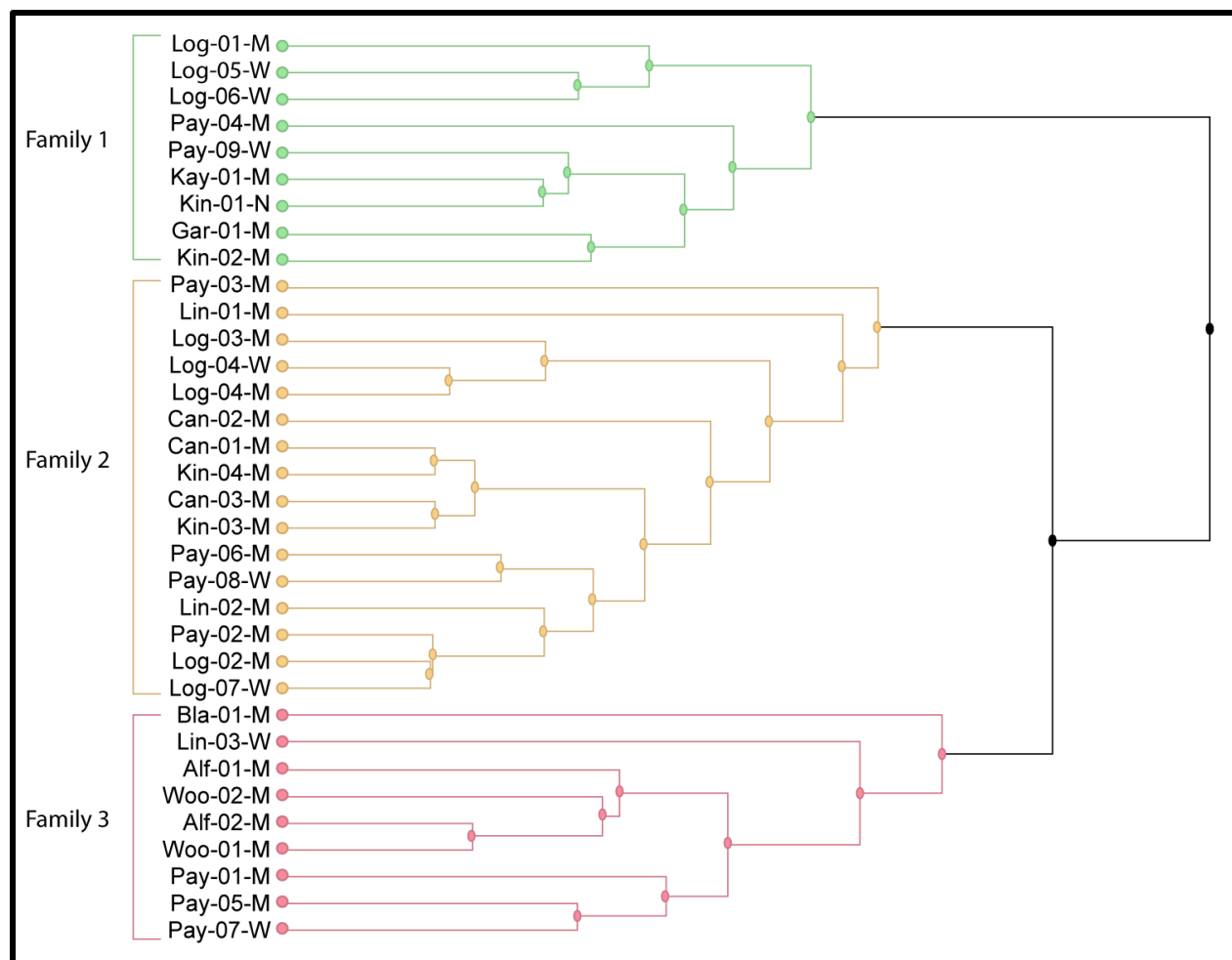
Figure 68: Dendrogram for a total of 34 crude-oil samples which are classified based on 35 geochemical parameters including biomarkers and isotopes into three oil families, Family-1 Mississippian sourced oils, Family 3 Woodford sourced oils and Family 2 potential mixture oils.

of the samples totaling at 17 crude oils showed biomarker signatures indicating possible mixtures of different degrees (Family-2). This classification was based on a total of 35 source parameters, including biomarker ratios and isotopic data, from which chemometrics was performed using Malcom Software by Schlumberger.

Figure 68 shows chemometric results of the hierarchal cluster analysis (HCA) with the grouping of the different oil families. The majority of the oil samples showed dual signatures, suggesting contribution of both Mississippian and Woodford source rocks. The mixture Family-2 oils appears to be in general closer to the Woodford-sourced oils, relative to the Mississippian end-member, which could indicate that the mixture oils have received a higher contribution from the Woodford relative to the Mississippian source contribution.

Geochemically, Family-1 oils are characterized by enrichment of lower and extended tricyclic terpanes, ranging from C_{23} to C_{39}. Moreover, hopanes are relatively low, with particularly higher extended tricyclic terpanes than homohopanes. Diahopane biomarker was also observed to occur in higher abundance than the rest of the oil families. On the steranes' biomarker class, Family-1 exhibited a slight shift towards ααα 20R cholestane relative to the rest of the regular sterane biomarkers. Diasteranes were overall higher than their regular sterane counterparts, with a slight enrichment of pregnanes/sterane ratios. Additionally, steranes were higher than hopanes in Family-1 oils, which suggests that eukaryotic organic-matter contribution is higher in Mississippian kerogen than in prokaryotic organic input. Isotopically, normal alkanes of Family-1 oils showed a relatively enriched δ13C signature ranging from −30 to −29. The Family-1 diamondoid fingerprint of dimethyldiamantane showed enrichment in 4,8-diemthyldiamantane relative to 4,9- and 3,4-dimethyldiamantane (Figure 59). Lastly, lighter hydrocarbons of C_7 compounds were higher in 2,3-dimethylpentane and 3-ehtylpentane relative to heptane isomers.

203

The, most noticeable biomarker signature of the Woodford end-member oils of Family-3 is the dominance of hopane in the terpane biomarker class. Hopanes and homohopanes were higher than extended tricyclic terapens, with extended tricyclic terpanes present up to C_{34}. Only trace amounts of diahopane were observed in the Family-3 oils. Moreover, steranes distribution featured an abundance of ααα 20R stigmastane relative to the rest of the regular steranes, and diasteranes were lower than their regular isomers. Overall, hopanes were higher in abundance in the sterane biomarkers, suggesting a higher input of prokaryote relative to eukaryote organic matter. Isotopically, normal alkanes showed a slightly more negative δ13C composition, ranging from −32 to −34. Diamondoids distribution of dimethyldiamantanes exhibits higher concentration of 3,4-dimethyldimantane relative to 4,9- and 4,8-dimethyldiamantane. In Family-3, some of the gasoline range hydrocarbons differed from the rest of the oil samples, with higher 3,3-dimethylpentane and 3-ethylpentane, relative to the rest of heptane isomers.

Family-2 oils have the most variable geochemical composition of biomarkers. Overall, Family-2 has a medium biomarker ratio of the discussed biomarkers for Family-1 and Family-3. For example, the presence of an enriched hopane signature together with the presence of extended tricyclic terpanes up to C_{38}. However, not all of the geochemical signature showed a systematic variation; that is, some favored a Woodford signature, whereas other showed a Mississippian contribution. Most notable is the isotopic signature, with the majority of this oil family showing a similar signature to Family-3, with a more negative δ13C composition of normal alkanes ranging from −32 to −34. In contrast, the C_7 star diagrams suggests a more Mississippian fingerprint, with high 2,3-dimethylpentane and 3-ethylpentane relative to rest of heptane isomers.

Sammon mapping classification was performed for the generated compositional data for the oil samples. Sammon mapping is a non-linear algorithm used primarily for multi-dimensional scaling for data analytics. This algorithm is used to reduce data variables into a representative two-dimensional map that still captures variations in each crude-oil sample. In our examined crude oils, 35 biomarker and isotopic data were reduced to a representative Sammon map. Figure 69 shows the crude oils Sammon map, with family marked according to hierarchical cluster analysis (HCA). The Sammon map confirms classification done by HCA, with two major end-members of Family-1 and Family-3, while oils falling in between can be grouped into Family-2. Unlike Family-1 and
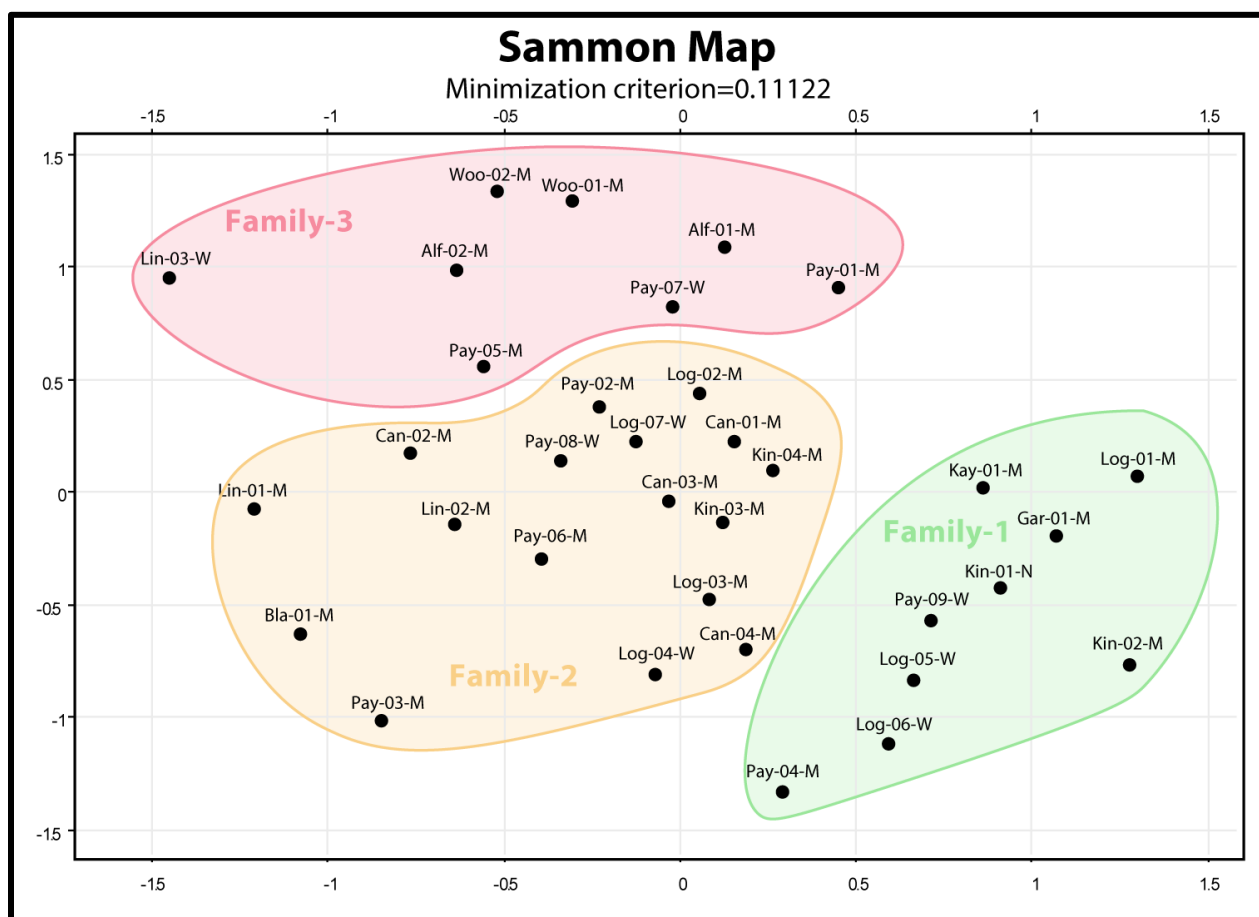
Figure 69: Sammon map for a total of 34 crude-oil samples which are classified based on 35 geochemical parameters including biomarkers and isotopes into three oil families, Family-1 Mississippian sourced oils, Family 3 Woodford sourced oils and Family 2 potential mixture oils.

Family-3, Family-2 oils show the most variation plotting in between Family-1 and Family-3, supporting the interpretation that Family-2 oils are a result of mixing between the two end-members with different proportions. While Sammon mapping is not a common approach in petroleum geochemistry studies, the agreement between the HCA and Sammon map suggests that this technique is a quick approach to reduce complex.

The spatial distribution of the oil families across the sampled geological provinces in Oklahoma (the Nemaha-uplift, Anadarko-Shelf and the Cherokee-platform) is shown in Figure 70. Mississippian sourced crude oils are observed to occur in Central-Oklahoma with highest occurrence at the eastern part of Logan and western of Payne Counties (Figure 70). Additionally,
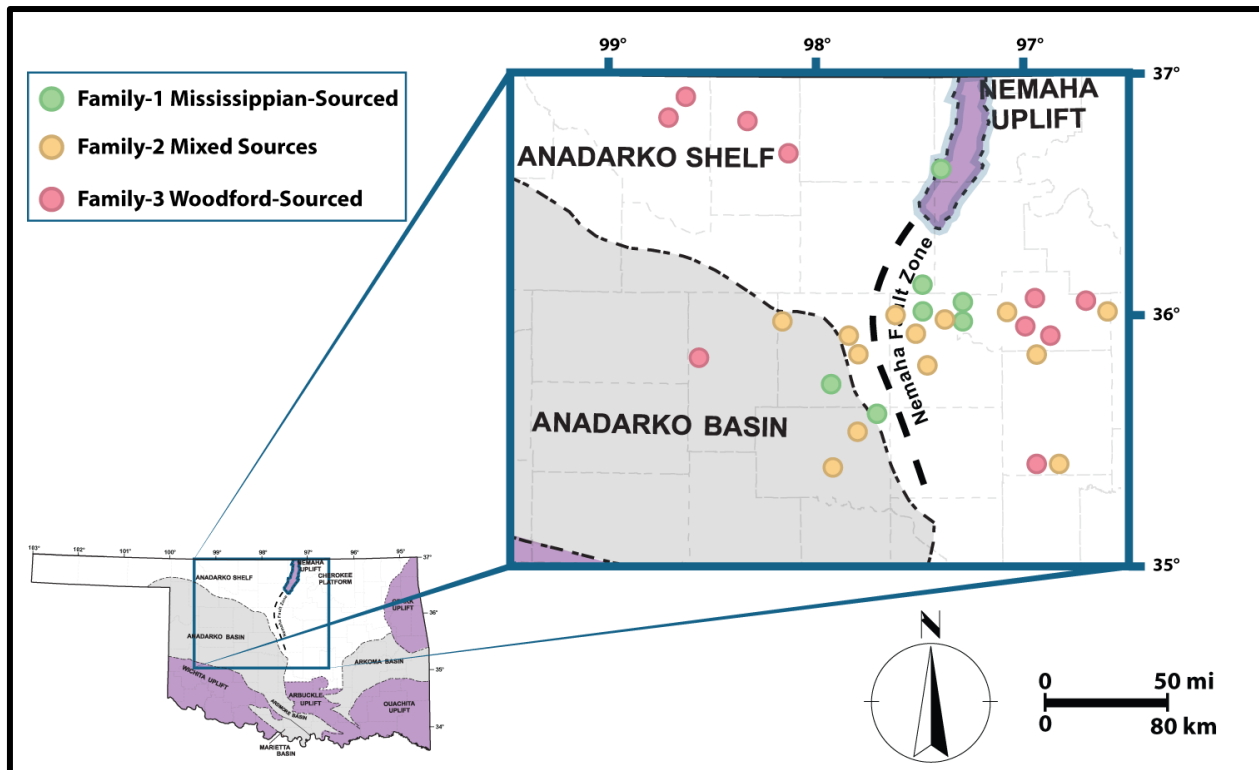
Figure 70: Map showing the oil families distribution across the central Oklahoma and the Anadarko Shelf and Sooner Trend Anadarko Basin Canadian and Kingfisher Counties (STACK) play provinces. Note the occurrence of Mississippian-sourced oils (Family-1) and mixed oils (Family-2) in close proximity to the Nemaha Uplift, while only Woodford-sourced oils are further away from the Nemaha Uplift.

206

two of the oils produced from the STACK Play showed a Mississippian end-member signature (i.e., Kin- 02-M and Kin-01-N). Uncommonly is the sample Kay-01-M the furthest to the North within the Nemaha-uplift province, showing a strong Mississippian signature. Family-2 is the largest in terms of oil samples co-existing close to Mississippian end-member oils, with the majority of Family-2 oils located east of the Nemaha-Uplift in Central-Oklahoma over Logan, Payne, and Lincoln counties and five oil samples within the STACK Play province. Overall, Family-2 mixed sourced crude-oils appear to be in close approximation to the Nemaha-uplift fault system suggesting that Nemaha-uplift faults might have some control over the degree of mixing between Mississippian and Woodford petroleum source rocks. It's important to note that the likelihood of petroleum mixing of these fluids could increase as some of these wells are stimulated by hydraulic fracturing. Family-3 which are Woodford sourced oil becomes more prominent as we move away from the Nemaha-uplift province to the west at Woods, Alfalfa and Blaine counties and in some areas of Payne and Lincoln counties to the east.

Spatial distribution of thermal maturity of crude oil was assessed using around 10 maturity-based ratios of the saturate and aromatic hydrocarbons. Then an average of a VRE was calculated using the relationship published in the literature, noting the concentration of diamondoids (Peters et al., 2005b). This approach is unique in that it evaluates thermal maturity of the C_{15+} hydrocarbons by examining biomarker-based ratio of saturate and aromatic fractions while indicating the presence of diamondoids as a proxy for the contribution of cracked hydrocarbons, which can normally be overlooked using the conventional biomarkers (Moldowan et al., 2015). Figure 71 shows the distribution of oils, color-coded by their average VRE value and by whether they contain a high concentration of diamondoids. Overall, oils within the STACK play are notably higher, with values ranging from 1.01 to 1.51%VRE with a high abundance of diamondoid

concentration, with 4- and 3-methyldiamantanes ranging from 3.2 to 18.9 ppm and with an average of 11.4 ppm. Such elevated thermal maturities and relatively high diamondoids presence suggest that these oils are a mixture of cracked and non-cracked hydrocarbons. Similarly, oils within the Anadarko Shelf were slightly lower in the vitrinite reflectance, ranging from 0.61 to 0.94%VRE, suggesting oils within early to peak oil-window, with the oils exhibiting an overall API gravity ranging from 21° to 36°. Given such gravities, it is tempting to suggest that these oils are low-to-middle maturity crudes, but diamondoid suggests that these oils are mixture of cracked and non-cracked hydrocarbons with 4- and 3-methyldiamantanes ranging from 6.9 to 13.7 ppm. In contrast, crude oils located in central Oklahoma and particularly east of the Nemaha Uplift showed a systematic decrease in thermal maturity, with 0.55–0.81%VRE along with trace amounts of
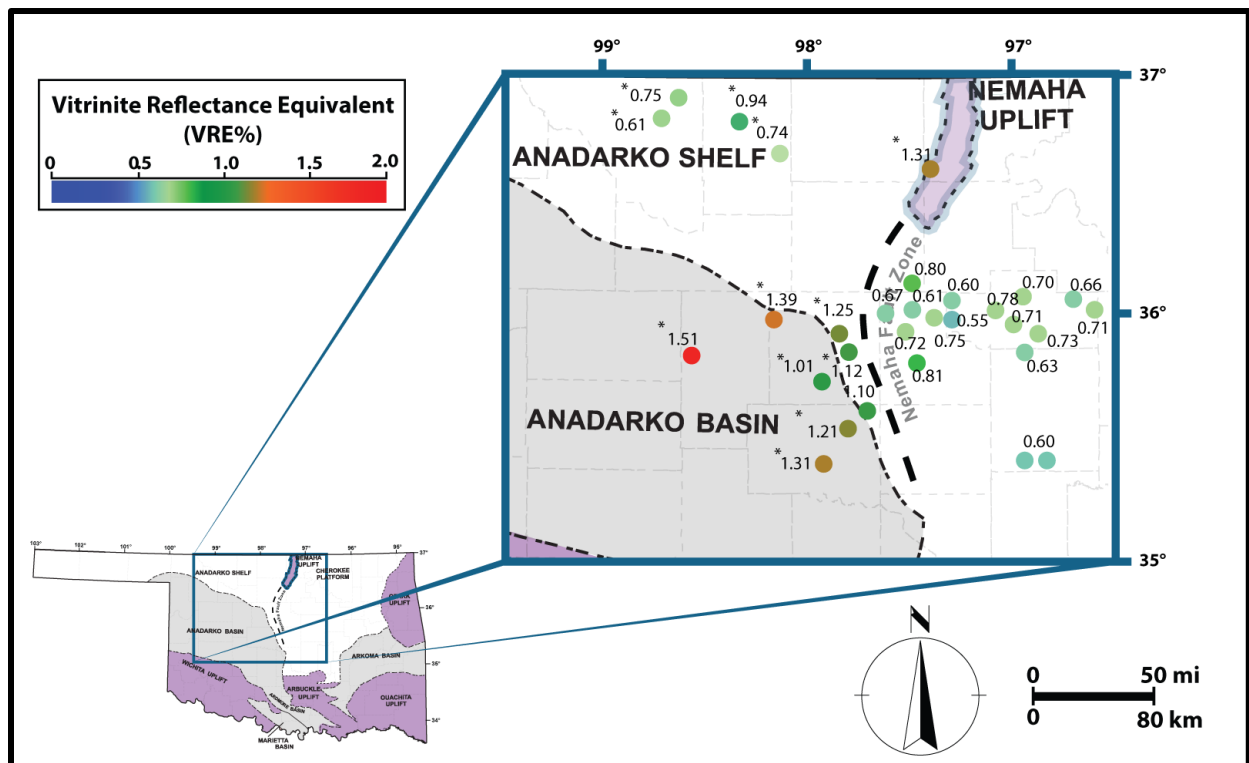
Figure 71: Map showing the oil vitrinite reflectance equivalent (VRE) values across the central Oklahoma and the Anadarko Shelf and Sooner Trend Anadarko Basin Canadian and Kingfisher Counties (STACK) play provinces. Oils marked with * indicate the presence of relatively high diamondoid concentrations.

208

diamondoids, with 4- and 3-methyldiamantanes ranging from 1.2 to 4.6 ppm and averaging at 2.6 ppm. Therefore, central-Oklahoma oils are mainly composed of non-cracked hydrocarbons, with maturity ranging from early to peak oil-window. Examined in detail, the central-Oklahoma Oils exhibit a maturity trend, particularly for oils in close proximity to the Nemaha Uplift, such as samples located in the western side of Logan County, with a maturity reaching up to 0.8% VRE. Interestingly, those oils are produced from relatively deeper depths than oils within Payne and Logan Counties. West Logan oils are recovered at depths ranging from 5500 to 5800 ft, while Mississippian formation is encountered at depths as shallow as 4300 ft in East Logan and Payne counties. This difference in depth could explain the slight increase in crude-oil maturity observed in Logan County, but another possibility is associated with elevated geothermal anomalies related to the Nemaha Uplift. Moreover, hydrothermal fluids associated with deep faults within the Nemaha Uplift have been suggested as a potential process causing Mississippian and Woodford kerogens to locally mature in areas where regional iso-reflectance vitrinite suggests otherwise (Cardott and Lambert, 1985; Higley, 2014a). This hypothesis was further confirmed through the isotope geochemistry of calcite-filled fractures within the Mississippian Limestone formation. Strontium isotopes ($^{87}Sr/^{86}Sr$) suggest that some calcite-filled fractures are associated with radiogenic fracture-filling calcite cements (Mohammadi et al., 2018). Hence, such geothermal activity could cause localized petroleum generation from organic-rich Mississippian and Woodford rocks. Therefore, the slightly elevated maturities of oils in Logan County is interpreted as related to local hydrothermal fluids. Such an interpretation can also be applied to oil sample Kay-01-M, which exhibits an unusually elevated maturity value of 1.31% VRE, whereas it is produced from a relatively shallow Mississippian Formation depth ranging from 3500–4000 ft. At such depths, iso-reflectance values are relatively low, ranging from 0.4 to 0.7% Ro, which cannot

explain the observed higher maturity of Kay-01-M oil (Cardott and Lambert, 1985). Therefore, the higher maturity of Kay-01-M oil (the furthest north sample within the Nemaha Uplift Province) can be explained by two possible mechanisms, both related to a high-temperature geothermal anomaly with varying causes: first, a high-temperature geothermal anomaly caused by hydrothermal fluids associated with the Nemaha Uplift deep faults, which resulted in localized thermal maturation of kerogens generating high-maturity oil. Second, the high-temperature geothermal anomaly can be caused by Precambrian basement anomaly, as observed from the total magnetic intensity map. The magnetic anomalies located west of the Nemaha Uplift within Kay County, which have been interpreted as related to the Mid-Continent rift system (Elebiju et al., 2011). Regardless of the cause of the high-temperature geothermal anomaly, it can cause the generation of high-maturity oils at shallower-than-expected depths. However, it is apparent that the Kay County geothermal anomaly is higher in magnitude than that of Logan County, resulting in the presence of higher diamondoid concentration in crude oil Kay-01-M.

CHAPTER VI

OIL-BEARING FLUID INCLUSIONS AND PETROLEUM-MIGRATION MILOMETERS

Introduction to Fluid Incisions

Conventional or unconventional reservoirs constitute the final product, and the most valuable accumulations of hydrocarbon in a petroleum system. An adequate understanding of the reservoir characteristics and evolution through geological time is crucial to further advance exploration and development efforts. After hydrocarbon is expelled from the source rock, it migrates in a liquid or gas state, leaving behind traces within the carrier beds on the scale of micro-sized interactions between rock minerals and hydrocarbon movement. Roedder Edwin, one of the early pioneers in the field of fluid inclusions, defines a fluid inclusion as "…small volumes of fluid trapped within a crystal during its growth from that fluid, or during subsequent healing of fractures in the presences of fluid" (Roedder, 2003). The micro-sized oil inclusions provide valuable evidence of paleo-oil composition. When carefully and meticulously handled and examined, hydrocarbon fluid inclusions can provide a better understanding of petroleum migration and accumulation. Specifically, biomarkers provide valuable insight into hydrocarbons inclusion composition in terms of organic-matter source, sedimentary depositional settings and level of thermal stress. All combined facilitate a better understanding of reservoir-filling history.

Fluid inclusion analysis can be divided into two main approaches, namely destructive and nondestructive methods. Firstly, nondestructive methods are those in which properties are measured without damaging the original fluid inclusion structure, including texture and pressure–volume–temperature (PVT) analysis. Texture examination is a petrographic observation of the

fluid inclusion patterns (Van den Kerkhof and Hein, 2001). Pressure-volume-temperature is the measurement of physical properties of the inclusions, such as freezing and melting points (Robert H. Goldstein, 1994). The second approach is the destructive method, in which the original inclusion is damaged, and entrapped fluids are released for bulk chemical composition analysis for analytes such as *n*-alkanes, biomarkers and isotopes (George et al., 2007). In this study, both approaches and associated data will be discussed, with more emphasis on the composition of oil-bearing fluid inclusions observed from Mississippian carbonates.

Fluid Inclusion Petrography and Microthermometry

Lithologies in the study area include argillaceous pelitic to siliceous mudstones, containing scattered fossils, and fine-grained, fossiliferous packstones and grainstones. Late diagenetic cement occurred as fracture-, vug- and breccia-filling (FBV) calcite.

Inclusions containing two phases (liquid and vapor) were observed in open-space-filling blocky calcite and quartz cement in Kingfisher, Payne, Canadian and Blaine Counties. Homogenization temperatures (Th) range from 48 to 148°C, and first melting (Tm) values range from −21.1 to 1.1°C (Table 23). Two-phase petroleum inclusions were identified only in calcite cement and were recognized by their light-blue- to cream-colored fluorescence under UV light (Figure 72). Sample CA-99336, located in Canadian County, exhibited the largest size fluid inclusions (Figure 72). Overall, measured homogenization temperatures vary dramatically for both aqueous and petroleum inclusions. The highest homogenization temperature values are observed in sample CA-99336, located in Canadian County, with a homogenization temperature of 148°C. Since the homogenization temperature of oil inclusions is highly affected by oil composition, in this study more emphasis is put on homogenization temperature of aqueous inclusions. As

212

indicated in Table 23, the highest homogenization temperature of aqueous inclusions is 148ºC from sample CA-1-99336 in Canadian County, followed by sample GS-9698 located at Blaine County, with average homogenization temperature of 105°C of primary and secondary aqueous inclusions. In contrast, fluid inclusion homogenization temperatures within Payne County were significantly lower than the rest of the samples listed in Table 23. The average homogenization temperature is 91ºC for aqueous inclusions in sample SMD-2216. A comparison of all homogenization temperatures in the samples listed in Table 23 makes apparent that the lowest Th values are reported in sample SMD-2216 in Payne County, which suggests milder thermal stress during fluid-inclusion entrapment there as compared with the other counties.

In the study area, the higher Th values indicate precipitation by hot basinal fluids during the later stages of diagenesis. Such fluids are observed in samples located west of the Nemaha Uplift, within Kingfisher, Canadian and Blaine Counties. In contrast, sample SMD-2216 in Payne County is characterized by lower Th and lower calculated fluid-inclusion salinities, as shown in Table 23, indicating an early diagenetic (marine and meteoric) cement stage, a significant porosity-reducing event in north-central Oklahoma.

Previous studies of Mississippian rocks in Oklahoma have reported the occurrence of fluid inclusions in the precipitated calcite (Mohammadi et al., 2017a; Mohammadi et al., 2017b). Those fluid inclusions were classified into two distinct end-member fluids based on salinity, including very saline fluids (above 12% wt. NaCl equivalent) and lower salinity fluids (below 5% wt. NaCl equivalent). The distribution of fluid inclusion geochemistry, along with carbon and oxygen isotope data for north-central Oklahoma indicate several fluid origins (Mohammadi et al., 2017a; Mohammadi et al., 2017b). These fluids include a lower salinity original fluid, which is likely comprised of Mississippian seawater and a mixture of seawater and fresh water. The original fluid

213

was displaced by high salinity hydrothermal fluids, which emanated from the lower stratigraphic section and moved upwards along faults and fractures during the late stages of diagenesis Mohammadi et al., 2018a)
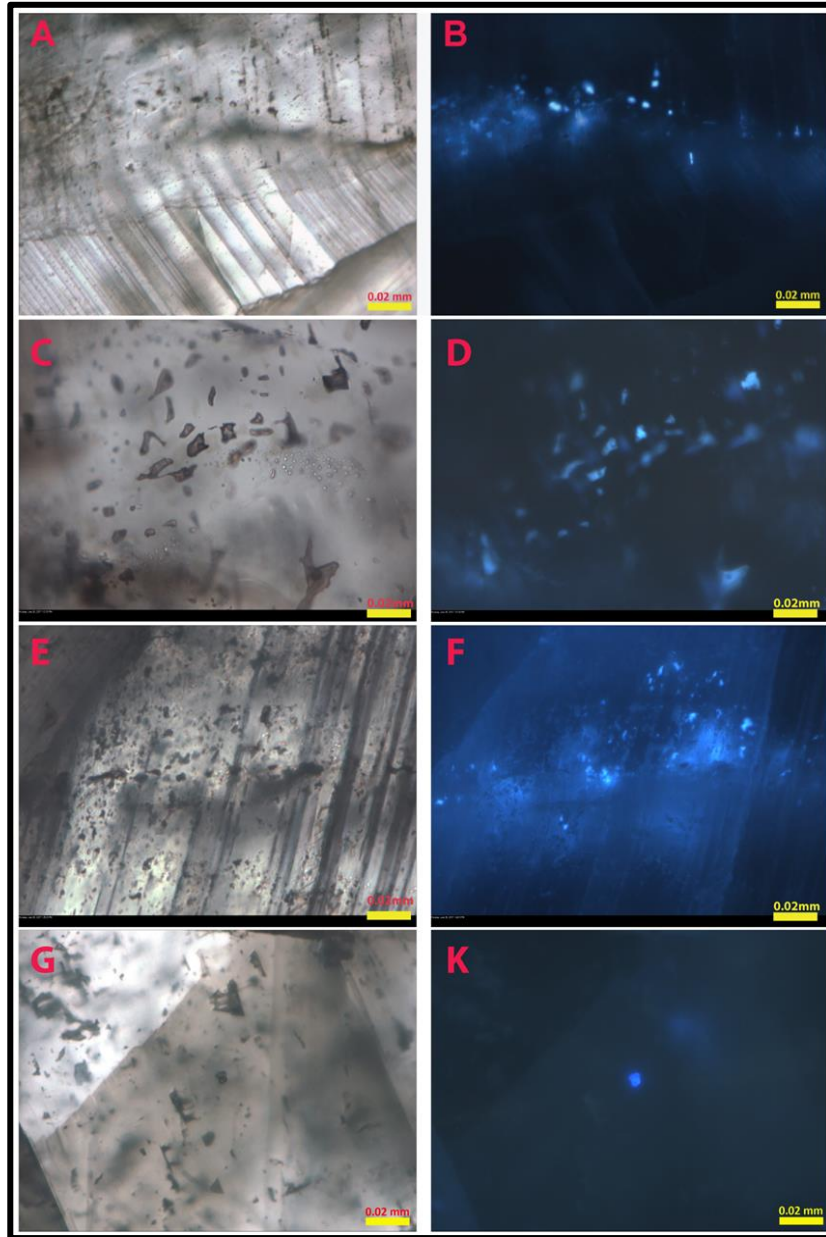
Figure 72: Photomicrographs of oil-bearing fluid inclusions in Mississippian rocks examined under transmitted plane light and blue fluorescence under ultraviolet (UV) light. (A, B) AM-8371 sample from Kingfisher County; (C, D) CA-99336 sample from Canadian County; (E, F) SMD-2216 sample from Payne County; (G, K) GS-9698 from Blaine County.

Table 24 Microthermometric data for fluid inclusions in carbonate cements. (Vertical = vertical fracture, Breccia = breccia fracture, Shear = shear zone, Solution = solution-enlarged fracture, Ptygmatic = ptygmatic fracture)(Mohammadi et al., 2018)

Sample ID	Location	Open space type	Asmbl[a]	Th (°C)[b]	Tm (°C)[c]	Calculated salinity (wt.% eq. NaCl)	Type
GS-9698	Blaine Co., OK (#2)	Breccia	1	87	-2.6	4.3	Primary Aqueous
			2	117			Primary Aqueous
					-2.5	4.2	
			3	110	-2.4	4.0	Secondary-petroleum
			4	106	-18.8	21.5	Secondary Aqueous
			5	115			
				115	-0.3	0.5	
				101			Secondary Aqueous
				101			
				101			
CA-1-99336-B	Canadian Co., OK	Vertical/shear	1	141			Primary Aqueous
			2	105	-1.1	1.9	Primary Aqueous
			3	48			
				48			
				48			
				48			
				48			Primary-petroleum
				48			
				48			
				48			
				48			
			4	111			Primary Aqueous
				111			
				148			
AM-8371	Kingfisher Co., OK	Ptygmatic	1	130	-2.5	4.2	Primary-petroleum

Table 23 continued.

Sample ID	Location	Open space type	Asmbl[a]	T_h (°C)[b]	T_m (°C)[c]	Calculated salinity (wt.% eq. NaCl)	Type
SMD-2216	Payne Co., OK (#2)	Vertical	1	80			Primary-petroleum
			2	74	-8.9	12.7	Primary Aqueous
			3	74	-21.1	23.2	Primary Aqueous
				78	-21.1	23.1	
			4	122	0.7		Primary Aqueous
				111	1.1		
			5	89	-2.1	3.5	Primary Aqueous

a: assemblage number, b: homogenization temperature; c: last ice-melting temperature

Oil-Inclusions Composition

Normal Alkanes and Acyclic Isoprenoids

Normal alkanes together with acyclic isoprenoids of oil inclusions varied among the four inclusion samples. The overall distribution of the *n*-alkane profile showed a bimodal distribution in oils from CA-1-99336 and GS-9698, maximizing at *n*-C_9 and *n*-C15 for sample GS-9698, and *n*-C_{15} together with *n*-C11 in sample CA-1-99336 (Figure 73). In contrast, both samples SMD-2216 and AM-8371 showed a unimodal distribution favoring long-chain hydrocarbons, with sample SMD-2216 maximizing at *n*-C_{20} and sample AM-8371 maximizing at *n*-C_{15}. Moreover, sample AM-8371 showed odd over even preference in carbon number, ranging from C_{15} to C_{21}. Even though the abundance of long-chain normal hydrocarbons is usually associated with terrigenous organic-matter input, the dominance of *n*-C_{20} is more related to evaporation loss than to organic-matter source, as is further supported by the pristane and phytane ratios of normal alkanes.
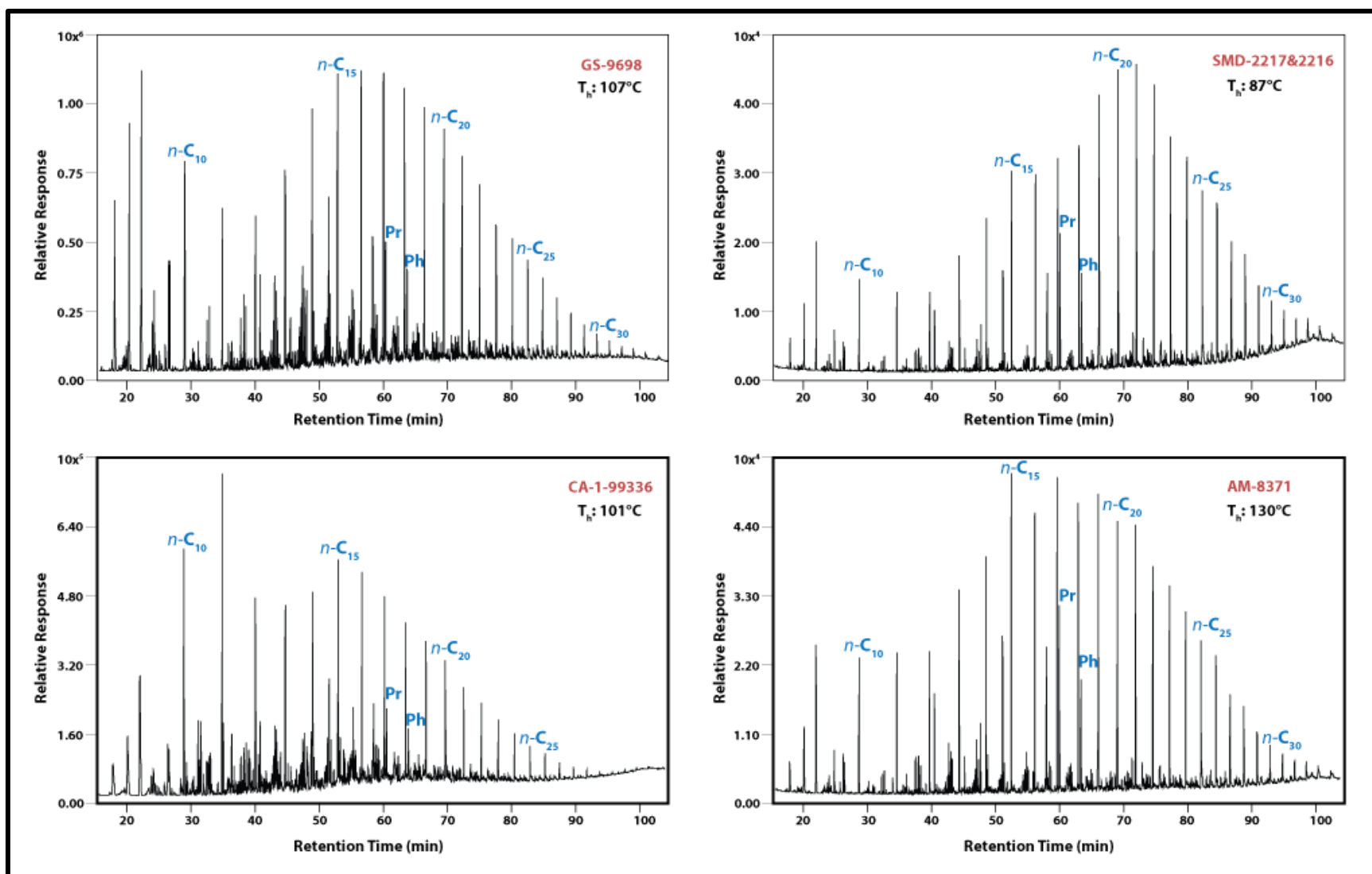
Figure 73: Partial *m/z* 85 mass chromatograms of oil inclusions depicting the distribution of normal alkanes. Pr: pristane, Ph: phytane.

The acyclic isoprenoid of the oil inclusions suggests that most of these oils originate from marine-derived kerogen deposited under relatively suboxic to anoxic redox condition. This finding is supported by pristane relative to n-C_{17} (Pr/nC17) together with n-C_{18} (Ph/nC18) relative to phytane, with sample GS-9698 showing a strong marine signature with Pr/nC17 at 0.57 and Ph/nC18 at 0.80. The rest of samples showed a potential mixed kerogen type contribution of Type II and Type III, with Pr/nC17 ranging from 0.58 to 0.93 and Ph/nC17 ranging from 0.39 to 0.65. Acyclic isoprenoids, particularly pristane and phytane, specificity is low for organic-matter type, as many sources can contribute to their presence. Hence, we examined detailed terpane and sterane biomarkers to delineate oil-inclusion relationship to produced crude oils.

Biomarkers

Biomarkers were observed in most of the samples except oil inclusions from Canadian County. Sample CA-1-99336 had a higher signal-to-noise ratio in most of the biomarker mass-chromatograms, while the rest of the samples had a reliable biomarker signal for interpretation. In general, terpane biomarkers of oil inclusions from both GS-9698 and AM-8371 samples were relatively similar, whereas SMD-2216 terpane biomarkers were unique. The samples GS-9698 and AM-8371 showed an abundance of hopane and homohopane biomarkers over the rest of terpane biomarkers observed from the m/z 191 mass fragmentogram (Figure 74). Moreover, both GS-9698 and AM-8371 samples exhibited relatively high C_{29} norhopane (Ts), with sample GS-9698 containing higher C_{29} norhopane (C29-Ts) than AM-8371. In the homohopane biomarkers, sample GS-9698 showed the steeper slope of decreasing homohopanes distribution with increasing carbon number, while sample AM-8371 exhibited a gently decreasing slope of homohopanes. Sample AM-8371 showed a unique abundance of the gammacerane biomarker, and only a trace amount is

218

observed from sample GS-9698. The distribution of tricyclic terpanes varied between GS-9698 and AM-8371 samples, with significantly higher C_{23} and C_{24} compared to C_{25} and C_{26} tricyclic terpanes in sample GS-9698, whereas sample AM-8371 had an almost equal abundance of these lower tricyclic terpane biomarkers. As to extended tricyclic terpanes, GS-9698 and AM-8371 oil inclusions showed trace amounts of extended tricyclic terpanes, reaching up to C_{31}. In contrast, sample SMD-2216 oil inclusions showed a unique terpane biomarker composition. Most notable is the dominance of tricyclic terpanes over hopane biomarkers, especially the increase in chromatogram complexity in the retention time range after the elution of hopane biomarker. Moreover, SMD-2216 exhibits higher C_{23} and C_{24} tricyclic terpanes over the rest of the homologous series (Figure 74). Unlike, GS-9698 and AM-8371, sample SMD-2216 contained a higher abundance of extended tricyclic terpanes reaching up to C_{36}, which elutes after the $C_{33}17\alpha$ (H) trishomohopanes. Compared to GS-9698 and AM-8371, sample SMD-2216 oil inclusions have lower C_{24} tetracyclic terpanes. In the hopane series, sample SMD-2216 exhibits higher C_{27} trisnorhopane (C_{27}-Ts) than C_{29} norhopane (C_{29}-Ts), whereas the inverse is observed in oil inclusions from GS-9698 and AM-8371, with higher C_{29} norhopane (C_{29}-Ts) than C_{27} trisnorhopane (C_{27}-Ts)

Sterane biomarkers and their rearranged counterpart showed a similar composition in samples GS-9698 and AM-8371, which coincide with similarities observed from the terpane biomarkers. Depicted in Figure 75 are stacked sterane mass fragmentogram for cholestanes, ergostanes, and stigmastanes. Overall, most of the oil inclusions showed a dominance of stigmastanes relative to the rest of the regular steranes. Oil inclusions from GS-9698 and AM-8371 exhibit an abundance of the stigmastane, while sample SMD-2216 had slightly higher cholestane. In all of the oil inclusions, diasteranes are higher than their regular sterane counterpart.

In all of the sample, regular sterane isomers with αββ 20S+R structural configuration prevailed compared to ααα 20S+R isomers, especially in ergostanes and stigmastanes. In contrast, isomers of C_{30} and C_{27} showed an equal abundance of both αββ 20S +R and ααα 20S+R. Moreover, oil inclusions from sample SMD-2216 exhibit the dominance of isomer ααα 20R relative to αββ 20S+R and ααα 20S, which is a unique distribution in the cholestane isomers of sample SMD-2216. In contrast, samples GS-9698 and AM-8371 showed higher αββ 20S+R isomers of the cholestane. Relative dominance of diasterane decrease at C_{30} steranes, with sample AM-8371 showing the least abundance C_{30} diasterane. Additionally, C_{30} regular steranes in GS-9698 and AM-8371 oil inclusions showed an equal abundance of αββ 20S and αββ 20R, and sample SMD-2216 showed a slight increase in αββ 20S over αββ 20R. Overall, the relative response of oil inclusions in samples GS-9698 and AM-8371 reflect higher hopane biomarkers than that of steranes, whereas sample SMD-2216 is uniquely high in stigmastane and cholestane biomarker, together with tricyclic terpanes. Such distribution in the terpane biomarker is a reflection of the type of organic-matter and source-rock lithology that those oil inclusion have been generated from, with a potential of diagenetic alteration during oil inclusion entrapment. The abundance of lower tricyclic together with extended tricyclic terpanes in sample SMD-2216 appear to be related to a specific type of planktonic algae that is documented to prevail in Mississippian source rocks (Atwah et al., 2018). Overall relatively low hopane and higher sterane indicate that the source rock that generated SMD-2216 oil inclusions had higher eukaryotic organic-matter input than input from prokaryotic organics. Moreover, the higher input of cholestane isomer ααα 20R relative to ergostane and stigmastane in SMD-2216 supports the potential contribution of planktonic algal organic-matter input as the major source to these oil inclusions. However, the abundance of ααα 20R stigmastane can also originate from
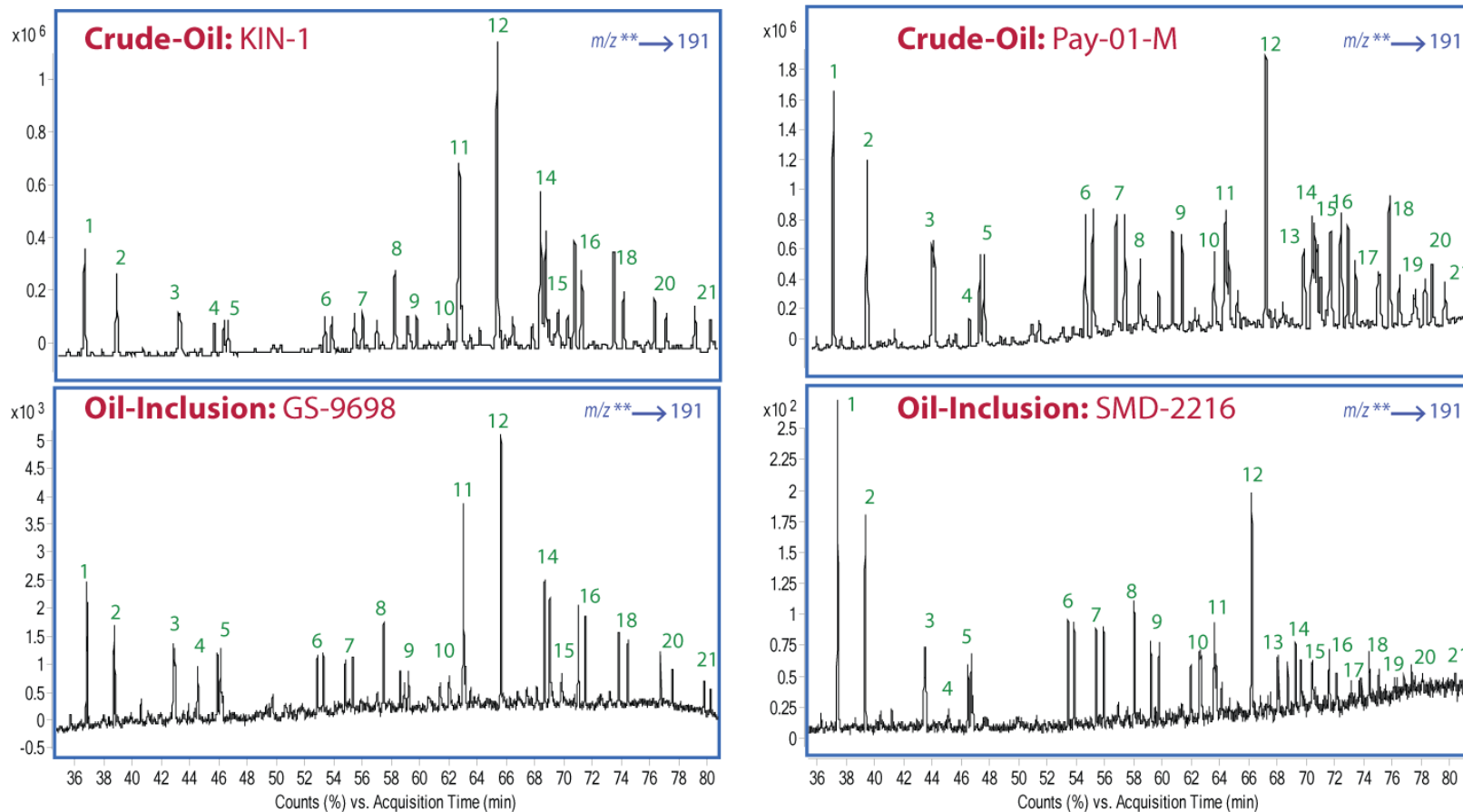
Figure 74: Extracted ion chromatograms of all product transitions to precursor *m/z*191 of oil inclusions depicting the distribution of terpane biomarkers, labeled peaks and associated compounds are listed in Table 24.

Table 25 Detailed compound list of terpane biomarkers labeled in Figure 74 and 77

Peak No.	Compound Name	MRM precursor to product transition
1	C_{23} tricyclic terpane	*m/z* 318→191
2	C_{24} tricyclic terpane	*m/z* 332→191
3	C_{25} tricyclic terpane (S+R)	*m/z* 346→191
4	C_{24} tetracyclic terpane	*m/z* 330→191
5	C_{26} tricyclic terpane (S+R)	*m/z* 360→191
6	C_{28} extended tricyclic terpane (S+R)	*m/z* 402→191
7	C_{29} extended tricyclic terpane (S+R)	*m/z* 370→191
8	C_{27} 18α(H)-trisnorneohopane Ts	*m/z* 416→191
9	C_{27} 17α(H)-trisnorhopane Tm	*m/z* 416→191
10	C_{30} extended tricyclic terpane (S+R)	*m/z* 416→191
11	C_{31} extended tricyclic terpane (S+R)	*m/z* 430→191
12	C_{29} Tm 17α(H)21β (H)-norhopane	*m/z* 398→191
13	C_{30} 17α(H)-hopane	*m/z* 412→191
14	C_{33} extended tricyclic terpane (S+R)	*m/z* 458→191
15	C_{31} 17 α(H) homohopane 22 (S+R)	*m/z* 426→191
g	gammacerane	*m/z* 412→191
16	C_{34} extended tricyclic terpane (S+R)	*m/z* 472→191
17	C_{32} 17α(H) bishomohopane 22 (S+R)	*m/z* 440→191
18	C_{35} extended tricyclic terpane (S+R)	*m/z* 486→191
19	C_{33} 17α(H) trishomohopane (S+R)	*m/z* 454→191
20	C_{36} extended tricyclic terpane (S+R)	*m/z* 500→191
21	C_{34} 17α(H) homohopane (S+R)	*m/z* 468→191
22	C_{35} 17α(H) homohopane (S+R)	*m/z* 482→191

marine algal kerogens, such as the case in the Woodford Shale (Romero and Philp, 2012).

Therefore, the enrichment of ααα 20R stigmastane in oil inclusions from GS-9698 and AM-8371

stigmastane indicates a Paleozoic marine source rock. With hopanes dominating the overall biomarker fragmentograms in samples GS-9698 and AM-8371, indicating a higher prokaryotic input rather than eukaryotic organic-matter input, from which these oil inclusions are generated. Overall, most of the samples had higher rearranged steranes relative to their regular-sterane counterpart, with basically a shift in the methylation group from potions C-10 and C-13 to C-5 and C-14. Such a rearrangement in the methyl-group has been attributed to different factors such as acidic condition, clay catalysis and high temperature (Rubinstein et al., 1975). The observed increase in diasteranes of oil inclusions could be related to diagenesis and associated acidity, especially given that some oil inclusions are found to occur with aqueous inclusions estimated to have high salinity and higher homogenization temperatures (Table 23). Therefore, this might have mediated the migration of methyl-groups in regular steranes, resulting in oil inclusions enriched in diasteranes

Using oil-inclusion molecular geochemistry, particularly both terpane and sterane biomarkers composition, we can delineate hydrocarbon charges and identify the sources that are contributing to those oil-incisions. In Payne County, where the SMD-2216 sample is located, it exhibits the unique presence of extended tricyclic terpanes, together with the limited occurrence of hopanes, which strongly matches previously examined bitumen associated with Mississippian organic-rich rocks. Mississippian bitumen is discussed in detail in Chapter IV, but in general, the SMD-2216 sample correlates with Mississippian source rock, suggesting that these oil inclusions mark periods of Mississippian hydrocarbon charge episodes. In contrast, samples GS-9698 and AM-8371 and their oil inclusions showed some signatures that are close to the Woodford Shale, such as the abundance of hopanes over tricyclic terpane, tougher with enrichment in stigmastane relative to ergostane and cholestane. However, other characteristics of those oil inclusions deviate

223

from the Woodford signature, such as the higher abundance of diasterane relative to regular-sterane, which potentially emerges from an alteration process during oil-inclusions entrapment.

Aromatic Hydrocarbons

Oil-inclusions aromatic hydrocarbons were measured for source-rock lithology and maturity assessment of the different oil-inclusion samples. Aromatic hydrocarbons exhibit higher thermal stability than that of biomarker compounds, so it was possible to analyze oil inclusions from sample CA-1-99336-B in which biomarkers were destructed. Table 25 lists some of the key aromatic ratios sensitive to both maturity and source of organic matter. Overall, CA-1-99336-B stands out compared to the rest of the oil-inclusion samples, with a higher ratio for maturity, starting with aromatic biomarker-based ratios such as monoaromatic and triaromatic steroids for maturity assessment of these oil inclusions. The monoaromatic steroid (MA (I)/MA (I + II) ratio is 0.72 for sample CA-1-99336-B, which is equivalent to approximately 1.0–1.3%Ro, reflecting late-oil to condensate maturity level. In contrast, oil inclusions in samples AM-8371, GS-9698 and SMD-2216 range from 0.20 to 0.45, with the lowest measured monoaromatic steroid ratio from sample SMD-2216 at 0.20, reflecting the onset of the oil-generation window at approximately 0.7%Ro. The TAS also showed a similar trend to that of monoaromatic steroid ratio, with slightly higher values for samples CA-1-99336-B and SMD-2216, and slightly lower for samples AM-8371 and GS-9698. Triaromatic steroid measured ratios reached as high as 0.82 for sample CA-1-99336-B, whereby oil inclusions at the latest stages of the oil window were at 1.2–1.4%Ro. The TASs for AM-8371, GS-9698, and SMD-2216 samples ranged from 0.31 to 0.39, in which SMD-2216 is at around 0.75%Ro and AM-8371 and GS-9698 reaches around 0.8%Ro (Peters et al., 2005b). In addition to maturity ratios, methyl triaromatic steroids are investigated as a source and
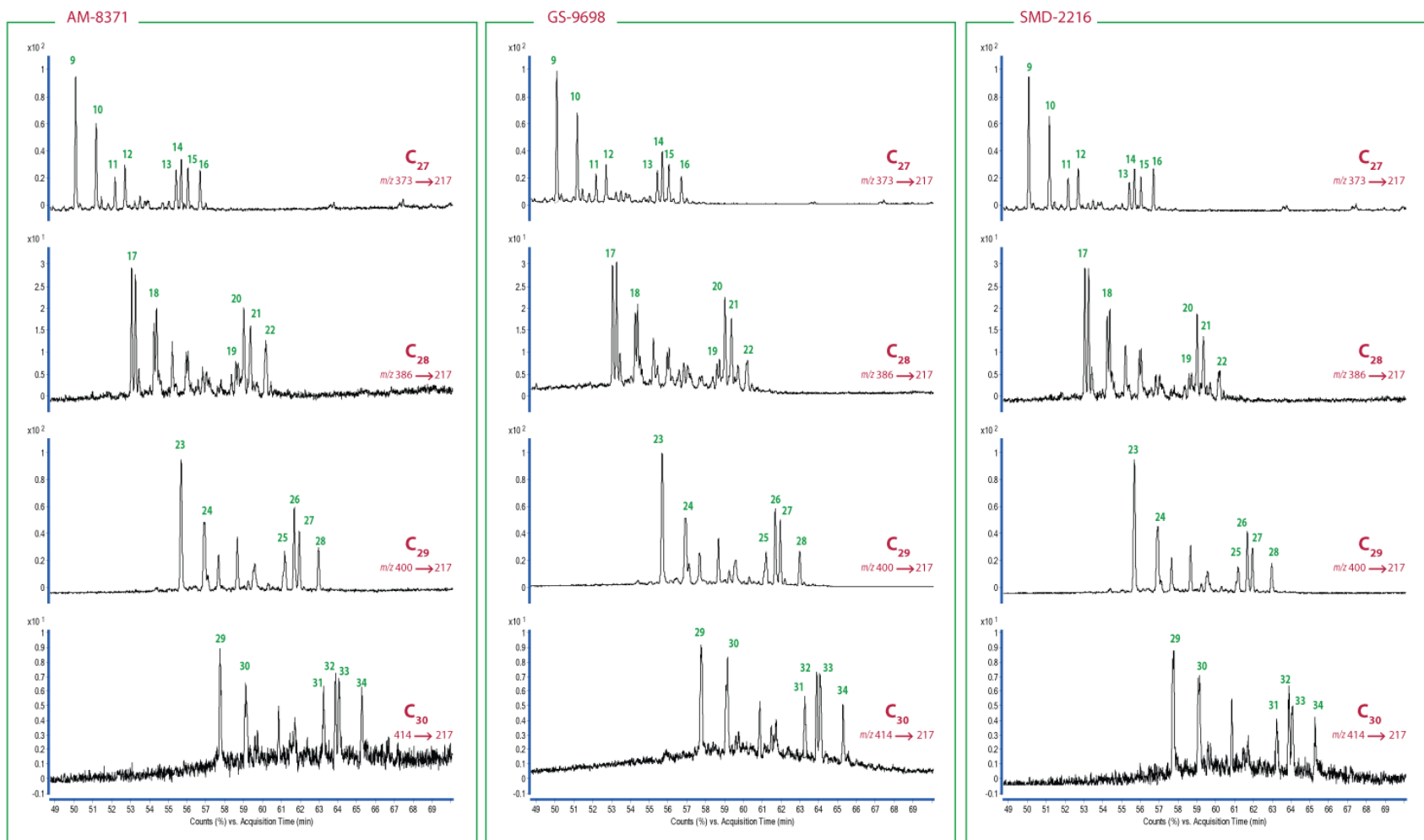
Figure 75: GC-MS/MS MRM mass fragmentogram of oil inclusion from samples AM-8371, GS-9698 and SMD-2216 ; fragmentogram shows stacked series of sterane biomarkers ranging C_{27} to C_{30}. Refer to Table 18 for peak number and associated compounds list

age-specific biomarkers, by which triaromatic dinosteroid is used as a biomarker to identify crude oils generated from pre-Jurassic source rocks (Moldowan et al., 2001). Methyl triaromatic steroid is documented in some compounds, particularly triaromatic dinosteroids, to originate from dinosterols with 4,23,24-trimethylcholestrols structural configuration found in modern marine dinoflagellates, and in some cases is related to temporal diversity of acritarchs (Moldowan et al., 2001; Peters et al., 2005b). In Table 25, TAS2/3 compares 2-methyl-24-ethylatriaromatic cholestanes to a series of 3-methyl triaromatic steroid isomers. The TAS2/3 in the oil inclusions is

Table 26 Key aromatic hydrocarbon ratios sensitive for maturity and source parameters

Aromatic ratio	AM-8371	CA-1-99336-B	GS-9698	SMD-2216
MA(I)/MA(I+II)[a]	0.46	0.72	0.45	0.20
TA(I)/TA(I+II)[b]	0.38	0.82	0.39	0.31
TAS2/3[c]	0.11	0.12	0.27	0.08
TNR-1[e]	6.34	12.69	10.92	4.90
DNR-1[e]	3.53	5.14	6.31	3.28
ENR[f]	1.77	2.41	2.36	1.21
TMNs/MNRg	1.41	1.48	1.92	1.62
MPI-1[h]	0.77	1.25	0.87	0.77
PP-1[i]	0.51	1.47	0.47	0.66
DBT/P[g]	1.29	0.46	0.65	1.13

a: MA(I)/MA(I+II): monoaromatic steroid ratio $(C_{21}+C_{22})/(C_{21}+C_{22}+C_{27}+C_{28}+C_{29};}$ b:) TA(I)/TA(II): triaromatic steroid ratio $(C_{20}+C_{21})/(C_{20}+C_{21}+C_{26}+C_{27}+C_{28})$; c : TAS2/3: 2-methyl-24-ethylatriaromatic cholestanes/ (3-methyl-24-ethy triaromatic steroid $C_{29}+$ 3-methyl-24-methy triaromatic steroid $C_{28}+$ 3-methyl-triaromatic steroid C27); d:TNR-1:trimethylnaphthalene ratio: 1,3,7-trimethylnaphthalene/1,3,5-+1,4,6-trimethylnaphthalenes; e: DNR-1: dimethylnaphthalene ratio 2,7-+3,6-dimethylnaphthalenes/1,5 dimethylnaphthalene; f: ENR: 2-ethylnaphthalene/1-ethylnaphthalene ratio; g: TMNs/MNR: (1,2,4-+ 1,2,5-+ 1,3,7-+ 1,3,6-+ 1,3,5-+1,4,6-+ 2,3,6-+1,2,7- 1,2,6+-1,6,7- trimethylnaphthalenes)/(2-+1-methylnaphthalenes); h: MPI-1: methylphenanthrene index: 1.5*(3-+2-methylphenanthrenes/ phenanthrene+ 1-+9-methylphenanthrenes); i: PP-1: 1-methylphenanthrene/ 3-+2-methylphenanthrenes; g: DBT/P: dibenzothiophene/phenanthrenes.

relatively low, ranging from 0.08 to 0.27, with SMD-2216 showing an unusually low abundance of 2-methyl-24-ethyltriaromatic, while the rest of the samples exhibit similar concentrations of 2-methyl-24-ethyltriaromatic biomarker. Methyl triaromatic steroid biomarkers and their saturated hydrocarbon counterparts have been observed to co-occur in marine kerogen enriched in acritarchs, such as the Silurian Qusaiba Shale (Al Atwah and Jacobi, 2017). Therefore, a higher ratio of TAS2/3 in sample GS-9698 at 0.27 could suggest that these oil inclusions originated from acritarchs-rich kerogen.

Non-biomarker aromatic hydrocarbons such as naphthalenes and phenanthrenes were examined as an additional maturity and as source parameters. In general, the higher values were observed for oil inclusions within sample CA-1-99336-B with some minor variability in ratio magnitude. Trimethylnaphthalene ratio (TNR-1) together with dimethylnaphthalene (DNR-1) are measured at 12.69 and 5.14, respectively, for oil inclusions in sample CA-1-99336-B, whereas the lowest measured ratios are from SMD-2216 oil inclusions at 4.90 and 3.28, respectively. Unlike the aromatic steroids, dimethylnaphthalene for sample GS-9698 is higher than CA-1-99336, even though maturity is higher at CA-1-99336. The GS-9698 higher dimethylnaphthalene can be created due to a preference for the formation of 2,7-dimethylnaphthalene or 3,6-dimethylnaphthalene by clay rearrangement reaction during the generation of these oil inclusions from their source or during their entrapment in calcite cements (Pu et al., 1990; Radke, 1988). Moreover, the ethylnaphthalene ratio (ENR) showed maturity trend similar to the previously discussed ratios among the oil-inclusion samples, but the difference in magnitude between the samples is significantly lower than between other ratios. The highest ENR value is 2.41 for CA-1-99336-B and 2.36 for GS-9698, whereas the lowest ENR is 1.21 for SMD-2216, located in Payne County. According to Radke et al. (1986), ENR ratio is largely influenced by type of kerogen, with Type III

showing a wider range of ENR with increasing maturity. For example kerogen Type III with ENR at 1.1 represents a maturity of 0.50Rm%, and with slight ENR to 1.5 maturity increases to 0.7Rm%; hence, it is suggested that such ratio must be calibrated to vitrinite reflectance for each kerogen to derive absolute maturity values (Radke et al., 1986). Lastly, naphthalene-based ratios are the sum of trimethylnaphthalenes relative to the sum of methylnaphthalenes, whereby organic-matter type and source-rock lithology will result in certain trimethylnaphthalene–methylnaphthalene ratios with clay-poor source rock with ratios <0.9 and clay-rich source rock with ratios >1.7 (Asahina and Suzuki, 2018). Overall, the examined oil inclusions showed trimethylnaphthalene–methylnaphthalenes in sample AM-8371 ranging from 1.41 to 1.92 at GS-9698. Relatively low values of AM-8371, CA-1-99336-B and SMD-2216 samples suggest that these oil inclusions have been generated in source rock with low clay content, such as carbonaceous and siliceous shale, whereas oil inclusions from GS-9698 have been generated from a source rock with relatively more clay-content, such as muddy shale and marlstones (Asahina and Suzuki, 2018).

Phenanthrenes and alkylated phenanthrenes, in conjunction with the organosulfur dibenzothiophene compounds, are reported in a number of ratios sensitive to maturity and source in Table 25. The methylphenanthrene index (MPI-1) range is most notably high for sample CA-1-99336-B with 1.80, which can be converted to a mean value of 1.3–1.5%Ro (Radke, 1983). Samples AM-8371, GS-9698 and SMD-2216 all exhibit relatively close MPI-1 values ranging from 0.77 to 0.87, which converts to a mean 0.7–0.9%Ro (Radke, 1983). Another methylphenantherne ratio is PP-1, which shows slightly lower values than MPI-I for samples AM-8371, GS-9698 and SMD-2216 ranging from 0.47 to 0.66, whereas PP-1 is higher for sample CA-1-99336-B at 1.47. Collectively, phenanthrenes maturity ratios coincide with maturity ratios

determined by aromatic biomarker, with sample CA-1-99336-B past the oil window to the condensate level, and the rest of the samples within the peak-oil stage of oil generation. Lastly, source-rock facies ratio of dibenzothiophene to phenanthrenes (DBT/P) is listed in Table 25. Oil-inclusion samples cluster into two groups, with samples AM-8371 and SMD-2216 with DBT/P >1 and samples CA-1-99336-B and GS-9698 with DBT/P <1. However, when compared with pristane and phytane ratios, all of the oil-inclusion samples plot within Zone 3, indicating a marine shale source for which those oil inclusions have been generated (Hughes et al., 1995).

Oil Inclusion and Produced Oil

Oil inclusions represents micron-sized evidence of paleo-oil migration, which can represent either an early-hydrocarbon charge, in which low maturity fluids start to fill the reservoir, or a later-hydrocarbon charge, in which reservoirs are high-graded with cracked hydrocarbons. Hence, comparing the paleo-oil composition as observed from oil inclusions with currently produced crude oil can shed light on the petroleum-migration process (George et al., 2007).

The composition of produced oils of different end-members (i.e. Mississippian end-member and Woodford end-member) were compared in terms of the composition of oil inclusions, with oils produced from Mississippian and Woodford zones. The overall distribution of *n*-alkanes was difficult to compare between oil inclusion and produced oils, due to the evaporation loss of light hydrocarbon from oil-inclusion samples during sample concentration and solvent evaporation. Loss of light hydrocarbons could be due to biodegradation, but since the *n*-alkanes of long-chain hydrocarbons are still intact, biodegradation is unlikely the cause of lost light hydrocarbons. Hence, long-chain hydrocarbons (C_{15+}) were more suitable for correlation application. Figure 76 shows the distribution of acyclic-isoprenoids relative to heptadecane (*n*-C_{17})

and octadecane (n-C_{18}). Three of the oil-inclusions plot closely to a cluster of oils produced from the Anadarko Shelf and central Oklahoma, while one of the oil inclusions shows a reducing marine signature with lower pristane/n-C_{17} values. Additionally, oil inclusion shows an overall trend with sample CA-1-99336-B with lowest Pr/n-C_{17} and Ph/n-C_{18}, which reflect an increase in thermal maturity. Moreover, while organic-acids have been reported to co-occur with normal alkanes from oil inclusions in Lower Permian Unayzah sandstones at the Ghazal Field located in the central Arabian Basin, partial mass-chromatogram of oil inclusion of the present study showed clear normal alkanes and acyclic isoprenoids with no evidence of organic-acids (Arouri et al., 2010a). Overall, the results of normal alkanes and acyclic isoprenoids show a general similarity between
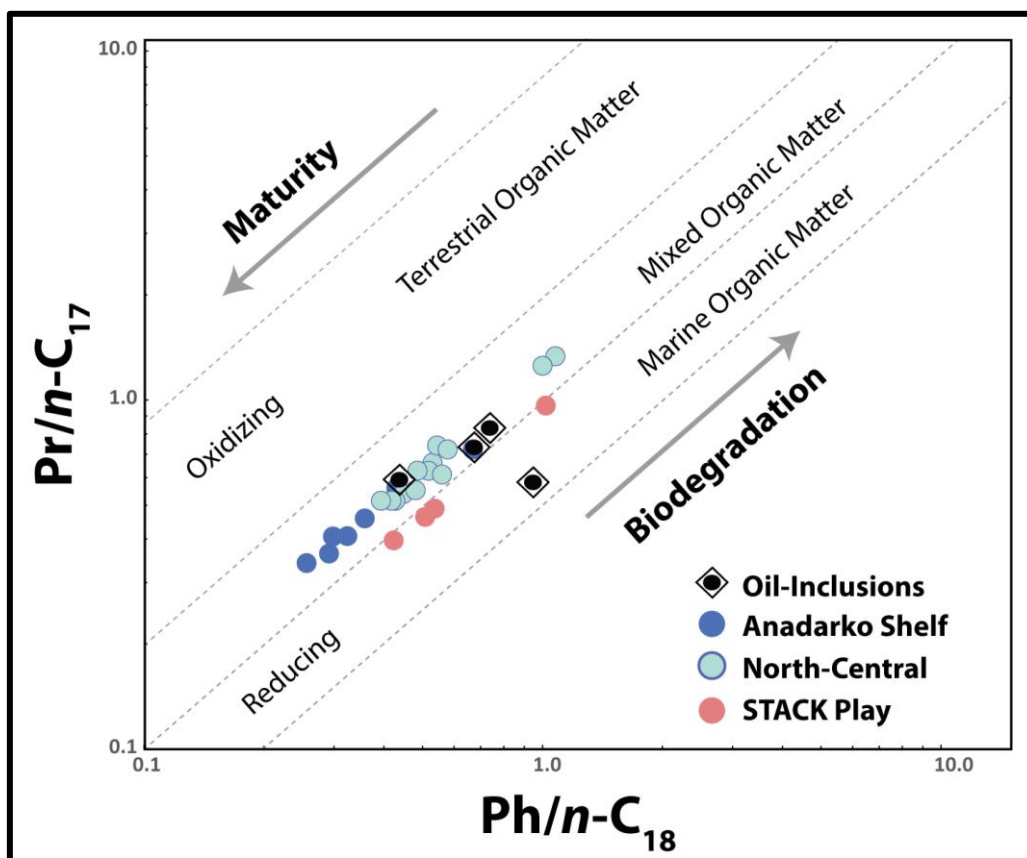
Figure 76: Cross plot comparing ratio of pristane to heptadecane (n-C_{17}) and the ratio of phytane to octadecane (n-C_{18}) of oil inclusions together with Mississippian and Woodford crude oils.

230

the oil inclusions and crude oils, but due to the specificity limitations of these compounds, as discussed in Chapter II, we further examined biomarkers in more detail.

The notable similarity of terpane biomarkers is observed between oil inclusions and produced crude oils. Mississippian end-member oils are characterized by their diagnostic extended tricyclic terpane signature, as exemplified by oil sample Pay-04-m. Such a biomarker signature is observed only in oil inclusions from SMD-2216 (Figure 77). Extended tricyclic terpanes are overall higher in crude oil than the oil inclusions, due to sample concentration and weight. Both Mississippian end-member oils and oil-inclusion SMD-2216 exhibit higher tricyclic terpane relative to hopane biomarkers, with extended tricyclic terpane reaching C_{38}. A mass fragmentogram of Mississippian end-members shows complex m/z191 at a retention time segment between 66 and 80 min, which reflects the co-elution of homohopanes with extended tricyclic terpanes. In the hopane biomarkers, SMD-2216 oil inclusions and Pay-04-M indicate a lower abundance of C_{29} Tm 17 α (H) 21β (H)-norhopane relative to C_{30} 17 α (H)-hopane. In those samples, C_{24} tetracyclic terpanes were relatively low in comparison with both C_{25} and C_{26} tricyclic terpanes. However, a slight difference is also observed between the oil-inclusion sample and the crude oil, such as the higher C_{23} and C_{24} tricyclic terpanes relative to hopane in the oil-inclusion SMD-2216, while the Pay-04-M oil sample showed higher hopane relative to C_{23} and C_{24} tricyclic terpanes. In contrast, oil inclusions recovered from sample GS-9698 from Blaine County reflect a strong Woodford end-member signatures. For example, both crude oil Woo-01-M and GS-9698 oil inclusions share the dominance of hopane and homohopanes over tricyclic terpanes (Figure 77). In both samples, extended tricyclic terpanes are observed up to C_{31} only in very low abundance. In addition, C_{29} Tm 17 α (H)21β (H)-norhopane and C_{24} tetracyclic terpane were observed to be higher in crude oil Woo-01-M and GS-9698 oil inclusions, compared to

Mississippian end-member samples. The GS-9698 oil inclusions differed from Woo-01-M in a slight depletion of C_{24} tetracyclic terpane, relative to nearby tricyclic terpanes.

Sterane biomarkers in oil inclusions shared a similar sterane composition observed in produced crude oils. Table 26 list key sterane biomarker ratios of crude oils along with oil inclusions. As with terpane biomarkers, similar sterane distribution between oil inclusion and produced petroleum samples. Crude-oil Pay-04-M representing a Mississippian end-member fingerprint shares similar sterane ratios to the SMD-2216 oil-inclusion sample, such as the dominance of cholestane over ergostane and stigmastane, particularly isomers of ααα20R configuration. Moreover, pregnanes are higher in Mississippian end-member oils and oil inclusion from SMD-2216. However, SMD-2216 differed from all the Mississippian end-member oils with a dominance of diasteranes over regular steranes in the range of C_{27} to C_{30} (Figure 77). In contrast, oil inclusions from GS-9698 and Woodford end-member oils exhibit enrichment of stigmastane relative to the ergostane and cholestane of different isomers, such as the aββ20S and ααα20R. Like Mississippian oil inclusion with high diasterane relative to regular-steranes, oil inclusion from GS-9698 differs from the Woodford end-member oil-sample in that they are enriched in diasteranes with the ratio of diasteranes relative to regular steranes in GS-9698 at 0.41 and the Woodford oil Woo-01-M at 0.27. Additionally, oil inclusions from AM-8371 showed sterane biomarkers slightly different from Mississippian and Woodford end-members oils; however, some similarities are observed between AM-8371 and mixture crude oils such as Can-01-M. Regular sterane in those samples showed an intermediate abundance of stigmastane relative to ergostane and cholestane
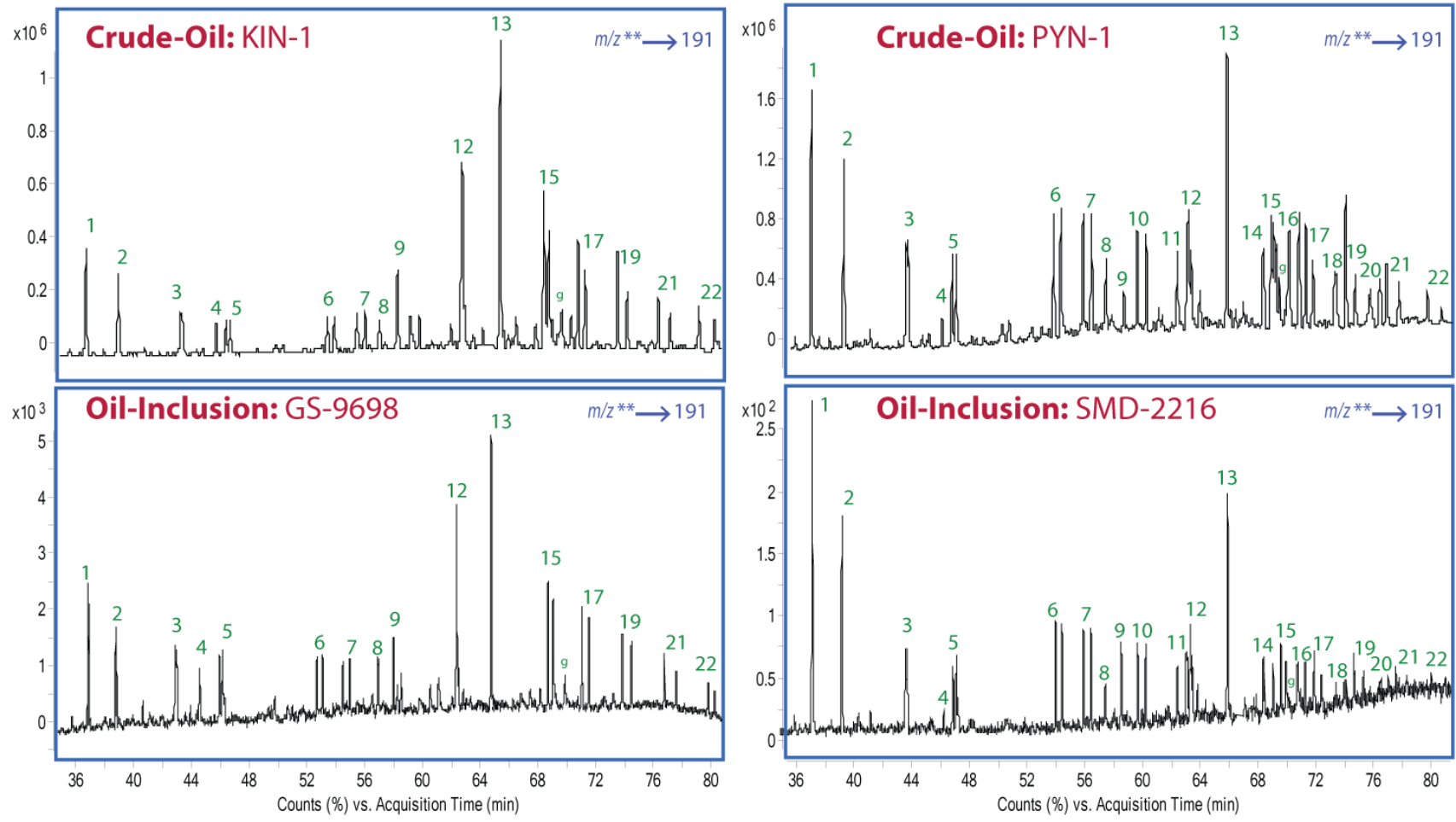
Figure 77: Extracted ion chromatograms of all product transitions to precursor *m/z*191 of oil inclusions and *m/z*191 mss-fragmentogram of crude oils depicting the distribution of terpane biomarkers. Labeled peaks and associated compounds are listed in Table 24.

with at 0.61 in AM-8371 oil inclusions and 0.51 in crude-oil Can-01-M, which potentially suggests

that these oil inclusions have a mixture component of both petroleum system end-members. The

AM-8371 oil inclusions, like the rest of the oil-inclusion samples, showed high diasterane relative

to the regular steranes at 0.51. Overall, such enrichment of diasteranes in both of the oil inclusions

compared to crude-oil samples may be caused by acidic clay-catalysis rearrangement of the

methylgroup at sterane biomarkers. Such a mechanism could be mediated during high salinity

hydrothermal fluids diagenesis, which is likely associated with calcite cementation and oil-

inclusion entrapment AM-8371.

Table 27 Key sterane biomarkers for crude-oils and oil-inclusions

Biomarkers	Crude-Oil Samples				Oil-Inclusion Samples		
	Woo-01-M	Pay-04-M	Can-01-M	Log-07-W	GS-9698	AM-8371	SMD-2216
%C_{27} $\alpha\alpha\alpha$R [a]	0.19	0.31	0.29	0.32	0.11	0.18	0.31
%C_{28} $\alpha\alpha\alpha$R [b]	0.15	0.27	0.2	0.2	0.18	0.21	0.11
%C_{29} $\alpha\alpha\alpha$R [c]	0.66	0.42	0.51	0.48	0.71	0.61	0.58
S/(S+R) (C_{29} $\alpha\alpha\alpha$) [d]	0.48	0.59	0.52	0.57	0.44	0.51	0.54
$\beta\beta$S/($\beta\beta$S+$\alpha\alpha$R) (C_{29})[e]	0.53	0.63	0.55	0.56	0.48	0.59	0.51
(C_{21+22})/($C_{27+28+29}$)[f]	0.09	0.11	0.13	0.07	0.06	0.09	0.13
Diast/(Diast+ster) [g]	0.27	0.30	0.36	0.21	0.41	0.51	0.61

a: C_{27} $\alpha\alpha\alpha$20R cholestane over the sum of C_{27} $\alpha\alpha\alpha$20R cholestane, C_{28} $\alpha\alpha\alpha$20R ergostane and C_{29} $\alpha\alpha\alpha$20R stigmastane; b: C_{28} $\alpha\alpha\alpha$20R ergostane over the sum of C_{27} $\alpha\alpha\alpha$20R cholestane, C_{28} $\alpha\alpha\alpha$20R ergostane and C_{29} $\alpha\alpha\alpha$20R stigmastane c: C_{29} $\alpha\alpha\alpha$20R stigmastane over the sum of C_{27} $\alpha\alpha\alpha$20R cholestane, C_{28} $\alpha\alpha\alpha$20R ergostane and C_{29} $\alpha\alpha\alpha$20R stigmastane; d: C_{29} $\alpha\alpha\alpha$20S stigmastane over sum of C_{29} $\alpha\alpha\alpha$20S+R stigmastanes f: sum of C_{21} and C_{22} sterane over sum of C_{27} $\alpha\alpha$ 20R, C_{28} $\alpha\alpha$ 20R and C_{27} $\alpha\alpha$ 20R C_{29} steranes; g: C_{27} $\alpha\beta\beta$20S cholestane over C_{29} $\alpha\beta\beta$20S stigmastane; h: C_{28} $\alpha\beta\beta$20S ergostane over C_{29} $\alpha\beta\beta$20S stigmastane.

Diamondoids in Oil Inclusion

Distribution of extended diamondoids fingerprint of CA-1-99336-B oil inclusion showed mixed signatures (Figure 78). Moreover, oil-inclusions diamondoids distribution relative to triamantane shows tetramantane isomers plotting over crude-oil Log-01-M, while pentamantane isomers together with cyclohexamantane plot over crude-oil Alf-01-M and Woo-01-M. However, pentamantane [1(2,3)4] (Pent-1) did not match any of the examined crude-oil diamondoid fingerprints. Such high pentamantane relative to tetramantane [123] could be a result of the presence of clay and carbonates minerals, with interaction with kerogen dominated with cyclic organic compounds. Based on an experimental study, pure compounds of cholestane in the presence of montmorillonite and calcium carbonate at 340°C for three days, which resulted in a higher yield of pentamantane [1(2,3)4] (Pent-1) relative to tetramantane [123] (Tet-3) (personal communication, Moldown). Hence, such higher pentamantane [1(2,3)4] could result from contribution Mississippian source-rock carbonate. Crude-oil Log-01-M is carbonate-sourced oils as observed from biomarkers and isotopes; however, it does not show similar enrichment of pentamantane [1(2,3)4], which could suggest a third source to the oil inclusions of CA-1-99336-B.

Quantitative extended diamondoid analysis of matured fluid helped fingerprint those fluids that are otherwise difficult to correlate using classic geochemical approaches. Samples such as Bla-01-M are condensates highly mature with no biomarker left, but some aromatic compounds were observed with light series of *n*-alkanes. Sample Bla-01-M showed a unique extended-diamondoids fingerprint, different from the examined crude-oils sand oil inclusions (Figure 78). Similarly, crude-oil Kay-01-M is light crude oil with API at 48°, with trace amount of biomarkers not adequate for identifying the source. With extended diamondoid distribution, Kay-01-M

showed a fingerprint similar to sample Alf-01-M and Woo-01-M. This observation implies that

Kay-01-M is dominantly sourced from the Woodford Shale, as Woo-01-M and Alf-01-M oils both

represent Woodford-sourced end-members, as confirmed by biomarker composition.
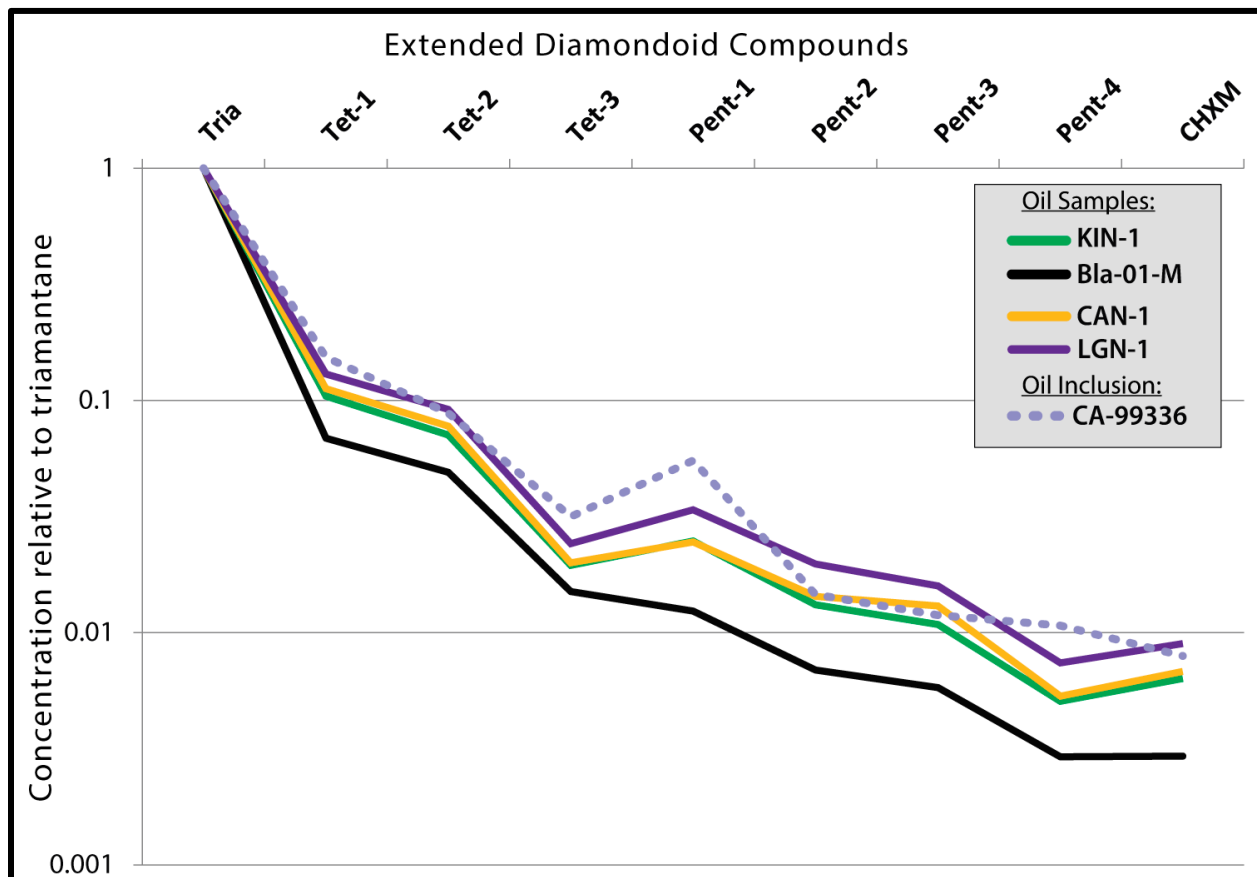
Figure 78: Diamondoids fingerprint comparing crude-oil samples with oil inclusions. Tria: Triamantane; Tet-1: Tetramantane [1(2)3]; Tet-2: Tetramantane [121]; Tet-3: Tetramantane [123]; Pent-1: Pentamantane [1(2,3)4]; Pent-2: Pentamantane [12(1)3]; Pent-3: Pentamantane [1212]; Pent-4: Pentamantane [1213]; CHXM: cyclohexamantane [123124]. Refer to Table 5 for

Carbazoles and Phenols in Crude-Oil

An improved understanding of migration time and distances traveled by crude oils from

source rocks to reservoirs is vital in the search for new petroleum accumulations. The migration

time and distance may be determined by modeling the evolution of a set of oil tracers along the

migration pathway from the source to the reservoir accumulation. The oil tracers are molecular

markers, such as carbazole and its derivatives, naturally generated along with crude oil. Moreover, these nitrogen aromatic compounds include carbazole, methylcarbazoles, dimethyl carbazoles, and benzocarbazoles. Similarly, phenol compounds can be used to track oil migration distance, but phenols are also sensitive to water-washing effects due to their high solubility in water.

Examined crude-oil carbazole and phenol compounds and their concentrations are listed in Table 27. Overall, carbazoles absolute concentration varied among the crude oils with 1,8-dimethylcarbazole showing highest concentration compared to the rest of the carbazoles compounds. Concentration of 1,8-dimethylcarbazole varied, ranging from 8.55 to 57.96 ppm and averaging 32 ppm. In contrast, distribution of benzocarbazoles showed notable differences, with high benzo[c]carbazole within oils at the Anadarko Shelf, while oils at central Oklahoma and STACK play with high benzo[a]carbazole compared to benzo[c]carbazole (Table 27). Moreover, the absolute concentration of the total benzocarbazole isomers ranged from 2.06 to 8.55 ppm, with the lowest values observed in oils at the Anadarko Shelf, whereas highest concatenations occur in crudes from central Oklahoma. Of the phenols compound class, phenol is the most abundant, with some samples showing a predominance of o-cresol over phenol, while in all crude-oil samples m-cresol is the least abundant among the phenol compounds. Overall, the total concentration of phenols ranged from 0.2 to 7.3 ppm, and particularly oils within the STACK play showed the highest abundance of phenols compared to oils located in the Anadarko Shelf and central Oklahoma (Table 27).

Table 28 Phenols and carbazoles compounds of selected oil samples from Anadarko Shelf, STACK Play and central Oklahoma.

Peak NO	Compounds	Alf-01-M	Kay-01-M	Can-01-M	Can-04-M	Gar-01-M	Kin-01-N	Lin-03-W	Log-01-M	Pay-04-M
P1	Phenol	0.15	0.13	1.40	1.34	1.48	1.17	0.35	0.50	0.48
P2	o-Cresol	0.28	0.19	0.62	0.92	0.92	0.88	0.06	0.30	0.22
P3	p-Cresol	0.12	0.18	0.71	0.56	0.36	0.36	0.04	0.12	0.09
P4	m-Cresol	0.03	0.07	0.34	0.02	0.12	0.27	0.01	0.04	0.05
1	Carbazole	5.90	2.71	11.72	27.36	2.31	3.57	0.45	1.53	0.82
2	1-Methylcrbz	17.25	11.62	18.11	14.20	5.11	11.21	0.86	3.62	2.19
3	3-Methylcrbz	3.60	2.37	8.97	1.77	1.40	3.84	0.64	0.88	0.68
4	2-Methylcrbz	5.36	2.92	8.96	6.21	1.69	4.79	0.45	1.11	0.75
5	4-Methylcrbz	8.67	6.39	11.80	17.48	2.39	6.63	0.37	2.47	1.33
6	1,8-DiMecrbz	18.91	22.34	47.79	50.69	8.55	21.17	12.01	50.22	54.86
7	1-Ethylcrbz	3.16	1.57	4.82	4.47	0.96	2.00	0.17	0.57	0.43
8	1,3-DiMecrbz	16.24	11.79	34.01	26.77	5.13	12.54	5.18	2.59	2.93
9	1,6-DiMecrbz	16.20	11.15	31.47	28.17	5.11	11.83	6.41	2.37	2.71
10	1,7-DiMecrbz	13.23	13.65	40.81	34.59	5.49	16.98	6.54	2.83	3.38
11	1,4-DiMecrbz	17.98	15.43	35.61	38.48	6.06	14.91	6.68	4.35	4.41
12	1,5-DiMecrbz	17.57	18.51	34.59	38.24	5.91	17.70	6.07	5.33	4.64
13	2,6-DiMecrbz	9.20	6.14	12.47	14.90	1.54	5.34	0.83	1.28	1.23
14	2,7-DiMecrbz	16.55	10.26	18.44	23.35	3.93	9.62	5.66	3.16	3.05
15	1,2-DiMecrbz	11.63	7.30	20.85	22.41	2.89	9.49	0.73	2.00	2.13
16	2,4-DiMecrbz	2.48	3.70	7.08	8.75	1.89	4.38	0.98	0.87	1.36
17	2,5-DiMecrbz	2.38	2.54	5.92	6.52	1.65	3.13	0.64	0.82	0.74
18	Benzo(a) crbz	1.11	0.85	3.36	4.11	4.64	3.20	2.31	4.48	3.83
19	Benzo(b) crbz	0.36	0.03	0.05	0.73	0.05	0.79	0.86	0.14	0.14
20	Benzo(c) crbz	2.13	1.18	1.80	2.22	1.83	1.63	1.39	3.31	1.34
	Sum of Benzocrbz	3.60	2.06	5.21	7.06	6.51	5.62	4.57	7.92	5.31
	BC ratio	0.34	0.42	0.65	0.65	0.72	0.66	0.62	0.57	0.74

The overall carbazole trend observed in crude oil reflects the migration distance of crude oil from source-rock–oil accumulation in the reservoirs through carrier beds. Crude oils within the Anadarko Shelf are produced from relatively shallow Mississippian reservoirs exhibiting the lowest BC ratio, below 0.5, ranging from 0.33 to 0.42. In such crude oil, benzo [c] carbazole is higher than benzo [c] carbazole isomer (Figure 80), suggesting that these oils are distally sourced and have interacted with carrier-bed the most. In contrast, most of the oils located in central Oklahoma showed a BC ratio higher than 0.5, ranging from 0.55 to 0.83. These oils exhibit an abundance of benzo [a] carbazole over benzo [c] carbazole isomer (Figure 80). Such benzocarbazole abundance evidences that central-Oklahoma oils are proximally sourced, suggesting that oils interacted the least with carrier beds during secondary migration. Oil samples within the STACK play showed comparable ratios to oils located in central Oklahoma, with BC ratio ranging from 0.47 to 0.72. Those oils of the STACK play are all above 0.5 except for sample Bla-01-M, at 0.45, suggesting a slight abundance of benzo [c] carbazole over benzo [a] carbazole. Sample Bla-01-M is a condensate with an API gravity of 49°, which also showed an elevated concentration of diamondoids, suggesting this particular sample has been exposed to thermal stress that might affect the BC ratio. The rest of the oils within the STACK play suggest a proximal source for the oils with relatively less migration distance than oils recovered from the Anadarko Shelf.

Benzocarbazoles and oil migration distance can vary among different petroleum sedimentary basins, depending on crude-oil source rocks type. According to Larter et al, (1995) crude-oil relative migration distance can be estimated using the benzocarbazole ratio, for example,

benzocarbazole ratio of oils from the foreland basin of western Canada showed a systematic

decrease with increasing migration distance ranging from 0.6 BC ratio for non-migrated oil, and
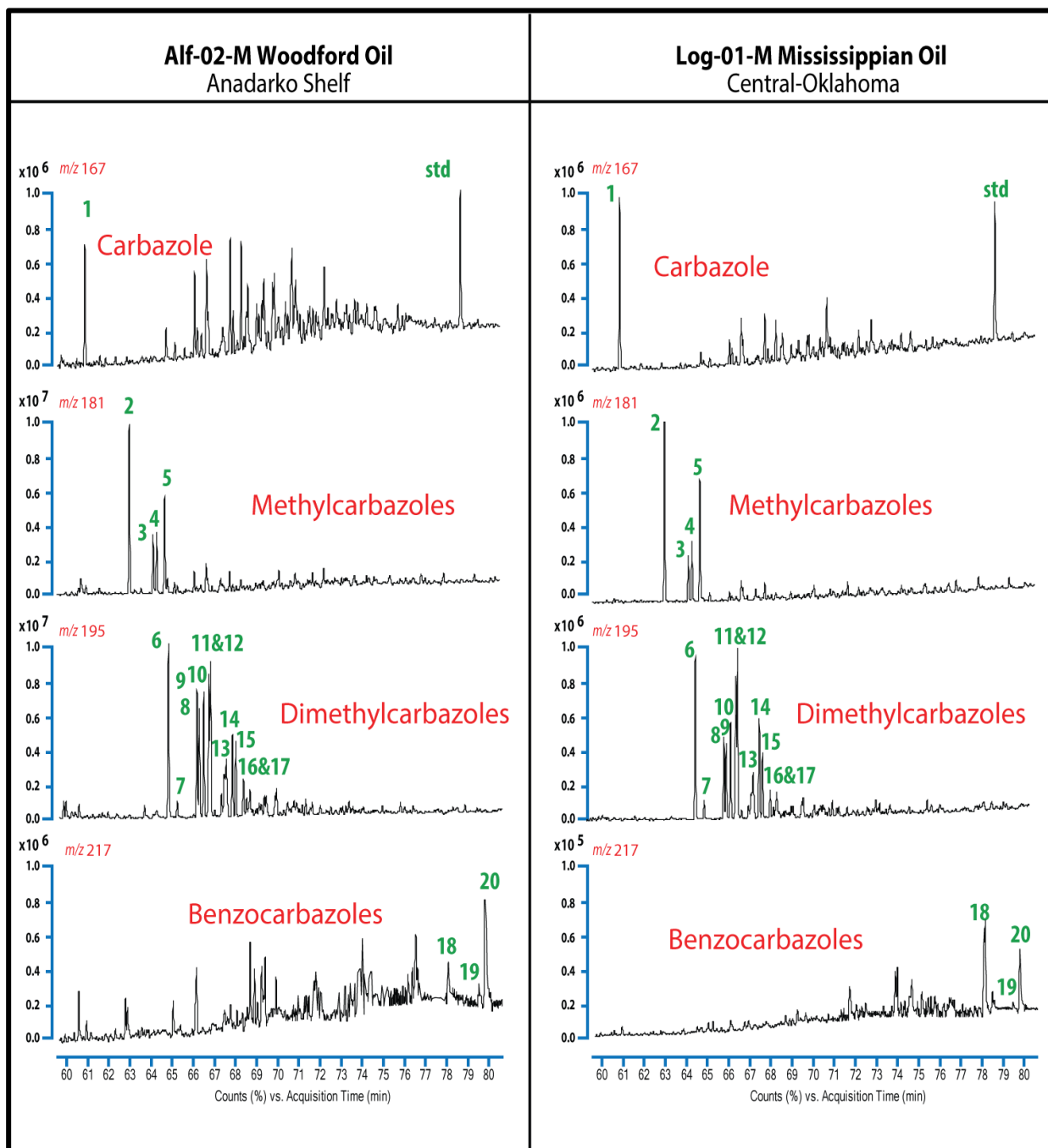
Figure 79 Series of carbazole compounds-fragmentograms of crude-oil samples comparing oil from central Oklahoma Log-01-M with oil sample from Anadarko Shelf Alf-02-M. Note the distribution of benzocarbazole in the two different oil samples, which is affected by oil migration distance. Labeled peaks and associated compounds are listed in Table 23.

240

0.3 BC ratio for oil with approximately less than 200 km of relative migration (Larter et al., 1996).

By assuming a similar relationship between BC ratio and migration distance, we estimated relative

oil migration distance of examined crude-oil samples. Based on the BC ratio, Anadarko Shelf oils

exhibit the lowest ratio, suggesting a higher migration distance, ranging from approximately 100

km to 200 km from the source kitchen area. In contrast, central-Oklahoma oils located east of the

Nemaha Uplift showed the highest BC ratios, with an estimated migration distance ranging from

10 km to 50 km. Benzocarbazole ratio showed a trend in the oil samples from Central Oklahoma,

particularly oils with close proximity to the Nemaha Uplift faults, which include most of oils at

Logan County. The highest BC ratio is observed in oil sample Log-02-M at 0.82, with a general

decrease towards the east at Payne County, suggesting a possible west-to-east oil migration

direction. Additionally, the relatively high BC ratios are observed in the Southern part of Payne

County as well as LNK, with a trend decreasing to the north. Such trend within central Oklahoma

indicates multiple oil migration pathways charging these reservoirs with hydrocarbon, with a

potential fill-and-spill series of oil accumulations (Figure 80). Oils within the STACK play showed

a wider range of BC ratios, which affected the range of oil migration distance, ranging from 50 km

to 80 km. Even though oil samples distribution is limited in the examined oils, some trends are

observed that could indicate an oil migration trend—particularly, three oils found in Canadian

County, including Can-01-M, Can-03-M, and Can-04-M samples. These oils showed a decreasing

BC ratio, starting as high as 0.72 and reaching 0.62 in sample Can-01-M, with an overall northeast

trend, which could reflect an oil migration pathway. This is a crucial observation, especially in

unconventional tight reservoirs, which shows that oil migration also occurs at a smaller scale

within mudrocks, which have long been thought of as either a source of hydrocarbon or as a cap rock sealing conventional sandstone reservoirs.

Phenol compounds are water-soluble polar compounds, and they can be used to assess crude-oil secondary alteration, such as water washing (Taylor et al., 1997). Unlike carbazoles, phenols dramatically change in abundance in the lab experiment simulating oil migration, as observed from core flooding experiments (Larter et al., 2000). Sorption effect on hydrophilic compounds including phenols will ultimately result in phenol separation from oil into water, then finally preferentially to a solid phase (Taylor et al., 1997). Therefore, while migration does influence
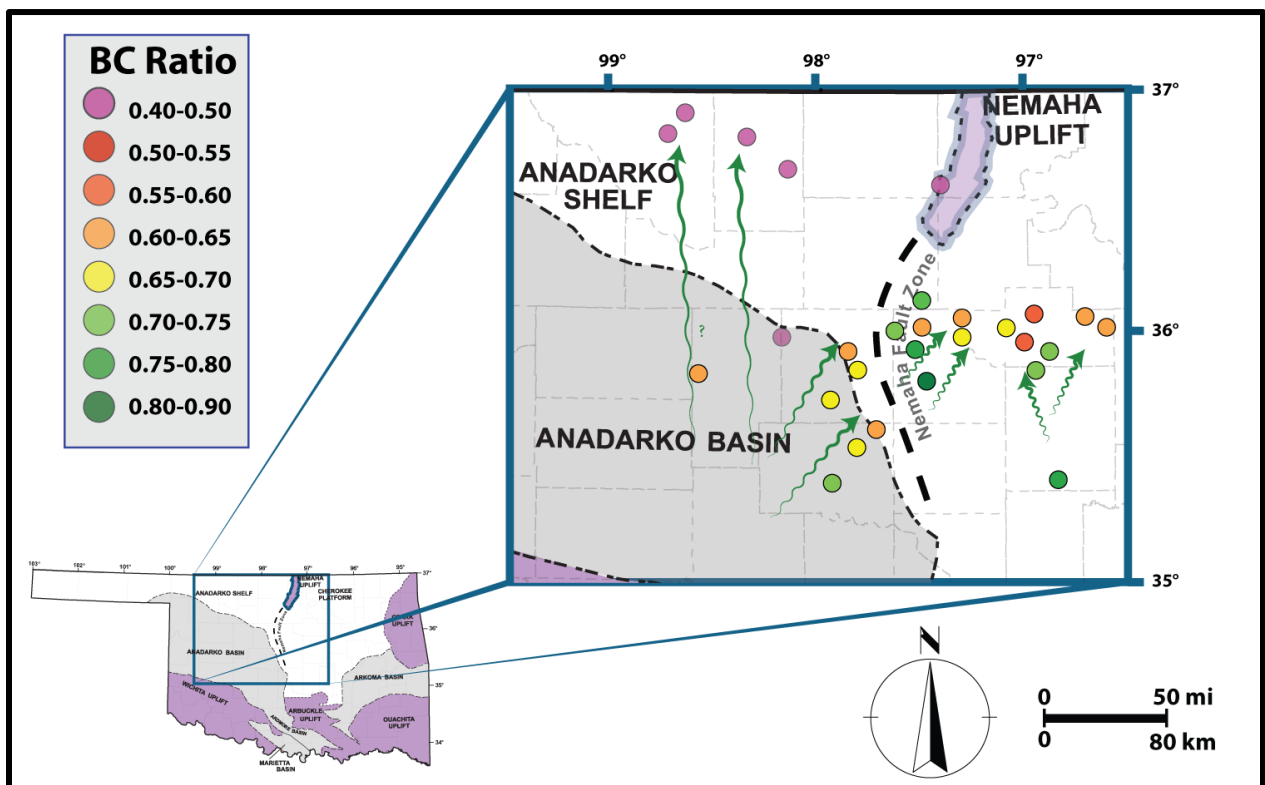
Figure 80: Map showing distribution of benzocarbazole ratio (BC ratio) with inferred oil migration direction of crude-oil samples from the Anadarko Shelf, the Sooner Trend Anadarko Basin Canadian and Kingfisher Counties (STACK) play and central Oklahoma.

phenols concentration, in-reservoir alteration such as oil-water interaction has significant control of phenols distribution (Peters et al., 2018).

In addition to oil production, the Mississippian limestone play in northern Oklahoma and southern Kansas is well-known for significant volumes of water production. The Mississippian Limestone play exhibits shallow reservoirs economically attractive to drill; however, associated saltwater production affects the economic success in such a play (Hall, 2012). Therefore, examining water-soluble compounds such as phenols in crude oil produced from the Mississippian reservoirs is crucial to evaluate the degree of water washing in these reservoirs. Total phenols in the examined oil samples ranged from 0.5 to 0.8 ppm within the Anadarko Shelf, whereas oil samples at the STACK play showed higher levels of phenols, ranging from 0.2 to 7 ppm, and oils from central Oklahoma ranged from 0.4 to 2 ppm. Figure 81 displays a cross plot comparing the concentration of phenol compounds against the sum of cresols, which include *ortho*-cresol, *meta*-cresol, and *para*-cresol. Most of the oils showed a dominance of phenols over cresol, except some oils within the Anadarko Shelf, such as sampleWoo-02-M and Kay-01-M, with higher *ortho*-cresol than phenol. For cresols, the isomer *ortho*-cresol with a methyl group at carbon position C-2 was the dominant cresol isomer in all of the crude-oil samples. Based on the concentration of phenols, crude oils within Anadarko Shelf are the highest in terms of water washing, followed by oils within central Oklahoma (Figure 81). Crude oils within the STACK play showed phenols intact with high abundance, suggesting they are the least affected by reservoir water washing. Such variation of phenol and cresols concentration can be interpreted to reflect fluid hydrodynamics with respect to interaction between crude oil and water, resulting in portioning of phenols from the crude oil to the water in samples located at the Anadarko Shelf and Central Oklahoma. In such settings, loss of phenols is influenced by oil migration distance and the reservoir pool seal-rock quality and

formation-water enrichment. In contrast, STACK play enrichment of phenols suggests minimal oil-water interaction, which could result from short oil migration distance or high-quality seal rocks, with the latter more likely to be the cause. Within the STACK play, oils are mainly produced from Mississippian reservoirs which are tight mudrocks with ultra-low permeability, where oils interact least with formation water
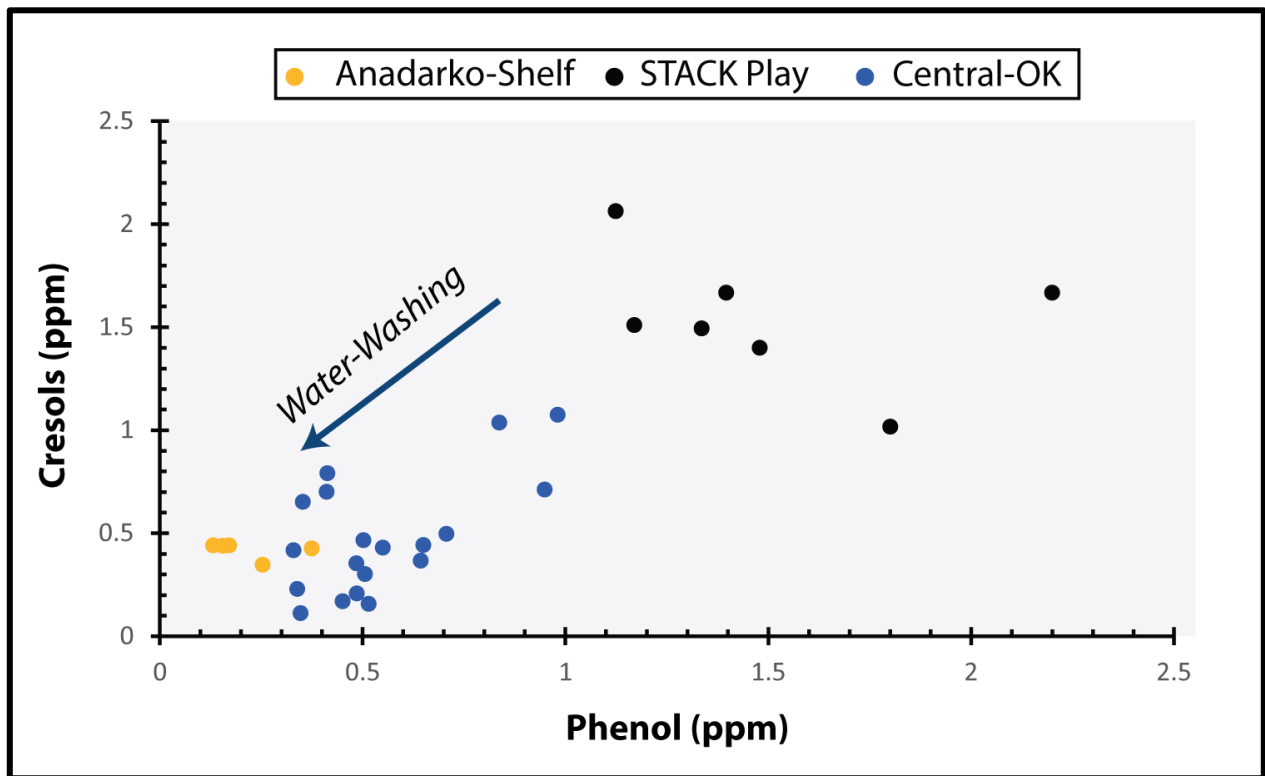
Figure 81: Cross-plot of crude-oil samples comparing the concentration of phenol in the x-axis against the sum of cresols which includes ortho-cresol, meta-cresol and para-cresol.

CHAPTER VII

BASIN AND PETROLEUM SYSTEMS MODELING OF DEVONIAN-MISSISSIPPIAN PETROLEUM SYSTEMS IN CENTRAL OKLAHOMA

Introduction

Basin and petroleum system modeling is a dynamic forward modeling tool that incorporates different geological input (e.g. rock thickness, lithology, age, etc.) and is calibrated through boundary conditions, which includes variables such as paleo-heat-flow (Hantschel and Kauerauf, 2009). Basin and petroleum system modeling offers very effective analysis that can be dynamically refined as more wells are drilled and more data is acquired. Moreover, mature basins such as the Anadarko Basin are very rich provinces in terms of data availability, providing crucial input for constructing a geologically sound basin model and production data constraints, which are scarce in exploratory frontier basins.

Historically, the approach of 1D basin modeling was first introduced in 1998 at site 397 as a part of the deep sea drilling project located on the continental rise of North Africa (Yükler MA, 1979). The first attempt at a basin modeling approach for the Anadarko Basin Province was carried out for the Cherokee Basin located in the southeastern region of Kansas. The Cherokee Basin is the shallow-shelf extension of the Anadarko and Arkoma basins strata, which are comprised of Cambrian to Mississippian carbonates interbedded with shales, and overlain by Pennsylvanian to Permian clastics interbedded with thin carbonates (Förster et al., 1998). Different scenarios of geohistory were modeled, including periods of sedimentation and erosion, together with modeling thermal maturation and diagenesis. In this study, basin modeling results suggest that the Cherokee Basin, even though at shallower depths than those of the Anadarko Basin, reached 70°C during

Late Permian (Förster et al., 1998). As to thermal maturation, the authors assumed heat conduction with a constant heat flow of 60 mW/m^2 from the basement, resulting in maximum maturation stage of 0.5%Ro for Pennsylvanian strata, and 0.6%R$_o$ for Devonian-Mississippian shales (Förster et al., 1998). The limitation of this basin modeling approach is attributed to the 1D approach, in which only four wells are used as data input. Thererfore, generated data and interpretations are limited to the location of the wells, so the study is localized and cannot be extended to cover the Anadarko Basin

The USGS performed a more recent 3D regional basin modeling study of the Anadarko Basin Province including Oklahoma, Kansas, Colorado and Texas. This is a crucial study that compiled published literature about the Anadarko Basin and synthesized it in a 3D basin model with the main objective of assessing undiscovered oil and gas by means of basin and petroleum system modeling principles (Higley, 2014b). The basin model takes into account major petroleum system elements and processes including source rocks, thermal-maturation, petroleum migration and accumulation, reservoir rocks, hydrocarbon traps and seal rocks (Higley and Gaswirth, 2014). In this study, petroleum systems of the Anadarko Basin were divided into two total petroleum classes, namely the Woodford petroleum system and the Pennsylvanian petroleum system, each of which is subdivided into a number of assessment units based on reservoir ages, with a total of 13 assessment units. The USGS 3D Anadarko Basin model considered conventional petroleum accumulation, represented as a total of nine assessment units (i.e. conventional reservoirs), together with continuous assessment units (i.e. unconventional shale reservoirs), which were subdivided into Devonian and Mississippian Woodford Shale gas and Woodford Shale oil continuous assessment units, as well as the Pennsylvanian Thirteen Finger Limestone–Atoka Shale continuous assessment units. The results of the simulation indicate that an estimated 80%

undiscovered oil within Mississippian Devonian reservoirs, along with 60% undiscovered gas resources. Moreover, the mean of estimated undiscovered oil within the Mississippian assessment unit is 17 million barrels, with the gas total at a mean of 367 billion cubic feet. In a probabilistic sense, it is estimated that the Mississippian assessment unit has a 90% chance of containing 5 million barrels of undiscovered oil, 15 billion cubic feet of gas and 3 million barrels of natural gas liquids. A more optimistic estimate suggests a 5% chance of finding 31 million barrels of undiscovered oil, 663 billion cubic feet of gas and 17 million barrels of natural gas liquids (Gaswirth and Higley, 2014). The Woodford Shale continuous assessment estimates were much higher than those of the Mississippian assessment unit, with mean undiscovered oil of 393 million barrels and with 15,973 billion cubic feet of gas, with a 95% likelihood of Woodford Shale containing 175 million barrels of oil, 8806 billion cubic feet of gas and 94336 million barrels of natural gas liquids. Lower likelihood (5%) scenarios suggest a total of 730 million barrels of undiscovered oil, 25 998 billion cubic feet of gas and 336 million barrels of natural gas liquids (Gaswirth and Higley, 2014). According to this study, Woodford Shale has a significantly higher potential of undiscovered oil and gas compared to that for the Mississippian formations. However, this study was carried out in 2013, and hence did not consider emerging liquid-rich plays in Oklahoma such, as the STACK and SCOOP plays. Even though these plays were first discovered in 2013, it was not until 2015 that they gained recognition, particularly when Newfield Exploration Company announced a significant capital expenditure of $700 million in exploration and production activities of the STACK play. To date, the potential within these unconventional plays has not been completely exploited (Brown, 2014).

The USGS study of the Anadarko Basin and petroleum-systems modeling is useful from a regional perspective, but it has various limitations. First, since the study covered a large area of interest, including four different states with a total of approximately 12 000 square miles, resulting in loss of resolution of details at a smaller scale. This lack of detail is clearly reflected in the structural grids of formation surfaces exhibiting smooth surfaces with low relief. Such a features greatly impact trap closure, and hence the distribution of hydrocarbon accumulation. Moreover, in the petroleum-migration and accumulation modeling of the USGS study, modeled petroleum accumulation bypassed a major oil field known as the Sooner Trend oil field (i.e. failed to show any accumulation around this oil field) (Higley, 2013). The Sooner Trend, first discovered in 1942 and was estimated to hold 320 million barrels of oil, believed to be hosted in fractured Mississippian carbonate rocks (Ball et al., 1991). Another limitation of the basin model is that it assumes the Woodford total petroleum system was sourced solely from the Woodford Shale. However, the evidence from petroleum geochemistry (presented in Chapter V) suggests multiple sources of hydrocarbon, in which a significant contribution stem from Mississippian source rock (Al Atwah et al., 2017a; Wang and Philp, 1997a). Mississippian petroleum source rocks have been shown to exhibit good generative potential (as discussed in Chapter IV), have unique geochemical fingerprint and petroleum generation kinetics indicating that they can generate oil at lower temperatures than the Woodford Shale. Including Mississippian source rock in the Anadarko Basin model is crucial, as it will control the volume of generated hydrocarbons and may match what has been observed in the field with respect to large volumes of hydrocarbons that are produced from tight carbonate within the STACK play. All limitations considered, the Anadarko Basin modeling would benefit from improving the 2D grid surfaces of formation tops to match present-day oil accumulation of known oil fields, together with the inclusion of petroleum source rock of

248

Mississippian age. In doing so, a better model could be achieved that is closely comparable to field and analytical observations of rocks and fluids recovered from Devonian-Mississippian petroleum systems within the Anadarko Basin.

Approach

The workflow of constructing the petroleum system analysis and basin modeling of the Anadarko Basin used three major input elements, some of which are data generated from this study; while another input is obtained from published literature and public data. Figure 82 shows the petroleum system analysis and basin modeling workflow used in this study. Overall, the workflow can be divided into three major stages, starting with model construction (data input), with different types of data set feeding into the building the model. The second step involved rock and fluid simulation in which parameters are set and constrained and tailored based on the major element that the model is testing, such as thermal maturation, oil migration, and so on. The last stage is model calibration, where the model was validated by comparing modeled results with observed and measured data.

Building the model involved different types of data sets including data that are generated in this study, and data from published literature. Geochemical data input generated in chapters IV, V and VI were used in defining important aspects in the basin model such as source rock organic-richness, hydrogen index, petroleum generation kinetics and kerogen type. Geological data input was extracted from published literature on the Anadarko Basin discussed in Chapter I, together with the publicly available data such as USGS digital data series 69-EE library on the Anadarko Basin province. An important building block of the model is the zmap-format, 2D grid of structural surface of the Anadarko basin's formations ranging from Precambrian to present-day topography,

with a total of 26 surfaces imported to the Schlumberger software PetroMod© 2016.2. The grid surfaces were built based on formation tops from more than 220 wells across the Anadarko Basin (Higley et al., 2014, and references therein). Table 28 shows a list of the surfaces used to build the basin model and the layers' associated properties. Division of the basin stratigraphy and formation nomenclature was based on formation lithology, and age information was based on published literature, Oklahoma Geological Survey stratigraphy chart of the Anadarko Basin and the Cherokee Platform (Boyd, 2008). Overall PetroMod lithologies are associated with crucial chemical and mechanical properties such as permeability, porosity, chemical compaction, seal property, thermal conductivity and fracturing, among others (Adler, 1971; Johnson et al., 1988b). Petroleum-generation kinetics was assigned to the Woodford Shale using the predefined kinetics within PetroMod under Lewan(2002)_TII_(WoodSh), which is based on

hydrous pyrolysis experiment using Woodford Shale samples (Lewan and Ruble, 2002). The Woodford Shale kinetic parameters were predefined according to Lewan and Ruble (2002): experiments with an activation energy (Ea) of 52.16 kcal/mol and a frequency factor of 6.51×10^{16} h^{-1}. Moreover, by using the kinetics editor tool within PetroMod, a custom kinetic parameter was modified for Mississippian source rocks from hydrous pyrolysis results presented in Chapter III. Mississippian source-rock kinetics are set at activation energy of 40.24 kcal/mol and with a frequency factor of 8.85×10^{12} h^{-1}.

The third type of data used in constructing the basin model is the boundary conditions (Figure 82). The boundary conditions included heat flow history, sedimentary-water temperature, and paleowater depth. Heat flow data were obtained from publicly available online database at SMU Geothermal Lab (Blackwell et al., 2011). Figure 83 shows the present-day heat flow distribution map of the basement along with basement faults. Paleo-heat-flow was estimated by
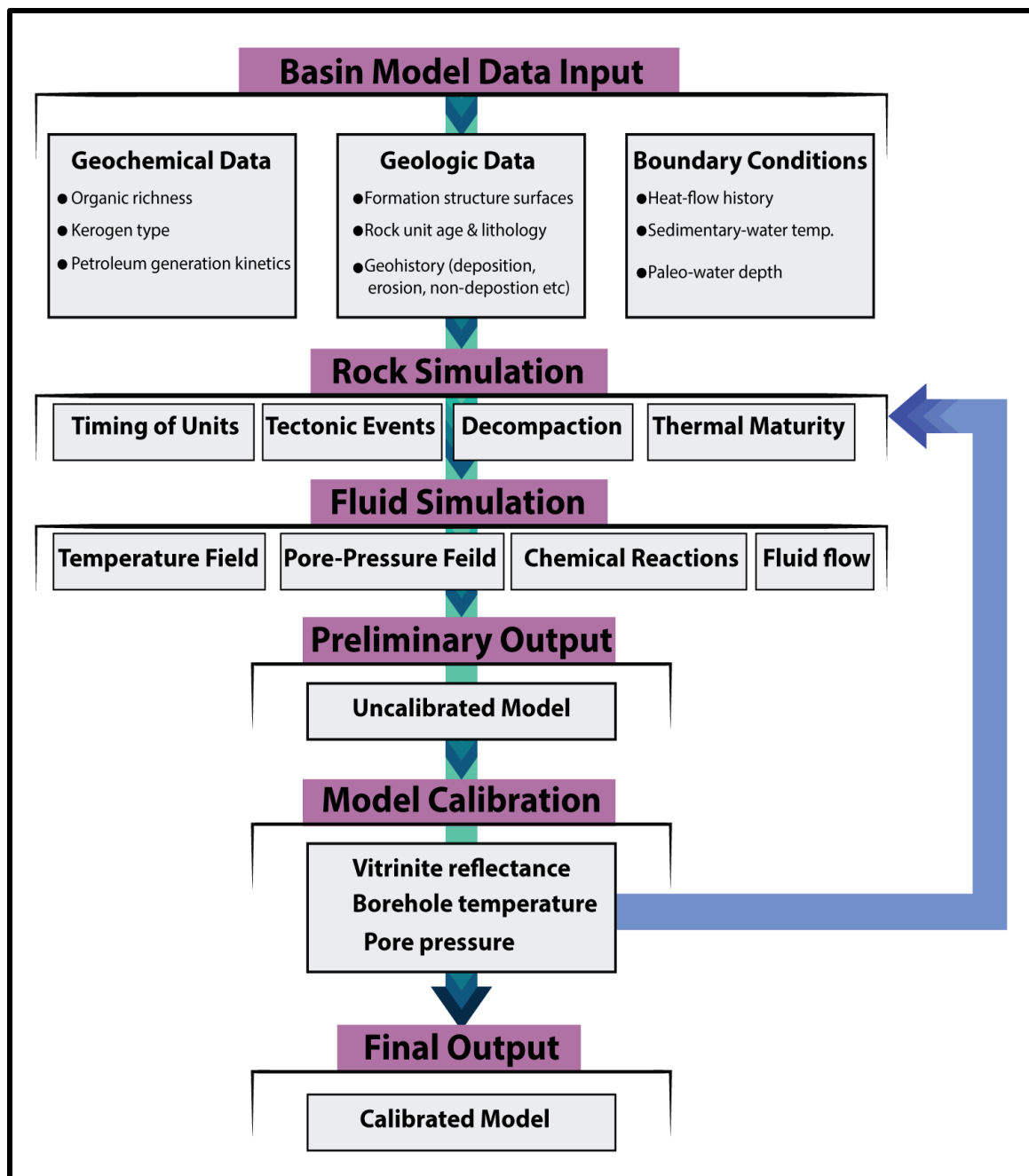
Figure 82: Basin modeling and petroleum system analysis workflow used in this study of the Anadarko Basin,. Adapted from (Peters, 2008).

Table 29 Key basin model stratigraphic input parameters including formation surfaces, age, deposition, erosion lithology, and petroleum system elements

Age	Surface Name	Deposition (Ma)		Erosion (Ma)		PetroMod Lithology	Petroleum System Element
		From	To	From	To		
Paleogene	Paleogene Erosion	0	0	50	0		
Cretaceous	Cretaceous Fm	110	50	0	0	Sandstone (clay rich)	Overburden
Permian	Permian Erosion	0	0	230	110		
Permian	Topography	256	230	0	0	Sandstone (clay rich)	Overburden
Permian	Chase Fm	302	256	0	0	Sandstone (clay rich)	Overburden
Pennsylvanian	Wabaunsee Fm	307	302	0	0	Sandstone (clay rich)	Overburden
Pennsylvanian	Douglas Fm	310	307	0	0	Sandstone (typical)	Overburden
Pennsylvanian	Cherokee Fm	312	310	0	0	Sandstone (typical)	Overburden
Pennsylvanian	Atokan Fm	315	312	0	0	Limestone (shaly)	Overburden
Pennsylvanian	Morrow Fm	320	315	0	0	Sandstone (typical)	Overburden
Mississippian	Springer Fm	332	320	0	0	Shale (typical)	Seal Rock
Mississippian	Miss Lime Fm	350	332	0	0	Limestone (ooid grainstone)	Reservoir Rock
Mississippian	U. Meramec Fm	355	350	0	0	Limestone (organic rich)	Source Rock
Mississippian	M Meramec Fm	370	355	0	0	Limestone (typical)	Reservoir Rock
Mississippian	L. Meramec Fm	375	370	0	0	Limestone (organic rich)	Source Rock
Devonian	Woodford Fm	443	375	0	0	Shale (organic rich, 8% TOC)	Source Rock
Silurian	Hunton Fm	446	443	0	0	Limestone (typical)	Underburden
Silurian	Sylvan Fm	457	446	0	0	Shale (typical)	Underburden
Ordovician	Viola Fm	461	457	0	0	Limestone (typical)	Underburden
Ordovician	Simpson Fm	488	461	0	0	Sandstone (typical)	Underburden
Cambrian	Arbuckle Fm	450	488	0	0	Limestone (ooid grainstone)	Underburden
Precambrian	Basement	1600	450	0	0	Granite (500 MA)	Underburden

calibrating the modeled paleo-heat-flow to match the measured vitrinite reflectance of the Woodford Shale across the Anadarko Basin. Vitrinite reflectance data was compiled from Brian Cardott from the Oklahoma Geological Survey (Cardott, 2012; Cardott and Lambert, 1985). Sediment-water temperature was estimated using the built-in tool within PetroMod for automatic calculation of SWT based on the study area latitude and longitude (Wygrala, 1989). Paleo-water depth was estimated using paleogeographic Blakey maps during Devonian-Mississippian time (Blakey, 2011).

After the model input was built and integrated, fluid and rock simulation was carried out through PetroMod 3D simulator module. In the simulator, certain parameters were adjusted to answer the study objectives. Within the basin model simulator, a total of 15 simulations were run, with the run control parameter set with previous readings of the temperate and pressure values to speed-up the computational time during the simulation. Moreover, the model sampling size was set at 1 km on both the *x* and *y* axes, with calculation steps set at a maximum time step duration of 1 Ma, with one maximum migration step calculation for each time step. The petroleum-migration simulation method was set at hybrid, which is a combination of Darcy and flowpath algorithms, together with a simplified version of percolation calculation. The hybrid migration method was defined using Darcy flow in cells with low permeability values, while flowpath was used at cells with high permeability, with the aim of speeding up the simulation processes. The determination of high and low permeability occurred via a preset permeability threshold within the reservoir-definition software dialog. Further, the reservoir definition is under the processes and tools as part of the simulation option that was adjusted, with a permeability threshold of 2.01 millidarcy and at 30% porosity. The edges of the basin were assumed to be closed during simulation, with faults were set as boundary elements, in which migration takes place along.
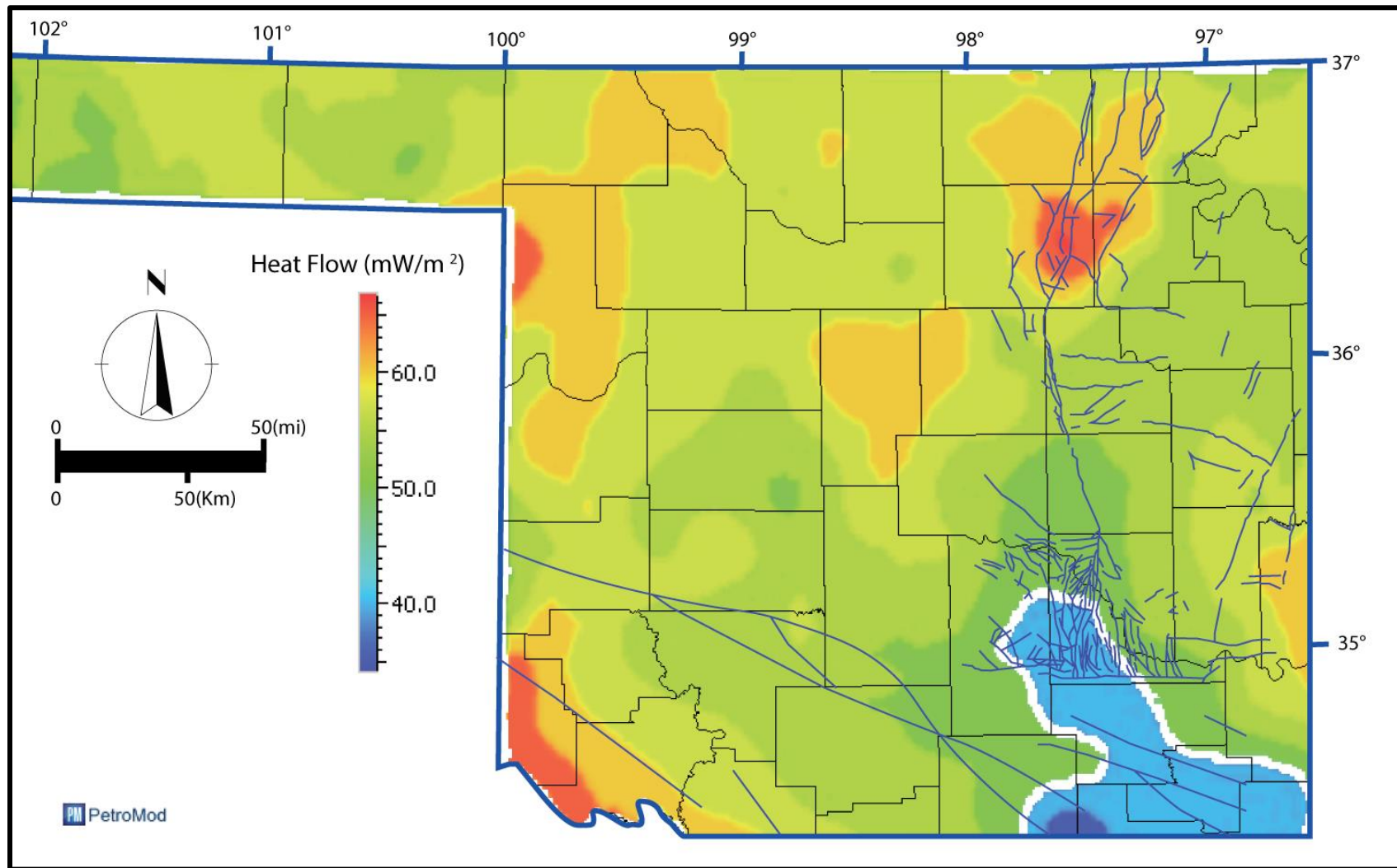
Figure 83: Present-day basement heat flow map of the Anadarko Basin superimposed on basement fault associated with Nemaha and Wichita uplifts, map was created using data downloaded from the Southern Methodist University Web site (http://smu.edu/geothermal/) (Blackwell et al., 2011).

254

the gridded fault boundary between the grid-cells of the formation surfaces. This approach is ideal for oil migration calculation through faults, whereby fault permeability is ignored, and assuming the faults without width where migration is controlled only by capillary pressure. Additionally, the secondary cracking option within the simulator processes and tools was adjusted to a maximum of 10 for the maturity-tracking factor. The tracking factor determines how many pseudo-components are used to generate and track their maturity as they evolve through geological time, with increasing the maturity tracking factor resulting in a more accurate secondary cracking calculation. The results of the simulation under the output overlays were set to generate basic, advanced and specialized output overlays

Quantitative diamondoid analysis modeling was carried out using a specialized diamondoid analysis tool. Modeling diamondoids involved four major steps including defining the diamondoid compounds, creating their kinetics, assigning the kinetics into the model and running the simulation. First, defining the diamondoid component within the oil was achieved by using the Components Editor. The kinetics of diamondoid formation was added to both Woodford and Mississippian source-rock kinetics in addition to the kinetics of black oil generation using the kinetics Editor tool in PetroMod. Then, the kinetics were assigned to source-rocks horizons within the 3D basin builder. The simulation process of quantitative diamondoid modeling is based on the following formula:

$$\% \; of \; liquid \; cracked \; to \; gas := \left[1 - {Co}/{Cc} \right] * 100, \hspace{2cm} \textbf{[Eq 6]}$$

where Co is the diamondoid baseline and Cc is the modeled diamondoid concentration as determined from PetroMod simulator. Afterward, simulation results were illustrated by overlying oil cracked to gas and then compared to actual measurements of diamondoids across the basin.

255

Burial History

      The modeled burial history of the Anadarko Basin reflects the four major basin phases through different sedimentation and subsidence rates. Figure 84 shows burial history extraction from the depocenter of the Anadarko Basin depicting the four major phases of the basin evolution. The first phase is characterized by a stable subsidence rate reflecting the first Precambrian igneous activities, which is associated with the failed rifting of the triple junction arm known as the SOA (Feinstein, 1981). This phase, according to our model, exhibited a slow subsidence and sedimentation rate. Subsequently, in the second phase during the Cambrian through Mississippian time, a cratonic passive-margin basin setting characterized the Oklahoma Basin; this setting is reflected in the burial history through the deposition of thick carbonates interbedded with shales. The subsidence and sedimentation rate were also higher than that of the first phase. Notably, the subsidence rate decrease in the middle of this phase, approximately during Silurian and Devonian time, likely due to lower energy depositional settings that resulted in the deposition of organic-rich Woodford Shale that is regionally pervasive with a lower thickness. The third phase of the Anadarko Basin's burial history marks the most active phase, tectonically. This is reflected in the modeled burial history with a dramatic increase in the subsidence rate during Pennsylvanian time (Figure 84). This phase persisted through Permian time, increasing sedimentary accommodation space together with an increase in sediments supply, shifting the sedimentary system from the low-energy carbonate-dominated system in Phase 2 to the clastic sedimentary system of Phase 3, which resulted in an overall shift from a passive margin and cratonic basin to foreland basin settings (Gilbert, 1992). From a regional tectonic perspective, it is believed that Phase 3 of the Anadarko Basin was initiated to the collision between the North American plate with the Gondwanan plate and the South American plate to the south, and the African plate to the east, as

manifested in the Ouachita-Marathon orogeny (Kluth, 1986). By the end of this phase, as indicated from the modeled burial history, the Anadarko Basin has reached the maximum burial depth approximately by the end of Permian and Early Triassic. This is crucial in delineating the maximum thermal stress of petroleum source rocks within the Anadarko Basin. Lastly, Phase 4 of the Anadarko Basin's evolution was the epeirogenic episode with episodes of basin uplift and erosion. This phase is signaled through the dominance of Permian rocks comprising the present-day topography sediments with minor deposition of Jurassic, Cretaceous and in some Paleogene rocks, suggesting that those rocks could have been deposited at a regional scale then subsequently eroded as the basin continued to uplift (Johnson, 1989b). Modeled burial history suggests a decrease in the overall basin subsidence rate followed by subtle subsidence then another period of erosion from Cretaceous to the present day, likely controlled by the Laramide Orogeny caused by the collision between the North American Plate with the Pacific Plate during the Late Cretaceous. During the fourth phase of the Anadarko Basin's history, many geological aspects remain
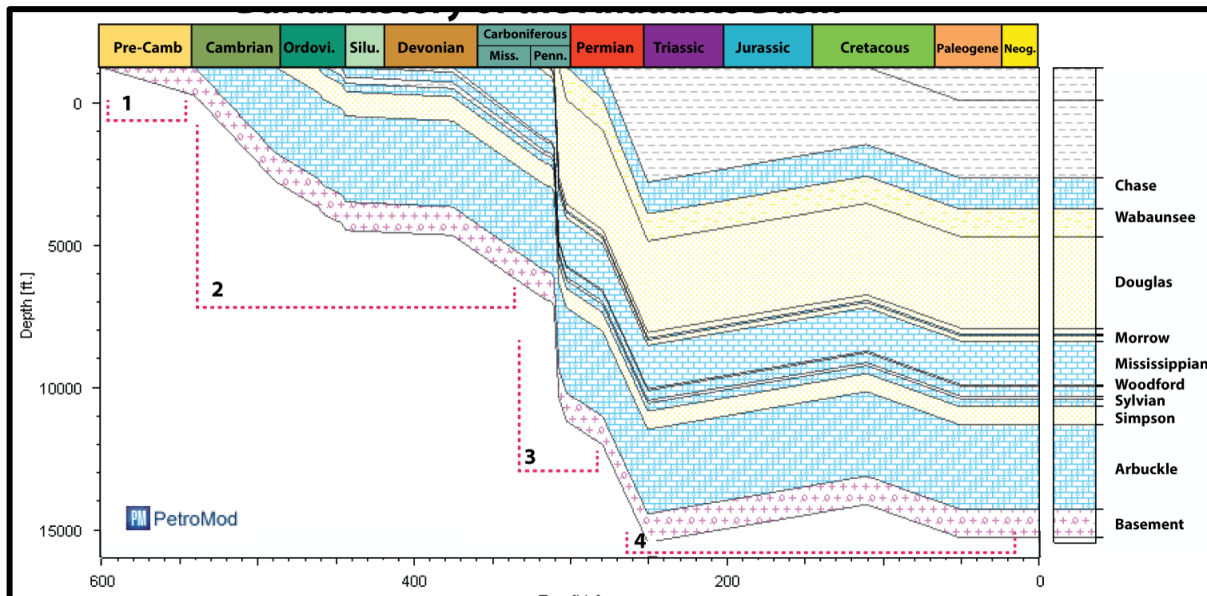
Figure 84: Burial history of the Anadarko Basin depocenter marked in numbers are the four major phases of the basin evolution which controlled sedimentation and subsidence rates.

unknown, partly because of the lack of direct evidence. Thererfore, some assumptions have to be made and then calibrated with indirect evidence, for example, the effect of uplift and the eroded section is one of the key factors in modeling the basin.

In general, the burial history is relatively stable across the basin with a difference in the magnitude of subsidence rate and sedimentary rock thicknesses, with higher magnitudes moving towards the basin depocenter and a decrease in those magnitudes moving away from the depocenter towards the Anadarko Shelf and the Nemaha Uplift. Interestingly, some localized depositional anomalies exist within the basin in close proximity to the Nemaha Uplift, in which erosion events were dramatic, as relatively young formations overlie the basement rocks. Therefore, due to the variation in the magnitude of deposited formation, the thicknesses, maximum burial history and associated thermal stresses also varied across the basin, which is also largely controlled by the subsidence rate and sediments supply, together with the thickness of the eroded section. With the latter being the most critical yet challenging task to accurately measure in the present-day geological settings due to the lack of evidence, however, a number of different techniques can be used to infer such information, as discussed in the following section.

Exhumation and Eroded Section

The inherent geological complexity of the Anadarko Basin's evolution involves a number of exhumation episodes that ultimately led to the erosion of sedimentary formations ranging in age from Permian to Pliocene. While the main Permian red-bed clay-rich formation covers most of the Anadarko Basin's topography, a limited occurrence of Mesozoic and Cenozoic units are observed in different localities within the Anadarko Basin. Jurassic- and Cretaceous-aged red-bed

formations are encountered in the subsurface in the western portion of the Oklahoma and Texas panhandle, which presumably extended to the eastern part of the Basin and subsequently eroded before Jurassic Cenozoic erosion event (Cunningham, 1961b). Another example of the eroded section includes the Cretaceous formation, as reported in western Oklahoma, suggesting that the basin at some point was covered with the Cretaceous formation (Adler, 1971; Johnson, 1989b). Late Miocene to Pliocene deposits are also absent throughout the Anadarko Basin, but those deposits are observed as fluvial deposits (i.e. Ogallala Formation) of 257 m thickness at the Texas Oklahoma panhandle region (Cunningham, 1961b). The overall limited presence of deposits ranging from Jurassic to Pliocene in age scattered across the Anadarko Basin suggests those formations may have been regionally deposited and eroded during different exhumation episodes as part of the Anadarko Basin's evolution.

Further evidence for exhumation and erosion within the Anadarko Basin is observed from geothermal profile discrepancies. Present-day depths and geothermal gradients do not match the observed thermal stresses to which the organic-rich shales have been exposed, which in turn reflects the paleo-geothermal settings. Moreover, measured vitrinite reflectance of the Woodford Shale across the Anadarko Basin showed a systematic increase with increasing depth, with the Woodford Shale reaching anthracite rank at 4.29% and 4.89%Ro, indicating that these rocks were exposed to temperatures up to 400°C. In contrast, the present-day geothermal gradient puts these rock at a maximum 250°C with a geothermal gradient of 20 to 24°C per km (Cardott and Lambert, 1985; Carter et al., 1998). This difference implies that overall strata of the Anadarko Basin were at higher temperatures and hence at greater depths, which subsequently exhumed and eroded deposits of Permian to Pliocene age. Therefore, the present-day geothermal structure of the

Anadarko Basin compared to paleo-geothermal history supports the stratigraphic evidence suggesting the Anadarko Basin has been exposed to episodes of uplift and erosion.

The accurate thickness of the eroded section across the Anadarko Basin is one of the major unknown aspects of the basin that can be inferred. Several attempts to estimate the missing section are published in the literature, using different approaches resulting in a significant difference, ranging from 1500 ft to 8000 ft. One of the approaches used to estimate the amount of sediment eroded is using the vitrinite reflectance depth profile, in which a regression line interpolation upward to intercept with $0.2\%R_o$ would estimate the thickness of eroded sediments. Waples (1980) used a model of vitrinite reflectance from worldwide basins, estimating about 3900 ft of sedimentary beds were eroded in the Anadarko Basin. Another study utilized the age spectra of microcline-baring clasts, estimating around 6550ft of sediments were removed (Harrison et al., 1987). Moreover, Schmoker (1986) assumed 2600ft of erosion taking place to model onset of the oil window within the Anadarko Basin, utilizing Loptin's time–temperature index (TTI). Overall, those studies used a single value of the eroded sediment thickness, and other studies used wide-variable thicknesses. According to Cardott and Lambert (1985), vitrinite reflectance and depth profile plotted in a semilog *x*-axis with linear regression fitting estimated erosion thickness across the Anadarko Basin ranging from 1500 ft to 4000 ft since the Permian. Maximum temperature was reached during the Wichita orogeny of Pennsylvanian, which is a much lower temperature than present-day conditions (Cardott and Lambert, 1985). A subsequent study also investigated vitrinite reflectance to better reconstruct the Anadarko Basin's burial history and argued that exhumation behavior differs based on sample location; for example, samples collected from the depocenter ought to exhibit higher erosion thickness than thin sediments within the shallow stable shelf region (Pawlewicz, 1990). Therefore, using this variable eroded-thickness approach, wells were classes

260

as shallow shelf or deep basin, whereby the shallow-shelf area is estimated to erode 3200 ft, and the missing section from the deep basin province is estimated at 8000 ft (Pawlewicz, 1990). In a more recent work, using a basin-modeling approach, an eroded section related to Permian-Cretaceous erosion was set at 1640 ft, while post-Tertiary erosion was estimated at 200 ft to 600 ft (Higley, 2014a).

The amount of eroded section was one of the unknowns in our study that we used as a boundary condition for calibration. However, some of the erosion aspects were inferred, as suggested by other workers, such as the variation of eroded thickness based on the overall basin geometry and the magnitude of the exhumation (Pawlewicz, 1990). After running different simulations, the best-model calibration was achieved by assigning maps of erosion surfaces during Mesozoic and Cenozoic time. Total erosion is estimated at 2500 ft at the Anadarko Basin depocenter, aligned with the SOA, which gradually decreased in eroded thickness towards the Anadarko Shelf, reaching valuse as low as 500 ft. Towards the Nemaha Uplift, particularly east of the Nemaha Uplift, is a structurally complex fault system, which could arguably be influenced by higher erosion due to reactivation of basement faults resulting in uplift of larger magnitude than the stable shallow shelf of the Anadarko Basin. In particular, the Nemaha faults system is believed to originate during the middle Ordovician, resulting in subtle paleo-high topography as a result of the Acadian orogenies to the east side of North American Plate (Gay Jr, 1999a). However, it was not until the Late Pennsylvanian that prominent Nemaha movement occurred, resulting from compressional forces linked to the Alleghenian orogeny and exhumation manifested in different fault systems (Gay Jr, 1999a, 2003b). Therefore, the erosion trend from the basin depocenter gradually decreased to 1000 ft towards the Nemaha Uplift Province to the east of the study area. While it is possible that erosion surfaces could have been more complex and heterogeneous with

respect to its topography than that of a simple decreasing trend from the basin outwards. However, in this study, we used a simple erosion trend which is adequate to achieve a calibrated model that matches measured maturity trends.

Model Calibration

Model calibration was based on two major measured elements including source-rock maturity and fluid types. Model calibration using source-rock maturity was based on vitrinite reflectance measurements of the Woodford Shale, with updated reflectance data included Cardott (1998) (Figure 34). Moreover, depth profiles of vitrinite reflectance values were taken from a collection of 14 wells, of which 14 one-dimensional basin models were used for thermal calibration (Figure 85). Moreover, geochemical data particularly related to maturity and oil cracking, together with diamondoid concentration for hydrocarbon mixing was compared to modeled oil-to-gas ratio and total bulk accumulation composition. The unknown variables that were calibrated to match
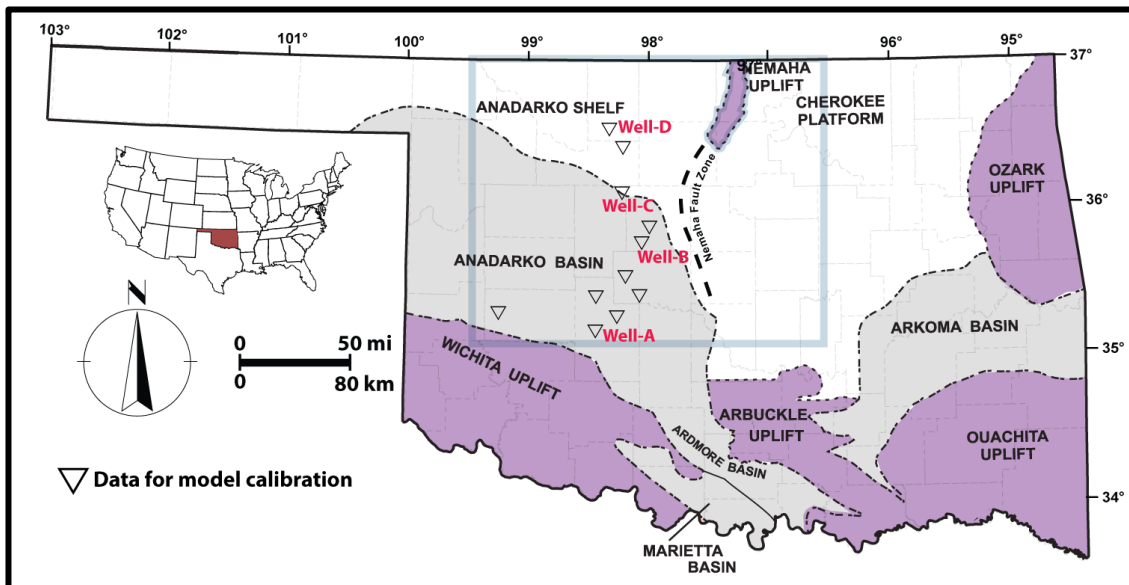
Figure 85: Distribution of wells used in calibrating the model with vitrinite and bottom-hole temperature, from (Pawlewicz, 1990).

observed rock maturity and fluid composition include paleo-heat-flow, erosion and uplift, and migration pathways. Those variables were adjusted based on maturity, following Sweeny and Burnham's (1999) easy vitrinite reflectance model in which modeled maturity best matched measured vitrinite reflectance depth profiles.

The best fit between measured and modeled thermal maturity and present-day geothermal gradient was determined by running a number of simulations. Shown in Figure 86 are examples of the 1D model calibration used as input for the 3D overall model calibration. This calibration was achieved by finding the optimal boundary condition values, together with fine-tuning the thickness of eroded sediments. For boundary conditions, paleo-heat-flow was adjusted with a decreasing trend of paleo-heat-flow with time. This helped best fit the high vitrinite reflectance values with modeled curves for sediments that are deeply buried within the Anadarko Basin. Since the basin had initially been exposed to intensive igneous activity during its early phases of development, this igneous activity suggests that it exhibited a higher geothermal gradient during Precambrian to Cambrian time, which gradually decreased during the second phase of cratonic basin settings. Figure 86 presents different sets of modeling scenarios; one model is calibrated with invoking series of depositions, uplifts and erosions in solid line, while the other uncalibrated model (doted line) shows continuous deposition. In the uncalibrated model, it is assumed that no erosion took place. Therefore, maximum burial depths are equivalent to the present-day depths. However, this model does not match the overall paleo-heat-flow that is measured from the reflectance of vitrinite, which indicates higher maturity stages. In this uncalibrated model, modeled thermal maturity is underestimated by $0.2\%R_o$, which increases with depth to about $0.5\%R_o$ offset. This offset could result underestimated maturity, in which case the basin model predicts that actual source rocks within the oil window to be thermally immature. Therefore, it is crucial to introduce
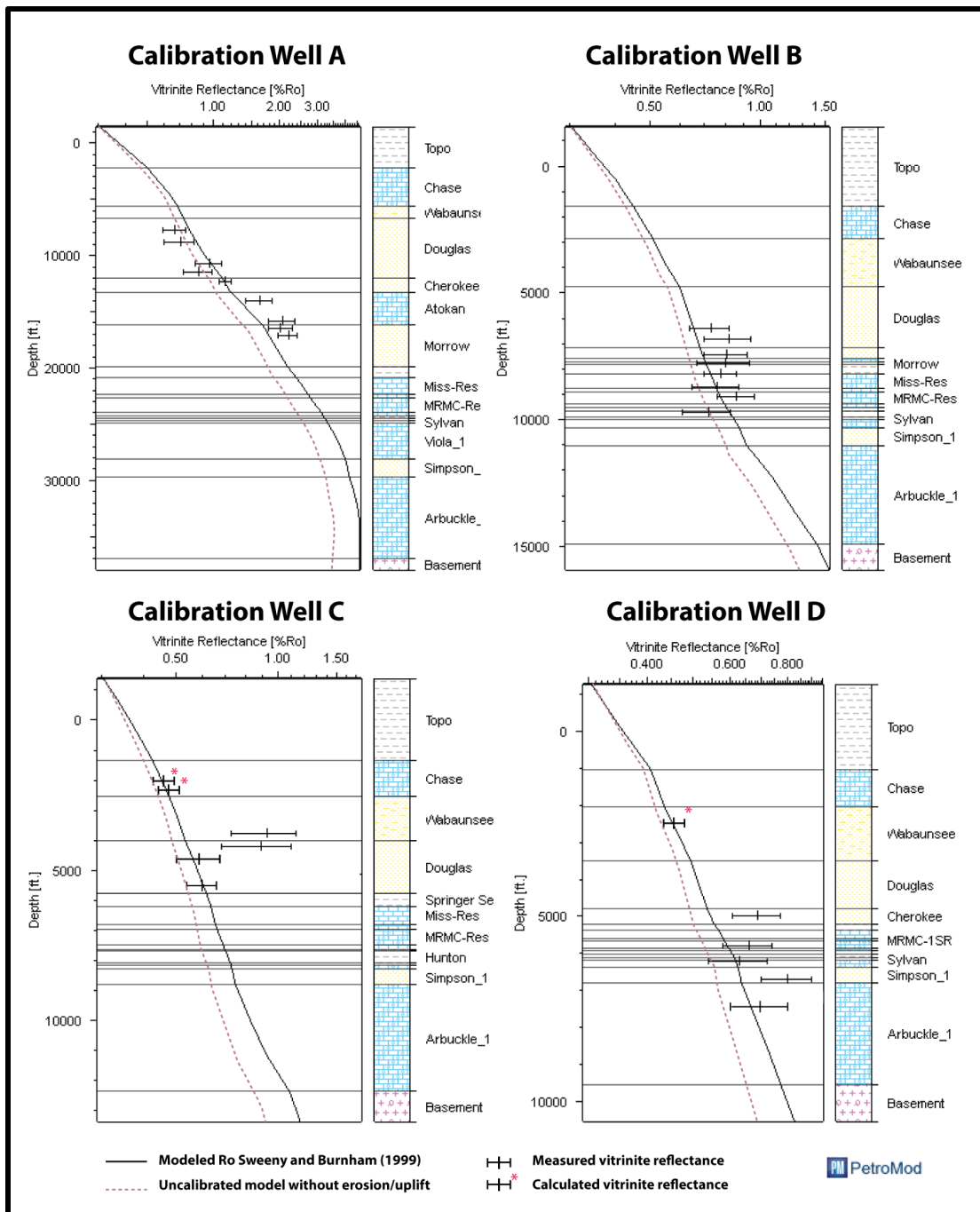
Figure 86: Examples of 1D model extraction from 3D basin modeling showing modeled maturity and measured vitrinite reflectance, with solid line representing calibrated model, while dotted line is the uncalibrated model, data point with asterisk are Tmax values converted into vitrinite reflectance.

episodes of erosion and uplift of the basin so that the modeled maturity trend closely matches observed maturity of the rocks. This calibration for best match also indicates that the maximum burial history was higher than the present-day depths.

Another data input used for calibrating the model is bottom-hole temperature and present-day thermal regime. Log-header bottom-hole temperatures are inherently hindered by different processes associated with drilling that alter the actual formation temperature. Therefore, a number of correction approaches have been developed to account for the drilling-mud circulation effects to back-calculate the actual formation temperature (Corrigan, 1997; Facer, 1991; Zare-Reisabadi et al., 2015). Temperature values were corrected using the Harrison and Luza's (1986) approach, and temperature data used are from the publicly published data set (Pawlewicz, 1990). The similar wells that were used for vitrinite reflectance to calibrate paleo-heat flow were used from a present-day temperate calibration shown in Figure 86. Present-day heat flow was included in the basin model as a 2D map, with values mostly averaging at around 50 mW/m^2 (Figure 87). The thermal regime of the present-day condition of the Anadarko Basin provided another line of evidence to check the validity of the model. Figures 86 and 87 display four example wells marked in the map of Figure 85. Good correlation is observed between the modeled temperature curve and measured temperature readings from those wells. The best correlation between bottom-hole temperatures and modeled temperature is observed in Wells B and D, followed by A and C. The overall temperature trend is observed to be higher in the deeper part of the basin, which decreases towards the Anadarko Shelf. Well A together with wells located in depocenter (Figure 87), and based on modeled temperature, indicates that Mississippian strata are at around 150°C in the deepest part of the basin, decreasing to around 50°C in Well D within the Anadarko Shelf.
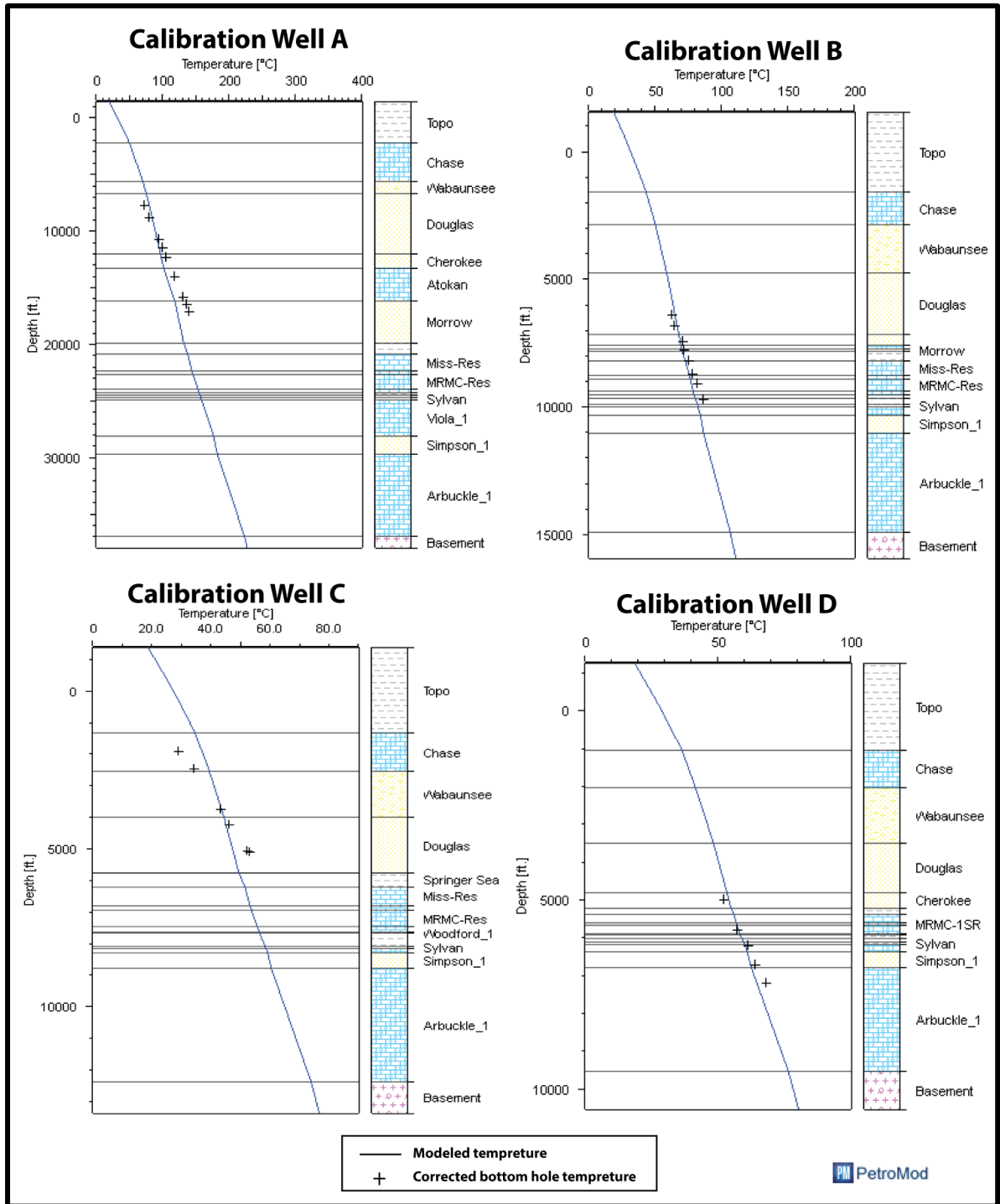
Figure 87: Examples of 1D model extraction from 3D basin modeling showing modeled present-day temperatures with measured corrected bottom-hole temperatures that are corrected using Harrison and Luza (1986) formula; temperature data source was used from Pawlewicz (1990).

Thermal maturity map for the Woodford Shale based on measured vitrinite reflectance served as another source of data for calibrating the basin model. The Woodford Shale is an extensively studied rock formations in Oklahoma, with a good data set for vitrinite reflectance having been published in a number of studies (Cardott, 1998, 2017; Cardott and Lambert, 1985). By utilizing maturity dataset, a 2D vitrinite reflectance map was built using a correlation-gridding technique with Trinity software (Zetaware), and gridding vitrinite reflectance values taking into consideration the overall structural surface of the Woodford Shale. Figure 88 shows the 2D maturity maps that were created from vitrinite reflectance measurements. This map was used to calibrate the model to achieve the best match by fine-tuning paleo-heat-flow. The modeled Woodford maturity maps were created using Sweeny and Burnham's (1999) thermal maturity modeling within PetroMod. A clear correlation between measured vitrinite reflectance and modelled results provides further evidence of the validity of the basin model calibration.

Petroleum Generation in Mississippian Rocks

The calibrated basin model of the Anadarko Basin shed light on petroleum generation and migration within the Mississippian organic-rich rocks. Particularly, strong geochemical evidence presented in this study suggests that organic-rich rocks within Mississippian formations are capable of generating hydrocarbons, with a unique oil fingerprint. Basin modeling results were used to assess the timing and volume of generated hydrocarbons within the Mississippian petroleum source rocks. The petroleum generation rate is higher in Mississippian source rocks compared to rocks of the Woodford Shale, which is largely controlled by the kinetic parameters of each rock formaiton and the heating rate over geological time. Figure 89 compares the transformation ratio results from basin modeling between Woodford and Mississippian source

267
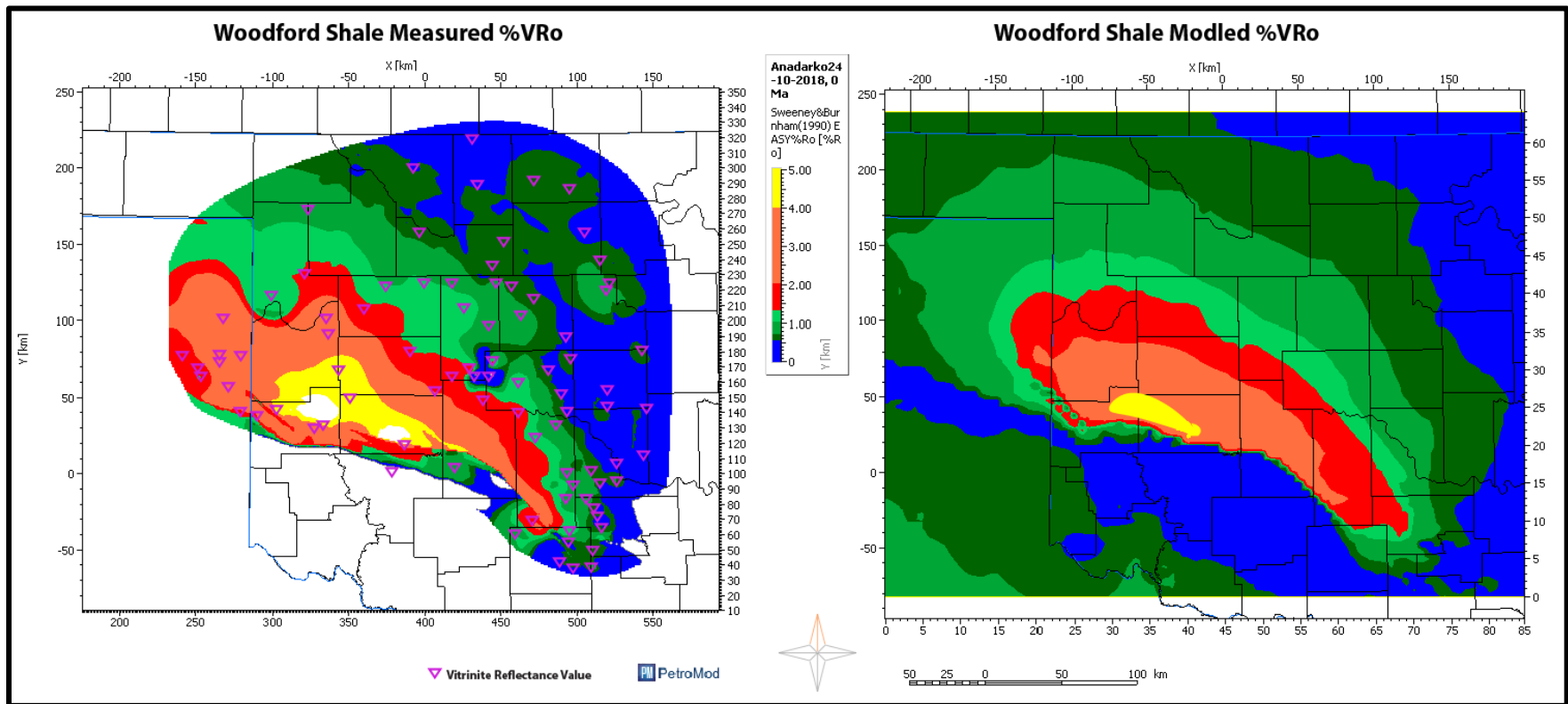
Figure 88: Maturity maps of the Woodford Shale comparing measured vitrinite reflectance (left) to modeled thermal maturity using Sweeny and Burnham (1999) Easy vitrinite reflectance model. Measured values are collected from Brian Cardott (1990).

rock. Transformation ratio is defined as the converted reactant hydrocarbons mass in comparison to the initial hydrocarbon potential, which is time- and temperature-dependent, as described by the Arrhenius's law (discussed in Chapter IV). While higher reaction orders of the transformation ratio can be used for nonlinear relationships, the transformation ratio is considered in this study as a first order reaction (Hantschel and Kauerauf, 2009). Evidence for the first-order reaction of petroleum formation from source rock is illustrated through time-series of hydrous pyrolysis experiments. Generated oil from hydrous pyrolysis with experiment times ranging from 22–238 h followed a linear relationship, validating the first-order relationship for oil generation, with expelled oil increasing over experiment time (Lewan and Ruble, 2002). Based on transformation ratios of modeled results from the depocenter of the Anadarko Basin, Mississippian source rocks start to increase in transformation ratio around 40 Ma earlier than the Woodford Shale (Figure 89). More specifically, 100% transformation of Mississippian source rocks is reached by Middle to
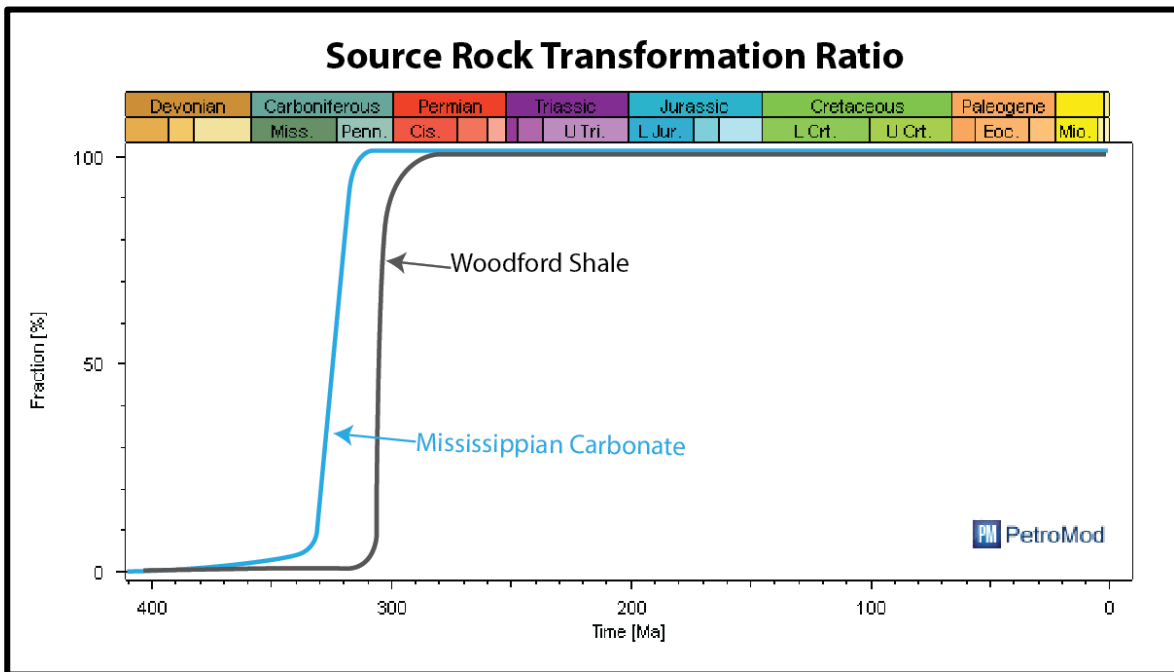
Figure 89: Transformation ratios of Mississippian Carbonate and Woodford Shale from the depocenter of the Anadarko Basin at Well A.

Late Pennsylvanian time, whereas Woodford Shale reaches complete transformation by Early Permian time. Although the Woodford Shale has been deposited prior to the deposition of Mississippian carbonate, Mississippian source rocks start petroleum generation earlier than the Woodford Shale.

Transformation ratios and thermal maturity varied across the different play types including Anadarko Shelf, STACK play and central Oklahoma. Figure 90 depicts a different burial histories, overlaid with the modeled thermal maturity of the different plays examined in this study. Thermal maturity of both Mississippian and Woodford source rocks within the Anadarko Shelf is not adequate for the observed petroleum accumulation in oil fields within the Shelf. Hence, this suggests that the majority of these oils are sourced from the deeper part of the basin. The Anadarko Shelf's burial history of Devonian-Mississippian formations reached a maximum depth of 5,500 ft according to modeled results. This depth not sufficient for older source rocks such as Simpson or Arbuckle Formations to generate oil locally. In contrast, the STACK play burial history and modeled maturity indicate that Devonian-Mississippian rocks are within the oil window, reaching a maximum depth at around 9000 ft, such local generation of those oils is very likely. Similarly, areas of Central Oklahoma are within the oil window, with Devonian-Mississippian source rocks reaching maximum burial at 6500 ft; suggesting local fluid sourcing of petroleum in these reservoirs is possible. However, thermal maturity is higher in the STACK play than in central Oklahoma, with modeled maturity suggesting peak-oil generation stage (Figure 90). It is also important to note that the maturity modeling did not consider any geothermal anomalies resulting from hydrothermal events. Those geothermal anomalies do exist, especially in closer proximity to the Nemaha faults system, so that modeling might be underestimating thermal maturity in areas where hydrothermal fluids played a role in the thermal maturation of Devonian-Mississippian

source rocks. While hydrothermal fluid activities were not considered in the Central Oklahoma Province, our basin modeling results suggest that these source rocks would still be within the early oil-window stage, regardless of the effect of hydrothermal fluids. The reason for not considering any geothermal anomalies within the Nemaha Province is due to the difficulty of mapping its distribution and identifying the timing of its occurrence. Some features associated with the gravity and magnetic maps were identified, and other geothermal anomalies are reflected in the vitrinite reflectance measurements. However, those anomalies are further east of the study area, close to the Ozark Uplift, so they were not included in the model (Cardott, 2012; Elebiju et al., 2011).

An important aspect of petroleum generation from Mississippian source rocks is organic richness and lateral continuity across the basin. While we present evidence that organic-rich beds within the Mississippian formation are capable of generating petroleum, it is not clear whether such facies are regionally present through the Anadarko Basin. Due to the complexity of the Mississippian carbonate depositional system of gently sloping carbonate ramp. In particular, Mississippian carbonate ramp exhibits a number of prograding clinoforms that varied spatially, hence, it is arguably plausible to postulate that Mississippian organic-rich beds are discontinuous geometries (Wilson et al., 2017). Several studies have investigated the stratigraphic distribution of the Mississippian formation subunits based on lithology and petrophysical log-response. A broad subgroup division was proposed to divide the Mississippian formation into Osagean, Meramecian, and Chesterian, and was mapped out throughout the Anadarko Basin (Jordan, 1959; Sutherland, 1988). A subsequent study did some work with Mississippian formation on a regional scale for the southern Midcontinent region and subdivided
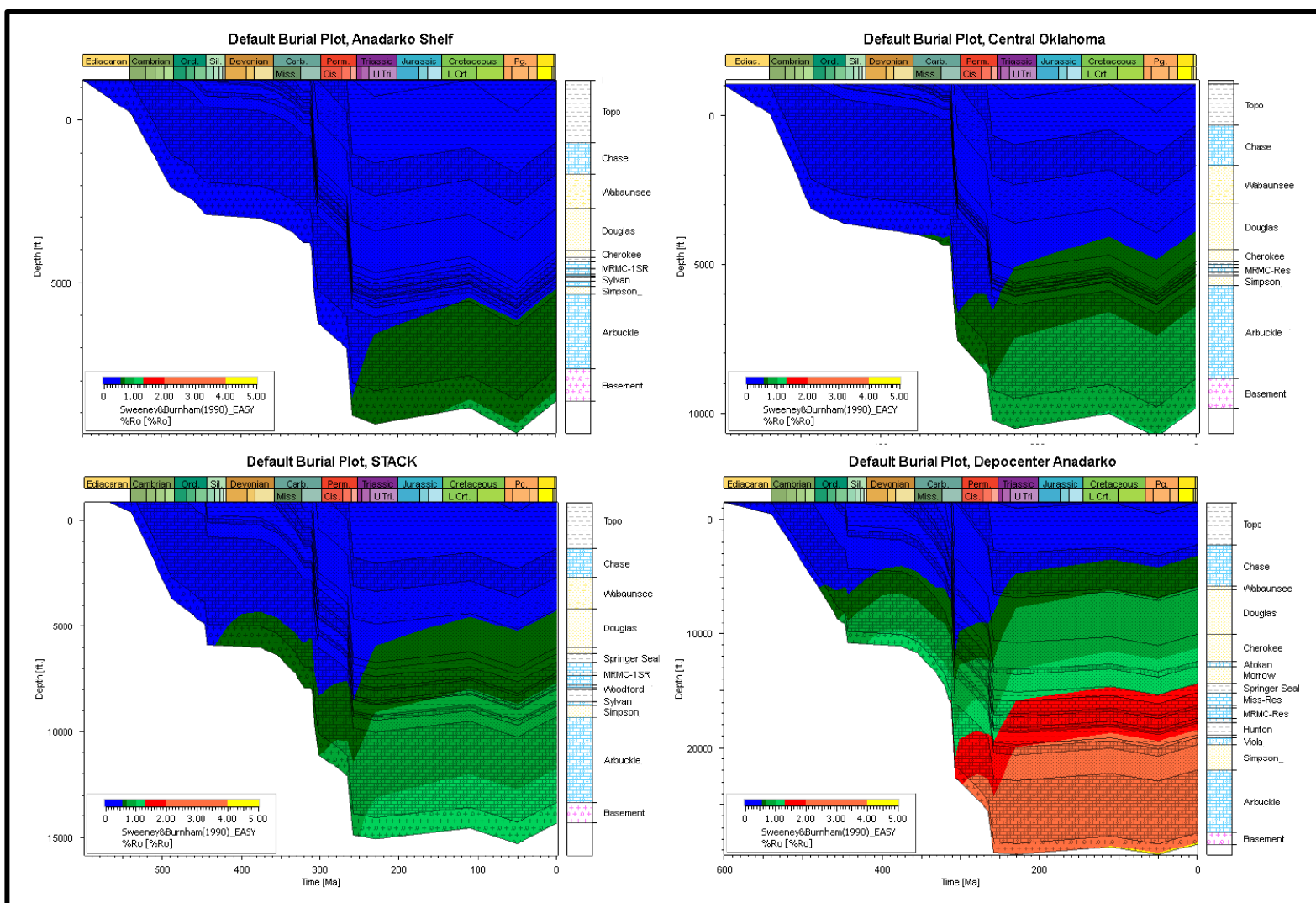
Figure 90: Burial history extractions from the 3D basin modeling over different plays within the Mississippian formation overlaid with modeled thermal maturity using Sweeny and Burnham (1990) Easy Ro model.

the Mississippian into upper and lower units (Johnson et al., 1988b). The Upper Mississippian encompasses the Chesterian and Meramecian Series, with limestone and shales being the predominant lithology, whereas the Lower Mississippian includes Osagean and Kinderhookian Series, composed of carbonate sandstone and shales. In this study, regional lithology trends were mapped, with no indication of organic-richness (Johnson et al., 1988b). Those general lithology trends were used to construct the facies maps in the basin model, with the assumption that Mississippian organic-rich zones are continuous throughout the basin for oil-generation. Therefore, the lateral extent of those Mississippian source rocks is a key factor controlling the volume of generated oil, and hence, future geological studies mapping those facies would be of great significance.

Hydrocarbon-Charge Timing

The element of timing is crucial in petroleum-system analysis studies, particularly with respect to evaluating petroleum prospects in conventional petroleum accumulations (Magoon and Dow, 1994). Moreover, determining the hydrocarbon-charge timing is a key factor of a petroleum system, in which it must occur after the trap formation. Combining petroleum systems and basin modeling analysis with fluid-inclusions study can shed light on episodes of petroleum migration. The petroleum system and basin modeling analysis is used to reconstruct the thermal history of the basin over geological time, while fluid-inclusion microthermometry is used to measure the temperature at which petroleum migration took place as reflected in homogenization temperature. Therefore, by comparing homogenization temperature to the thermal history of a basin, one could infer the timing of hydrocarbon charge. For example, a study of Ghazal field in Saudi Arabia examined fluid inclusions in Lower Permian Unayzah sandstones within the Arabian Basin (Arouri

et al., 2010b). The field is known for its predominant gas and condensate production, in which it necessitates a geological-geochemical understanding to predict prospectivity of nearby structures and optimizing field development of existing discoveries. Hydrocarbon charge-timing was determined by measuring the homogenization temperatures of oil inclusions and coexisting aqueous inclusions, and these were compared to time-temperature plots generated from the basin model. All combined, the authors concluded that Ghazal field accumulations are a result of multiple hydrocarbon charges from the kitchen area, which included four major periods of oil and condensate migration episodes (Arouri et al., 2010b). More specifically, within the Anadarko Basin, attempts to identify petroleum-generation timing were made solely through a basin-modeling approach, with no evidence of microthermometry of fluid inclusions. According to Higley (2013), the onset of the Woodford Shale petroleum generation took place during Late Mississippian time (330 Ma), whereas peak-oil generation was from 300 to 220 Ma. However, timing provided in this study only reflect generation timing based on thermal maturity modeling, and which is not necessarily representative of secondary petroleum migration and timing of reservoir filling episodes. To answer such questions related to the timing of hydrocarbon charge we combined fluid inclusion with basin modeling of the Anadarko Basin.

The calibrated basin model of the Anadarko Basin was used to generate time-temperature plots depicting thermal history at locations where fluid inclusions were recovered. An overall temperature time-plot of the Anadarko Basin reflect the geohistory of the basin with its four major phases. Figure 91 shows a temperature-time plot with inferred timing of hydrocarbon charge episodes. Homogenization temperatures of aqueous-inclusions co-existing with oil inclusions are described in Chapter VI. In general, hydrocarbon charge can be divided into four periods of hydrocarbon charge, three of which occurred prior to the third phase of the Anadarko Basin

geological evolution. First oil entrapment as evidenced from homogenization temperatures of fluid inclusions occurred at 282 Ma from sample SMD-2216. This is the lowest temperature compared to the rest of inclusion measurements. This indicates that SMD-2216 within central Oklahoma marked the first hydrocarbon charge of lower maturity fluids. Second hydrocarbon charge occurred at 262 Ma from AM-8371 inclusions within Kingfisher County. Third and possibly fourth hydrocarbon charge periods are more challenging to interpret, with the possibility of two events at different geological periods exhibiting similar temperatures modeled temperature of those inclusions. Moreover, oil and aqueous inclusions obtained from Blaine (GS-9698), and Canadian (CA-1-99336-B) counties exhibited the highest homogenization temperatures of primary inclusions at 149°C. According to the modeled temperature history of the Mississippian formation, homogenization temperature values of GS-9698, and CA-1-99336-B samples could have occurred at 255 Ma or 55 Ma. It is very likely that inclusion entrapment occurred on both periods, representing the highest maturity hydrocarbon-charge contribution to Mississippian reservoirs. It is presumably possible for higher maturity fluids to be migrating as the Anadarko Basin continued to subside during the third phase of the Anadarko Basin geological evolution as reflected in the burial history (Figure 84). This is also supported by the modeled thermal maturation, during 255 Ma the depocenter of the Anadarko Basin have entered the gas window (Figure 90). Similarly, it is very likely for oil tertiary migration to occur at later stages of the Anadarko Basin, particularly after the fourth phase where uplift and tilting associated with the Laramide orogeny took place (Johnson et al., 1988b). Additionally, diamondoid results of oils recovered from areas west of the Nemaha Uplift suggest a mixing element of oils with various maturity stages. Those could reflect the observed entrapment periods of those fluid inclusions (Figure 91). Therefore, oils within STACK play and the Anadarko Shelf mixing took place with first low maturity hydrocarbons

filling Mississippian from 282 Ma to 262 Ma, while subsequent mature hydrocarbon charge took place during 255 Ma, together with the possibly of petroleum re-migrate during Paleogene time (55 Ma). Such information is crucial in exploring for oil, particularly for areas within the west of the Nemaha Uplift in-which hydrocarbon charge occurred over different periods, ultimately lowering the hydrocarbon charge risk (hydrocarbon charge is very likely). In contrast, areas east of the Nemaha Uplift exhibited a single hydrocarbon charge that likely took place during 282 Ma. Therefore, for the trapping of those fluids in structural and stratigraphic closures must occur prior to 282 Ma, so that area can be characterized with a higher risk of hydrocarbon charge.

The timing of hydrocarbon charge in Mississippian reservoirs is not restricted to the periods discussed above. Arguably, hydrocarbon charge could have occurred at a different timing than suggested. Perhaps, for example, the examined fluid inclusions are not necessarily representative of the complex process of petroleum migration over the vast area within the Anadarko Basin. However, this approach provides a measured line of evidence that can be improved with more examination of fluid inclusion samples, which could in future refine the periods of hydrocarbon charge by providing a statistically significant number of data inputs. Moreover, the mechanism of fluid-inclusion entrapment preserves much information reflecting the fluid physical and chemical properties at which it was entrapped as a crystal impurity of Mississippian rocks. Therefore, it is very likely that hydrocarbon charge and reservoir filling occurred in the periods suggested in Figure 91, but hydrocarbon charge is not strictly exclusive to those periods.

Petroleum Migration and Diamondoid Modeling

Petroleum-migration and diamondoid modeling results suggest a different petroleum migration-and-accumulation mechanisms across the Anadarko Basin and the different

Mississippian plays. Figure 92 illustrates modeled petroleum migration pathways within the Mississippian reservoirs, depicting the different migration mechanisms across the Nemaha Uplift. Starting with petroleum migration modeling, two mechanisms can be attributed to the Devonian-Mississippian petroleum systems, including hybrid-distance migration and short-distance migration. Modeling results suggest that the hybrid-distance migration is likely occurring west of the Nemaha Uplift, mainly across the Anadarko Basin and the broad shallow shelf extending from north Oklahoma into Kansas. The modeled hybrid-distance migration is dominantly associated with the long-distance migration pathways, with some areas associated with a short-distance migration pathways. Therefore, Mississippian reservoirs are distally and proximally sourced, over areas such as the STACK play and oil fields within the Anadarko Shelf. Moreover, modeled
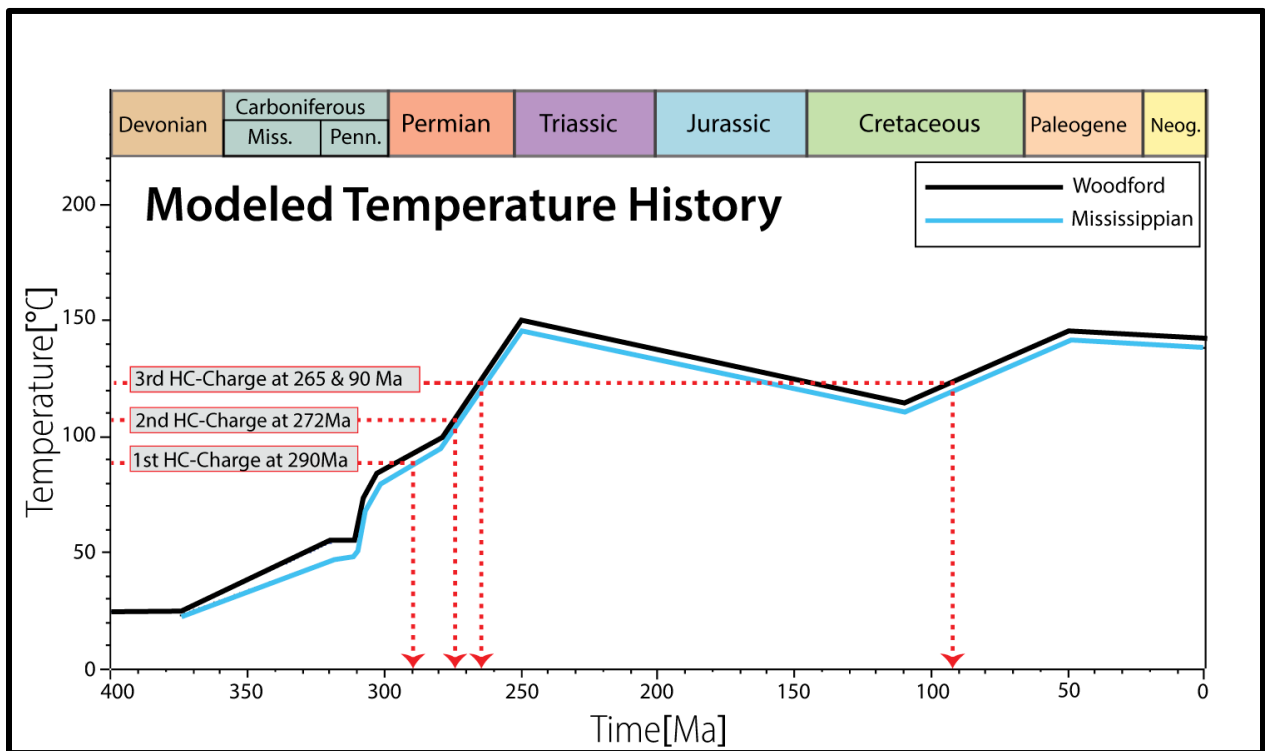
Figure 91: Temperature–time plot of locations where fluid inclusions were obtained; modeled temperature is extracted from 3D calibrated basin model; entrapment time of fluid inclusions are marked in million years (Ma).

277

diamondoids indicate that oil accumulation associated with the hybrid-distance migration mechanisms also exhibit elevated concentrations of diamondoids. This is explained by the contribution of a high maturity fluid contribution from the Anadarko depocenter migrating a short-to long-distances. Therefore, the major control on the high diamondoid concentration in oil accumulation west of the Nemaha Uplift is related to communication with deep Anadarko Basin in which Woodford and Mississippian source rocks are within the gas window as shown in Figure 88. The contribution of cracked hydrocarbons, which typically are enriched in diamondoids due to their thermal stability result in oil accumulation with high diamondoid concentration (Dahl et al., 1999b). The short-distance migration mechanism is modeled across the east-side of the Nemaha Uplift in the central Oklahoma region.

The short-distance migration pathways resulted in a modeled petroleum accumulations that are proximally sourced from Mississippian as well as Devonian source rocks, which exhibits a small fetch area. Modeled petroleum accumulation as a result of the short-distance pathways exhibits low diamondoids concentration; that is, modeled diamondoids are associated with early-petroleum generation charges, where the concentration of diamondoids are diluted with saturate and aromatic hydrocarbons. Therefore, the modeled oil accumulations of central Oklahoma, unlike the STACK play and Anadarko Shelf accumulations, do not have good communication with the Anadarko Basin depocenter. Contribution from the basin depocenter is hindered by the presence of the Nemaha Uplift, which acts as a petroleum-migration barrier. It can also be argued that
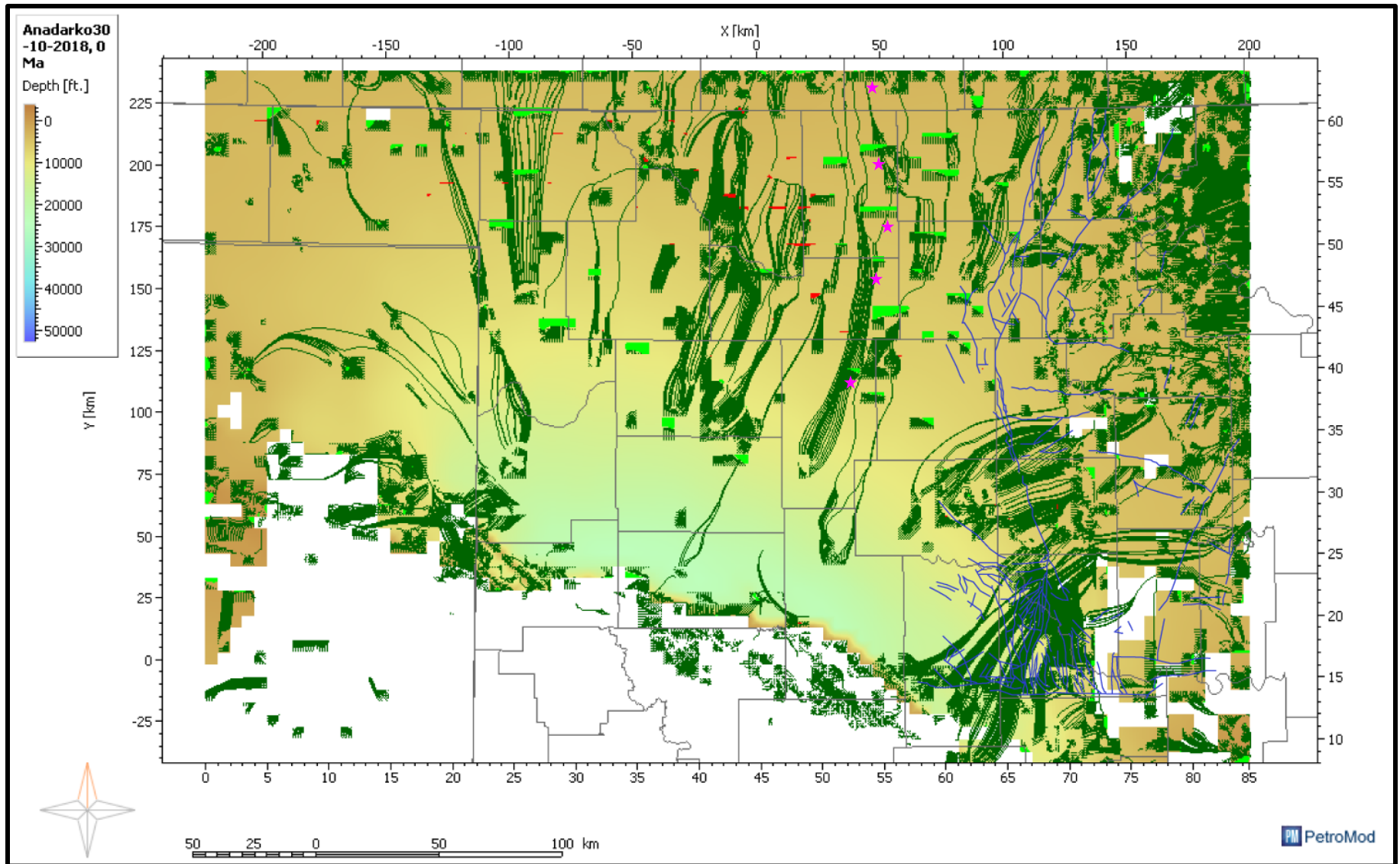
Figure 92: Modeled petroleum migration and major oil accumulation within Mississippian formations. Marked accumulations with a star represent a series of spill-to-fill accumulations associated with a continuous long-distance migration pathways.

late-tectonic activity associated with the last phase of the geological evolution of the Anadarko Basin could have affected the remigration of petroleum. This petroleum's Tertiary migration resulted from tectonic tilting and uplift during Cretaceous time caused by the Laramide orogeny (Johnson, 1989b). Therefore, such tilting could have preferentially migrated oils toward the north and northwest outward from the Anadarko Basin.

Diamondoid modeling was used as another calibration tool for constraining hydrocarbon-charge history and oil mixing. Measured diamondoid concentrations discussed in Chapter V of the 34 oil samples were used as a calibration input to quality check the output result of the basin model. Most of the modeled oil accumulations in the east of the Nemaha Uplift within Mississippian central Oklahoma play exhibit low modeled diamondoid concentration ranging from about 0.4 to 8% of total accumulation, with an overall average of 1.5%. This modeled diamondoid distribution ensured that hydrocarbon charge within the east of the Nemaha Uplift consisted of single low-to-medium maturity petroleum. Oil accumulations in Mississippian reservoirs within the west of the Nemaha Uplift, particularly areas of the Anadarko Shelf and STACK play, showed a more complex distribution of modeled diamondoids. Mass percentage of total modeled diamondoid varied from 1% to 80%, with high diamondoids associated with the presence of a considerable amount of gas. The variability in modeled diamondoids within the Anadarko Shelf and STACK play areas reflect the episodic hydrocarbon-charge mechanism, with diamondoids increasing in abundance as lighter and more mature fluids fill Mississippian reservoirs and the Anadarko Basin subsides into the gas window. Diamondoids proved an effective tool to calibrate the basin model, providing an independent calibration tool besides temperature measurement (BHT) and maturity measurement (%Ro). The significance of diamondoids is that they can be measured in crude oil

and can reveal the mixing of hydrocarbons of various maturities. This fluid-based calibration is crucial to quality check the validity of the basin model.

An important aspect of modeled accumulations could shed light on the mechanism by which conventional traps within Mississippian reservoir have been filled. Especially in areas where long-distance migration is established within deep parts of the Anadarko Basin. Some of the modeled accumulation along the Sooner Trend Province and the broad Anadarko Shelf result from a number of fill-to-spill structures aligning along the major petroleum-migration pathway. Figure 92 shows a number of examples of fill-to-spill accumulations; for example, pink stars represent a series of fill-to-spill Mississippian oil accumulations. Moreover, the fill-to-spill accumulations within the west area of the Nemaha Uplift extend from south to north radially away from the basin, with each fill-to-spill accumulation sharing the same modeled petroleum-migration pathway system. Using the fill-to-spill tool within the PetroMod 3D viewer module, the fill-to-spill accumulations can be tracked, such that the sequence of reservoir filling is revealed. Table 29 list details of a series of fill-to-spill accumulations sorted by the sequence in which they received hydrocarbon charge. First accumulations are situated near the deep Anadarko Basin, so those would be under high-pressure and temperature conditions in which they are at the liquid phase at reservoir condition and becoming in the vapor at surface conditions (e.g. accumulations 6751675 and 6751567). Interestingly, modeled diamondoids, as illustrated by the formula of Eq 6, followed a reasonable trend, with diamondoids enriched in hydrocarbon accumulations near the deeper area of the Anadarko Basin, with a decreasing trend in the diamondoid abundance the further the

modeled accumulation from the depocenter. This trend is expected, especially that hydrocarbons accumulation near the depocenter are exposed to higher thermal stress, so secondary cracking of hydrocarbon fragments most of the hydrocarbons into smaller molecules, whereas the ultra-thermal stability of diamondoids preserves them from alteration. Thus, they increase in abundance. This sequence of fill to spill is apparent in the abundance of vapor in hydrocarbon accumulations that are proximal to the depocenter, while hydrocarbon accumulations such as 6751986 and 6751912 contain both liquid and vapor phases at surface condition, with GOR decreasing from 27

Table 30 An example of fill to spill oil accumulations along the same migration pathways from deep Anadarko Basin to the shallow shelf

Accumulation ID	Sequence of filling	Volume of liquid at Reservoir (MMbbls)*	Volume of Vapor at Reservoir (mcf)*	Diamondoid abundance (%)	GOR (m^3/m^3)*	At surface phase
6751675	1st	0.15.	0	80.0	0	Vapor
6751567	2nd	0.29	0	75.0	0	Vapor
6751698	3rd	0.44	0	67.0	0	Vapor
6751616	4th	0	8.23	17.7	0	Vapor
6751666	5th	0	0.08	0	0	Vapor
6751577	6th	0	12.9	0	0	Vapor
6751986	8th	0.61	16.64	42.0	27373.23	Vapor & Liquid
6751912	9th	41.58	0	25.0	1724.4	Vapor & Liquid

* (MMbbls): Million barrels of oil, (mcf): thousands of cubic feet of gas, (GOR): gas to oil ratio

373.23 m^3 of gas to 1724.4 to m^3 of oil (Table 29). However, it is unclear why accumulations 6751666 and 6751577 did not contain any diamondoids; a possible explanation is a phase, where diamondoids preferentially favor the liquid phase as opposed to the vapor phase. However, accumulation 6751616 contained only the vapor phase but showed a presence of low diamondoid abundance. Therefore, we are not sure why the model predicts the absence of diamondoid in some vapor hydrocarbon accumulations.

A detailed comparison between the basin model results and measured crude-oil composition was examined between STACK play and central-Oklahoma areas. A good correlation is observed in the model between well locations coinciding with oil accumulations. Figure 93 shows model results of accumulations and associated wells from which oil samples were investigated in Chapter V. Overall, oil accumulations within central Oklahoma showed low measured diamondoids, as observed in Figure 58; similarly, modeled diamondoid percentage is low for most of the central-Oklahoma oil accumulations. For example, the crude-oil sample Pay-01-M and Pay-03-W are oils produced from the Mississippian formation and the Woodford Shale subsequently, with the measured concentration of diamondoids for Pay-01-M at 2.4 ppm, with Pay-03-W at 2.8 ppm. The modeled diamondoids in accumulations associated are slightly higher in some cases, while in others matched measured concentrations. Oil sample Pay-03-W had a measured concentration of 2.8 ppm; however, modeled diamondoids are at 8.4 ppm. A better match is observed at modeled accumulation near Pay-01-M, with measured diamondoid concentration of 2.8 ppm and modeled concentration of 2.0 ppm (Figure 93). The STACK play crude oils examined, overall, had higher diamondoid concentrations (Figure 58). For example, diamondoids are measured at 11.1 ppm from sample Kin-01-N and 12.5 2 ppm from sample Can-03-M, whereas modeled results at those similar localities are 11.0 ppm in oil accumulation at Kin-

01-N and 13.5 ppm for oil accumulation (Figure 93). The overall trend of modeled diamondoids can be extended to estimate their abundance in areas where we do not have samples for measurements. Figure 93 demonstrates an example of estimated diamondoids within oil accumulations located on the eastern side of Custer County, where the Woodford is within the wet-gas window. Modeled diamondoids suggest that if accumulation is present there, it would be in the vapor phase, with 68% of gas by mass, while diamondoids abundance is at 29.9%. However, the overestimation of diamondoids at Pay-03-W is unclear, and other oil accumulations also are questionable because modeling results suggest a 99% mass of diamondoids, which is unrealistic. Diamondoids represent a very minute component of hydrocarbons, and at the magnitude of a part per million; however, it is not impossible to find hydrocarbon accumulations composed solely of diamondoids, as such fluids were found in the Smackover Formation (Wingert, 1992). In general, though, diamondoid-only fluids have not been observed within the Anadarko Basin. Even though such overestimation of diamondoids is limited to about 10% of the total modeled oil accumulation, certainly the model would benefit from optimizing for better diamondoid estimation through more simulations and expanded coverage of measured diamondoids.

Controls of Hydrocarbon Charge

Hydrocarbon charge within Mississippian reservoir is a complex process that is controlled by different elements. Overall, those elements include thermal maturity, basin fill and structural evolution together with seal quality. Thermal maturity is key, as illustrated by diamondoids results previously in Chapter V, with some oil accumulation consisting of different hydrocarbon charges of various maturities. Moreover, the different phases of the Anadarko Basin history and major structural elements greatly impacted the distribution of hydrocarbons within Mississippian rocks.
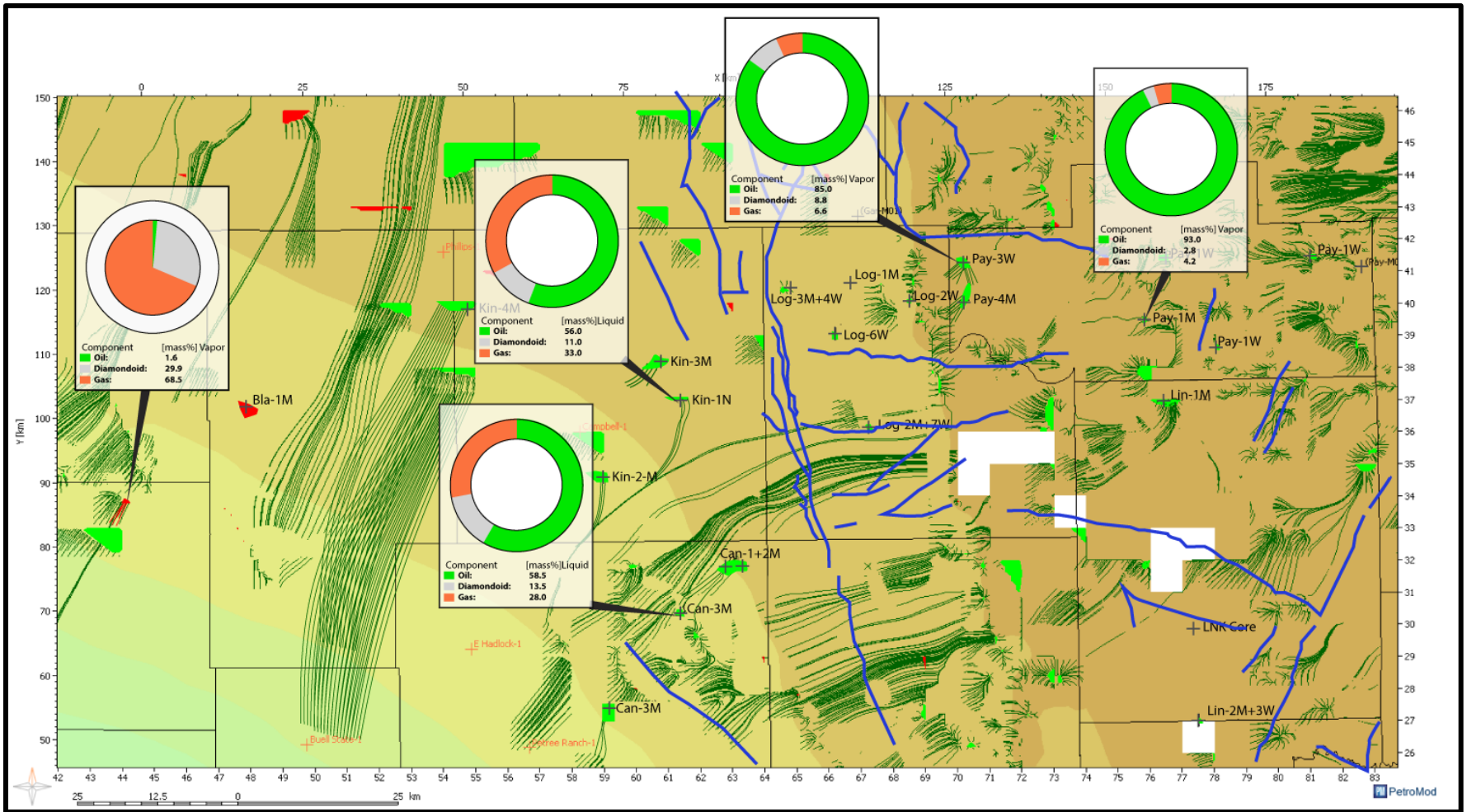
Figure 93: Modeled petroleum accumulations and associated composition indicated by mass percentage, whereas diamondoids are in parts per million. The two examples shown are within the Sooner Trend Anadarko Basin Canadian and Kingfisher Counties (STACK) play, including Can-03-M and Kin-01-N; two examples are from the central Oklahoma play, including Pay-01-M and Pay-03-W; and one example is of modeled accumulations where there is no well control from Custer County.

In particular, the Nemaha Uplift fault system that separates the STACK play from the central-Oklahoma accumulations within the Cherokee Platform. The Nemaha fault systems, as observed in the petroleum-migration models, indicate that it served as migration pathways for younger layers overlaying the Mississippian formation, so it possibly acted as a lateral migration barrier. This possibility also can be inferred from the depletion of diamondoid concentrations in oil accumulations within central Oklahoma, indicating there were no hydrocarbon charges received from the basin depocenter. Therefore, it is arguably possible that the relatively low volumes and quality of hydrocarbons produced from central Oklahoma compared to STACK play production are due to hydrocarbon charge loss caused by the Nemaha Uplift fault system. Additionally, it is reasonable to suggest that the likelihood of the water washing of hydrocarbons in central Oklahoma due to the abundance of faults in that region, together with the shallower Mississippian depths. Such an interpretation is inferred from oil composition evidence shown in Chapter VI, with water-soluble phenol compounds depleted from oils in central Oklahoma and the Anadarko Shelf.

An important petroleum system element that influences petroleum accumulation and migration within different Mississippian plays is the seal rock presence and quality. It is well known that Pennsylvanian shales overlay Mississippian formations. However, internally within the Mississippian Formations, the stratigraphy is complex; lithologies interchange, with siltstones, mudrock, solid carbonate and cherty weathered carbonates. It has long been suggested that weathered cherty Osagean Mississippian limestone (known as Miss Chat) is the best target for exploring for oil in Mississippian formations, specifically for oil-fields within north-central of Oklahoma (Rogers, 2001). However, accumulations reservoired in Miss Chat are disadvantaged from the high saturation of water and water production associated with oil production. Measured saturation from a core sample located at Osage County exhibits average water saturation ranging

from 56 to 73% and average oil saturation ranging from 6 to 19% (Suneson, 2012). Large volume

production of water greatly impacts the economics of developing the Miss. Chat. From a petroleum

systems analysis perspective, Miss Chat diagenesis results from rock fluids interaction with rock

matrix, particularly infiltration of meteoric waters, possibly during periods of Anadarko Basin

Uplift. Such processes impacted seal quality in central Oklahoma and the shallow Anadarko Shelf,

so petroleum production is associated with high water production. In contrast, STACK play

reservoirs consist of solid carbonates interbedded with silt and clay organic-rich beds, as described

in the LNK core. The dual effect of tight mudstones within Mississippian carbonate provides an

exceptional seal, together with a source for generating hydrocarbons. Therefore, STACK play oil

production is economically superior to that of central Oklahoma and the Anadarko Shelf, due to

the lower water saturation caused by the presence of good seal quality rocks within Mississippian

formation in the STACK play. Tight rocks within Mississippian formations vary in lithology from

clay-rich siltstone to organic-rich muddy carbonates and marlstones. These types of seals are

present in discontinuous geometries across the Anadarko Shelf and increase in thickness and mud-

content towards the depocenter, which pinches out towards the shallower depths across the

Anadarko Shelf (Johnson et al., 1988a). Therefore, seal rock distribution and lithology are one of

the key elements that control hydrocarbon accumulations quality and volume within Mississippian

reservoirs.

Petroleum System Charts

The petroleum system event charts provide a representation of all elements and processes

of a specific petroleum system through time (Magoon and Dow, 1994). The chart compares

petroleum system elements and processes on the *y*-axis and geological time on the *x*-axis. The

petroleum system elements' sequence of occurrence was the conventional wisdom for the exploration of conventional hydrocarbon accumulations, but with the emerging unconventional tight source-rock reservoir, the importance of those elements has changed. In conventional hydrocarbon accumulations, it is important to have all the elements intact and in place prior to the hydrocarbon-charge process, followed by robust preservation to the present day, whereas an unconventional source-rock reservoir system depends less on time, while it is largely controlled by organic richness, thermal maturity, and rock brittleness. All in all, the petroleum system event chart provides a summarized illustration of the petroleum system elements in time, which can be converted into risk chart for evaluating a hydrocarbon play or prospect (Magoon and Dow, 1994).

The petroleum system event charts resulting from the basin model are divided into three geological areas: the Anadarko Shelf, STACK and central-Oklahoma plays (Figure 94). Anadarko Shelf petroleum system events are unique in various respects. Even though the Woodford Shale extends to the shallow shelf, source rocks are immature for petroleum generation; therefore, only oil accumulation from migration is considered for this type of play (Figure 94). Additionally, Mississippian source-rock facies are absent, resulting in a very limited number of seal rocks, including some of the Pennsylvanian shales. Trap formation is interpreted to take place during the major tectonic event during which the Anadarko Basin shifted into a foreland basin, setting at the third phase of the basin evolution, as discussed earlier. As determined from oil-inclusions homogenization temperatures and the thermal history of the basin, oil migration likely took place during two episodes during Late Pennsylvanian followed by another hydrocarbon charge during the Paleogene time. One persistent major high-risk consideration within the Anadarko Shelf play is the preservation of hydrocarbons, in particular, hydrocarbon loss due to seal quality, together with basin exhumation. Estimating the hydrocarbon loss is a difficult task; however, it can be

inferred that hydrocarbon preservation is challenging for the Anadarko Shelf hydrocarbon accumulations for two reasons. First, the composition of oils within the Anadarko Shelf exhibits trace amount of phenols, which are water-soluble compounds, indicating that those oils have been interacting with water or have possibly been water washed. This aspect ultimately suggests a dynamic fluid flow system where hydrocarbons are not completely sealed from interacting with water. Second, the variability in GOR could reflect variability in seal presence and effectiveness, in which high GOR indicating good quality of seal rock capable of holding higher columns of hydrocarbons, while low GOR suggests poor seal quality, whereby seal rock leaks gas and is not capable of accumulating higher hydrocarbon column. Seal quality within the Anadarko Shelf is controlled by two factors including rock quality and basin evolution. Rock type is controlled by depositional and diagenetic alteration of Mississippian rocks of the shallow Anadarko Shelf. Furthermore, during the third phase of the Anadarko Basin history, intense tectonic activity and associated basin exhumation could have impacted seal quality within the Anadarko Shelf. Therefore, the Anadarko Shelf play's critical moment is marked just after hydrocarbon charges have ceased, whereby reservoirs have received the highest volume possible of hydrocarbon.

The central-Oklahoma Mississippian play shares some elements with the Anadarko Shelf but it differs in others. Most notably, thermal maturation of Devonian-Mississippian source rocks is within the early-to-peak oil-generation window (Figure 94). Therefore, unlike the Anadarko Shelf, source rocks within central Oklahoma are capable of oil and gas generation. Furthermore, as evidenced by biomarkers geochemistry indicating that multiple source rocks have contributed to the hydrocarbon accumulations in central Oklahoma. Since petroleum generation is within central Oklahoma, oil migration and accumulation are proximal, resulting in short-distance migration pathways. Reservoir rocks span between Devonian Woodford Shale and multiple zones
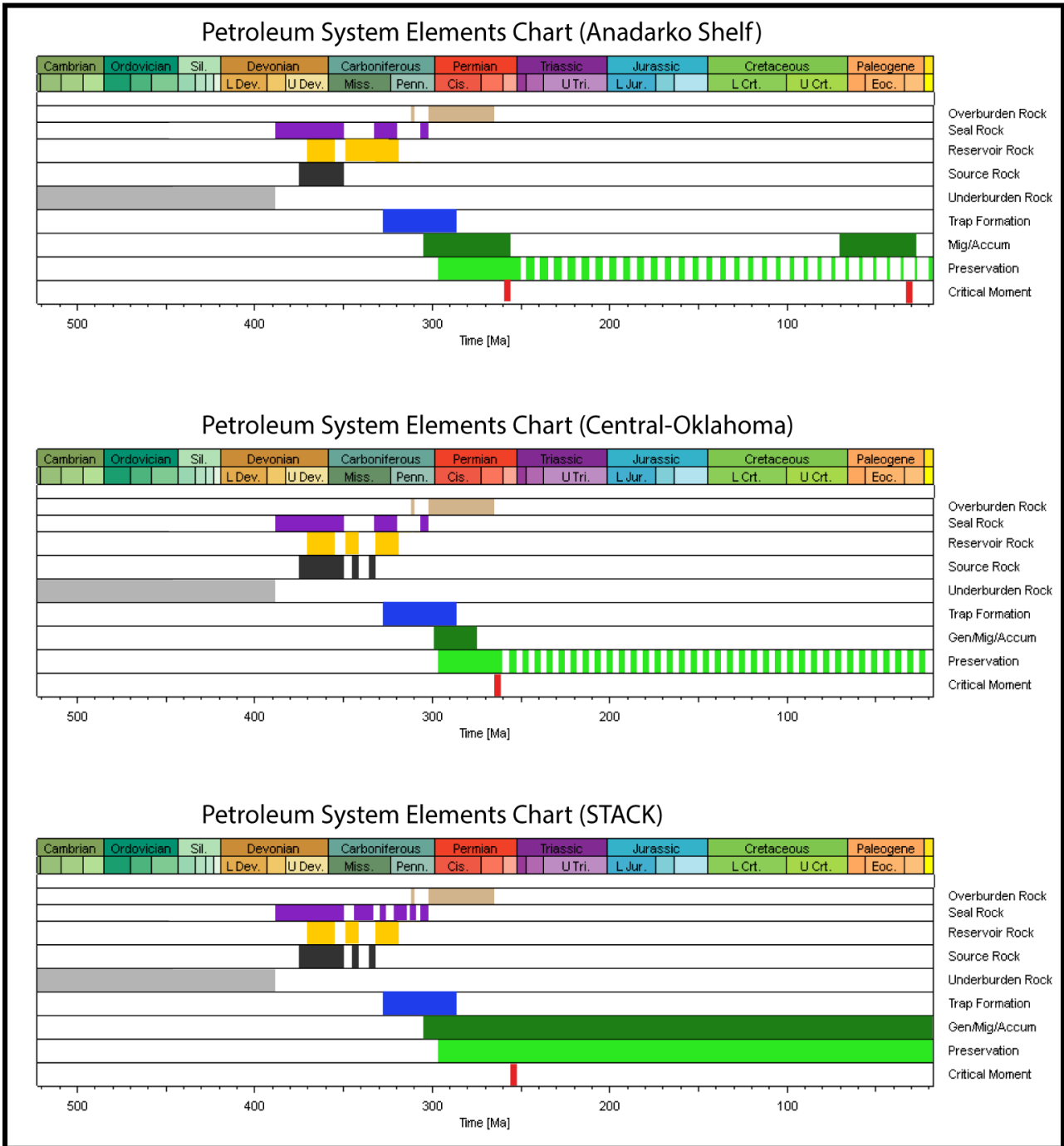
Figure 94: Petroleum systems event chart showing different Devonian-Mississippian petroleum systems including the Anadarko Shelf and the Central Oklahoma and Sooner Trend Anadarko Basin Canadian and Kingfisher Counties (STACK) plays.

within Mississippian carbonate formations (Figure 94). As to traps formation within central Oklahoma, they are likely to have formed during the Early Pennsylvanian as part of Ouachita-Marathon orogeny, during the third phase of the Anadarko Basin's evolution. Petroleum generation started during Pennsylvanian time, as evidenced from basin modeling results, but it was not until the Early Permian (282 Ma) that oil expulsion and migration took place, as determined from fluid-inclusion microthermometry (Figure 94). In central Oklahoma, trap formations did form prior to hydrocarbon charge, occurring in the ideal sequence for oil accumulation. However, hydrocarbon preservation is problematic for oil accumulations within central Oklahoma. This is inferred because of the fault systems associated with the Nemaha Uplift and its evolution along with the Anadarko Basin. While the Nemaha Uplift is believed to originate as a paleo-topographic high during the Proterozoic, it has been a structurally dynamic province in which fault systems are reactivated as a function of tectonic activities (Berendsen and Blair, 1995; Gay Jr, 2003a). In particular, tectonic activity including Ouachita orogeny during Pennsylvanian and to a lesser extent the Laramide orogeny during Late Cretaceous collectively contributed to the reactivation of the fault system within the Nemaha Uplift, potentially resulting in loss of accumulated hydrocarbons in traps, together with the loss of hydrocarbon during petroleum migration. This hydrocarbon loss is also associated with higher water production and oils produced bearing a geochemical signature suggesting water washing. Therefore, similar to oil accumulations within the Anadarko Shelf, Central Oklahoma Mississippian plays carry a higher risk for hydrocarbon preservation due to structural deformation influencing the seal quality of hydrocarbon traps. In central Oklahoma, the critical moment is defined at the maximum burial depth of Devonian-Mississippian source rocks. Since hydrocarbon generation in these reservoirs is proximal to the source, maximum burial would imply the maximum thermal maturation, hence the larger volume of hydrocarbon charge. From an

unconventional petroleum system perspective, tight Woodford Shale and Mudrocks within Mississippian carbonate can be classified as unconventional source-rock reservoirs. However, those unconventional reservoirs would be at higher risk with regards to thermal maturity, since these reservoirs are at an early phase of maturity. Moreover, for economical liquid hydrocarbon production from source-rock reservoirs within Oklahoma, the thermal maturity of source rocks and associated hydrocarbons must have reached early stages of hydrocarbon cracking, hence late-oil to wet-gas stages of thermal maturation. In addition to thermal maturity, higher production of water in central Oklahoma together with oil composition lacking phenols indicating water-washing alteration.

The petroleum system event chart of the STACK play exhibits unique characteristics, as compared to those of central Oklahoma and Anadarko Shelf, starting with the number of seal rocks present within Mississippian formations, including a number of mudstones, wackestone and siltstone deposits within the Meramec formation and overlying by the Springer shale formation. As to source rocks, both Woodford Shale and lower Mississippian mudrocks are of good petroleum-generation potential. A unique characteristic of the STACK play is its thermal maturity level based on modeling results indicating late oil-window stage at present-day settings. Modeled vitrinite reflectance within the STACK play ranges from 0.9% to 1.7%, with its close proximity to the basin depocenter increasing the likelihood of additional hydrocarbon charge of lighter hydrocarbon contribution from over-mature depocenter. Moreover, the STACK play shares a similar trap formation timing to that of central Oklahoma and Anadarko Shelf, but the STACK play traps are predominantly stratigraphically controlled, with some structural closures for hydrocarbon accumulation. Those stratigraphic taps of hydrocarbons are a function of the change in lithology from porous carbonates to tight mudrocks and siltstones forming packages of a mixed

292

carbonate-siliciclastic depositional system (Hill, 2018). As indicated by modeling results, the onset of petroleum generation in the STACK area occurred in the Late Pennsylvanian, whereas oil migration took place during early Permian to Paleogene; therefore, petroleum migration and accumulation is presented as a continuous process (Figure 94). The measured microthermometry result of fluid inclusions suggests that fluid entrapment occurred during approximately 262 Ma and 55 Ma, but this suggestion does not exclude other periods of oil migration. Hydrocarbon preservation is distinctively uninterrupted for oil accumulations within the STACK play for a number of factors, including seal quality and minimum structural deformation. The presence of tight mudrock beds within STACK play together with minimal faulting resulted in better preservation of hydrocarbon accumulation, as reflected in the oil composition. Unlike oils from Anadarko Shelf and Central Oklahoma, the composition of STACK play oils exhibits unaltered concentration of hydrophilic compounds, such as phenols, suggesting minimum interaction with water due to adequately sealed mudrock facies. Furthermore, unlike Mississippian plays in the Central Oklahoma and Anadarko Shelf, water production is very minimal within STACK play reservoirs, which supports oil-composition evidence and suggests insignificant interaction with water. The critical moment is defined in the late Permian, with the maximum burial of Devonian-Mississippian strata. As an unconventional source-rock reservoir, the STACK play has certain elements that make it more productive than other Mississippian plays in Oklahoma: thermal maturity, rock brittleness together with rock cyclicity, and inherent compartmentalization. The STACK play from a maturity standpoint is within the peak-to-late oil-window, which corresponds to 0.8 to 1.4%Ro; also, migration of more mature fluids to the STACK play high-grades those fluids as evidenced from diamondoids concentration. Rock brittleness is a result of the high content of calcite and lower clay-minerals in some of the Mississippian units, with a shoaling upward

sequence stratigraphic framework resulting in compartmentalized unconventional reservoirs, whereby calcite-rich brittle reservoirs are juxtapositioned between organic-rich and mud-dominated beds. The reservoir source-rock pairs coexisting in stacked and repeated architecture makes the STACK play one of the most productive unconventional tight reservoirs in Oklahoma.

CHAPTER VIII

CONCLUSIONS

Devonian-Mississippian petroleum systems within the Anadarko Basin contain most hydrocarbon resources in Oklahoma. Estimates of undiscovered oil and gas suggest that almost 80% of technically recoverable hydrocarbons are trapped within Devonian-Mississippian petroleum systems. While major conventional oil-fields have been discovered in Oklahoma since the first oil discovery in 1897, major geological challenges persist to the present day, particularly with the emerging of unconventional self-sourced reservoirs, such as STACK and SCOOP plays. A major contributor to the success within both conventional and unconventional reservoirs is due to horizontal drilling combined with hydraulic fracturing stimulation. Such technologies allowed for uncapping large volume of oil and gas in what was previously thought of as a hydrocarbon source rock incapable of storing hydrocarbons. However, other aspects related to well performance and the composition of produced fluids raise many questions. Many factors control the success of hydrocarbon producibility from Devonian-Mississippian petroleum systems in Oklahoma, including rock mineralogy, thermal maturity and organic richness. Petroleum sourcing in these Mississippian reservoirs is complex, encompassing multiple hydrocarbon charges from different source rocks, in addition to the Woodford Shale. In this study, a comprehensive geochemical investigation, together with petroleum system and basin modeling analysis, was carried for a collection of various samples including source rocks, crude oils and fluid inclusions. All of the measured data, collectively, was used as a calibration tool for optimizing the Anadarko Basin modeling results by which conclusions were achieved concerning the petroleum system.

Woodford Shale together with Mississippian mudrock intervals are both of good petroleum-generation quality. Both rocks exhibit predominantly marine-derived organic matter with the Woodford Shale composed of a mixture of Type-I and -II kerogens, with liptinite as the dominant macerals and uniquely preserved morphology within the kerogen, such as *Tasmanites*. Mississippian mudrocks, including those produced unconventionally in the northern Oklahoma Mississippi limestone play and the STACK play in central Oklahoma, contain a number of organic-rich beds with dominantly Type-II kerogen and trace amounts of terrigenous organic matter. These beds are capable of generating hydrocarbons, as evidenced by pyrolysis data. The presence of multiple stacked source rocks within the Mississippian section increases the generation potential within these unconventional source-rock reservoirs. Additionally, diterpenoids together with extended tricyclic terpanes are unique biomarkers that are much more abundant in the Mississippian rocks. These biomarkers are believed to be an indicator of depositional setting and environmental conditions such as water salinity and proximity to paleoshoreline during the Mississippian time. Sedimentological features, together with macerals and biomarkers, provide the evidence to suggest a generalized shoaling-upward sedimentary sequence from the Woodford Shale to the upper unit of the Mississippian limestone. The three subunits within the Mississippian limestone were based on organic-richness, mineralogy and key biomarker ratios. The lower unit could represent a better unconventional reservoir target due to its low clay content dominance of beds with carbonate- and silica-based mineralogy interbedded with organic-rich beds.

Petroleum generation kinetics of Mississippian source rocks was investigated using a series of hydrous pyrolysis experiments, then was compared to the Woodford petroleum generation kinetics. Hydrous pyrolysis expelled oil from Mississippian rocks suggest that Mississippian mudrock exhibits lower activation energy and a lower frequency factor than previously known

kinetics parameters for the Woodford Shale. Mississippian petroleum source rocks are capable of generating oil and gas at a lower temperature than the Woodford Shale; therefore, petroleum generation in Mississippian rocks could have started at shallower depths than the previously well-accepted depths for the Woodford Shale. The low kinetic parameters of petroleum generation in Mississippian source rocks is postulated due to organic-matter structure co-occurring as infused amorphonite and bituminite within the mineral matrix. The large surface area between the macerals and the mineral matrix increases the reactivity, with clays acting as catalysts for petroleum generation.

Mississippian and Woodford crude oils' geochemistry shed light on the sources and history of hydrocarbons produced from three major play areas, including the Anadarko Shelf, central Oklahoma and STACK plays. Further, based on source-rock–crude-oil geochemical correlation, two major petroleum systems were identified, including the Woodford end-member petroleum system and Mississippian end-member petroleum system, each of which bears a unique geochemical fingerprint. Molecular and isotopic compositions of over 250 compounds were measured and examined statistically using hierarchical cluster analysis together with the Summon mapping technique. Overall, crude oils cluster into three main families based on the saturate and aromatic biomarkers together with compound-specific isotope signatures of normal alkanes. Family-1 samples are composed of crude oils with a close relationship to Mississippian source-rock extracts, suggesting that Family-1 samples are Mississippian-sourced crude oil. Family-3 samples resemble a geochemical fingerprint close to the Woodford rock extracts; hence, Family-3 fluids are Woodford-sourced crude oil. Family-2 showed a mixed fingerprint of varying degrees, very likely resulting from hydrocarbon mixing from Mississippian and Woodford sources. Distribution of those oil families geographically exhibits a trend that could be closely controlled

by the Nemaha Uplift and associated faults system. Family-1 and Family-2 are observed in close proximity to the faults, co-occurring on both sides of the Nemaha Uplift, and they are present in STACK play and central Oklahoma. Family-3 is observed further away from the Nemaha Uplift those are found within the Anadarko Shelf and central Oklahoma. Diamondoids coupled with biomarkers of crude oil unraveled the extent of petroleum mixing, within Devonian-Mississippian petroleum systems. Anadarko Shelf samples together with oils at the STACK play showed enrichment of diamondoids and biomarkers, indicative of mixed hydrocarbons with various degrees of maturities. In contrast, oils in central Oklahoma were enriched in biomarkers and depleted in diamondoids, reflecting oils with minimal mixing.

Geological information embedded in fluid inclusions' composition has defined regional petroleum-migration patterns within different plays within Devonian-Mississippian petroleum systems. Aqueous-inclusions and coexisting oil-bearing fluid inclusions were investigated for biomarkers composition for identifying oil inclusions sources, together with comparing fluid-inclusion microthermometry with entrapped-hydrocarbons thermal maturity. Homogenization temperatures of aqueous-inclusions coincided with the level of thermal maturation at the molecular scale of oil inclusions. Biomarkers fingerprint of oil inclusions suggests predominant Woodford contribution for inclusions west of the Nemaha Uplift, while inclusions located east of the Nemaha Uplift reflected a Mississippian biomarker fingerprint. Moreover, two major populations were identified based on molecular-maturity-sensitive biomarkers together with measured homogenization temperatures; the first group of inclusions a exhibited high maturity signature and elevated homogenization temperatures occurring within the STACK play. In contrast, lower homogenization temperature coincided within low thermal maturity ratios, as observed within the

central Oklahoma. Fluids inclusion data was combined with basin modeling results to gain insight into episodes of hydrocarbon charge.

Migration-sensitive and naturally occurring geotracers in crude oils helped defined regional trends in petroleum migration into different reservoirs of the Devonian-Mississippian petroleum systems. The carbazole compound class was closely examined due to its members' sorptive forces into clay minerals within migration pathways; hence, carbazoles decrease in concentration with an increase in crude-oil migration distance from the source rock. The phenols compound class comprises hydrophilic compounds that revealed crude-oil secondary-alteration post-accumulation. The carbazole results suggest different migration patterns across the different oil samples, with BC ratios indicating a south-to-north long-distance migration trend within oils west of the Nemaha Uplift, including the STACK and Anadarko Shelf plays. Benzocarbazole ratios of oils east of the Nemaha Uplift showed a west-to-east decreasing trend. Estimation of the migration distance of each group of oil samples varied from 50 km to 200 km, with lower migration distances for oils within Central Oklahoma (less than 50 km), while long-distance migration is observed in oils at the Anadarko Shelf and STAK play (higher than 50 km). Phenols results revealed that some of the Mississippian oils are altered, while others remain intact. Particularly, oils in Central Oklahoma and the Anadarko Shelf are both water-washed, while oils within STACK play do not show a water-washing effect. Water washing of crude oil is likely due to poor seal quality, by which meteoric water has breached the seal rock, whereas intact phenols suggest good seal quality with minimal water-hydrocarbons interaction.

Measurement of diamondoids in fluid inclusions is a novel technique that has been first developed in this study, which opens a new field of petroleum geochemistry. Particularly for fluids of high maturity, classical geochemical approaches are not adequate for correlation purposes. Until

very recently, it was impossible to confidently correlate high-maturity fluids to their source rocks or to other high-maturity fluids. However, it has been shown that these correlations can be accurately and confidently made using the distributions of large diamondoids, an analytical technique termed QEDA. Therefore, QEDA provided a unique tool to unravel petroleum sources and fingerprint highly cracked oil inclusions with their source rocks. The results suggest that oil inclusions obtained from Canadian County are the most mature. They contain abundant diamondoids and lack biomarkers. Quantitative extended diamondoid analysis allowed for fingerprinting such mature oil inclusions and correlation with black crude oils. The results suggest that the oil inclusions are a mixture containing both Mississippian and Woodford source-rock contributions. Moreover, other oil inclusions located in Kingfisher and Blaine counties bear a strong sterane and terpane Woodford fingerprint. Maturity-sensitive ratios such as triaromatic steroids, methyl phenanthrene index and microthermometry analysis indicate different episodes of petroleum charges, with low maturity 06–0.8%VRE, low homogenization temperatures (78°C) and a high maturity hydrocarbon 1.2–1.4%VRE charge associated with high diamondoid concentrations and high homogenization temperatures (148°C). This study introduces an entirely new geochemical field (i.e., the correlation of high-temperature fluid inclusions to their source rocks using QEDA).

Built-basin and petroleum-systems modeling of Devonian-Mississippian petroleum systems honored the observed key geological factor controlling petroleum migration and accumulation in Mississippian reservoirs. Basin modeling calibration was achieved using multiple independent data inputs, including geothermal data from rock and temperature, together with fluids composition. A number of 3D simulations were run until model optimization achieved good alignment between modeled results and actual measurements. One of the key factors that greatly

impact the model is basin exhumation and eroded thickness of sediments. Basin modeling best-fit results suggest that the Anadarko Basin featured around 2500 ft of sediment, which gradually decreased to 500 ft of removed sediment thickness within the Anadarko Shelf. By combining basin modeling results of thermal history together with homogenization temperatures of fluid inclusions, episodes of hydrocarbon charge can be inferred. Hydrocarbon charge started in the Late Pennsylvanian up to Paleogene time and occurred in multiple episodes. Modeled burial history of the Anadarko Basin coincides with geologic and tectonic observations with four major phases, including the first-phase igneous episode during Precambrian to Middle Cambrian time, the second-phase epeirogenic episode during Cambrian through Mississippian time, the third-phase orogenic episode during Pennsylvanian time, and the final-phase epeirogenic episode, from the Permian to the present day. Secondary cracks and fluids' thermal maturity were appraised through the diamondoid tool. Accumulated hydrocarbons in Mississippian reservoirs were optimized to match diamondoid in measured crude oils. All in all, the basin modeling results suggest that various elements control hydrocarbon accumulation and composition within Mississippian plays, including the Anadarko Shelf, STACK and central Oklahoma plays. Hydrocarbon preservation due to seal quality is a cortical element increasing the risk in seeking economically viable accumulations within central Oklahoma and Anadarko Shelf. Hydrocarbon charge with mixed short- and long-distance migration is observed within the Anadarko Shelf and STACK plays, while central Oklahoma play is associated with proximal hydrocarbon charge with short-distance migration pathways. From the unconventional perspective, the STACK play exhibits a sweet spot among unconventional targets due to several factors, including thermal maturity, rock brittleness, rock cyclicity and inherent compartmentalization.

REFERENCES

Abrams, M. A., C. Gong, C. Garnier, and M. A. Sephton, 2017, A new thermal extraction protocol to evaluate liquid rich unconventional oil in place and in-situ fluid chemistry: Marine and Petroleum Geology, v. 88, p. 659-675.

Adhikari, P. L., R. L. Wong, and E. B. Overton, 2017, Application of enhanced gas chromatography/triple quadrupole mass spectrometry for monitoring petroleum weathering and forensic source fingerprinting in samples impacted by the Deepwater Horizon oil spill: Chemosphere, v. 184, p. 939-950.

Adler, F. J., 1971, Future Petroleum Provinces of the Mid-Continent, Region 7, *in* I. H. Cram, ed., Future Petroleum Provinces of the United States—Their Geology and Potential, Volumes 1 & 2, American Association of Petroleum Geologists.

Al-Arouri, K. R., D. M. Mckirdy, and C. J. Boreham, 1998, Oil-source correlations as a tool in identifying the petroleum systems of the southern Taroom Trough, Australia: Organic geochemistry, v. 29, p. 713-734.

Al Atwah, I., M. Alshaikh, S. T. Sweet, A. Knap, and B. Hascakir, 2018a, Extension of Existing Screening Criteria Tables for Thermal Enhanced Oil Recovery Methods Through Compositional Analyses of Heavy Oils, SPE Western Regional Meeting, Garden Grove, California, USA, Society of Petroleum Engineers.

Al Atwah, I., and D. Jacobi, 2017, Acritarchs in the Silurian Qusaiba Shale and Related Biomarkers: Implication for Identifying Paleozoic Hydrocarbon Charge: AAPG Annual Convention and Exhibition.

Al Atwah, I., S. Mohammadi, S. Sweet, A. Knap, and M. Becker, 2018b, Geochemistry of Oil-Bearing Fluid Inclusions Insight Into Hydrocarbon Charge in Devonian-Mississippian Petroleum Systems, Anadarko Basin, AAPG Annual Convention and Exhibition, Salt Lake City, AAPG.

Al Atwah, I., J. Puckette, J. Pantano, K. Arouri, and J. M. Moldowan, 2019, Organic Geochemistry and Crude Oil Source Rock Correlation of Devonian-Mississippian Petroleum Systems in Northern Oklahoma, *in* J. M. G. G. M. Grammer, J. O. Puckette, P. Jaiswal, S. J. Mazzullo, M. J. Pranter, and R. H. Goldstein, ed., Mississippian Reservoirs of the Midcontinent, v. 122, AAPG Memoir

Al Shaieb, Z., and J. Puckette, 2002, Sequence stratigraphy of Hunton Group ramp facies, Arbuckle Mountains and Anadarko Basin, Oklahoma: Platform carbonates of the southern mid-continent, 1996 symposium: Oklahoma Geological Survey Circular, p. 131-137.

Alexander, R., R. Kagi, and G. Woodhouse, 1981, Geochemical correlation of Windalia oil and extracts of Winning Group (Cretaceous) potential source rocks, Barrow Subbasin, Western Australia: AAPG Bulletin, v. 65, p. 235-250.

Alexander, R., R. I. Kagi, S. J. Roland, P. N. Sheppard, and T. V. Chirila, 1985, he effects of thermal maturity on distributions of dimethylnaphthalenes and trimethylnaphthalenes in some ancient sediments and petroleum: Geochimica et Cosmochimica Acta, v. 49, p. 385–95.

Alexander, R., R. I. Kagi, and P. N. Sheppard, 1983, Relative abundance of dimethylnaphthalene isomers in crude oils: Journal of Chromatography, v. 267, p. 367–72.

Alexander, R., A. V. Larcher, R. I. Kagi, and P. L. Price, 1992, An oil-source correlation study using age-specific plant-derived aromatic biomarkers, *in* P. A. a. R. P. P. J.M. Moldowan, ed., Biological Markers in Sediments and Petroleum: Englewood Cliffs, NJ, Prentice-Hall, p. 201–21.

Alexander, R., M. G. Strachan, R. I. Kagi, and W. Van Bronswijk, 1986, Heating rate effects on aromatic maturity indicators: Organic Geochemistry, v. 10, p. 997-1003.

Amati, L., and S. R. Westrop, 2006, Sedimentary Facies and Trilobite Biofacies Along an Ordovician Shelf to Basin Gradient, Viola Group, South-Central Oklahoma: Palaios, v. 21, p. 516-529.

Amsden, T. W., 1975, Hunton Group, Late Ordovician, Silurian, and Early Devonian in the Anadarko Basin of Oklahoma, v. 121, Oklahoma Geological Survey

Amsden, T. W., and G. Klapper, 1972, Misener Sandstone (Middle-Upper Devonian), North-Central Oklahoma: AAPG Bulletin, v. 56, p. 2323-2334.

Anders, D. E., and W. E. Robinson, 1971, Cycloalkane constituents of the bitumen from Green River shale: Geochimica et Cosmochimica, v. 35, p. 661-678.

Aquino Neto, F. d., 1983, Occurrence and formation of tricyclic and tetracyclic terpanes in sediments and petroleum: Advances in Organic Geochemistry 1981, p. 659-667.

Aquino Neto, F. R., Restle, A., Connan, J., Albrecht, P.,Ourisson, G., Aquino Neto, F. R., 1982, Novel tricyclic terpanes (C19±C20) in sediments and petroleums: Tetrahedron Letters, v. 23, p. 2027-2030

Arouri, K., P. F. Greenwood, and M. R. Walter, 1999, A possible chlorophycean affinity of some Neoproterozoic acritarchs: Organic Geochemistry, v. 30, p. 1323-1337.

Arouri, K. R., P. D. Jenden, and A. A. Al-Hajji, 2010a, Petroleum inclusions atop Unayzah gas condensate reservoir: Signpost for an undocumented chapter of the Arabian Basin filling history?: Organic Geochemistry, v. 41, p. 698-705.

Arouri, K. R., and D. M. McKirdy, 2005, The behaviour of aromatic hydrocarbons in artificial mixtures of Permian and Jurassic end-member oils: application to in-reservoir mixing in the Eromanga Basin, Australia: Organic Geochemistry, v. 36, p. 105-115.

Arouri, K. R., P. J. Van Laer, M. H. Prudden, P. D. Jenden, W. J. Carrigan, and A. A. Al-Hajji, 2010b, Controls on hydrocarbon properties in a Paleozoic petroleum system in Saudi Arabia: Exploration and development implications: AAPG bulletin, v. 94, p. 163-188.

Asahina, K., and N. Suzuki, 2018, Methylated naphthalenes as indicators for evaluating the source and source rock lithology of degraded oils: Organic Geochemistry, v. 124, p. 46-62.

Atwah, I., S. Sweet, J. Pantano, and A. Knap, 2019, Light Hydrocarbon Geochemistry: Insight into Mississippian Crude Oil Sources from the Anadarko Basin, Oklahoma, USA: Geofluids, v. 2019, p. 15.

Atwah, I. A., J. Puckette, M. Becker, and J. M. Moldowan, 2018, Source-Rock Reservoirs Geochemistry of Lower Mississippian Mudrocks in Central Oklahoma AAPG Bulletin.

Azevedo, D. A., R. R. Aquino Neto, and B. R. T. Simoneit, 1998, Extended ketones of the tricyclic terpane series in a Tasmanian tasmanite bitumen: Organic Geochemistry, v. 28, p. 289-295.

Bakel, A. J., and R. P. Philp, 1990, The distribution and quantitation of organonitrogen compounds in crude oils and rock pyrolysates: Organic Geochemistry, v. 16, p. 353-367.

Balaban, A. T., and P. V. Ragé Schleyer, 1978, Systematic classification and nomenclature of diamond hydrocarbons—I: Graph-theoretical enumeration of polymantanes: Tetrahedron, v. 34, p. 3599-3609.

Ballentine, C. J., R. K. O'Nions, and M. L. Coleman, 1996, A Magnus opus: Helium, neon, and argon isotopes in a North Sea oilfield: Geochimica et Cosmochimica Acta, v. 60, p. 831-849.

Bann, K. L., S. C. Tye, J. A. Maceachern, C. R. Fielding, and B. G. Jones, 2008, Ichnological and sedimentologic signatures of mixed wave-and storm-dominated deltaic deposits: Examples from the Early Permian Sydney Basin, Australiaa; Recent advances in models of siliciclastic shallow-marine stratigraphy: Special Publication—Society for Sedimentary Geology, v. 90, p. 293-332.

Barrie, C. D., K. W. Taylor, and J. Zumberge, 2016, Measurement of compound-specific carbon isotope ratios (δ13C values) via direct injection of whole crude oil samples: Rapid Communications in Mass Spectrometry, v. 30, p. 843-853.

Bastow, T. P., B. G. K. van Aarssen, G. E. Chidlow, R. Alexander, and R. I. Kagi, 2003, Small-scale and rapid quantitative analysis of phenols and carbazoles in sedimentary matter: Organic Geochemistry, v. 34, p. 1113-1127.

Beach, F., T. M. Peakman, G. D. Abbott, R. Sleeman, and J. R. Maxwell, 1989, Laboratory thermal alteration of triaromatic steroid hydrocarbons: Organic Geochemistry, v. 14, p. 109-111.

Beaumont, C., R. Boutilier, A. S. Mackenzie, and J. Rullkotter, 1985, Isomerization and aromatization of hydrocarbons and the paleothermometry and burial history of Alberta foreland basin: AAPG Bulletin, v. 69, p. 546-566.

Behar, F., M. Vandenbroucke, Y. Tang, F. Marquis, and J. Espitalie, 1997, Thermal cracking of kerogen in open and closed systems: determination of kinetic parameters and stoichiometric coefficients for oil and gas generation: Organic Geochemistry, v. 26, p. 321-339.

Behrens, A., P. Schae€er, S. Bernasconi, and P. Albrecht, 1999, 17(E)-13 (H)-malabarica-14(27),17,21-triene, an unexpected tricyclic hydrocarbon in sediments: Organic Geochemistry, v. 30, p. 379-383.

Berendsen, P., and K. Blair, 1995, Structural development of the Nemaha tectonic zone in Kansas, *in* K. S. Johnson, ed., Structural styles in the southern Midcontinent,, v. Circular 97, Oklahoma Geological Survey, p. 208-214.

Berner, R. A., M. R. Scott, and C. Thomlinson, 1970, Carbonate Alkalinity in the Pore Waters of Anoxic Marine Sediments1: Limnology and Oceanography, v. 15, p. 544-549.

Bird, C. W., J. M. Lynch, F. J. Pirt, W. W. Reid, C. J. W. Brooks, and B. S. Middleditch, 1971, Steroids and Squalene in Methylococcus capsulatus grown on Methane: Nature, v. 230, p. 473.

Bjorøy, M., K. Hall, P. Gillyon, and J. Jumeau, 1991, Carbon isotope variations in n-alkanes and isoprenoids of whole oils: Chemical Geology, v. 93, p. 13-20.

Blackwell, D., M. Richards, Z. Frone, J. Batir, A. Ruzo, R. Dingwall, and M. Williams, 2011, Temperature at depth maps for the conterminous US and geothermal resource estimate: GRC Transactions, v. 35.

Blakey, R., 2011, Paleogeography and geologic evolution of North America, Colorado Plateau Geosystems, Inc. http://cpgeosystems.com/nam.html

Blumer, M., R. R. L. Guillard, and T. Chase, 1971, Hydrocarbons of marine phytoplankton: Marine Biology, v. 8, p. 183-189.

Brassell, S., G. Eglinton, I. Marlowe, U. Pflaumann, and M. Sarnthein, 1986, Molecular stratigraphy: a new tool for climatic assessment: Nature, v. 320, p. 129.

Braun, J. C., 1961a, A stratigraphic study of the Sycamore and related formations in the southeastern Anadarko Basin.

Braun, J. C., 1961b, A stratigraphic study of the Sycamore and related formations in the southeastern Anadarko Basin: The Shale Shaker Digest v. 9-11, p. 150-164.

Brewer, J., R. Good, J. Oliver, L. Brown, and S. Kaufman, 1983, COCORP profiling across the Southern Oklahoma aulacogen: Overthrusting of the Wichita Mountains and compression within the Anadarko Basin: Geology, v. 11, p. 109-114.

Brody, F., and P. R. Ruby, 1960, Synthetic and Natural Sources of the Pyridine Ring, *in* E. Klingsberg, ed., Chemistry of Heterocyclic Compounds: Pyridine and its Derivatives I, v. 14: London, Interscience, p. 613.

Brooks, J. D., K. Gould, and J. W. Smith, 1969, Isoprenoid Hydrocarbons in Coal and Petroleum: Nature, v. 222, p. 257.

Brown, A. A., and J. T. Sentfle, 1997, Source potential of the Viola Springs Formation, southern limb of the Arbuckle anticline, Arbuckle Mountains, *in* K. S. Johnson, ed., Simpson and Viola Groups in the southern Midcontinent, v. Circular 99, Oklahoma Geological Survey p. 102.

Brown, D., 2014, Here's the SCOOP, Oklahoma plays offer untapped potential: AAPG Explorer, v. 35, p. 8,10.

Brown, S. W., and P. J. Swetland, 1992, Arbuckle oils—an overview, *in* K. S. a. C. Johnson, B.J., ed., Source rocks in the southern Midcontinent, v. Circular 93, Oklahoma Geological Survey, p. 175.

Brown, W., 1984, Washita Valley fault system—a new look at an old fault.

Burruss, R. C., and J. R. Hatch, 1989a, Geochemistry of oils and hydrocarbon source rocks, Greater Anadarko basin: evidence for multiple sources of oils and long distance oil migration, *in* K. S. Johnson, ed., Oklahoma Geological Survey, v. Circular 90: Anadarko Basin symposium, p. 53-64.

Burruss, R. C., and J. R. Hatch, 1989b, Geochemistry of oils and hydrocarbon source rocks, Greater Anadarko basin: evidence for multiple sources of oils and long distance oil migration, *in* K. S. Johnson, ed., Anadarko Basin symposium, v. Circular 90, Oklahoma Geological Survey, p. 53-64.

Cardott, B. J., 1989, Thermal maturation of the Woodford Shale in the Anadarko Basin,, *in* K. S. Johnson, ed., Anadarko basin symposium, v. Circular 90, 1988: Oklahoma Geological Survey p. 32-46.

Cardott, B. J., 2012, Thermal maturity of Woodford Shale gas and oil plays, Oklahoma, USA: International Journal of Coal Geology, v. 103, p. 109-119.

Cardott, B. J., and M. W. Lambert, 1985, Thermal maturation by vitrinite reflectance of Woodford Shale, Anadarko basin, Oklahoma: AAPG Bulletin, v. 69, p. 1982-1998.

Cardott, B. J., C. R. Landis, and M. E. Curtis, 2015, Post-oil solid bitumen network in the Woodford Shale, USA—a potential primary migration pathway: International Journal of Coal Geology, v. 139, p. 106-113.

Carter, D. W., 1982, A Study of Strike-Slip Movement Along the Washita Valley Fault Arbuckle Mountains, Oklahoma.

Carter, L. S., S. A. Kelley, D. D. Blackwell, and N. D. Naeser, 1998, Heat flow and thermal history of the Anadarko Basin, Oklahoma: AAPG bulletin, v. 82, p. 291-316.

Cassani, F., O. Gallango, S. Talukdar, C. Vallejos, and U. Ehrmann, 1988, Methylphenanthrene maturity index of marine source rock extracts and crude oils from the Maracaibo Basin, *in* L. Mattavelli, and L. Novelli, eds., Organic Geochemistry In Petroleum Exploration: Amsterdam, Pergamon, p. 73-80.

Chen, J., Y. Bi, J. Zhang, and S. Li, 1996a, Oil-source correlation in the Fulin basin, Shengli petroleum province, East China: Organic Geochemistry, v. 24, p. 931-940.

Chen, J., J. Fu, G. Sheng, D. Liu, and J. Zhang, 1996b, Diamondoid hydrocarbon ratios: novel maturity indices for highly mature crude oils: Organic Geochemistry, v. 25, p. 179-190.

Chenoweth, P. A., J. C. Braun, S. C. Champlin, and J. D. Prestridge, 1959, Sycamore and related formations of southern Oklahoma: Symposium of the Mississippian of Oklahoma and Kansas: Tulsa Geological Digest, v. 27, p. 113-123.

Cheynier, V., G. Comte, K. M. Davies, V. Lattanzio, and S. Martens, 2013, Plant phenolics: Recent advances on their biosynthesis, genetics, and ecophysiology: Plant Physiology and Biochemistry, v. 72, p. 1-20.

Clark, J. P., and R. P. Philp, 1987, Geochemical characterization of evaporite and carbonate depositional environments and correlation of associated crude oils in the Black Creek Basin, Alberta: Canadian Petroleum Geologists Bulletin, v. 37, p. 401-416.

Clark, T., T. M. Knox, M. A. McKervey, H. Mackle, and J. J. Rooney, 1979, Thermochemistry of bridged-ring substances. Enthalpies of formation of some diamondoid hydrocarbons and of perhydroquinacene. Comparisons with data from empirical force field calculations: Journal of the American Chemical Society, v. 101, p. 2404-2410.

Clayton, C. J., and M. Bjorøy, 1994, Effect of maturity on 13C12C ratios of individual compounds in North Sea oils: Organic Geochemistry, v. 21, p. 737-750.

Coffey, W. S., 2001, Lithostratigraphy and Porosity Characterization of the Sycamore Formation (Mississippian), and it's Relationship to Reservoir Performance, Carter-Knox Field, Grady and Stephens County, Oklahoma: The Shale Shaker v. 52, p. 9-17.

Comer, J. B., 1992, Potential for producing oil and gas from the Woodford Shale (Devonian-Mississippian) in the southern mid-continent, USA: AAPG Bulletin (American Association of Petroleum Geologists);(United States), v. 76.

Connan, J., J. Bouroullec, D. Dessort, and P. Albrecht, 1986, The microbial input in carbonate-anhydrite facies of a sabkha palaeoenvironment from Guatemala: A molecular approach: Organic Geochemistry, v. 10, p. 29-50.

Connock, G. T., T. X. Nguyen, and R. P. Philp, 2018, The development and extent of photic-zone euxinia concomitant with Woodford Shale deposition: AAPG Bulletin, v. 102, p. 959-986.

Corbett, R., and R. Smith, 1969, Lichens and fungi. Part VI. Dehydration rearrangements of 15-hydroxyhopanes: Journal of the Chemical Society C: Organic, p. 44-47.

Crone, A. J., and K. V. Luza, 1990, Style and timing of Holocene surface faulting on the Meers fault, southwestern Oklahoma: GSA Bulletin, v. 102, p. 1-17.

Cunningham, B., 1961a, Stratigraphy Oklahoma-Texas Panhandles.

Cunningham, B., 1961b, Stratigraphy Oklahoma-Texas Panhandles: oil and gas fields of the Texas and Oklahoma Panhandles: Amarillo: Panhandle Geological Society, p. 45-60.

Curiale, J. A., 1992, Petroleum geochemistry of Texas and Oklahoma oils along the Marathon—Ouachita fold-thrust belt, south-central U.S.A: Chemical Geology, v. 98, p. 151-173.

Curiale, J. A., and J. B. Curtis, 2016, Organic geochemical applications to the exploration for source-rock reservoirs – A review: Journal of Unconventional Oil and Gas Resources, v. 13, p. 1-31.

Curtiss, D., and D. Wavrek, 1997, The Oil Creek-Arbuckle Petroleum System, Major county, Oklahoma: Ames Structure in Northwest Oklahoma and Similar Features: Origin and Petroleum Production (1995 Symposium), p. 240-258.

Da Wang, H., and R. P. Philp, 1997, Geochemical study of potential source rocks and crude oils in the Anadarko Basin, Oklahoma: AAPG Bulletin, v. 81, p. 249-275.

Dahl, J., S. Liu, and R. Carlson, 2003, Isolation and structure of higher diamondoids, nanometer-sized diamond molecules: Science, v. 299, p. 96-99.

Dahl, J., J. M. Moldowan, K. Peters, G. Claypool, M. Rooney, G. Michael, M. Mello, and M. Kohnen, 1999a, Diamondoid hydrocarbons as indicators of natural oil cracking: Nature, v. 399, p. 54-57.

Dahl, J., J. M. Moldowan, R. E. Summons, M. A. McCaffrey, P. Lipton, D. S. Watt, and J. M. Hope, 1995, Extended 3β-alkyl steranes and 3-alkyl triaromatic steroids in crude oils and rock extracts: Geochimica et Cosmochimica Acta, v. 59, p. 3717-3729.

Dahl, J. E., J. M. Moldowan, K. E. Peters, G. E. Claypool, M. A. Rooney, G. E. Michael, M. R. Mello, and M. L. Kohnen, 1999b, Diamondoid hydrocarbons as indicators of natural oil cracking: Nature, v. 399, p. 54.

Dale, J., S. Larter, A. Aplin, and G. Macleod, 1995, The organic geochemistry of North Sea oil field production waters: Organic Geochemistry: Developments and Applications to Energy, Climate, Environments, and Human History. Selected papers from the 17th International Meeting on Organic Geochemistry, p. 4-8.

De Grande, S. M. B., F. R. Aquino Neto, and M. R. Mello, 1993, Extended tricyclic terpanes in sediments and petroleums: Organic Geochemistry, v. 20, p. 1039-1047.

Demaison, G., 1984, The Generative Basin Concept: Petroleum Geochemistry and Basin Evaluation: AAPG Memoir 35, p. 1-14.

Derenne, S., C. Largeau, E. Casadevall, J. S. Sinninghe Damsté, E. W. Tegelaar, and J. W. de Leeuw, 1990, Characterization of Estonian Kukersite by spectroscopy and pyrolysis: Evidence for abundant alkyl phenolic moieties in an Ordovician, marine, type II/I kerogen: Organic Geochemistry, v. 16, p. 873-888.

Didyk, B. M., B. R. T. Simoneit, S. C. Brassell, and G. Eglinton, 1978, Organic geochemical indicators of palaeoenvironmental conditions of sedimentation: Nature, v. 272, p. 216.

Difan, H., L. Jinchao, and Z. Dajiang, 1990, Maturation sequence of continental crude oils in hydrocarbon basins in China and its significance: Organic Geochemistry, v. 16, p. 521-529.

Dolton, G. L., and T. F. Finn, 1989, Petroleum geology of the Nemaha uplift, central mid-continent, Dept. of the Interior, US Geological Survey.

Donovan, R., M. Gilbert, K. Luza, W. Marchini, and D. Sanderson, 1983, Possible Quaternary movement on the Meers fault, southwestern Oklahoma: Oklahoma Geology Notes, v. 43, p. 124-133.

Donovan, R. N., 1986, Geology of the Slick Hills: Oklahoma Geological Survey Guidebook v. 24, p. 1-12.

Dorbon, M., J. M. Schmitter, P. Arpino, and G. Guiochon, 1982, Carbozoles et lactames du petrole methode d'extraction et caraterisation: Journal of Chromatography A, v. 246, p. 255-269.

Dorbon, M., J. M. Schmitter, P. Garrigues, I. Ignatiadis, M. Ewald, P. Arpino, and G. Guiochon, 1984, Distribution of carbazole derivatives in petroleum: Organic Geochemistry, v. 7, p. 111-120.

Dott, R. H., 1934, Overthrusting in Arbuckle Mountains, Oklahoma: AAPG Bulletin, v. 18, p. 567-602.

Dow, W. G., 1974, Application of oil-correlation and source-rock data to exploration in Williston Basin: AAPG bulletin, v. 58, p. 1253-1262.

Dyni, J. R., 2006, Geology and Resources of Some World Oil-Shale Deposits, Reston, VA, U.S. Geological Survey, U.S. Department of the Interior.

Dzou, L. I. P., and W. B. Hughes, 1993, Geochemistry of oils and condensates, K Field, offshore Taiwan: a case study in migration fractionation: Organic Geochemistry, v. 20, p. 437-462.

Edwards, D. S., D. M. McKirdy, S. J. Rowland, D. J. Heath, and P. S. Gray, 2018, Waxy bitumen stranding in southern Australia: A geochemical study of multiple oil families and their likely origins: Organic Geochemistry, v. 118, p. 132-151.

Eglinton, T. I., 1994, Carbon isotopic evidence for the origin of macromolecular aliphatic structures in kerogen: Organic Geochemistry, v. 21, p. 721-735.

Eglinton, T. I., and G. Eglinton, 2008, Molecular proxies for paleoclimatology: Earth and Planetary Science Letters, v. 275, p. 1-16.

EIA, 2015, Lower 48 states shale plays, U.S. Energy Information Administration

https://www.eia.gov/oil_gas/rpd/shale_gas.pdf.

EIA, U. S., 2018, U.S. Crude Oil and Natural Gas Proved Reserves, Year-end 2016, *in* U. S. D. o. Energy, ed., Washington, DC 20585, U.S. Energy Information Administration.

Elebiju, O. O., S. Matson, G. R. Keller, and K. J. Marfurt, 2011, Integrated geophysical studies of the basement structures, the Mississippi chert, and the Arbuckle Group of Osage County region, Oklahoma: AAPG bulletin, v. 95, p. 371-393.

Elias, M. K., and C. C. Branson, 1959, Type section of the Caney Shale, University of Oklahoma.

England, W. A., A. S. Mackenzie, D. M. Mann, and T. M. Quigley, 1987, The movement and entrapment of petroleum fluids in the subsurface: Journal of the Geological Society, v. 144, p. 327-347.

Espitalie, J., M. Madec, and B. Tissot, 1980, Role of mineral matrix in kerogen pyrolysis: influence on petroleum generation and migration: AAPG Bulletin, v. 64, p. 59-66.

F.G. Poole, and G. E. Claypool, 1984, Petroleum source-rock potential and crude-oil correlation in the Great Basin, *in* e. a. J. Woodward, ed., Hydrocarbon Source Rocks of the Greater Rocky Mountain Region, Rocky Mountain Assoc. Geol, p. 179-229.

Faulon, J.-L., P. G. Hatcher, G. A. Carlson, and K. A. Wenzel, 1993, A computer-aided molecular model for high volatile bituminous coal: Fuel Processing Technology, v. 34, p. 277-293.

Feinstein, S., 1981, Subsidence and thermal history of southern Oklahoma aulacogen: implications for petroleum exploration: AAPG Bulletin, v. 65, p. 2521-2533.

Förster, A., D. F. Merriam, and P. Hoth, 1998, Geohistory and thermal maturation in the Cherokee basin (mid-continent, USA): results from modeling: AAPG bulletin, v. 82, p. 1673-1693.

Foster, C. B., Reed, J.D. and Wicander, R., 1989, Gleoecapsomorpha prisca Zalessky, 1917: A new study, Part I: Taxonomy, geochemistry and paleoecology: Geobios, v. 22, p. 735-759.

Foster, C. B., Wicander, R. and Reed, J.D., 1990, 1990, Gleoecapsomorpha prisca Zalessky, 1917: A new study, Part II: Origin ofkukersite, a new interpretation. : Geobios, v. 23, p. 133-140.

Freeman, K. H., J. M. Hayes, J.-M. Trendel, and P. Albrecht, 1990, Evidence from carbon isotope measurements for diverse origins of sedimentary hydrocarbons: Nature, v. 343, p. 254.

Galimberti, R., C. Ghiselli, and M. A. Chiaramonte, 2000, Acidic polar compounds in petroleum: a new analytical methodology and applications as molecular migration indices: Organic Geochemistry, v. 31, p. 1375-1386.

Garner, D. L., and D. L. Turcotte, 1984, The thermal and mechanical evolution of the Anadarko basin: Tectonophysics, v. 107, p. 1-24.

Gaswirth, S. B., and D. K. Higley, 2013, Petroleum system analysis of the Hunton Group in West Edmond field, OklahomaHunton Group in West Edmond Field, Oklahoma: AAPG bulletin, v. 97, p. 1163-1179.

Gaswirth, S. B., and D. K. Higley, 2014, Chapter 5: Geologic Assessment of Undiscovered Oil and Gas Resources in the Cambrian Devonian Stratigraphy of the Anadarko Basin, Oklahoma, Kansas, Texas, and Colorado, *in* C. b. D. Higley, ed., Petroleum systems and assessment of undiscovered oil and gas in the Anadarko Basin Province, Colorado, Kansas, Oklahoma, and Texas—USGS Province, v. 58, USGS.

Gatewood, L. E., 1970, Oklahoma City field--anatomy of a giant.

Gatewood, L. E., 1979, Stratigrapic Trap Possibilities in the Arbuckle Group: General Relationships.

Gatewood, L. E., 1992, Can carbonates be source rocks for commercial petroleum deposits?, *in* K. S. Johnson, and B. J. Cardott, eds., Source rocks in the southern Midcontinent, v. Circular 93, Oklahoma Geological Survey, p. 270–281.

Gay Jr, S. P., 1999a, Strike-slip, compressional thrust-fold nature of the Nemaha system in eastern Kansas and Oklahoma: AAPG Midcontinent Section Meeting p. 39-50.

Gay Jr, S. P., 1999b, Strike-slip, compressional thrust-fold nature of the Nemaha system in eastern Kansas and Oklahoma.

Gay Jr, S. P., 2003a, The Nemaha Trend-A system of compressional thrust-fold, strike-slip structural features in Kansas and Oklahoma,(Part 2, conclusion).

Gay Jr, S. P., 2003b, The Nemaha Trend-A system of compressional thrust-fold, strike-slip structural features in Kansas and Oklahoma,(Part 2, conclusion): The Shale Shaker, v. 54 p. 39-49.

Gelpi, E., H. Schneider, J. Mann, and J. Oro, 1970, Hydrocarbons of geochemical significance in microscopic algae: Phytochemistry, v. 9, p. 603-612.

George, S. C., H. Volk, and M. Ahmed, 2007, Geochemical analysis techniques and geological applications of oil-bearing fluid inclusions, with some Australian case studies: Journal of Petroleum Science and Engineering, v. 57, p. 119-138.

Gilbert, C., 1983, Timing and chemistry of igneous events associated with the Southern Oklahoma Aulacogen: Tectonophysics, v. 94, p. 439-455.

Gilbert, M. C., 1992, Speculations on the origin of the Anadarko basin, Basement Tectonics 7, Springer, p. 195-208.

Godwin, C. J., D. R. B. II, and J. O. Puckette, 2017, Meramecian-Chesterian (Upper Viséan) conodont biostratigraphy and revised lithostratigraphy along the southwestern flank of the Ozark Uplift, southern mid-continent, U.S.A., *in* J. M. G. G. M. Grammer, J. O. Puckette, P. Jaiswal, S. J. Mazzullo, M. J. Pranter, and R. H. Goldstein, ed., Mississippian Reservoirs of the Midcontinent, v. 116, AAPG Memoir p. 116.

Gough, L., 1964, Conifer resin constituents, SOC CHEMICAL INDUSTRY 14 BELGRAVE SQUARE, LONDON SW1X 8PS, ENGLAND, p. 2059-2060.

Graebe, J. E., D. T. Dennis, C. D. Upper, and C. A. West, 1965, Biosynthesis of Gibberellins I. The Biosynthesis of (-)-Kaurene,(-)-Kauren-19-Ol, and Trans-Geranylgeraniol in Endosperm Nucellus of Echinocystis Macrocarpa Greene: Journal of Biological Chemistry, v. 240, p. 1847-1854.

Grammer, M. C. a. G. M., 2017, Characteristics of Debris Flows and Outrunner Blocks – Evidence for Mississippian Deposition on a Distally Steepened Ramp, *in* J. M. G. G. M.

Grammer, J. O. Puckette, P. Jaiswal, S. J. Mazzullo, M. J. Pranter, and R. H. Goldstein, ed., Mississippian Reservoirs of the Midcontinent, v. Memoir 116, AAPG.

Greenwood, P. F., K. R. Arouri, and S. C. George, 2000, Tricyclic terpenoid composition of Tasmanites kerogen as determined by pyrolysis GC-MS: Geochimica et Cosmochimica Acta, v. 64, p. 1249-1263.

Greenwood, P. F., and R. E. Summons, 2003, GC–MS detection and significance of crocetane and pentamethylicosane in sediments and crude oils: Organic Geochemistry, v. 34, p. 1211-1222.

Hall, A. P., 2012, he Kansas oil and gas industry--An enduring model of high-tech entrepreneurship, The Center for Applied Economics, Technical Report 12-1116, 95 p., University of Kansas School of Business.

Halpern, H. I., 1995, Development and applications of light-hydrocarbon-based star diagrams: AAPG Bulletin, v. 79, p. 801-815.

Ham, W. E., R. E. Denison, and C. A. Merritt, 1964, Basement rocks and structural evolution of southern Oklahoma: AAPG Bulletin, v. 48, p. 529-529.

Ham, W. E., and J. L. Wilson, 1967, Paleozoic epeirogeny and orogeny in the central United States: American Journal of Science, v. 265, p. 332-407.

Hanson, A. D., B. D. Ritts, D. Zinniker, J. M. Moldowan, and U. Biffi, , 2001, Upper Oligocene lacustrine source rocks and petroleum systems of the northern Qaidam basin, northwest China: AAPG Bulletin, v. 85, p. 601-619.

Hantschel, T., and A. I. Kauerauf, 2009, Fundamentals of basin and petroleum systems modeling, Springer Science & Business Media.

Harris, S. A., 1975a, Hydrocarbon Accumulation in "Meramec-Osage" (Mississippian) Rocks, Sooner Trend, Northwest-Central Oklahoma: AAPG Bulletin, v. 59, p. 633-665.

Harris, S. A., 1975b, Hydrocarbon accumulation in "Meramec-Osage" (Mississippian) Rocks, Sooner Trend, Northwest-Central Oklahoma: AAPG Bulletin, v. 59, p. 633-664.

Harrison, T., M. Heizler, and K. Burke, 1987, Aspects of thermal evolution of Anadarko Basin, Oklahoma: AAPG (Am. Assoc. Pet. Geol.) Bull.;(United States), v. 71.

Harvey, H. R., and G. B. McManus, 1991, Marine ciliates as a widespread source of tetrahymanol and hopan-3β-ol in sediments: Geochimica et Cosmochimica Acta, v. 55, p. 3387-3390.

Hatch, J. R., S. R. Jacobson, B. J. Witzke, J. B. Risatti, D. E. Anders, W. L. Watney, K. D. Newell, and A. K. Vuletich, 1987, Possible late Middle Ordovician organic carbon

isotope excursion: evidence from Ordovician oils and hydrocarbon source rocks, mid-continent and east-central United States: AAPG Bulletin, v. 71, p. 1342-1354.

Hatch, J. R., Rice, D.D., Burruss, R.C., Schmoker, J.W., and Clayton, J.L,, 1986, Thermal maturity modeling and geochemical characterization of hydrocarbon source rocks, oils, and natural gases of the Anadarko Basin, *in* L. M. H. Carter, ed., USGS Research on Energy Resources, v. Circular 974, US Geological Survey p. 21-23.

Hester, T. C., J. W. Schmoker, and H. L. Sahl, 1990, Log-derived regional source-rock characteristics of the Woodford Shale, Anadarko basin, Oklahoma, Department of the Interior, US Geological Survey.

Higley, D. K., 2013, 4D Petroleum System Model of the Mississippian System in the Anadarko Basin Province, Oklahoma, Kansas, Texas, and Colorado, USA: The Mountain Geologist, v. 50, p. 81-98.

Higley, D. K., 2014a, Thermal maturation of petroleum source rocks in the Anadarko basin province, Colorado, Kansas, Oklahoma, and Texas: DK Higley, comp., Petroleum systems and assessment of undiscovered oil and gas in the Anadarko Basin Province, Colorado, Kansas, Oklahoma, and Texas—USGS Province, v. 58.

Higley, D. K., 2014b, Petroleum systems and assessment of undiscovered oil and gas in the Anadarko Basin Province, Colorado, Kansas, Oklahoma, and Texas—USGS Province 58: U.S. Geological Survey Digital Data Series, v. DDS–69–EE, p. 327 p.

Higley, D. K., and S. B. Gaswirth, 2014, Chapter 2: Overview: Petroleum Systems and Assessment of Undiscovered Oil and Gas in the Anadarko Basin Province, Colorado, Kansas, Oklahoma, and Texas—USGS Province 58, *in* C. b. D. Higley, ed., Petroleum systems and assessment of undiscovered oil and gas in the Anadarko Basin Province, Colorado, Kansas, Oklahoma, and Texas—USGS Province, v. 58, USGS.

Higley, D. K., N. J. Gianoutsos, M. P. Pantea, and S. M. Strickland, 2014, Chapter 13: Precambrian to Ground Surface Grid Cell Maps and 3D Model of the Anadarko Basin Province, *in* C. b. D. Higley, ed., Petroleum systems and assessment of undiscovered oil and gas in the Anadarko Basin Province, Colorado, Kansas, Oklahoma, and Texas—USGS Province, v. 58, USGS.

Hill, E., 2017, Core and Wireline Log Based, Shelf to Basin Stratigraphic Framework of Mississippian Strata, East-Central Oklahoma, Oklahoma State University, Stillwater, Oklahoma.

Hill, E., 2018, Core and Wireline Log Based, Shelf to Basin Stratigraphic Framework of Mississippian Strata, East-Central Oklahoma: The Shale Shaker, v. 69, p. 230-191.

Hill, R. J., D. M. Jarvie, J. Zumberge, M. Henry, and R. M. Pollastro, 2007, Oil and gas geochemistry and petroleum systems of the Fort Worth Basin: AAPG bulletin, v. 91, p. 445-473.

Holba, A., L. Ellis, I. Dzou, A. Hallam, W. Masterson, J. Francu, and A. Fincannon, 2001, Extended tricyclic terpanes as age discriminators between Triassic, Early Jurassic and Middle-Late Jurassic oils: 20th International Meeting on Organic Geochemistry, p. 464.

Holba, A. G., J. E. Zumberge, B. J. Huizinga, H. Rosenstein, and L. I. Dzou, 2003, Extended tricyclic terpanes as indicators of marine upwelling: (abs.): 21st International Meeting on Organic Geochemistry, Krakow, v. Book of Abstracts, p. 131.

Holz, G. G., and N. L. Conner, 1973, The composition, metabolism and roles of lipids in Tetrahymena., *in* A. M. Elliott, ed., In Biology of Tetrahymena, Dowen, Hutchinson & Ross, Stroudburg., p. 99- 122.

Huang, W.-Y., and W. G. Meinschein, 1979, Sterols as ecological indicators: Geochimica et Cosmochimica Acta, v. 43, p. 739-745.

Huffman, G. G., 1955, Geology of the Ozark uplift, northeastern Oklahoma.

Hughes, W. B., 1984, Use of thiophenic organosulfur compounds in characterizing crude oils derived from carbonate versus siliciclastic sources, *in* J. G. Palacas, ed., Petroleum Geochemistry and Source Rock Potential of Carbonate Rocks: Tulsa, OK, American Association of Petroleum Geologists, p. 181–196.

Hughes, W. B., A. G. Holba, and L. I. P. Dzou, 1995, The ratios of dibenzothiophene to phenanthrene and pristane to phytane as indicators of depositional environment and lithology of petroleum source rocks: Geochimica et Cosmochimica Acta, v. 59, p. 3581-3598.

Hunt, J. E., 2017, Conodont Biostratigraphy in Middle Osagean to Upper Chesterian Strata, North-Central Oklahoma, U.S.A., Master's thesis, Oklahoma State University, Stillwater, Oklahoma, USA, 180 p.

Hunt, J. M., 1996, Petroleum geochemistry and geology, v. 2, WH Freeman New York.

Ioppolo, M., R. Alexander, and R. I. Kagi, 1992, Identification and analysis of C0–C3 phenols in some Australian crude oils: Organic Geochemistry, v. 18, p. 603-609.

Jacobi, D. J., J. J. Breig, B. LeCompte, M. Kopal, G. Hursan, F. E. Mendez, S. Bliven, and J. Longo, 2009, Effective Geochemical and Geomechanical Characterization of Shale Gas Reservoirs From the Wellbore Environment: Caney and the Woodford Shale, SPE Annual Technical Conference and Exhibition, New Orleans, Louisiana, Society of Petroleum Engineers, p. 20.

Jarvie, D., B. Claxton, F. Henk, and J. Breyer, 2001, Oil and shale gas from the Barnett Shale, Fort Worth Basin, Texas: AAPG Annual Meeting Program, v. 10, p: A100.

Jarvie, D. M., 2012, Shale resource systems for oil and gas: Part 2—Shale-oil resource systems.

Jenkins, W., 1970, Chitinozoa from the Ordovician Sylvan shale of the Arbuckle mountains, Oklahoma: Palaeontology, v. 13, p. 261-288.

Jiang, C., M. Li, K. G. Osadetz, L. R. Snowdon, M. Obermajer, and M. G. Fowler, 2001, Bakken/Madison petroleum systems in the Canadian Williston Basin. Part 2: molecular markers diagnostic of Bakken and Lodgepole source rocks: Organic Geochemistry, v. 32, p. 1037-1054.

Johnson, K. S., 1989a, Geologic evolution of the Anadarko basin: Anadarko basin symposium: Oklahoma Geological Survey Circular, p. 3-12.

Johnson, K. S., 1989b, Geologic evolution of the Anadarko basin, *in* K. S. Johnson, ed., Anadarko basin symposium: , Oklahoma Geological Survey Circular 90, p. 3-12.

Johnson, K. S., T. W. Amsden, R. E. Denison, S. P. Dutton, A. G. Goldstein, B. Rascoe, P. Sutherland, and D. Thompson, 1988a, Southern Midcontinent Region, *in* L. L. Sloss, ed., Sedimentary cover, North American Craton: U.S., v. 2: Evanston, Illinois, The Geological Society of America, p. 307-360.

Johnson, K. S., T. W. Amsden, R. E. Denison, S. P. Dutton, A. G. Goldstein, J. B. Rascoe, P. K. Sutherland, and D. M. Thompson, 1988b, Southern Midcontinent region, *in* L. L. Sloss, ed., Sedimentary Cover—North American Craton, Geological Society of America.

Jones, P. J., and R. P. Philp, 1990, Oils and source rocks from Pauls Valley, Anadarko Basin, Oklahoma, U.S.A: Applied Geochemistry, v. 5, p. 429-448.

Jordan, L., and Rowland, T. L., , 1959, Mississippian rocks in northern Oklahoma: Tulsa Geological Society Digest, v. 27, p. 124-136.

Katz, B., V. Robison, W. Dawson, and L. Elrod, 1994, Simpson-Ellenburger (.) petroleum system of the Central Basin Platform, West Texas, USA: Memoirs-American Association of Petroleum Geologists, P. 453-453.

Katz, B. J., 1983, Limitations of 'Rock-Eval' pyrolysis for typing organic matter: Organic Geochemistry, v. 4, p. 195-199.

Katz, B. J., and L. W. Elrod, 1983, Organic geochemistry of DSDP Site 467, offshore California, Middle Miocene to Lower Pliocene strata: Geochimica et Cosmochimica Acta, v. 47, p. 389-396.

Kaźmierczak, J., and B. Kremer, 2009, Spore-like bodies in some early Paleozoic acritarchs: Clues to chlorococcalean affinities: Acta Palaeontologica Polonica, v. 54, p. 541-551.

Keller, G. R., E. G. Lidiak, W. J. Hinze, and L. W. Braile, 1983, The role of rifting in the tectonic development of the midcontinent, U.S.A: Tectonophysics, v. 94, p. 391-412.

Keranen, K. M., M. Weingarten, G. A. Abers, B. A. Bekins, and S. Ge, 2014, Sharp increase in central Oklahoma seismicity since 2008 induced by massive wastewater injection: Science, v. 345, p. 448-451.

Killops, S., 1991, Novel aromatic hydrocarbons of probable bacterial origin in a Jurassic lacustrine sequence: Organic geochemistry, v. 17, p. 25-36.

Killops, S. D., J. I. Raine, A. D. Woolhouse, and R. J. Weston, 1995, Chemostratigraphic evidence of higher-plant evolution in the Taranaki Basin, New Zealand: Organic Geochemistry, v. 23, p. 429-445.

Kirkland, D., R. Denison, D. Summers, J. Gormly, K. Johnson, and B. Cardott, 1992, Geology and organic geochemistry of the Woodford Shale in the Criner Hills and western Arbuckle Mountains, Oklahoma, Oklahoma Geological Survey Circular, v. 93, p. 38-69.

Kluth, C., 1986, Plate tectonics of the Ancestral Rocky Mountains: Part III. Middle Rocky Mountains, *in* J. E. Peterson, ed., Paleotectonics and Sedimentation in the Rocky Mountain Region, United States.

, AAPG Memoir 41, p. 353-369.

Knebel, G. M., and G. Rodriguez-Eraso, 1956, Habitat of some oil: AAPG Bulletin, v. 40, p. 547-561.

Kuuskraa, V., S. H. Stevens, and K. D. Moodhe, 2013, Technically recoverable shale oil and shale gas resources: an assessment of 137 shale formations in 41 countries outside the United States, US Energy Information Administration, US Department of Energy.

Langworthy, T. A., W. R. Mayberry, and P. F. Smith, 1976, A sulfonolipid and novel glucosamidyl glycolipids from the extreme thermoacidophile Bacillus acidocaldarius: Biochimica et Biophysica Acta (BBA) - Lipids and Lipid Metabolism, v. 431, p. 550-569.

Larter, S., B. Bowler, E. Clarke, C. Wilson, B. Moffatt, B. Bennett, G. Yardley, and D. Carruthers, 2000, An experimental investigation of geochromatography during secondary migration of petroleum performed under subsurface conditions with a real rock: Geochemical Transactions, v. 1, p. 54.

Larter, S. R., and A. C. Aplin, 1995, Reservoir geochemistry: methods, applications and opportunities: Geological Society, London, Special Publications, v. 86, p. 5-32.

Larter, S. R., B. F. J. Bowler, M. Li, M. Chen, D. Brincat, B. Bennett, K. Noke, P. Donohoe, D. Simmons, M. Kohnen, J. Allan, N. Telnaes, and I. Horstad, 1996, Molecular indicators of secondary oil migration distances: Nature, v. 383, p. 593.

LeBlanc, S. L., 2014, High resolution sequence stratigraphy and reservoir characterization of the" Mississippian Limestone" in north-central Oklahoma, Oklahoma State University, Stillwater, Oklahoma.

Levine, D. G., R. H. Schlosberg, and B. G. Silbernagel, 1982, Understanding the chemistry and physics of coal structure (A Review): Proceedings of the National Academy of Sciences, v. 79, p. 3365-3370.

Lewan, M., 1985, Evaluation of petroleum generation by hydrous pyrolysis experimentation: Phil. Trans. R. Soc. Lond. A, v. 315, p. 123-134.

Lewan, M. D., M. J. Kotarba, J. B. Curtis, D. Więcław, and P. Kosakowski, 2006, Oil-generation kinetics for organic facies with Type-II and -IIS kerogen in the Menilite Shales of the Polish Carpathians: Geochimica et Cosmochimica Acta, v. 70, p. 3351-3368.

Lewan, M. D., and T. E. Ruble, 2002, Comparison of petroleum generation kinetics by isothermal hydrous and nonisothermal open-system pyrolysis: Organic Geochemistry, v. 33, p. 1457-1475.

Li, M., S. R. Larter, D. Stoddart, and M. Bjoroey, 1992, Liquid chromatographic separation schemes for pyrrole and pyridine nitrogen aromatic heterocycle fractions from crude oils suitable for rapid characterization of geochemical samples: Analytical Chemistry, v. 64, p. 1337-1344.

Li, M., N. Zhong, S. Shi, L. Zhu, and Y. Tang, 2013, The origin of trimethyldibenzothiophenes and their application as maturity indicators in sediments from the Liaohe Basin, East China: Fuel, v. 103, p. 299-307.

Liang, Q., Y. Xiong, C. Fang, and Y. Li, 2012, Quantitative analysis of diamondoids in crude oils using gas chromatography–triple quadrupole mass spectrometry: Organic Geochemistry, v. 43, p. 83-91.

Lochte, H. L., and E. R. Littmann, 1955, The petroleum acids and bases: New York, Chemical Publishing Company.

Longman, M. W., and S. E. Palmer, 1987, Organic geochemistry of mid-continent Middle and Late Ordovician oils: AAPG Bulletin, v. 71, p. 938-950.

Lu, H., G. Sheng, P. a. Peng, Q. Ma, and Z. Lu, 2011, Identification of C24 and C25 lanostanes in Tertiary sulfur rich crude oils from the Jinxian Sag, Bohai Bay Basin, Northern China: Organic Geochemistry, v. 42, p. 146-155.

Luza, K. V., and J. E. Lawson Jr, 1983, Seismicity and tectonic relationships of the Nemaha uplift in Oklahoma, Part V, (final report): Oklahoma Geological Survey Open-File Report v. 1-83, p. 115.

Mackenzie, A. S., S. C. Brassell, G. Eglinton, and J. R. Maxwell, 1982a, Chemical Fossils: The Geological Fate of Steroids: Science, v. 217, p. 491-504.

Mackenzie, A. S., N. A. Lamb, and J. R. Maxwell, 1982b, Steroid hydrocarbons and the thermal history of sediments: Nature, v. 259, p. 223–6.

Magoon, L. B., and W. G. Dow, 1994, The petroleum system: chapter 1: Part I. Introduction.

Mahato, S. B., and S. Sen, 1997, Advances in triterpenoid research, 1990–1994: Phytochemistry, v. 44, p. 1185-1236.

Mango, F. D., 1987, An Invariance in the Isoheptanes of Petroleum: Science, v. 237, p. 514-517.

Maughan, T. J., and D. Deming, 2006, Gas occurrence in the Caney Shale, part 1.

McConnell, D., 1987, Paleozoic structural evolution of the Wichita uplift, southwestern Oklahoma, Texas A&M University, College Station, Texas.

McKee, E. D., E. J. Crosby, G. O. Bachman, K. G. Bell, G. H. Dixon, S. E. Frezon, E. E. Glick, W. P. Irwin, W. W. Mallory, and W. J. Mapel, 1975, Paleotectonic investigations of the Pennsylvanian System in the United States, part I: introduction and regional analyses of the Pennsylvanian System, US Government Printing Office.

Mei, M., K. K. Bissada, T. B. Malloy, L. M. Darnell, and E. B. Szymcyk, 2018, Improved method for simultaneous determination of saturated and aromatic biomarkers, organosulfur compounds and diamondoids in crude oils by GC–MS/MS: Organic Geochemistry, v. 116, p. 35-50.

Meissner, F. F., J. Woodward, and J. L. Clayton, 1984, Stratigraphic relationships and distribution of source rocks in the greater Rocky Mountain region: in J. Woodward, F.F. Meissner, and J. L. Clayton, eds., Hydrocarbon source rocks of the greater Rocky Mountain region: Denver, CO, Rocky Mountain Association of Geologist, p. 1-34.

Mello, M. R., P. C. Gaglianone, S. C. Brassell, and J. R. Maxwell, 1988, Geochemical and biological marker assessment of depositional environments using Brazilian offshore oils: Marine and Petroleum Geology, v. 5, p. 205-223.

Meredith, W., S. J. Kelland, and D. M. Jones, 2000, Influence of biodegradation on crude oil acidity and carboxylic acid composition: Organic Geochemistry, v. 31, p. 1059-1073.

Miceli Romero, A., and R. P. Philp, 2012, Organic geochemistry of the Woodford Shale, southeastern Oklahoma: How variable can shales be?: AAPG bulletin, v. 96, p. 493-517.

Milam, K., 2013, OSU-Industry consortium eyes Mississippian:: AAPG Explorer, v. 34, p. 36-39.

Mitchell, J., 2011, Horizontal drilling of deep granite wash reservoirs, Anadarko Basin, Oklahoma and Texas.

Mohammadi, S., T. A. Ewald, J. M. Gregg, and K. L. Shelton, 2017, Diagenesis of Mississippian carbonate rocks in north-central Oklahoma, USA, *in* J. M. G. G. M. Grammer, J. O. Puckette, P. Jaiswal, S. J. Mazzullo, M. J. Pranter, and R. H. Goldstein, ed., Mississippian Reservoirs of the Midcontinent, v. Memoir 116, AAPG

Mohammadi, S., T. A. Ewald, J. M. Gregg, and K. L. Shelton, 2018, Diagenesis of Mississippian carbonate rocks in north-central Oklahoma, USA, *in* J. M. G. G. M. Grammer, J. O. Puckette, P. Jaiswal, S. J. Mazzullo, M. J. Pranter, and R. H. Goldstein, ed., Mississippian Reservoirs of the Midcontinent, v. Memoir 116, AAPG

Moldowan, J., Zinniker, D., Liu, Z., Rovenskaya-Nemchenko, A., Nemchenko, T., , 2011, Geochemical parameters for unravelling mixtures. Examples from the South Atlantic continental margins and the giant north-central West Siberian gas fields. In: Proceedings of the 25th International Meeting on Organic Geochemistry IMOG 2011, Interlaken, Switzerland, 18–23 September, p. 424 (Book of Abstracts, P-291).

Moldowan, J. M., J. Dahl, D. Zinniker, and S. M. Barbanti, 2015, Underutilized advanced geochemical technologies for oil and gas exploration and production-1. The diamondoids: Journal of Petroleum Science and Engineering, v. 126, p. 87-96.

Moldowan, J. M., F. J. Fago, R. M. K. Carlson, D. C. Young, G. an Duvne, J. Clardy, M. Schoell, C. T. Pillinger, and D. S. Watt, 1991, Rearranged hopanes in sediments and petroleum: Geochimica et Cosmochimica Acta, v. 55, p. 3333-3353.

Moldowan, J. M., S. R. Jacobson, J. Dahl, A. Al-Hajji, B. J. Huizinga, F. J. Fago, A. Zhuravlev, and R. Riding, 2001, Molecular fossils demonstrate Precambrian origin of dinoflagellates: The ecology of the Cambrian radiation, p. 474-493.

Moldowan, J. M., W. K. Seifert, and E. J. Gallegos, 1983, Identifcation of an extended series of tricyclic terpanes in petroleum: Geochimica et Cosmochimica Acta, v. 47, p. 1531-1534.

Moldowan, J. M., W. K. Seifert, and E. J. Gallegos, 1985, Relationship between petroleum composition and depositional environment of petroleum source rocks: AAPG bulletin, v. 69, p. 1255-1268.

Moldowan, J. M., and N. M. Talyzina, 1998, Biogeochemical evidence for dinoflagellate ancestors in the Early Cambrian: Science, v. 281, p. 1168-1170.

Moldowan, M., Dahl, J.E., Moldowan, S.M., Takaki, T., Mello, M.R., Barbanti, S.M., , 2014, Determining multiple sources, facies and oil-mixtures of the South Atlantic Margins: Africa and Brazil: In: AAPG Datapages/Search and Discovery Article #90189 © 2014 AAPG Annual Convention and Exhibition, Houston, Texas, USA, April 6–9, 2014b.

Molinares-Blanco, C. E., and R. M. Slatt, 2014, Thomas Amsden's Pre-Woodford Sub-Crop Maps and the Late Devonian–Early Mississippian Unconventional Plays in the Arkoma Basin.

Murray, A. P., R. E. Summons, C. J. Boreham, and L. M. Dowling, 1994, Biomarker and n-alkane isotope profiles for Tertiary oils: relationship to source rock depositional setting: Organic Geochemistry, v. 22, p. 521-IN6.

Murris., R. J., 1984, Introduction, *in* R. J. Murris, ed., Petroleum Geochemistry and Basin Evaluation, v. Memoir 35: Tulsa, Oklahoma, merican Association of Petroleum Geologists, p. x–xii.

Nakahara, S., S. Stauss, T. Kato, T. Sasaki, and K. Terashima, 2011, Synthesis of higher diamondoids by pulsed laser ablation plasmas in supercritical CO_2: Journal of Applied Physics, v. 109, p. 123304.

Noble, R. A., R. Alexander, R. I. Kagi, and J. Knox, 1985, Tetracyclic diterpenoid hydrocarbons in some Australian coals, sediments and crude oils: Geochimica et Cosmochimica Acta, v. 49, p. 2141-2147.

Noble, R. A., R. Alexander, R. I. Kagi, and J. K. Nox, 1986, Identification of some diterpenoid hydrocarbons in petroleum: Organic Geochemistry, v. 10, p. 825-829.

Oshima, F., S. Stauss, C. Ishii, D. Z. Pai, and K. Terashima, 2012, Plasma microreactor in supercritical xenon and its application to diamondoid synthesis: Journal of Physics D: Applied Physics, v. 45, p. 402003.

Ourisson, G., P. Albrecht, and M. Rohmer, 1982, Predictive microbial biochemistry from molecular fossils to procaryotic mebranes: Trends in Biochemical Sciences, v. 7, p. 236-239.

Ourisson, G., P. Albrecht, and M. Rohmer, 1984, The Microbial Origin of Fossil Fuels: Scientific American, v. 251, p. 44-51.

Ourisson, G., M. Rohmer, and K. Poralla, 1987, Prokaryotic hopanoids and other polyterpenoid sterol surrogates: Annual Reviews in Microbiology, v. 41, p. 301-333.

Pawlewicz, M. J., 1866, Thermal maturation of the eastern Anadarko basin: Oklahoma: US Geological Survey Bulletin.

Pawlewicz, M. J., 1990, Thermal Maturation of the Eastern Anadarko Basin, Oklahoma: By Mark J. Pawlewicz, Department of the Interior, US Geological Survey.

Peace, H., 1994, Mississippian facies relationships, eastern Anadarko basin: Oklahoma: Oklahoma City Geological Society Shale Shaker, v. 45, p. 26-35.

Perrodon, A., 1992, Petroleum systems: models and applications: Journal of Petroleum Geology, v. 15, p. 319-325.

Perry, W. J., 1989, Tectonic evolution of the Anadarko Basin region, Oklahoma, Department of the Interior, US Geological Survey.

Peters, C. A., C. Hallmann, and S. C. George, 2018, Phenolic compounds in oil-bearing fluid inclusions: Implications for water-washing and oil migration: Organic Geochemistry, v. 118, p. 36-46.

Peters, K., J. M. Moldowan, A. Driscole, and G. Demaison, 1989, Origin of Beatrice oil by co-sourcing from Devonian and Middle Jurassic source rocks, inner Moray Firth, United Kingdom: AAPG Bulletin, v. 73, p. 454-471.

Peters, K., C. C. Walters, and J. M. Moldowan, 2005a, The biomarker guide: biomarkers and isostopes in the environment and human history, v. 2, Cambridge University Press, 704 p.

Peters, K., C. C. Walters, and J. M. Moldowan, 2005b, The biomarker guide: biomarkers and isostopes in the environment and human history. 1, v. 1, Cambridge University Press, 704p.

Peters, K. E., 2000, Petroleum tricyclic terpanes: predicted physicochemical behavior from molecular mechanics calculations: Organic Geochemistry, v. 31, p. 497-507.

Peters, K. E., and M. G. Fowler, 2002, Applications of petroleum geochemistry to exploration and reservoir management: Organic Geochemistry, v. 33, p. 5-36.

Peters, K. E., and J. M. Moldowan, 1993, The biomarker guide: interpreting molecular fossils in petroleum and ancient sediments, Prentice Hall.

Peters, K. E., J. M. Moldowan, and P. Sundararaman, 1990, Effects of hydrous pyrolysis on biomarker thermal maturity parameters: Monterey Phosphatic and Siliceous members: Organic Geochemistry, v. 15, p. 249-265.

Peterson, F. A., 1983, Foreland detachment structures, *in* J. D. Lowell, and R. R. Gries, eds., Rocky Mountain Foreland Basins and Uplifts Rocky Mountain Association of Geologists Guidebook, p. 65-77.

Philp, R. P., and T. D. Gilbert, 1986, Biomarker distributions in Australian oils predominantly derived from terrigenous source material: Organic Geochemistry, v. 10, p. 73-84.

Philp, R. P., and L. Mansuy, 1997, Petroleum geochemistry: concepts, applications, and results: Energy & fuels, v. 11, p. 749-760.

Philp, R. P., J. Oung, and C. A. Lewis, 1988, Biomarker determinations in crude oils using a triple-stage quadrupole mass spectrometer: Journal of Chromatography A, v. 446, p. 3-16.

Picha, F. J., and K. E. Peters, 1998, Biomarker oil-to-source rock correlation in the Western Carpathians and their foreland, Czech Republic: Petroleum Geoscience, v. 4, p. 289-302.

Pickel, W., J. Kus, D. Flores, S. Kalaitzidis, K. Christanis, B. J. Cardott, M. Misz-Kennan, S. Rodrigues, A. Hentschel, M. Hamor-Vido, P. Crosdale, and N. Wagner, 2017, Classification of liptinite – ICCP System 1994: International Journal of Coal Geology, v. 169, p. 40-61.

Powell, T. G., and D. M. McKirdy, 1973, Relationship between ratio of pristane to phytane, crude oil composition and geological environment in Australia: Nature Physical Science, v. 243, p. 37.

Pu, F., R. P. Philip, L. Zhenxi, and Y. Guangguo, 1990, Geochemical characteristics of aromatic hydrocarbons of crude oils and source rocks from different sedimentary environments: Organic Geochemistry, v. 16, p. 427-435.

Puckette, J., A. Abdalla, A. Rice, and Z. Al-Shaieb, 1996, The Upper Morrow reservoirs: complex fluvio-deltaic depositional systems: Circular-Oklahoma Geological Survey, v. 98, p. 47-84.

Puckette, J., D. Boardman, and W. Watney, 2013, Woodford Shale, correlating rock properties in outcrop and core with wireline log characteristics, PowerPoint presentation. Double Tree by Hilton, Wichita, KS.

Quan, T. M., E. N. Adigwe, N. Riedinger, and J. Puckette, 2013, Evaluating nitrogen isotopes as proxies for depositional environmental conditions in shales: Comparing Caney and Woodford Shales in the Arkoma Basin, Oklahoma: Chemical geology, v. 360, p. 231-240.

Radke, M., 1988, Application of aromatic compounds as maturity indicators in source rocks and crude oils: Marine and Petroleum Geology, v. 5, p. 224-236.

Radke, M., D. H. Welte, and H. Willsch, 1982a, Geochemical study on a well in the Western Canada Basin: relation of the aromatic distribution pattern to maturity of organic matter: Geochimica et Cosmochimica Acta, v. 46, p. 1-10.

Radke, M., D. H. Welte, and H. Willsch, 1986, Maturity parameters based on aromatic hydrocarbons: Influence of the organic matter type: Organic Geochemistry, v. 10, p. 51-63.

Radke, M., H. Willsch, D. Leythaeuser, and M. Teichmüller, 1982b, Aromatic components of coal: relation of distribution pattern to rank: Geochimica et Cosmochimica Acta, v. 46, p. 1831-1848.

Radke, M. W., D. H. , 1983, The methylphenanthrene index (MPI): a maturity parameter based on aromatic hydrocarbons, in D. L. J. W. a. L. G. W. M. Schenck P. A., ed., Advances in Organic Geochemistry 1981 Wiley, Chichester, p. 504-512.

Ramezani, H., and G. A. Mansoori, 2007, Diamondoids as molecular building blocks for nanotechnology, Molecular Building Blocks for Nanotechnology, Springer, p. 44-71.

Ramondetta, P. J., 1990, El Dorado: An old field with potential: Oil and Gas Journal, v. 26, p. 110-116.

Reed, J. D., H. A. Illich, and B. Horsfield, 1986, Biochemical evolutionary significance of Ordovician oils and their sources: Organic Geochemistry, v. 10, p. 347-358.

Requejo, A., 1992, Quantitative analysis of triterpane and sterane biomarkers: methodology and applications in molecular maturity studies, *in* P. A. a. R. P. P. J. M. Moldowan, ed., Biological Markers in Sediments and Petroleum: NJ, Prentice-Hall, Englewood Cliffs, p. 222-240.

Requejo, A. G., G. B. Hieshima, C. S. Hsu, T. J. McDonald, and R. Sassen, 1997, Short-chain (C21 and C22) diasteranes in petroleum and source rocks as indicators of maturity and depositional environment: Geochimica et Cosmochimica Acta, v. 61, p. 2653-2667.

Rieley, G., R. J. Collier, D. M. Jones, G. Eglinton, P. A. Eakin, and A. E. Fallick, 1991, Sources of sedimentary lipids deduced from stable carbon-isotope analyses of individual compounds: Nature, v. 352, p. 425.

Robert H. Goldstein, T. J. R., 1994, Systematics of fluid inclusions in diagenetic minerals, SEPM Society for Sedimentary Geology.

Roedder, E., 2003, Fluid Inclusions, *in* R. A. Meyers, ed., Encyclopedia of physical science and technology (Third Edition): New York, Academic Press, p. 71-77.

Rogers, S. M., 2001, Deposition and diagenesis of Mississippian chat reservoirs, north-central Oklahoma: AAPG Bulletin, v. 85, p. 115-129.

Rohmer, M., P. Bouvier-Nave, and G. Ourisson, 1984, Distribution of hopanoid triterpenes in prokaryotes: microbiology, v. 130, p. 1137-1150.

Romero-Sarmiento, M.-F., D. Pillot, G. Letort, V. Lamoureux-Var, V. Beaumont, A.-Y. Huc, and B. Garcia, 2016, New Rock-Eval method for characterization of unconventional shale resource systems: Oil Gas Sci. Technol. – Rev. IFP Energies nouvelles, v. 71, p. 37.

Romero, A. A. M., T. Nguyen, and R. P. Philp, 2017, Organic geochemistry of the Eagle Ford Group in Texas: AAPG Bulletin.

Romero, A. M., and R. P. Philp, 2012, Organic geochemistry of the Woodford Shale, southeastern Oklahoma: How variable can shales be?: AAPG Bulletin, v. 96, p. 493-517.

Rontani, J.-F., and P. Bonin, 2011, Production of pristane and phytane in the marine environment: role of prokaryotes: Research in Microbiology, v. 162, p. 923-933.

Ross, C. A., 1979, Late Paleozoic collision of North and South America: Geology, v. 7, p. 41-44.

Rubinstein, I., O. Sieskind, and P. Albrecht, 1975, Rearranged sterenes in a shale: occurrence and simulated formation: Journal of the Chemical Society, Perkin Transactions 1, p. 1833-1836.

S. J. Mazzullo, B. W. W., Darwin R. Boardman, Beau T. Morris, Cory J. Godwin, 2017, Lithostratigraphy, Biostratigraphy, Stratigraphic Architecture, and Depositional Systems in Lower to Middle Mississippian Strata on the Western Flank of the Ozark Dome, Midcontinent USA, *in* J. M. G. G. M. Grammer, J. O. Puckette, P. Jaiswal, S. J. Mazzullo, M. J. Pranter, and R. H. Goldstein, ed., Mississippian Reservoirs of the Midcontinent, v. Memoir 116, AAPG

Sacksteder, K. A., M. Protopopova, C. E. Barry, K. Andries, and C. A. Nacy, 2012, Discovery and development of SQ109: a new antitubercular drug with a novel mechanism of action: Future microbiology, v. 7, p. 823-837.

Schever, P., 2012, Chemistry of marine natural products, Elsevier.

Schmitter, J., and P. Arpino, 1983, Possible origin and fate of α-methylquinolines and α-methylbenzo [h] quinolines from crude oils, Advances in Organic Geochemistry 1981, Wiley Chichester, p. 808-812.

Schmoker, J., 1986, Oil generation in the Anadarko basin, Oklahoma and Texas: Modeling using Lopatin's method, Oklahoma Geological Survey.

Schowalter, T. T., 1979, Mechanics of secondary hydrocarbon migration and entrapment: AAPG bulletin, v. 63, p. 723-760.

Schulz, L. K., A. Wilhelms, E. Rein, and A. S. Steen, 2001, Application of diamondoids to distinguish source rock facies: Organic Geochemistry, v. 32, p. 365-375.

Seifert, W. K., and J. M. Moldowan, 1979, The effect of biodegradation on steranes and terpanes in crude oils: Geochimica et Cosmochimica Acta, v. 43, p. 111-126.

Seifert, W. K., and J. M. Moldowan, 1981, Paleoreconstruction by biological markers: Geochimica et Cosmochimica Acta, v. 45, p. 783-794.

Seifert, W. K., and J. M. Moldowan, 1986, Use of biological markers in petroleum exploration, *in* J. R. B, ed., Methods in Geochemistry and Geophysics, v. 24, p. 61-290.

Seifert, W. K., J. M. Moldowan, and R. W. Jones, 1980, Application of biological marker chemistry to petroleum exploration: Proceedings of the Tenth World Petroleum Congress. Bucharest, Romania. September, 1979. Paper SP8, Heyden, p. 425-440.

Serpa, L., T. Setzer, and L. Brown, 1989, COCORP seismic-reflection profiling in northeastern Kansas: Geophysics in Kansas: Kansas Geological Survey Bulletin, v. 226, p. 165-176.

Shan-Tan, L., and I. R. Kaplan, 1992, Diterpanes, triterpanes, steranes and aromatic hydrocarbons in natural bitumens and pyrolysates from different mimic coals: Geochimica et Cosmochimica Acta, v. 56, p. 2761-2788.

Shanafelt, T. D., Y. K. Lee, N. D. Bone, A. K. Strege, V. L. Narayanan, E. A. Sausville, S. M. Geyer, S. H. Kaufmann, and N. E. Kay, 2005, Adaphostin-induced apoptosis in CLL B cells is associated with induction of oxidative stress and exhibits synergy with fludarabine: Blood, v. 105, p. 2099-2106.

Shannon Jr, J. P., 1962, Hunton Group (Silurian-Devonian) and related strata in Oklahoma: AAPG Bulletin, v. 46, p. 1-29.

Sieminski, A., 2014a, Statement of Adam Sieminski, Administrator, Energy Information Administration, before the Committee on Energy and Commerce, Subcommittee on Energy and Power, U.S. House of Representatives, December 11, 2014: EIA Testimonies. Retrieved July 31, 2015, from

http://www.eia.gov/pressroom/testimonies/sieminski_12112014.pdf.

Sieminski, A., 2014b, US Oil and Natural Gas Outlook: IAEE International Conference.

Simoneit, B. R. T., J. O. Grimalt, T. G. Wang, R. E. Cox, P. G. Hatcher, and A. Nissenbaum, 1986, Cyclic terpenoids of contemporary resinous plant detritus and of fossil woods, ambers and coals: Organic Geochemistry, v. 10, p. 877-889.

Sivan, P., G. C. Datta, and R. R. Singh, 2008, Aromatic biomarkers as indicators of source, depositional environment, maturity and secondary migration in the oils of Cambay Basin, India: Organic Geochemistry, v. 39, p. 1620-1630.

Sofer, Z., 1984, Stable carbon isotope compositions of crude oils: application to source depositional environments and petroleum alteration: AAPG bulletin, v. 68, p. 31-49.

Sonnenberg, S. A., and L. Meckel, 2016, Our current working model for unconventional tight petroleum systems: oil and gas, AAPG Annual Convention and Exhibition, Calgary Canada.

Statler, A. T., 1965, Stratigraphy of the Simpson Group in Oklahoma: Tulsa Geological Society Digest, v. 33 p. 162-211.

Sullivan, K. L., 1985, Organic facies variation of the Woodford Shale in western Oklahoma.

Summons, R. E., and R. J. Capon, 1991, Identification and significance of 3β-ethyl steranes in sediments and petroleum: Geochimica et Cosmochimica Acta, v. 55, p. 2391-2395.

Suneson, N. H., 2012, Arkoma Basin Petroleum-Past, Present, and Future: Shale Shaker, v. 36, p. 38-70.

Sutherland, P. K., 1988, Late Mississippian and Pennsylvanian depositional history in the Arkoma basin area, Oklahoma and Arkansas: Geological Society of America Bulletin, v. 100, p. 1787-180.

Sven, S., I. Chikako, Z. P. David, U. Keiichiro, and T. Kazuo, 2014, Diamondoid synthesis in atmospheric pressure adamantane–argon–methane–hydrogen mixtures using a continuous flow plasma microreactor: Plasma Sources Science and Technology, v. 23, p. 035016.

Svingen, P. A., A. Tefferi, T. J. Kottke, G. Kaur, V. L. Narayanan, E. A. Sausville, and S. H. Kaufmann, 2000, Effects of the bcr/abl Kinase Inhibitors AG957 and NSC 680410 on Chronic Myelogenous Leukemia Cells in Vitro: Clinical Cancer Research, v. 6, p. 237-249.

Swanson, D. C., 1979, Deltaic deposits in the Pennsylvanian upper Morrow Formation of the Anadarko basin.

Talyzina, N. M., J. M. Moldowan, A. Johannisson, and F. J. Fago, 2000, Affinities of Early Cambrian acritarchs studied by using microscopy, fluorescence flow cytometry and biomarkers: Review of Palaeobotany and Palynology, v. 108, p. 37-53.

Tanner, J. H., 1967, Wrench fault movements along Washita Valley fault, Arbuckle Mountain area, Oklahoma: AAPG Bulletin, v. 51, p. 126-134.

Taylor, P., S. Larter, M. Jones, J. Dale, and I. Horstad, 1997, The effect of oil-water-rock partitioning on the occurrence of alkylphenols in petroleum systems: Geochimica et Cosmochimica Acta, v. 61, p. 1899-1910.

Ten Haven, H. L., J. W. De Leeuw, and P. A. Schenck, 1985, Organic geochemical studies of a Messinian evaporitic basin, northern Apennines (Italy) I: Hydrocarbon biological markers for a hypersaline environment: Geochimica et Cosmochimica Acta, v. 49, p. 2181-2191.

Ten Haven, H. L., M. Rohmer, J. Rullkötter, and P. Bisseret, 1989, Tetrahymanol, the most likely precursor of gammacerane, occurs ubiquitously in marine sediments: Geochimica et Cosmochimica Acta, v. 53, p. 3073-3079.

Thomas, B. R., 1969, Kauri Resins—Modern and Fossil, *in* G. Eglinton, and M. T. J. Murphy, eds., Organic Geochemistry: Methods and Results: Berlin, Heidelberg, Springer Berlin Heidelberg, p. 599-618.

Thompson, K. F. M., 1983, Classification and thermal history of petroleum based on light hydrocarbons: Geochimica et Cosmochimica Acta, v. 47, p. 303-316.

Thompson, K. F. M., 1987, Fractionated aromatic petroleums and the generation of gas-condensates: Organic Geochemistry, v. 11, p. 573-590.

Tissot, B., R. Pelet, and P. Ungerer, 1987, Thermal history of sedimentary basins, maturation indices, and kinetics of oil and gas generation: AAPG bulletin, v. 71, p. 1445-1466.

Tissot, B., and D. Welte, 1984, Petroleum Formation and Occurrence: Berlin, Springer

Trendel, J. M., A. Restlé, J. Connan, and P. Albrecht, 1982, Identification of a novel series of tetracyclic terpanes (C24□C27): Journal of the Chemical Society, Chemical Communications, p. 304-306.

Turner, B. W., C. E. Molinares-Blanco, and R. M. Slatt, 2015, Chemostratigraphic, palynostratigraphic, and sequence stratigraphic analysis of the Woodford Shale, Wyche Farm Quarry, Pontotoc County, Oklahoma: Interpretation, v. 3, p. SH1-SH9.

Van den Kerkhof, A. M., and U. F. Hein, 2001, Fluid inclusion petrography: Lithos, v. 55, p. 27-47.

Volkman, J. K., S. M. Barrett, S. I. Blackburn, M. P. Mansour, E. L. Sikes, and F. Gelin, 1998, Microalgal biomarkers: A review of recent research developments: Organic Geochemistry, v. 29, p. 1163-1179.

Volkman, J. K., P. Kearney, and S. W. Jeffrey, 1990, A new source of 4-methyl sterols and 5α(H)-stanols in sediments: prymnesiophyte microalgae of the genus Pavlova: Organic Geochemistry, v. 15, p. 489-497.

Wang, D. W., and R. P. Philp, 1997a, Geochemical study of potential source rocks and crude oils in the Anadarko Basin, Oklahoma: AAPG Bulletin, v. 81, p. 249-275.

Wang, D. W., and R. P. Philp, 1997b, A Geochemical Study of Viola Source Rocks and Associated Crude Oils in the Anadarko Basin, Oklahoma, *in* K. S. Johnson, ed., Simpson and Viola Groups in the southern Midcontinent, v. Circular 99, Oklahoma Geological Survey p. 102.

Wang, G., X. Chang, T.-G. Wang, and B. R. Simoneit, 2015a, Pregnanes as molecular indicators for depositional environments of sediments and petroleum source rocks: Organic Geochemistry, v. 78, p. 110-120.

Wang, G., X. Chang, T. G. Wang, and B. R. T. Simoneit, 2015b, Pregnanes as molecular indicators for depositional environments of sediments and petroleum source rocks: Organic Geochemistry, v. 78, p. 110-120.

Wang, G., T. G. Wang, B. R. T. Simoneit, L. Zhang, and X. Zhang, 2010, Sulfur rich petroleum derived from lacustrine carbonate source rocks in Bohai Bay Basin, East China: Organic Geochemistry, v. 41, p. 340-354.

Waples, D. W., 1980, Time and temperature in petroleum formation: application of Lopatin's method to petroleum exploration: AAPG bulletin, v. 64, p. 916-926.

Wavrek, D., 1992, Characterization of Oil Types in the Ardmore and Marietta Basins, Southern Oklahoma aulacogen, *in* K. S. Johnson, and B. J. Cardott, eds., Source Rocks in The

Southern Midcontinent, v. Circular 93, Oklahoma Geological Survey Circular, p. 185-195.

Wavrek, D. A., M. A. Garcia, and C. D. Ferebee, 1997, The Viola Group as a petroleum system: Implications for horizontal-drilling prospects, *in* K. S. Johnson, ed., Simpson and Viola Groups in the southern Midcontinent, v. Circular 99, Oklahoma Geological Survey p. 78-86.

Webb, G. W., 1976, Oklahoma City oil—Second crop from preserved subunconformity source rocks: AAPG Bulletin, v. 60, p. 115-122.

Wei, Z., J. M. Moldowan, and A. Paytan, 2006, Diamondoids and molecular biomarkers generated from modern sediments in the absence and presence of minerals during hydrous pyrolysis: Organic Geochemistry, v. 37, p. 891-911.

Weston, R. J., R. P. Philp, C. M. Sheppard, and A. D. Woolhouse, 1989, Sesquiterpanes, diterpanes and other higher terpanes in oils from the Taranaki basin of New Zealand: Organic Geochemistry, v. 14, p. 405-421.

Wilson, E. N., W. L. Watney, and G. M. Grammer, 2017, An Overview of the Giant Heterogeneous Mississippian Carbonate System of the Midcontinent: Ancient Structure, Complex Stratigraphy, Conventional Traps and Unconventional Technology in a High Fluid Volume World, *in* J. M. G. G. M. Grammer, J. O. Puckette, P. Jaiswal, S. J. Mazzullo, M. J. Pranter, and R. H. Goldstein, ed., Mississippian Reservoirs of the Midcontinent, v. 116, AAPG Memoir.

Wingert, W. S., 1992, G.c.-m.s. analysis of diamondoid hydrocarbons in Smackover petroleums: Fuel, v. 71, p. 37-43.

Wolff, G. A., N. A. Lamb, and J. R. Maxwell, 1986, The origin and fate of 4-methyl steroids—II. Dehydration of stanols and occurrence of c30 4-methyl steranes: Organic Geochemistry, v. 10, p. 965-974.

Wygrala, B. P., 1989, ntegrated study of an oil field in the southern Po Basin, northern Italy, University of Cologne, Germany, 217 p.

Yamamoto, M., 1992, Fractionation of azaarenes during oil migration: Organic Geochemistry, v. 19, p. 389-402.

Yang, Y., and K. Arouri, 2016, A Simple Geotracer Compositional Correlation Analysis Reveals Oil Charge and Migration Pathways: Scientific Reports, v. 6, p. 23066.

Yükler MA, C. C., Welte DH 1979, Simulation of geologic, hydrodynamic, and thermodynamic development of a sediment basin — a quantitative approach., *in* W. B. F. R. U. von Rad, and al., ed., Initial Reports of the Deep Sea Drilling Project, v. 47, part 1: Washington, p. 761-771.

Zhang, S., and H. Huang, 2005, Geochemistry of Palaeozoic marine petroleum from the Tarim Basin, NW China: Part 1. Oil family classification: Organic Geochemistry, v. 36, p. 1204-1214.

Zhang, S., H. Huang, Z. Xiao, and D. Liang, 2005, Geochemistry of Palaeozoic marine petroleum from the Tarim Basin, NW China. Part 2: Maturity assessment: Organic Geochemistry, v. 36, p. 1215-1225.

Zinniker, D. A., 2005, New insights into molecular fossils: the fate of terpenoids and the origin of gem-dialkylalkanes in the geological environment, PhD dissertation, Stanford University, Stanford, California.

Zou, C., 2017, Unconventional petroleum geology, Elsevier.

Zumberge, J. E., 1987, Prediction of source rock characteristics based on terpane biomarkers in crude oils: A multivariate statistical approach: Geochimica et Cosmochimica Acta, v. 51, p. 1625-1637.